FACULTY OF **MEDICINE AND HEALTH SCIENCES**

Intensity modulated radiation therapy and arc therapy: validation and evolution as applied to tumours of the head and neck, abdominal and pelvic regions

Wim Duthoy

Promotor:
Prof. Dr. W. De Neve

Thesis submitted to fulfil the requirements for achievement
of the degree of Doctor in Medical Sciences

Ghent, January 2006

Department of radiotherapy

Universiteit Gent
Faculty of Medicine and Health Sciences
Department of radiotherapy

Intensity modulated radiation therapy and arc therapy: validation and evolution as applied to tumours of the head and neck, abdominal and pelvic regions

Wim Duthoy

Thesis submitted to fulfil the requirements for the degree of Doctor in Medical Sciences
February 2006

Promotor

Prof. Dr. W. De Neve	Department of radiotherapy Ghent University Hospital

President of the examination commission

Prof. Dr. C. De Wagter	Department of radiotherapy Ghent University Hospital

Examination commission

Prof. Dr. Y. De Deene	Department of radiotherapy Ghent University Hospital
Ir. W. De Gersem	Department of radiotherapy Ghent University Hospital
Prof. Dr. M. Peeters	Department of gastro-enterology Ghent University Hospital
Prof. Dr. G. Storme	Department of radiotherapy Free University of Brussels
Prof. Dr. D. Verellen	Department of radiotherapy Free University of Brussels
Prof. Dr. H. Vermeersch	Department of head and neck surgery Ghent University Hospital
Prof. Dr. E. Wong	Department of Oncology Department of Applied Mathematics University of Western Ontario, London Regional Cancer Centre, London, Ontario, Canada

From 1-10-2000 until 30-9-2004, Wim Duthoy was an Aspirant of the FWO-Vlaanderen

Contents

Abbreviations

3D	three-dimensional
3D-CRT	three-dimensional conformal radiotherapy
aSOWAT	arc-therapy adapted segment outline and weight adaptation tool
ABST	anatomy-based segmentation tool
ADR	angular delivery rate
BEV	beam's eye view
CP(s)	control point(s)
CT	computed tomography
CTV(s)	clinical target volume(s)
DMLC	dynamic multileaf collimator
DVH(s)	dose-volume histogram(s)
FDG	2-[^{18}F]fluoro-2-deoxy-D-glucose
GTV	gross tumour volume
GUH	Ghent University Hospital
Gy	gray
HNC	head and neck cancer
IGRT	image-guided radiation therapy
IMRT	intensity-modulated radiation therapy
IMAT	intensity-modulated arc therapy
linac(s)	linear accelerator(s)
LNR(s)	lymph node region(s)
LPO	leaf position optimization
LVC	leaf velocity constrainer
MLC	multileaf collimator
MLS	maximal leaf speed
PGD	polymer gel dosimetry
MRI	magnetic resonance imaging
MS(s)	machine state(s)
MU(s)	monitor unit(s)
NTCP	normal tissue complication probability
OAR(s)	organ(s) at risk
PET	positron emission tomography
PTV(s)	planning target volume(s)
SMLC	static multileaf collimator
TCP	tumour control probability
TPS	treatment planning system
WAPRT	whole abdominopelvic radiation therapy

List of Figures

List of Tables

I Summary – Samenvatting – Résumé

Summary

Intensity-modulated radiotherapy (IMRT) is a relatively new approach for the old quest of three-dimensional conformal radiation technique (3D-CRT). IMRT allows for a greater control over the distribution of the delivered dose and by this, enables to create concave dose distributions and to conformally spare organs at risk (OARs), like the spinal cord, the optic pathways or the parotid salivary gland. Technically, there are several approaches to both the planning (segment creation, optimization and dose computation) and the delivery (static gantry, rotational, dynamic or static multileaf collimator (MLC)). At the Ghent University Hospital (GUH), a unique treatment planning system (TPS) was developed, built on anatomy-based segmentation and leaf position optimization (LPO), driven by a bio-physical optimization function.

At GUH, IMRT has been clinically implemented for a variety of sites, of which the implementation for head and neck cancer (HNC) is the focus of the first part of this thesis. The planning strategy is described for re-irradiation of recurrent or second primary HNC and for HNC originating from the pharynx or oral cavity. Furthermore, the implementation of IMRT for the irradiation of sino-nasal cancer has shown that IMRT results in at least equal local control (LC) and overall survival (OS) as conventional radiation techniques, and clinically confirms the sparing of the optic pathways. None of the patients who were irradiated by means of IMRT lost vision due to radiation-induced toxicity. A review of the clinical results of IMRT in HNC, summarizing the experience of the leading IMRT centers shows a parallel conclusion: IMRT results in a favourable toxicity profile, but until now, no effect on LC or OS has been shown in a well-controlled trial. The observation that most of the HNC relapse within the “high-dose” region, indicates that these conventional “high dose” levels (+/- 70 Gy) are not sufficient to eradicate all clonogenic cancer cells. Therefore, we studied the possibility of dose escalation, guided by biological imaging (positron emission tomography; PET) within a clinical phase I trial, with a stepwise dose escalation protocol.

Besides the implementation and clinical validation of static-gantry IMRT, the second focus of this dissertation is on the development of intensity-modulated arc therapy (IMAT). IMAT is a rotational, MLC-based delivery technique, in which the modulation of the intensity is obtained by overlapping arcs. The anatomy-based approach, in conjunction with the LPO, makes our TPS suitable for the transition from IMRT to IMAT. IMAT has some distinct advantages over IMRT in selected cases. In situations where a large concavity in the dose distribution is needed, IMAT offers an infinite number of beam directions. Another situation where IMAT could be beneficial over IMRT occurs when multiple dose peaks have to be created within a lower "dose bath", a situation often encountered in biological imaging guided radiotherapy. A planning strategy for IMAT was developed, and a class solution for whole abdominopelvic radiotherapy and radiotherapy for rectal cancer were implemented, after the formulation of target delineation guidelines. IMAT was compared with non-intensity-modulated 3D-CRT, and showed a better OAR sparing for equal or better target coverage. IMAT was dosimetrically verified by polymer gel dosimetry (PGD), which allows 3D absolute dosimetry. PGD showed a good correlation between calculated and measured dose. Finally, IMAT is discussed in comparison with helical tomotherapy: both delivery systems are rotational, and have the same indications. Future research will concentrate on the improvement of LC in HNC by careful dose escalation, compiling and analyzing the observed toxicity in IMRT and on the further automation, development and implementation of IMAT.

Samenvatting

Intensiteitsgemoduleerde radiotherapie (IMRT) is een relatief recente benadering van een oud radiotherapeutisch streefdoel, namelijk de driedimensionale conformele radiotherapie (3D-CRT). IMRT laat een betere controle over de dosisdistributie (DD) toe dan conventionele 3D bestralingstechnieken. Zo is het met IMRT mogelijk om concave DDs te bereiken en om de risico-organen, zoals het ruggenmerg, de speekselklier, het oog en de oogzenuwen, conformeel uit te sparen. Vanuit een technisch oogpunt zijn er verschillende benaderingen voor IMRT mogelijk, zowel op het vlak van planning (creëren van segmenten, optimalisatie en dosisberekening) als van de uitvoering (statische versus roterende gantry, statische versus dynamische multileaf collimator). In het Universitair Ziekenhuis Gent (UZG) werd er een uniek planningssysteem ontwikkeld, dat voornamelijk steunt op anatomie gebaseerde segmentatie (ABS) en de optimalisatie van de segmentvorm (SVO) en het relatieve belang

van elk van deze segmenten. De optimalisatie wordt gestuurd door een bio-fysische objectieve functie.

IMRT werd in het UZG klinisch toegepast voor een hele waaier van tumorlocalisaties. De toepassing van IMRT voor de bestraling van hoofd- en halstumoren (HHT) vormt het onderwerp van het eerste deel van deze thesis. De planningsstrategie voor herbestralingen en bestraling van HHT, uitgaande van de keel en de mondholte wordt beschreven, evenals de eerste klinische resultaten hiervan. De studie van de implementatie van IMRT voor tumoren van de neus(bij)holten heeft aangetoond dat IMRT in deze indicatie leidt tot minstens even goede lokale controle (LC) en overleving als conventionele bestralingstechnieken. Bovendien werd het op planning uitsparen van de optische structuren bevestigd door de klinische resultaten: geen van de patiënten die met IMRT behandeld werden, ontwikkelde blindheid tengevolge van stralingsgeïnduceerde schade. Een overzicht van de bereikte klinische resultaten van IMRT in HHT in andere centra levert een gelijkaardige conclusie op: IMRT leidt tot een gunstiger toxiciteitprofiel maar heeft tot op heden nog geen bewijs kunnen leveren van een gunstig effect op LC of overleving. De meeste hervallen van HHT worden gezien in het gebied dat tot een hoge dosis bestraald werd, wat erop wijst dat deze “hoge dosis” (+/- 70 Gy) niet volstaat om alle clonogene tumorcellen uit te schakelen. We startten een studie op, om de mogelijkheid van dosisescalatie uit te testen. Hierbij wordt de dosis verhoogd op geleide van informatie van biologische beeldvorming (positron emissie tomografie; PET).

Naast de toepassing en klinische validatie van IMRT bestond het werk in het kader van deze thesis ook uit de ontwikkeling en het klinisch opstarten van intensiteitgemoduleerde arc therapie (IMAT). IMAT is een rotationele vorm van IMRT (d.w.z. de gantry draait rond tijdens de bestraling), waarbij de modulatie van de intensiteit bereikt wordt door overlappende arcs. Dankzij de ABS, samen met de SVO, is het planningssysteem dat aan het UZG ontwikkeld werd uitermate geschikt om naast IMRT ook IMAT aan te kunnen. IMAT heeft enkele duidelijke voordelen ten opzichte van IMRT in bepaalde situaties. Als het doelvolume concaaf rond een risico-orgaan ligt met een grote diameter, biedt IMAT eigenlijk een oneindig aantal bundelrichtingen aan. Ook als er verschillende dosispieken bereikt dienen te worden, die elk omringd zijn door relatief lagere dosis, kan IMAT voordelen hebben. Deze laatste situatie doet zich vaak voor bij radiotherapie op geleide van de biologische beeldvorming. Een planningsstrategie voor IMAT werd ontwikkeld, en type-oplossingen voor totaal abdominale bestraling en rectumbestraling werden onderzocht en klinisch toegepast. Dit

laatste kon uiteraard enkel gebeuren nadat duidelijke richtlijnen voor de bepaling en intekening van het doelvolume waren opgesteld. In vergelijking met conventionele 3D technieken, werden betere planningsresultaten bekomen met IMAT. De dosimetrische controle van IMAT gebeurde aan de hand van polymeer gel dosimetrie, een techniek die een 3D absolute dosimetrie toelaat. Er werd een goede overeenkomst gevonden tussen de berekende DD, en de met PGD opgemeten DD. Tenslotte wordt een theoretische vergelijking gemaakt tussen IMAT en tomotherapy, die beide rotationele therapieën zijn en beide dezelfde indicaties hebben. Toekomstig onderzoek zal zich voornamelijk richten op het verbeteren van de LC bij HHT, het bijhouden en analyseren van de bijwerkingen van IMRT, en het verder automatiseren, ontwikkelen en toepassen van IMAT.

Résumé

La radiothérapie conformationnelle avec modulation d'intensité (RCMI) est une technique relativement nouvelle, qui sert le vieux rêve de la radiothérapie conformationnelle tridimensionnelle (RC-3D). RCMI permet une plus grande influence sur la distribution de la dose (DD) dans le patient. En utilisant RCMI, il est devenu possible de créer une distribution concave de la dose déposée, ce qui permet donc d'épargner d'une façon conformationnelle les organes à risque (OAR), comme les structures oculaires, les parotides et la moelle. Au niveau du plan technique, plusieurs possibilités de RCMI existent, aussi bien en ce qui concerne la planification (génération des faisceaux, l'optimisation, et le calcul dosimétrique), que le traitement lui-même (collimateur multilame (MLC) statique ou dynamique, technique rotationele ou faisceaux statiques). A l'Hôpital Universitaire de Gand (HUG), un système de planification a été développé, basé sur la génération de segments en partant de l'anatomie du patient (anatomy-based segmentation; ABS). L'ABS est complétée par l'optimisation de la position des lames (OPL) et de l'importance relative de chaque faisceau. Cette optimisation est basée sur une fonction objective à part biologique et physique.

A l'HUG, la RCMI a été introduite dans la pratique clinique depuis plusieurs années et pour un éventail de localisations tumorales. L'application de la RCMI pour les tumeurs de la tête et du cou (TTC) est le sujet de la première partie du travail présenté. La stratégie de planification RCMI et les résultats dosimétriques aussi bien que cliniques pour les ré-irradiations et l'irradiation primaire de tumeurs originelles de l'oropharynx et la cavité orale sont discutés. L'application de la RCMI dans le traitement des tumeurs des fosses nasales et paranasales (TFPN) a résulté dans un contrôle local (CL) et une survie qui est au moins comparable aux

résultats obtenus avec les techniques conventionnelles. Sur le plan de toxicité oculaire, aucun patient traité par la RCMI n'a développé une perte de vue à cause d'une pathologie radio-induite. Une mise au point de l'expérience et des résultats publiés des centres de radiothérapie, renommés pour la CRMI, nous donne le même message : la CRMI a un profil de toxicité avantageux, mais une amélioration du CL reste jusqu'à aujourd'hui a prouver. Dans la plupart des patients avec une TTC, qui souffrent d'une récidive, la récidive se développe dans la région qui a reçu une dose « maximale ». Cette observation nous montre que cette dose, dite « maximale » (d'environ 70 Gy), est insuffisante pour éliminer tous les cellules cancéreuses. Nous avons initié une étude d'escalade de dose. La dose escalée est dirigée par l'imagerie biologique (la tomographie à émission de positrons, TEP).

Au delà de l'application et la validation de la RCMI, une nouvelle technique de traitement à modulation d'intensité a été développée, à savoir l'arc-thérapie à modulation d'intensité (ATMI). La modulation d'intensité est obtenue par la superposition de plusieurs arcs. Grâce à l'ABS et l'OPL, notre système de planification est bien équipé pour l'ATMI. L'ATMI a plusieurs avantages par rapport à la RCMI. Dans les cas où le volume-cible est drapé autour d'un OAR avec un grand diamètre, l'ATMI offre un nombre infini de faisceaux. Aussi dans la radiothérapie dirigée par l'information de l'imagerie biologique, l'ATMI pourrait avoir un rôle. L'ATMI a été développée pour la radiothérapie abdominopelvienne et pour le traitement radiothérapeutique du cancer du rectum. Pour ce dernier, une définition du volume-cible a été proposée, basée sur des données de la littérature. Comparé à des techniques 3D, l'ATMI résulte dans une protection dosimétrique des tissues normales. Le contrôle de qualité dosimétrique pour l'ATMI a été fait à l'aide de gels radiosensibles. Ces gels sont un important atout, vue que ces gels sont des dosimètres absolus en 3D. Une bonne corrélation a été trouvée entre les DD calculées et mesurées. Dans le proche futur, l'amélioration du CL dans les TTC sera un sujet de recherche important. L'incidence de toxicité, et la relation entre l'incidence et la dose délivrée, serra analysée, et pour l'ATMI, l'automatisation de planification et le développement du traitement viendront au premier plan.

II Objectives and outline of the thesis

Intensity-modulated radiation therapy (IMRT) is a relatively new technique for delivering radiation dose to the patient. IMRT permits more control over the distribution of the delivered dose than conventional radiotherapy and three-dimensional conformal radiotherapy (3D-CRT). This results in some new possibilities:

(1) Creation of concave dose distributions, allowing to homogeneously irradiate a target volume that is wrapped around an organ at risk (OAR) [1].

(2) Conformal sparing of normal tissue.

(3) Delivery of multiple dose levels per fraction, creating the possibility of optimization of radiobiological characteristics [2].

The clinical implementation of IMRT aims at an improved complication-free loco-regional control. Although IMRT has been increasingly used around the world, clinical validation of its results is still scarce (although hardly needed).

By creating new possibilities, IMRT also raises new questions. The most important question introduced by IMRT is concerning the definition of target volumes. Unlike in conventional radiotherapy, the outline of the beams is defined by the delineated structures. Therefore, tissue wrongly not assigned as target volume will be underdosed. On the other hand, the possibility of sparing the OAR is largely influenced by the delineation of the target volume(s) [3]. Another related question is how we can use IMRT in order to further improve local control by focused dose escalation and how these volumes for dose escalation can be best identified.

One of the disadvantages of IMRT is the prolonged treatment time which increases with the number of beams. It can be shown that for target volumes with a large inner radius, or with multiple prescribed dose peaks, more beam directions are needed in order to obtain similar results regarding target volume homogeneity and sparing of OARs. Current IMRT delivery techniques might be sub-optimal for treating large tumours, and show room for further improvement.

The objectives for this thesis were to:

1. validate the implementation hypothesis for IMRT:

IMRT was implemented for several head and neck cancer (HNC) sites. A clinical protocol was developed, specifying the indications, target delineation and planning goals. IMRT has been implemented for oral cavity, pharyngeal, laryngeal and sinonasal tumours. For sinonasal carcinoma, radiation therapy plays an important role in the multidisciplinary approach. Conventional radiotherapy, however, might lead to ocular toxicity, resulting in (bilateral) blindness. With IMRT, it is possible to spare the optic pathways without compromising the dose to the target volume. IMRT for this site was therefore implemented with the hypothesis of higher complication-free local control rates. This has previously been shown for the acute toxicity [4]. It was investigated whether the implementation hypothesis was valid by examining the treatment results and the long-term toxicity.

2. incorporate biological imaging technologies into IMRT planning:

For advanced stage HNC, radiotherapy, in combination with chemotherapy, is a possible treatment option, and even standard treatment for inoperable cases. Despite optimal radiotherapy techniques, a large proportion of these patients will suffer disease relapse. The majority of these recurrences are mostly located in the original gross tumour volume (GTV). This urges for higher doses to those regions in which clonogenic cells survive. Dose escalation should be directed to a small volume, in order to keep toxicity acceptable. The incorporation of 2-[^{18}F]fluoro-2-deoxy-D-glucose positron emission tomography (FDG-PET, further referred to as PET) in IMRT treatment planning for guiding the dose escalation was explored.

3. develop and implement intensity-modulated arc therapy

Some clinical situations, in which static-gantry IMRT would possibly result in sub-optimal results, were identified. An anatomy-based planning approach for intensity-modulated arc therapy (IMAT) was developed, and class solutions were set up for whole abdominopelvic and pelvic (rectal) irradiation and compared with 3D-CRT techniques on the treatment planning level. Before bringing conformal techniques for rectal cancer into clinical practice, a clear definition of the target volume, and delineation guidelines were developed. Polymer gel dosimetry was used for dosimetrical control of the planning and delivery.

III Intensity-modulated radiation therapy

IMRT was previously described as "an advanced form of 3D-CRT that uses non-uniform radiation beam intensities that have been determined using various computer-based optimization techniques" [5]. Crucial in this description is the modulation of the intensity (or fluence, which would be a more appropriate term [6]) throughout the beam. The most common form of intensity modulation is the use of wedges. However, this is not considered as IMRT, as it is not an advanced form of 3D-CRT. There has been an exponentially growing interest in the development and the clinical use of IMRT, as reflected by the number of publications on this subject (Figure 1).

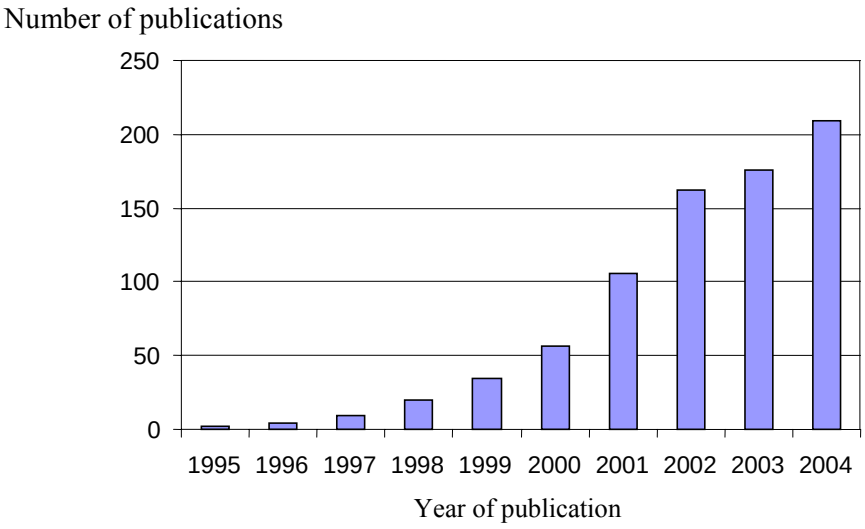

Figure 1: Evolution of the number of publications on IMRT. A Medline (http://www.pubmed.com) search was done on June 1st, 2005 using the following terms: [(intensity AND (modulation OR modulated) AND (radiotherapy OR radiation OR irradiation)) OR IMRT] in Title.

It is beyond the scope of this work to exhaustively review all the previously described aspects of IMRT. IMRT has been excellently reviewed both concerning its physical aspects [5;7] as well as the clinical implementation of IMRT [8]. This section on IMRT will give a brief summary on IMRT, putting the emphasis on the approach used at Ghent University Hospital (GUH).

III. 1. Physical principles of IMRT

Brahme *et al* [9] tackled the problem of a concave target volume, wrapped around an OAR. A clinical example of this often, but not exclusively, encountered situation is HNC, in which the tumour and the regional lymph nodes lie concavely around the spinal cord. He showed that, for rotational therapy, it is possible to calculate an intensity profile that would result in a

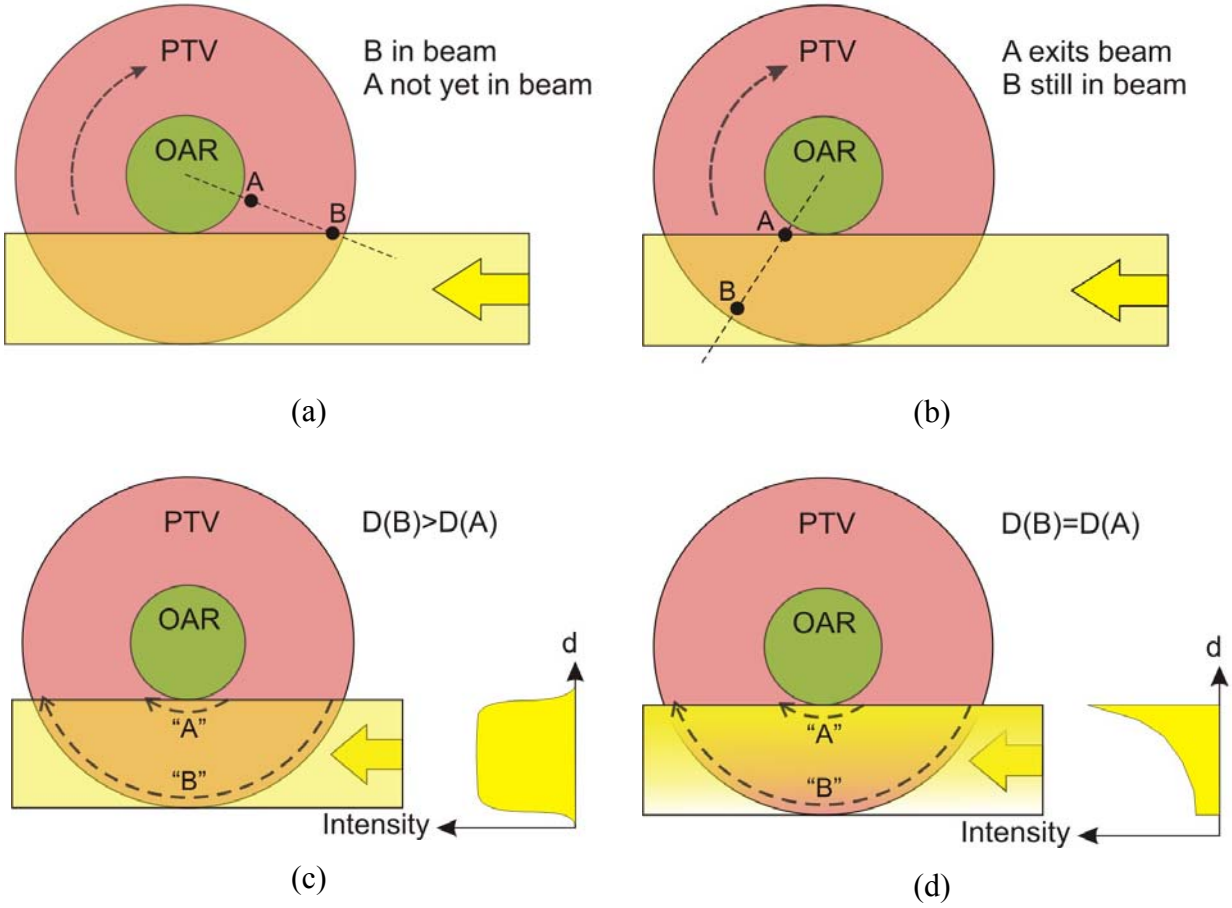

Figure 2: Visual and simplified representation of the work of Brahme *et al* [9]. The circle represents a simple phantom, in which the inner circle represents the organ at risk (OAR), while the outer ring (red) represents the planning target volume (PTV), as indicated. The bar represents a simplified beam, with omission of attenuation and penumbra. Instead of rotating the beam (as it is the case in rotational therapy), the phantom is rotating and the beam is kept stationary, which represents, in fact, the same relative situation. Two points in the PTV are followed: one point (A) lies close to the OAR, while the other (B) lies far away from the OAR. When the points are "irradiated" by the idealized beam (i.e. they lie in the bar), they accumulate dose. Thus, as the rotation progresses (panels (a) and (b)), point B will accumulate more dose (D(B)>D(A)), when the beam has a flat intensity profile (c). Brahme has shown that an intensity profile can be calculated for which the accumulated dose in all points (represented by A and B; D(B)=D(A)) in the PTV is equal, or, in other words, the PTV is homogeneously irradiated (d).

homogeneous absorbed dose in such a target volume. This intensity profile is as follows: the closer a point in the beam profile is to the OAR, the higher the intensity should be in this point. This is graphically explained in Figure 2. This paper is considered as the kick-off for IMRT by authorities in the field of IMRT [10-12]. In his paper (time is then 1982), Brahme

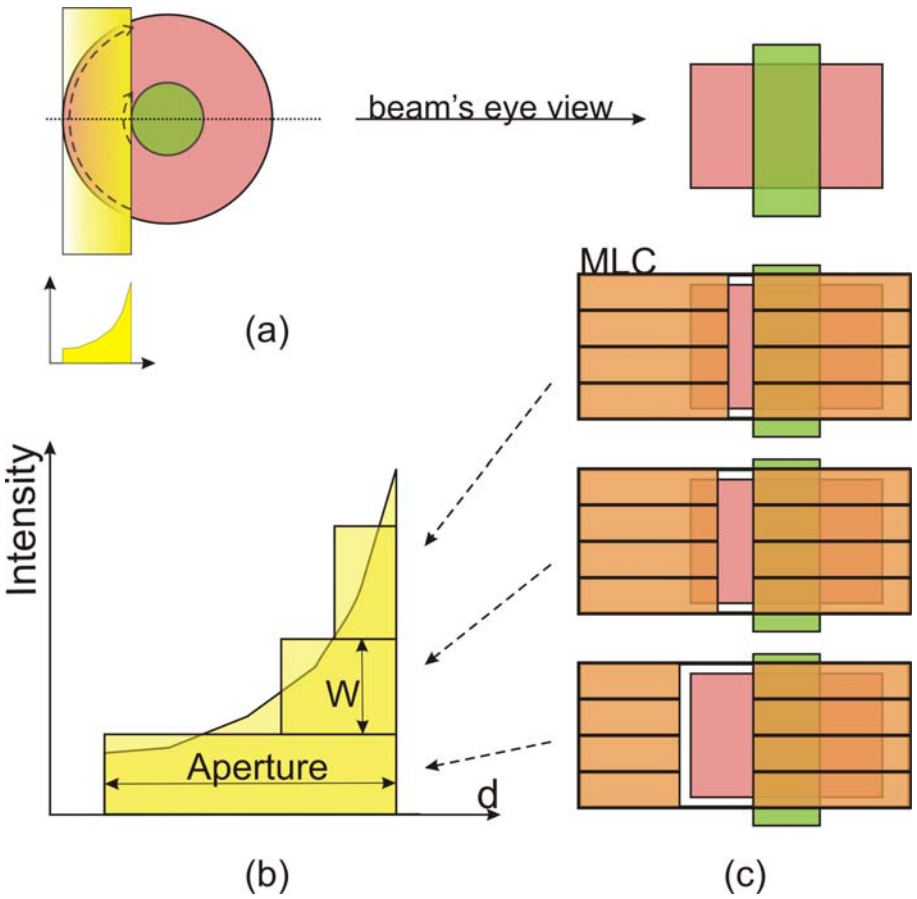

Figure 3: Representation of the MLC delivery technique for intensity modulation. In the left upper corner (a), panel (d) from Figure 2 is portrayed, and the desired intensity profile (curve) is enlarged in (b). The ideal intensity profile can be approximated by the superposition (in time) of three beams (or segments) with a flat intensity. The two parameters for optimization, to be known the aperture of the segment (defined by the leaf positions), and the relative weight "W", are indicated by the arrows. Whereas the phantom is looked at in a transverse view in (a), the same setup is represented in a beam's eye view in (c). A simplified MLC, with two banks of 4 leaves, defines the three segments. In the SMLC delivery technique ("step-and-shoot"), the radiation will be switched off between the leaf transition from one segment to the following. In the DMLC delivery technique ("sliding window" or "close-in"), the leaves will travel during radiation, thus giving a more precise approximation of the desired intensity profile.

suggested the use of a non-linear wedge-shaped filter to obtain this intensity profile. There have been several methods for delivering intensity-modulated beams. The one most resembling to the linear wedge is the use of cast metal compensators. However, this is a

cumbersome technique, as the compensators have to be changed between each beam, and have to be made on a patient- and beam-specific basis.

The first established IMRT delivery technique used the MIMiC multileaf collimator (MLC) from the NOMOS® company [7]. This (serial) tomography approach is discussed in section IV. 1 on p. 44.

Today, however, most IMRT treatments are delivered using a MLC, as shown in Figure 3**.** Two modes of delivery exist, known as dynamic MLC delivery (DMLC), in which the leaves travel during irradiation, and static MLC (SMLC) delivery. The former form of delivery is sometimes referred to as "sliding window" or "close-in" technique, while the latter is more commonly known as "step-and-shoot" (Figure 3). In SMLC delivery, the modulation of the intensity is obtained by superposed segments. Two parameters can be optimized: the aperture of the segment (leaf position) and the relative weight (W) of the segments.

III. 2. IMRT treatment planning

The treatment planning strategies for IMRT were historically divided into "forward" and "inverse" planning. These terms refer to the points where the planning starts, and where it ends. In this view, "inverse planning" starts with defining the goals of the treatment plan, and works to an optimized solution, which will ultimately result in a set of beams and segments. One could indeed call this "inverse", as opposed to, e.g. 3D-CRT, in which the beams are defined first while their relative weights are then optimized iteratively (by human interaction or computer-based). In the same thinking frame, forward IMRT planning denotes the planning strategy in which the segments are generated as a first step and then optimized in order to reach the predefined goals. However, these descriptions are troublesome, as one could say that even for a conventional planning of two tangential fields (as for a breast cancer radiation treatment), the goals of the treatment plan are also preset, and a solution (wedge factor and relative weights) is also searched for by iteration. Therefore, we suggest adopting the nomenclature as proposed by the Intensity Modulated Radiation Therapy Collaborative Working Group [5]. Forward planning is then defined as "treatment planning in which the planner defines the beam directions and shapes, beam weights, wedges, and so on, followed by the dose calculation and then the display and evaluation of the dose distribution. Iteration through the process is performed manually to reach an acceptable plan". Inverse planning is

then defined as “treatment planning in which the clinical objectives are specified mathematically and a computer optimization algorithm is used to automatically determine beam parameters that will lead to the desired dose distribution”. Although unambiguous, these definitions fail to propose a useful classification of IMRT planning approaches. Indeed, it is theoretically possible to make a forward IMRT planning [1], but it is evident that a computer-based optimization algorithm will result in a better solution (as was also proven, e.g. [13;14]). Therefore, using the proposed definition, all IMRT plans are considered to be “inverse”. Still, two largely differing groups of planning strategies can be identified, based on the method of segment generation: (1) “optimized fluence map”-based segmentation; and (2) anatomy-based segmentation.

III. 2.1. “Optimized fluence map”-based segmentation

Most commercially available IMRT treatment planning systems use the “optimized fluence map”-based planning approach. An introduction to the different aspects involved is given in a recent review [10]. Briefly, it goes as follows: the planner defines a number of beam parameters (gantry and collimator angle, energy, modality) and a number of goals (planning constraints). Then, for each chosen beam direction, a two dimensional grid is made out of “elementary beams” (called beamlets or bixels), after which a fast calculation algorithm (referred to as pencil beam algorithm) calculates the dose delivered per beamlet. These data form the basis for the subsequent optimization process. The optimization can be separated into two components: (1) the objective function; and (2) the search algorithm.

An objective function (also called cost function) is a mathematical description of the clinical objectives for the treatment plan optimization [5]. In fact, an objective function should closely mimic the clinical decision-making of an experienced radiation oncologist and physicist. However, a computer is unable to visually inspect and compare dose distributions, and take a clinical decision on which would be the preferred plan. Therefore, all these data have to be summarized into one value (the “cost” or “score”). Several types of objective functions exist:

- Dose- and/or dose-volume-based objective functions: some simple dose or dose-volume points are used to describe the treatment goals. Some examples are: maximal dose, minimal dose, maximal volume receiving more than 20 Gy.
- Biological model-based objective functions: more integrative criteria like normal tissue complication probability (NTCP) and tumour control probability (TCP) are used in the objective function.

Thus, any situation of the relative weights of the beamlets can be reduced to one value. However, in optimization, we want to compare several situations. Therefore, the weights of the beamlets (or other parameters that could be optimized) will have to be adapted, and the new situation re-evaluated. If we consider an IMRT plan with 6 beam directions, where all beams are divided into 100 beamlets and each 10 possible intensity levels, there would be $100x10^6$ possible "plans" to evaluate. Obviously, this cannot be done by human interaction. Thus, the weight of the beamlets is adapted by a search algorithm. Search algorithms define how the next beamlet weight will be adapted. Here too, several methods exist, of which gradient search [15] and simulated annealing [16] are the most widespread. An overview of these methods is given elsewhere [17]. For each new situation, a score is calculated by the objective function. By minimizing (or maximizing, depending on the characteristics of the objective function) this score, optimized fluence maps can be made for each beam direction. However, these optimized fluence maps cannot be delivered as such, and have to be converted to deliverable segments.

In this conversion, an algorithm tries to define the outlines (for SMLC-IMRT) or the leaf trajectories (for DMLC-IMRT) of the MLC leaves that are required to produce a deliverable intensity distribution that closely matches the distribution obtained by the optimized fluence maps. This "conversion" from optimized fluence maps to a deliverable series of segments, or leaf sequence generation, is one of the main disadvantages of the "optimized fluence map"-based planning approach.

Indeed, this procedure will lead to a deterioration of the optimized plan quality [18], as the number of segments will usually be limited, and the MLC leaves have some physical constraints that have to be obeyed. The conversion of optimized fluence maps is further explained in Figure 4. Another source for the deterioration of the quality of the optimized plan lays in the use of fast (but approximative) dose calculation algorithms for this optimization. A fast dose calculation, like the pencil beam method, is indispensable in optimization, as the optimization algorithm will go through it for thousands of times. For the sake of speed, these algorithms harbour serious flaws, such as inaccurate computation of scatter dose and a limited number of dose points in the structures that are included in the objective function. These flaws will be abused by the optimization algorithm. After leaf sequencing and final dose calculation using a more precise dose calculation algorithm, the final plan might therefore differ substantially from the optimized one, even urging for a new cycle of optimization.

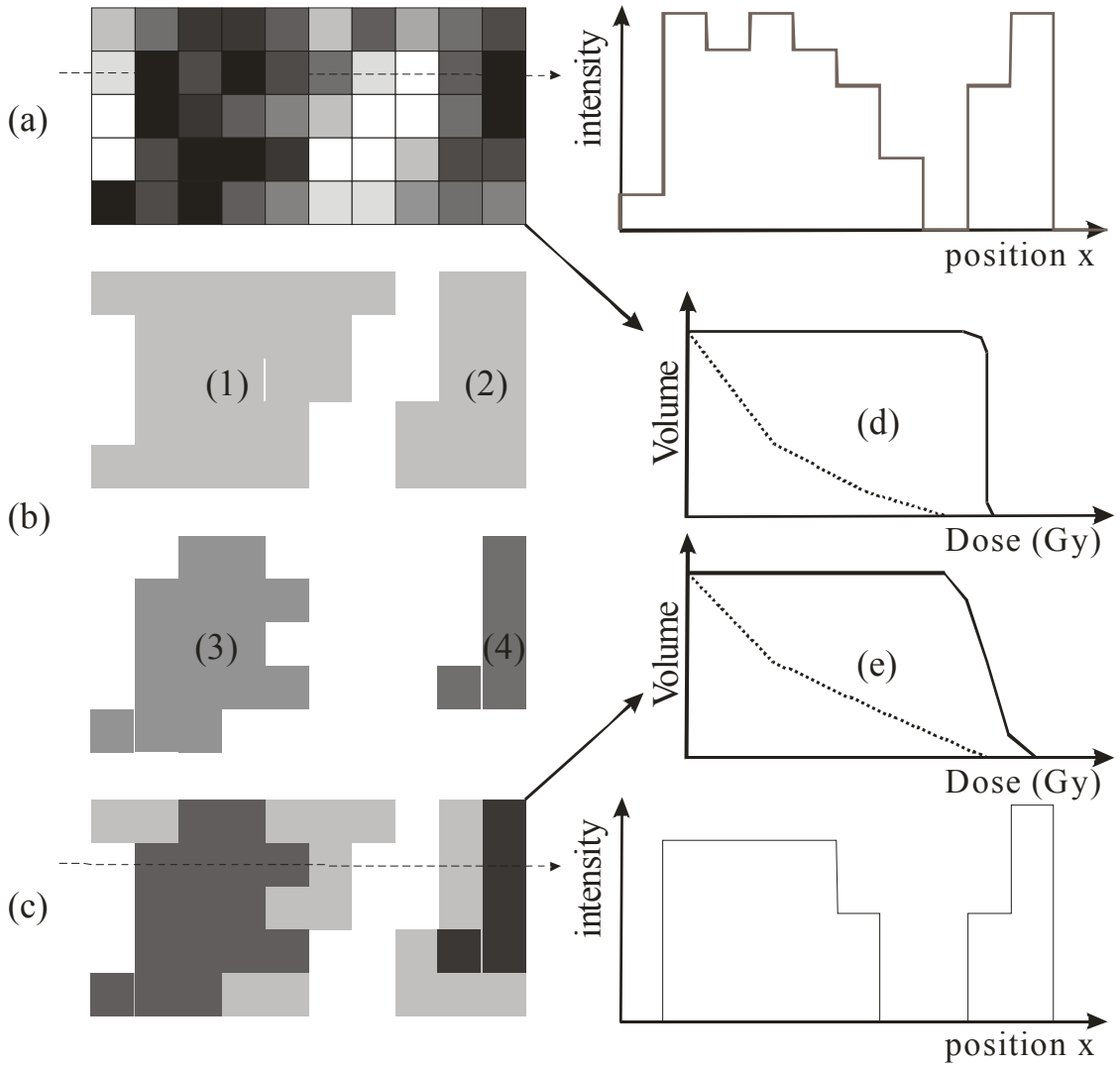

Figure 4: The process of leaf sequencing in "optimized fluence map" IMRT planning. (a) typical optimized fluence map for one beam direction. The darker the bixels (= elementary beamlet, see text), the higher the intensity. At the right, a one-dimensional (1-D) intensity profile along the dashed line is shown. (b) shows the 4 segments (1-4) that will be used to approximate the optimized fluence map. The deliverable fluence map is shown in (c), with the 1-D intensity profile at the right side. As the eventual fluence map deviates from the optimized fluence map, the resulting dose distribution of the optimized plan and the deliverable plan (presented here as dose-volume histograms in (d) and (e), respectively) will also differ. This difference can also be caused by the different calculation algorithm used during optimization (mostly a simple pencil-beam algorithm) and for final dose calculation (see text).

III. 2.2. Anatomy-based segmentation

Although the work of Brahme [9] was carried out for an ideal cylindrical phantom, using an ideal beam (no attenuation, no penumbra), it is obvious that the principle also stands for the more complex human anatomy, and for "real life" beams. In contrast to the previous approach, here, the creation of segments is the first planning step. Therefore, the number of

segments is known before optimization, and cannot increase by the optimization. The optimization can be based on very accurate dose calculations, as effects like head scatter or leaf leakage can easily be accounted for. Anatomy-based segmentation is also more intuitive than "optimized fluence map"-based IMRT plans, thus minimizing reluctance at its implementation, and simplifying quality control procedures. The creation of these segments can be done in a number of ways, be it manual, or using a computer algorithm. The GUH implementation of anatomy-based segmentation is discussed in more detail below.

III. 3. IMRT at Ghent University Hospital

De Neve *et al* [1] repeated the mathematical exercise from Brahme for static beams, and implemented the methodology for the concave sparing of the spinal cord. The idea behind this development was that, at that time, IMRT (then called beam intensity modulation or BIM) could only be planned using a dedicated treatment planning system (TPS). De Neve *et al* [1] showed that it was possible to plan and deliver an IMRT plan with a standard 3D TPS. Since this proof of principle, several software tools have been developed in-house, resulting in a unique anatomy-based TPS, which we will discuss into more detail.

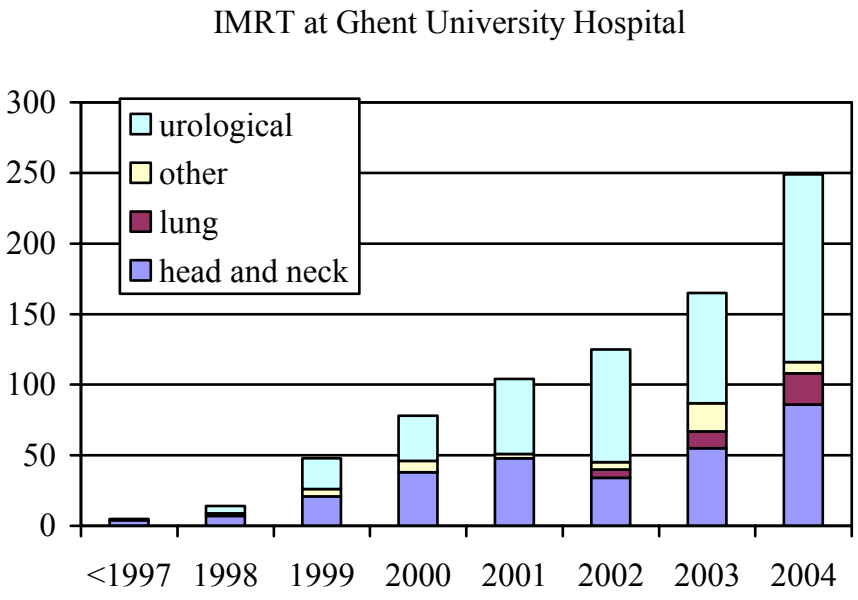

Figure 5: Number of patients treated with IMRT at GUH. Data from the year 1996 have been grouped with 1997.

IMRT was first applied for patients with a recurrent or second primary tumour of the head and neck region, who had been irradiated previously. In this group of patients, the main goal was to enable full-dose re-irradiation by selective sparing of the spinal cord [19]. Since then, the number of indications for IMRT has been growing to include prostate cancer, lung cancer and the majority of HNC. One of the three linear accelerators (linacs) at GUH is dedicated to IMRT treatments. The number of patients, treated with IMRT, reached 250 in 2004, and will approximate 300 patients in 2005, thus representing one fourth of all treated patients at GUH (Figure 5). The number of indications is likely to include gynaecological tumours (cervical and/or endometrial cancer) and gastro-intestinal cancer (rectal cancer) in the near future.

The GUH TPS is a planning system that is largely based on in-house developed software, and uses the GRATIS® virtual simulator [20]. As shown previously by Brahme *et al* [9] and De Neve *et al* [1], the optimal beam intensity profile can be calculated for any given situation. Although both calculations are based on a simplified phantom model, the same principle is valid for clinical anatomical situations. Thus, segment widths and weights can be roughly calculated in advance. This lead to the development of a segmentation tool, creating segments based on the anatomy of the patient (anatomy-based segmentation tool, ABST) [21]. The input that is provided to ABST consists of one (ore more) planning target volume(s) (PTVs) and one or more OARs, the skin contour, and a template beam, defining the isocenter, the beam incidence, the linac, the radiation modality and beam quality. The segments are then created in a nine-step algorithm:

1. All PTVs and OARs are projected on the isocentric plane along raylines from the source.
2. A rectangular grid, encompassing the PTV projection, is formed, with a pixel size of 1x1 mm^2. All pixels are assigned a value of zero. This grid is further called segmentation grid
3. Per PTV, all pixels within the PTV projection (=PTV-pixels) are assigned a value of 1.
4. In the same way, the values of all OAR-pixel are decremented by five.
5. All pixels with a positive value are divided by (1+D), with D the distance of the pixel to the nearest contour point of the OAR projection. This procedure is repeated for each OAR.
6. Rays are traced from the source point to each pixel, and the distance d from the skin to the isocentric plane is determined. The value of each positive pixel is multiplied by its respective (1+d) value.

7. The contours of the segments are now based on the iso-value lines of the segmentation grid. A first set of iso-value lines encompasses all grid points with positive values. This will form "exclusion contours", covering parts of the PTV(s), but excluding all OAR(s). Further iso-value lines (inside the exclusion contours) are then selected in such that they result in segment contours with increasing area. The area of the smallest contour is user-defined, as is the multiplication factor, which will define the area of the next contour (minimal area x multiplication factor). Contours are further created by repeating this procedure, until the area of the segment would be larger than the area of the exclusion segment.
8. Leaves and jaws are placed by closing-in on the previously determined segment contours. During this step, the minimal distance constraint of the Elekta MLC – opposed and diagonally opposed leaves should be separated with at least 1 cm - is disregarded.
9. During the last step, the leaf settings are adapted in order to meet the minimal distance constraint. This is done in such a way that adaptations away from the OARs will be favoured, and that the total repositioning distance is minimized

ABST will result in a number of segments, with an increasing number of (superposed) segments the closer a point gets to the OAR. Unlike for "optimized fluence map"-based IMRT, no dose computation is needed for the generation of segments. This makes ABST a fast method for the generation of segments which serve as a starting point for further optimization. A disadvantage of ABST is that it needs an OAR that runs through the projection of the PTV in a direction perpendicular to the direction of the leaf motion. Therefore, it is sometimes necessary to create a "dummy" structure that complies with this prerequisite (like in publication V. 7).

At GUH, typically, class solutions are developed per site (and disease stage, if appropriate). The IMRT Collaborative Working Group describes a class solution as "… a set of criteria for optimization (the form of the objective function and the values of its parameters) and the specifications of the beam techniques used, typically including beam directions and number (of beams). …" [5]. A class solution for a given disease site (and stage) should be designed in such a way that its application will lead to an acceptable plan in e.g. 90% or 95% of the cases. The major advantage of the use of class solutions is a reduction in planning time (by eliminating a priori a lot of parameters that could otherwise be optimized, e.g. beam direction, energy,…). Other advantages include homogeneity of the treatments, which is important for

the delivery (no “unexpected” collision problems; radiographers are more confident) and reporting. By definition, however, the use of a class solution – for a given patient - will result in a plan that is sub-optimal (clearly, the optimum plan does never exist [10]!). Therefore, it is important to specify the criteria that will be used for plan acceptance or rejection. It is obvious that each “candidate class solution” should be tested against these acceptance criteria before it can be adopted as “class solution”. Ideally, a class solution in clinical use should be re-analysed regularly over a group of treated patients, to see if it complies with the needs.

By using class solutions, only two treatment parameters remain for optimization: (a) the relative weight of the segments and (b) the leaf positions of the segments. The optimization of both parameters is driven by a bio-physical cost function [14]. As can be inferred from its name, both a biological and a physical term are used in this case. For the biological part of the objective function, the NTCP is calculated according to the earlier work of Burman *et al* [22] and Kutcher *et al* [23].

In this model, three parameters were determined by fitting clinically-derived dose-toxicity data points [24], namely (a) “TD_{50}” : dose to the whole organ (or to a reference volume, V_{ref}) that would lead to a complication probability of 50%; (b) volume parameter “n” and (c) the slope of complication probability “m” (more details are provided in Figure 6). All these data were entered in a database used by our TPS. Some new - virtual - organs were added to the database, in order to deal with specific clinical situations. As an example, for re-irradiation of the head and neck region, it is clear that other biological parameters are needed for the earlier irradiated spinal cord. One could set the TD_{50} to 30 gray (Gy) instead of 65 Gy, and increase the slope of the dose-NTCP function by decreasing the slope parameter “m”. These parameters for the spinal cord have lost their relationship with the clinical observations by Emami *et al* [24] from which the original parameters were extracted [22]. Still, these “virtual organs” have proven to be very useful, and, theoretically, one could extract these parameters from clinical data (in this case, from a series of re-irradiated head and neck patients). In the same philosophy, virtual organs were constructed which are (ab)used as a replacement for physical parameters. By setting both the slope parameter “m” and the volume parameter “n” to a very low value, a physical constraint for maximum dose is mimicked, as any point in the volume of interest, to which these parameters are assigned, receiving a dose higher than the TD_{50}, will give rise to a very high NTCP, and will be severely penalized by the optimization algorithm.

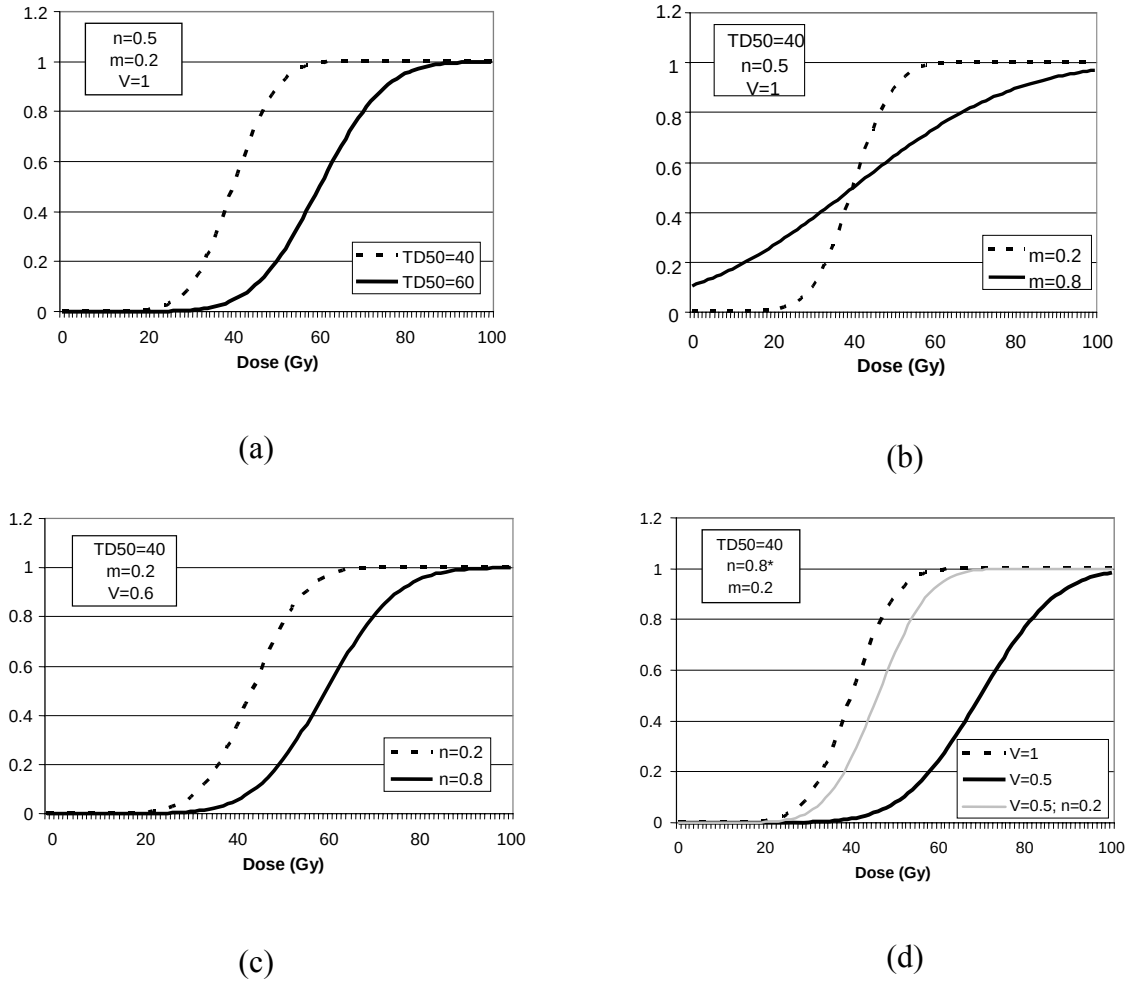

Figure 6: Relation between dose (Gy) and normal tissue complication probability (NTCP), showing the effect of the three parameters on the dose-NTCP relation. TD50 (in Gy) = dose to the whole organ (or to a reference volume, V_{ref}) that would lead to a complication probability of 50%; n = volume dependence of the NTCP; m = the slope of the NTCP curve; V = relative volume of the organ that receives a specified dose. For each panel, the parameters that were kept constant are shown in the left upper legends box, while the variable parameter is displayed in the legend box in the right lower legend box. (a) shows the effect of the TD50 on the dose-NTCP curve. (b) shows the impact of the slope parameter "m", while the influence of the volume dependence parameter is presented in (c). Subpanel (d) shows the influence of the relative volume "V" that was irradiated, for two different volume dependence parameters "n", namely n=0.8 (black lines) and n=0.2 (black dashed line and grey line). As the relative volume V equals unity for the black dashed line, there is no impact of "n" on this curve.

The TCP is also incorporated in the biological term, but mostly, the TCP factor is set to unity, because to date, for most tumour sites, there are not enough clinical and biological data to provide accurate TCP calculations. When using this TCP/NTCP model as the sole base for optimization, the dose in (parts of) the target volume (and thus the TCP) will increase, as long as the influence of this higher dose on the NTCP of the neighbouring OARs does not outweigh the gain in TCP. This might result in dose distributions with very high doses in parts

of the PTV. To date, no clinical experience exists for such a type of dose distributions. It is clear that such dose to the target volumes might lead not only to higher tumour control rates, but also to higher complication probabilities, due to chronic injury to the connective tissue, in which the tumour is embedded. The use of a purely biological optimization function, or the addition of a physical function, has been discussed in more detail elsewhere [25;26]. It can be concluded that, from a theoretical point of view, a purely biological optimization will always lead to a higher rate of uncomplicated tumour control, on condition that the biological models used fully reflect the in vivo (radio)biologic processes. This assumption cannot be made to date, and present TCP models have evident flaws, urging the use of additional physical factors in order to control the dose to and inside the target volume(s). The TPS allows the use of several physical factors, like maximally allowed inhomogeneity and root-mean-square-deviation minimization.

Besides the optimization of the segment weights, the position of the leaves is also optimized [27]. This leaf position optimization (LPO) starts from an existing dose distribution, calculated by any dose calculation algorithm, and is used as a tool for customization of an existing plan. Deliverable segments and the corresponding calculated dose distribution (per segment) serve as input for LPO. A leaf adaptation value (e.g. +1 cm) is selected, and the leaf position of the first leaf is adapted according to that value (+ stands for an outward placement of the leaf). The effect of the change on the dose matrix of the given segment is calculated using a fast calculation algorithm, and this effect is accounted for in the summed (over all segments) dose distribution. Then, the objective function (as described earlier) is recalculated, and if the change in leaf position results in an improvement, the new position is retained ("accept"), and the dose matrix for that segment is updated. In case of no improvement, the leaf is reset to its original position ("reject"). This procedure is executed for all collimating leaves of all segments, and represents one cycle in the LPO process. Each LPO cycle is followed by a (short) segment weight optimization. Subsequently, the next leaf adaptation value (e.g. -1 cm) is picked, and the whole procedure is repeated. The values that are used become progressively smaller (in absolute value), with bounces, and are partly user-defined. After all cycles are completed, the new segments are saved, and a final dose calculation (using an external dose calculation algorithm) is performed. This final dose calculation is necessary, as the dose distributions obtained after LPO are (partly) resulting from the fast (but approximate) calculation engine inside the LPO tool. The objective function in LPO was initially identical to the one used for segment weight optimization, but this sometimes resulted

in segments with a highly irregular aperture. This kind of segments is undesirable due to the tongue and groove effect [28], and the difficulty and/or uncertainty for the dose calculation of such segments. For this reason, an additional factor was added to the objective function in order to minimize these irregular forms (W. De Gersem, data unpublished). It has been shown that LPO results in significantly better IMRT plans for HNC [29] without any increase in the number of segments (and thus delivery time). Other groups have adapted a similar strategy, under the name of "direct aperture optimization" [30]. In a small, unpublished planning exercise, Claus showed that, for a head and neck case, it is perfectly possible to generate a clinically acceptable plan starting from 5 rectangular "segments" per beam direction (typically 6), and allowing the LPO algorithm to shape the segments in order to meet the planning requirements (Filip Claus, personal communication). Claus' experiment illustrates how thin the line between anatomy-based IMRT planning and "optimized fluence map"-based planning can be. A summary of the comparison between both strategies is given in Table 1.

	Favourable characteristics	**Unfavourable characteristics**
"Optimized fluence map"-based planning	• Implemented in most commercially available planning platforms. • Independent of any anatomical "relationship" between OAR and PTV.	• Number and shape of segments largely dependent on the quality of the conversion algorithm. • Generally less MU efficient* than anatomy-based approach.
Anatomy-based planning	• Segments are deliverable at any time in the optimization • The number of segments is known and constant at the start of optimization. • Results in more intuitive and smooth segment shapes.	• Specifically developed for situations in which the OAR runs through the PTV in BEV projection • Requires additional, dedicated optimization software (LPO)

Table 1: Summary of favourable and unfavourable characteristics of "optimized fluence map"- based planning and anatomy-based planning. Abbreviations: PTV = planning target volume; OAR = organ at risk; MU = monitor unit; BEV = beam's eye view; LPO = leaf position optimization. * MU efficiency: a measure for the number of MUs needed to obtain a certain specified dose. The clinical relevance of the MU efficiency is discussed on p. 178.

The problem of deterioration of the planning quality in "optimized fluence map"-based planning has also been described by the protagonists of these planning systems [10]. Several research groups are working on the incorporation of the MLC restrictions into the optimization part, in order to avoid the need for re-optimization [31;32]. It can be expected

that both planning strategies will learn from each others weaknesses and advantages, and will tend to converge. This "fusion" is already apparent in some commercially available TPSs like PrecisePLAN (Elekta) and Pinnacle (Philips Medical Systems) [33].

III. 4. Clinical implementation of IMRT for HNC

III. 4.1. Challenges in head and neck radiotherapy

HNC is a collective term harbouring a range of tumours, all arising from the head and neck region and usually from epithelial origin, differing not only in anatomical subsite, but also in risk factors, histological type and natural history. Mainly, six sites are considered under HNC [34]: (1) lip and oral cavity ;(2) pharynx, subdivided into nasopharynx, oropharynx and hypopharynx; (3) larynx; (4) nasal cavity and paranasal sinuses; (5) salivary glands and (6) thyroid gland. The most prevalent HNC sites are the oral cavity, the pharynx and larynx. Cancer of the thyroid gland largely differs from the other sites in terms of pathology, treatment and prognosis, and will not be considered here. The treatment of HNC is based on a multidisciplinary approach towards the patient, in which surgery, radiotherapy and, more recently, chemotherapy are sequentially or concomitantly combined. Radiotherapy for HNC deals with some problems, which can be grouped into two classes: (1) loco-regional failure and (2) toxicity (acute and chronic). Both problems are related to one another, and depend on the combination of irradiated volume and delivered dose. Conventional radiotherapy is associated with some technical limitations, possibly inducing suboptimal treatments leading to an unfavourable outcome. IMRT allows for more flexibility in the dose distributions, with creation of concave dose distributions, and conformal avoidance of OARs. The general hypothesis for the implementation of IMRT for head and neck radiotherapy is that IMRT would widen the therapeutic window, thus resulting in a higher complication-free loco-regional control.

➔ A general overview on IMRT for HNC is given in publication V. 1 (p. 62).

III. 4.1.1. Loco-regional failure

The origin of loco-regional failure lies in the survival of at least one clonogenic tumour cell. This can be caused by (1) a geographical miss or (2) an insufficient delivered dose, or a combination of both. In standard treatment protocols, there are mainly three levels of dose

prescriptions, depending on the load of clonogenic tumour cells. For macroscopic tumour, doses of (at least) ± 70 Gy are needed in order to eradicate all clonogenic tumour cells. In regions at high risk of microscopic tumour, like the post-surgical tumour bed, doses of ± 60 Gy are applied. For regions deemed at moderate to low risk for microscopic disease, doses around 50 Gy are delivered [35]. Knowledge about the pattern of spread, both locally and regionally, is indispensable in the definition of the target volumes, be it at simulation, or on the planning computed tomography (CT) and in the formulation of the dose prescription. Independent of the definition problem of the target volumes of HNC, good dose coverage to the PTV is necessary in order to obtain loco-regional control. The most commonly adopted technique in conventional radiotherapy consists of two lateral fields and one anterior lower neck field to cover the whole PTV. However, due to the limited tolerance of the spinal cord, the end dose with this beam configuration is around 40-44 Gy. At this dose, the posterior border of the lateral photon beam is set anteriorly to the spinal cord, and the posterior part of the neck is from then on irradiated using electrons, thus sparing the spinal cord (Figure 7).

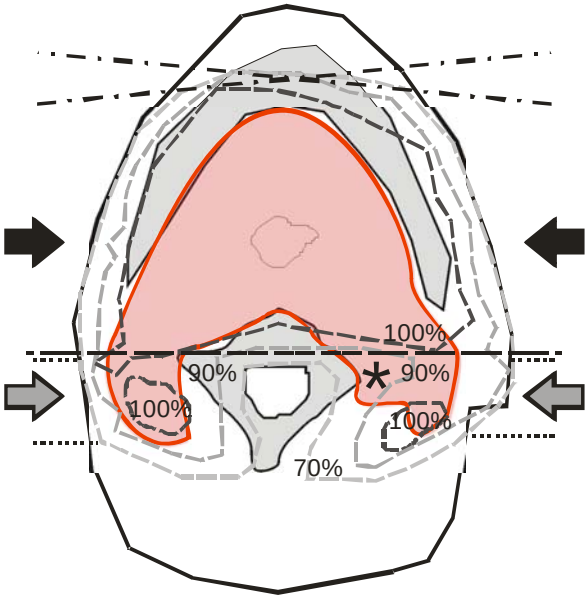

Figure 7: Illustration of the underdosage, induced by the use of a photon-electron match line technique. A transverse slice through a patient is shown, with the mandible and the vertebra (grey shaded structures). The planning target volume is indicated by the red/darker shaded structure. The two lateral photon beams are depicted by the dashed-dotted line (black arrows), while the dotted lines represent the posterior electron beams (grey arrows). The dashed lines represent the isodose lines (expressed as percent of the prescribed dose). The asterisk indicates the region in the PTV that receives less than 90% of the prescribed dose.
Adapted from Fogliata *et al* [36].

However, this field matching between the photon and the electron beam can be responsible for gaps between the fields, resulting in an underdosage at the junction [36]. In the anterior lower neck field, a central block is placed in order to shield the spinal cord. For low-lying tumours, like laryngeal and hypopharyngeal carcinoma, this can result in shielding of microscopic disease or even of the macroscopic tumour. This is routinely solved by using isocentric table top rotations, thus treating the lower neck by lateral photon fields only. Due to

the larger radiological path length, however, this nearly always results in underdosage in the lower neck region. Both problems can be avoided using IMRT, as the concave dose distributions spare the spinal cord during the whole treatment, omitting the need for electron beams.

III. 4.1.2. Treatment related toxicity

Radiation-induced toxicity is rather arbitrarily divided in acute toxicity and chronic toxicity. Acute toxicity starts during radiotherapy, and usually resolves within three months after the commencement of the radiotherapy course. Acute toxicity originates from the radiation-induced loss of the proliferative capacity of the so-called "target cells" , e.g. the clonogenic keratinocytes in the skin and oral mucosa, in addition to the ongoing physiological cell loss at epithelial surfaces [37]. This imbalance results in tissue hypoplasia and function loss. Other processes, like acute vascular response and other inflammatory reactions also play an important role in the clinical presentation and course of the acute toxicity [38].

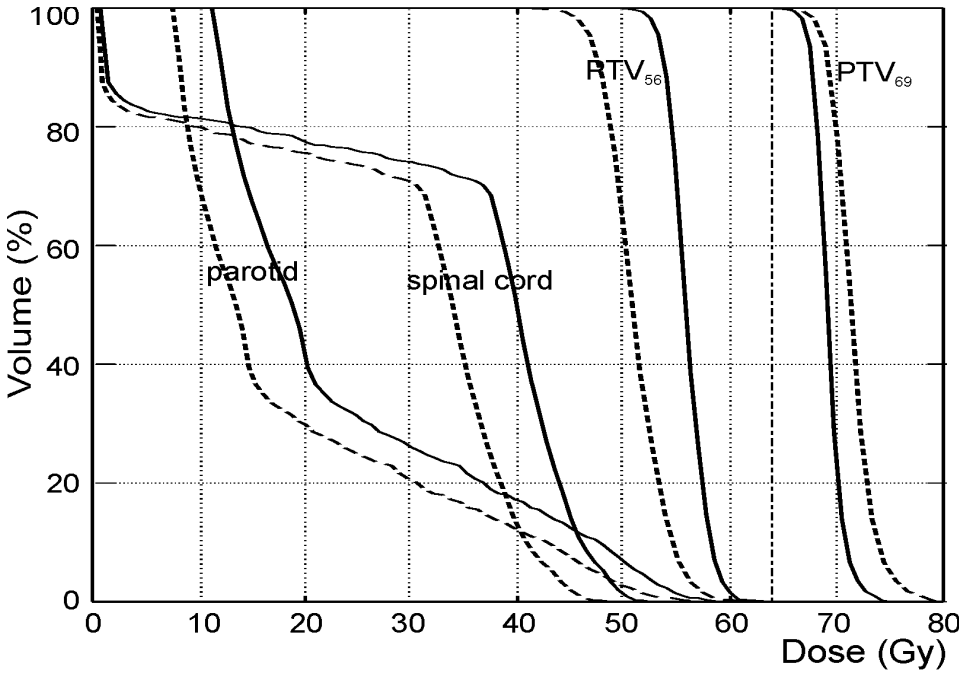

Figure 8: Dose-volume histograms (DVHs) for PTV_{69}, PTV_{56}, the spinal cord and the spared parotid. The DVHs represent the result of a typical IMRT plan for head and neck cancer, consisting of 32 fractions (more details are provided in III. 4.2.2 on page 33). The definition of PTV_{69} and PTV_{56} is given in Table 2 (p. 34). The full lines represent the total physical dose in Gy, while the dashed lines represent the 2Gy-normalized iso-effective dose – volume histograms ($NID_{2Gy}VH$) for the same structures. The $NID_{2Gy}VH$ are computed from the DVH data, by applying the formula given by Lee *et al* [39] with the same parameters as given in the caption of Table 2.

Chronic toxicity, by convention, appears from 90 days onwards after the start of radiotherapy, is considered irreversible and is characterized by vascular injury and tissue fibrosis [40]. Apart from other factors, like co-morbidity, genetic susceptibility, and concomitant chemotherapy, toxicity is influenced by the total dose, the irradiated volume, and the dose per fraction (for the sake of completeness, it should be mentioned that the dose per fraction will have a larger impact on chronic toxicity than on acute toxicity). Therefore, IMRT can result not only in physical selectivity (= the physical dose to the OARs is lower than the dose to the PTV), but also in biological selectivity [41]. Indeed, the sparing of the OARs in IMRT is not the result of coning down the treatment fields, like in conventional radiotherapy, but mainly by selective sparing through the whole treatment. IMRT results in a lower dose per fraction to the OARs than to the PTV, and so, the biological advantage of IMRT will even be more pronounced when the ratio of the α/β-values for tumour and OARs is larger than unity. An example is given in Figure 8. Here, both the physical dose for the whole treatment is given, as well as the normalized iso-effective dose (NID). The NID_{2Gy} represents the biologically effective dose, as if the dose was given in 2 Gy fractions [39].

In head and neck radiotherapy, the target volumes are in the vicinity of multiple OARs:

(1) **Spinal cord:** Radiation-induced spinal cord injury leads to the loss in function, not only of the stricken segment of the spinal cord, but to the part of the spinal cord that is located distally to this segment. On the macroscopic level, the grey matter and the white matter can be easily distinguished. The grey matter (centrally located in the spinal cord) is radioresistant in comparison with the white matter. As the white matter is mainly composed by longitudinally running myelinated axons, white matter necrosis is responsible for downstream paralysis. It is believed that the target cells for radiation damage are both the endothelial cells (thus compromising the blood supply), and the glial cells (resulting in demyelinisation of the axons, and so in loss of signal transduction). Besides the role of endothelial and glial cells, there is emerging knowledge on the influence of cytokines and growth factors in white matter necrosis. Clinical presentation largely depends on the position of the injured segment of the spinal cord. However, spinal cord injury is a never tolerated side effect of radiotherapy. Therefore, the spinal cord will always have the highest importance in planning. The $TD_{5/5}$ (the total dose, given in 2 Gy fractions, that is associated with a chance of a certain endpoint of 5% at 5 years after administration) for spinal cord necrosis is 50 Gy [22]. Detailed information about the biological response of the spinal cord to radiation can be found elsewhere [42]. We

adopted a hard constraint of 50 Gy to the planning risk volume around the spinal cord (dose per fraction is then around 1.5 Gy)

(2) **Optic nerve and optic chiasm:** Just like the spinal cord, the optic nerves are serial structures. Radiation optic neuropathy can lead to vision field defects and, if severe, (bilateral) loss of vision [43]. The threshold dose for radiation-induced optic neuropathy lies between 50 and 60 Gy [22;43]. For doses above 60 Gy, the dose per fraction seems to be a very important factor. A dose limit of 60 Gy was adopted as a hard constraint for optic chiasm and optic nerves, keeping in mind that the dose per fraction for a 70 Gy prescription in 35 fractions of 2 Gy to the target volume would thus result in 1.7 Gy per fraction to these optic structures.

(3) **Retina:** radiation retinopathy is caused by injury to the vascular supply of the retina, causing ischemia, hypoxia and neovascularization. In its turn, this can cause retinal haemorrhages, neovascular glaucoma and retinal detachments [44;45]. Retinal damage caused by radiation is observed at doses from 45 Gy on [22;46], although Takeda *et al* [47] found no retinal toxicity at doses below 50 Gy.

(4) **Salivary glands:** There are three major salivary glands, to be known the parotid, the submandibular and the sublingual gland. Furthermore, minor salivary glands are dispersed over the mucosa of the oral cavity (mostly buccal, labial, palatal and lingual). Saliva moistens the oral mucosa (and dry food), acts as a solvent for molecules that stimulate taste buds, contains amylase and lipase for food digestion, and has anti-bacterial actions. A deficient salivation leads to the subjective feeling of a dry mouth (=xerostomia), difficulties with eating (dry) food, decreased taste and dental caries, and affects the patient's quality of life. The salivary glands are relatively sensitive to radiation, with a TD_{50} (whole organ irradiation) of 28 Gy [48] for the parotid salivary gland. The reasons for this radiosensitivity are not completely understood, although a possible mechanism suggests a role for redox-active metal ions, that are associated with the secretion granules [49]. Serious efforts have been done for sparing the parotid salivary gland by using 3D-CRT [50] or IMRT techniques [3;51;52]. A mean dose below 26 to 30 Gy is advised when sparing of the parotid is achievable [53].

(5) **Mandible:** Mandibular osteoradionecrosis is a serious adverse effect that is relatively frequently encountered in head and neck cancer. It is nearly never seen at doses below 60 Gy, [54;55], but can reach an incidence of around 10% at doses of 70 Gy. Known risk factors for osteoradionecrosis are dose per fraction, invasion of the mandible by the tumour, dental extraction after radiotherapy (but also too close before radiotherapy), and concomitant chemotherapy [54-56].

(6) **Swallowing apparatus:** Swallowing is a complex physiological process [57]. The deglutition reflex is initiated by the voluntary action of collecting the oral content on the tongue, and propelling it backward to the pharynx. From then on, a wave of involuntary contraction in the pharyngeal musculature pushes the bolus towards the oesophagus. Just caudal to the pharyngo-oesophageal junction, the tension in the oesophagus is high at rest. This works as a physiological sphincter. The tension decreases as a part of the swallowing reflex. Inhibition of respiration and glottic closure are also essential parts of the reflex. It is clear that many different structures play an important role, and that the coordination between all the events is of utmost importance. In many patients suffering from a HNC, swallowing is already affected by the tumour itself. However, serious swallowing dysfunction can be seen in more than half of HNC patients, treated with concurrent chemotherapy, with aspiration in 60% of the patients [58].

III. 4.2. IMRT implementation for pharyngo-laryngeal carcinoma

In HNC, squamous cell carcinoma originating from the larynx and pharynx (oro-, hypo- and nasopharynx) represents the largest group. The main reasons to implement IMRT in this group of patients is to avoid the photon-electron matchline problem, and to spare the parotid gland in well-selected cases [53].

➔ **The implementation of IMRT for oropharyngeal and oral cavity tumours, together with the first clinical results, are discussed in publication V. 2 (p. 78).**

III. 4.2.1. Target volume definition and delineation

The delineation process results in various CTVs, depending on the estimated tumour load they contain. A PTV is constructed by applying a 3D expansion to each CTV, using a margin of 3mm. A description of all PTVs is given in Table 2.

➔ **The target definition and delineation process as used for pharyngo-laryngeal carcinoma is given in publication V. 4 (p. 108) and in [59].**

III. 4.2.2. Dose prescription and IMRT planning

In conventional radiotherapy, the different dose levels result from a “cone-down technique”: the neck region, including both macroscopic and subclinical disease, is irradiated up to a dose of e.g. 56 Gy, in 2 Gy fractions. After that dose level is reached, the fields are reduced so to encompass the macroscopic tumour with an adequate margin, and the treatment is continued

until the end dose of 70 Gy is reached, again in 2 Gy fractions. Theoretically, this could be done in IMRT treatments too, resulting in one plan per dose level. In this approach, the first IMRT plan would deliver a dose of 2 Gy per fraction to PTV_{All}, a PTV structure containing all different target volumes. After the first dose level (e.g. 56 Gy) is reached, a new plan is made in order to deliver 2 Gy per fraction to the remaining PTVs (= PTV_{All} minus PTV_{56}), and so on. The advantage of this approach is that conventional fractionation can be used for all target volumes. Still, this approach has some clear disadvantages: (1) multiple plans are needed, and thus more planner time is needed; (2) during subsequent plans, the previous dose level (e.g. PTV_{56} in the second plan) would accumulate dose that was not accounted for during the first plan, and thus, in the end-result, would receive more dose than initially prescribed. No evident planning tools exist to take previous IMRT planning results into account. This could result in a treatment that violates some planning constraints, like maximal dose to the spinal cord, even if this constraint had been met in all separate plans.

Another approach is to deliver the different dose levels in one plan. This approach is called the simultaneous integrated boost (SIB) technique. It has previously been shown that this SIB technique results in the more conformal dose distributions than when several IMRT plans are used for one treatment [60]. The fractionation scheme used at GUH is shown in Table 2.

Target volume	Description	Dose/fx (Gy)	TPD (Gy)	NID_{2Gy} (Gy)
PTV_{69}	PTV around the regions containing macroscopic tumour.	2.16	69.1	72.5
PTV_{66}	PTV around the (post-operative) tumour bed and resected LNR containing positive lymph nodes with capsular rupture	2.06	65.9	67.2
PTV_{62}	PTV around (resected) LNR containing positive lymph nodes without capsular rupture.	1.94	62.1	60.9
PTV_{56}	PTV around LNR that are to be irradiated electively	1.75	56.0	51.1

Table 2: Fractionation strategy for head and neck IMRT at GUH. *Abbreviations:* fx: fraction; TPD: total physical dose; NID_{2Gy}: normalized iso-effective dose, as for 2 Gy fractions, and calculated according to Lee *et al* [39], with: (1) a total treatment time that is calculated as 7(n-1)/5 with n the number of fractions; (2) an α/β-value of 10 Gy; (3) a β-value of 0.035/Gy² [61] and (4) a potential doubling time of 4 days; PTV: planning target volume; LNR: lymph node region.

The use of multiple PTVs introduces a new problem of priority ranking. Indeed, as the CTVs are lying against each other, an overlap region will be created by the expansion of CTVs to PTVs. The points in this overlap region will be submitted to a double request concerning the delivered dose. It is clear that the PTV with the highest dose prescription (=PTV_{high}) has priority over the PTV with the lower dose prescription (=PTV_{low}). To obtain this, the PTV_{low} is split up into an optimization volume (=$PTV_{low\text{-}optim}$) from which the PTV_{high} is subtracted with a specific margin. By this method, the overlap region is prevented, and the priority to PTV_{high} is assured. The dose gradient will be laid between the PTV_{high} and the $PTV_{low\text{-}optim}$.

The beam-defining part of the class solution that is used for IMRT treatments of patients with a pharyngo-laryngeal carcinoma consists of 6 non-opposed, non-equidistant coplanar beams (Figure 9). This beam arrangement is rather different than the generally proposed 9 equidistant coplanar beams [62]. Although the beam directions (45°, 75°, 165°, 195°, 285° and 315°) are on themselves non-equidistant , their trajectories could be viewed as 12

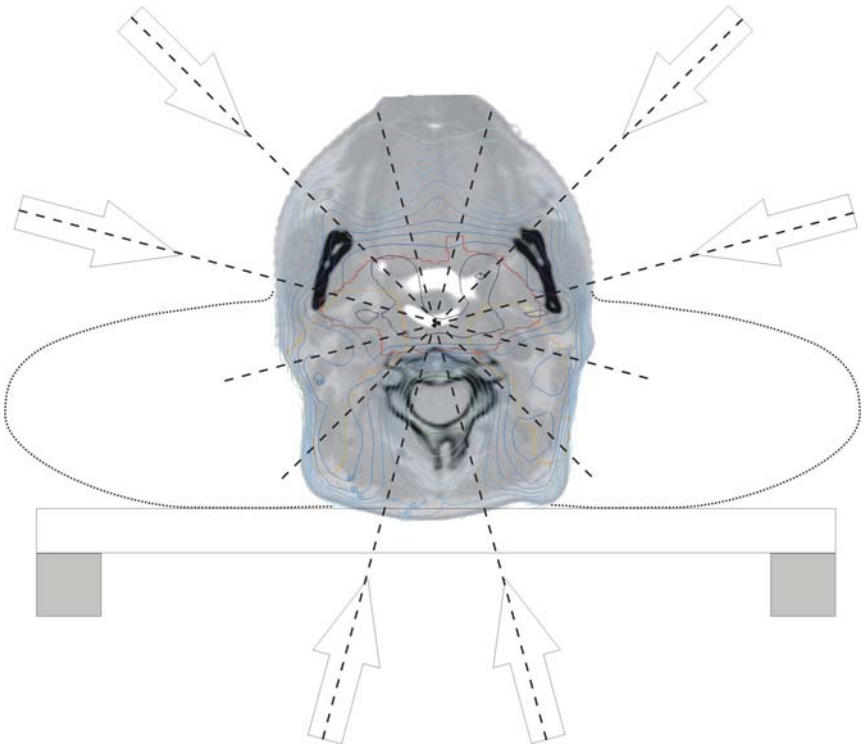

Figure 9: Beam arrangement for head and neck IMRT treatment, as applied at Ghent University Hospital. The six beam directions (45°, 75°, 165°, 195°, 285° and 315°) are depicted by the arrows and dashed lines. A transverse slice of the planning CT through the oropharynx is shown, as well as a projection of the shoulders (dotted lines). The couch is shown, together with the metal components of the Elekta table top, in their most outward position (as placed for these treatments).

equidistant directions (every 30°). The directions are chosen in such a way that the entrance dose through the oral cavity is minimized and beams entering via the (rather mobile) shoulders are avoided, as are the metal components of the table couch (see Figure 9).

Although the use of more beam directions might lead to a better planning result [63], it will also lead to longer treatment times. Therefore, the number of beams will always be a compromise between delivery time and planning quality. It should also be kept in mind that the gain in planning quality is not always clinically relevant. It is only in a minority of the patients that the planning goals and constraints, as specified in [59], cannot be reached with this setup. In these few patients, an individualized beam arrangement has to be looked for.

III. 4.2.3. Planning evaluation

The evaluation of an IMRT plan is done on basis of the dose-volume data and a visual inspection of the dose distributions on multiple slices in the three planes. The dose-volume data are visually inspected on cumulative dose-volume histograms (DVHs), and automatically checked using a UNIX-based shell script. The script checks all imposed constraints for all OARs and for the PTV homogeneity (the specific constraints can be found elsewhere [59]). If a constraint is violated, the reason for this can often be found by close inspection of the dose distribution. As an example, an underdosage in the PTV can be caused by a neighbouring OAR. In such a case, a clinical decision has to be made as whether respecting the constraint for the OAR is less or more important than reaching the goals for the PTV minimal dose. If such a conflicting situation is encountered, an extra optimization cycle is initiated, with a new evaluation at the end.

The use of objective planning evaluation constraints should be a dynamic process, with regular review of the applied constraints: if all consecutive plans pass all constraints, constraints might be too loose (or the class solution might be too complex for the given clinical situation). On the other hand, if no plan can reach all imposed constraints, these might be too tight (or the class solution might be inadequate). Of course, clinical treatment results (published and own experience) will also play an important role in the evaluation of the constraints.

III. 4.3. IMRT implementation for sinonasal cancer

Sinonasal sinus carcinoma groups all cancers arising from the nasal cavity and the paranasal sinuses. The incidence of this type of cancer is very low, representing only +/- 5% of all HNC

[64]. Most prevalent histological types are adenocarcinoma and squamous cell carcinoma, while other histological types like esthesioneuroblastoma, melanoma, lymphoma etc. are less frequent [65]. The treatment of sinonasal carcinoma is mainly based on a surgical approach in combination with radiotherapy [66]. Indeed, these tumours are in close proximity to important OARs like the optic apparatus. Also, these tumours often only cause symptoms in a relatively advanced stage, when surrounding organs are already affected. This makes radical surgery difficult to achieve. Therefore, at GUH, radiotherapy is a standard treatment modality for these tumours. One of the major concerns in the irradiation of sinonasal cancer is the risk of radiation-induced blindness. In older reported patient series, up to 30% of surviving patients developed radiation-induced blindness [67;68]. At GUH, IMRT was implemented for sinonasal cancer with the hypothesis that it would result in a higher uncomplicated local control. The planning strategy has been reported previously [69]. Briefly, seven beam directions (of which 5 in the sagittal plane) are used (see also Figure 2 in publication V. 1). Since July 1998, all patients suffering from a sinonasal cancer are treated by IMRT. Acute toxicity of this treatment is typically mild, and there is a reduction of dry eye syndrome [4]. Long-term results confirm these findings [45], and show equal treatment results in terms of local control and overall survival for IMRT as for conventional techniques. However, such a comparison is difficult to interpret, due to the patient selection bias that is typically associated with this rare cancer.

➔ **The long-term results of IMRT for post-operative irradiation of sinonasal carcinoma are presented and discussed in publication V. 3 (p. 90).**

III. 4.4. Introducing biological imaging in IMRT planning

III. 4.4.1. Introduction

Biological or functional imaging – as opposed to anatomical imaging - denotes all imaging modalities that visualize some biological properties of tissues. The use of biological imaging can serve three different goals in radiation therapy:

1. **Improving diagnostic and staging accuracy:**

   The choice of therapy ultimately relies on an accurate staging. In HNC, the presence and location of involved lymph nodes has important therapeutic implications, not only for surgery, but also concerning the radiation field size and dose prescription. Anatomical imaging, like CT, largely relies on measurements of diameter of lymph

nodes [70]. In a prospective study with histopathological control, Adams *et al* found a sensitivity and specificity of +/- 80% for CT and magnetic resonance imaging (MRI) (anatomical imaging), while this was 90% (sensitivity) and 95% (specificity) for FDG-PET [71].

Also in other sites, and most clearly in non-small cell lung cancer, biological imaging (and mainly FDG-PET) has provided promising results in staging. A review of all these sites is beyond the scope of this thesis, and is given elsewhere [72].

2. **Guidance for target delineation and dose distributions**

   Target delineation is the cornerstone of conformal radiotherapy. Until present, anatomical imaging has been the basis for this delineation. CT and MRI both provide excellent resolution in the axial plane (+/- 1 mm), but the discrimination between malignant and surrounding non-malignant tissue is not always easy. Biological imaging might add important information on the extent of the tumour. Daisne *et al* showed that FDG-PET-based automated delineation of the GTV corresponded better to tumour macroscopy than CT- or MRI-based GTV delineation for laryngeal cancer [73].

   Biological imaging is also capable of indicating tumour characteristics that are important with regard to the tumour response to radiation. Therefore, they could be used to create subvolumes within the GTV, each of which could be prescribed a different dose, as proposed by Ling *et al* [74]. The most important radiobiological properties that can be imaged currently, are presented in (the non-exhaustive) Table 3.

3. **Therapeutic response evaluation:**

   Currently, response to treatment is evaluated by physical examination, anatomical imaging, and follow-up. Although important, physical examination is difficult after treatment, and is not always sensitive. The major problem with anatomical imaging is that it is difficult to differentiate between necrotic tumour, post-therapy oedema and/or fibrosis, and tumour recurrence. Waiting for an evident recurrence might preclude an adequate second-line treatment. Moreover, early identification of non-responders might allow interrupting the therapy and to start alternative treatments, or define the need for additional therapy. Biological imaging with FDG-PET, executed early during treatment, has shown to be predictive for local control and survival in HNC [75].

The work presented in this thesis focuses on the use of biological imaging (more specifically FDG-PET) in the guidance of target delineation and dose distributions.

Tumour characteristic	Tracer	Imaging modality
Hypoxia	^{18}F-misonidazole	PET
	^{60}Cu-ATSM	PET
	[lactate]/[NAA] ratio	MRS
	^{19}F-MRI	MRI
Proliferation	^{18}F-fluorothymidine	PET
	^{11}C-methyl-methionine	PET
	[choline+creatine]/[citrate] ratio	MRS
Apoptosis	^{99m}Tc-Annexin V	SPECT
Microvasculature leakage	DCE-MRI	MRI

Table 3: Biological imaging for radiobiologically important tumour characteristics. Data from the table were extracted from [72;76-79]. Abbreviations: ATSM: diacetyl-bis(N-4-methylthiosemicarbazone); DCE: dynamic contrast enhanced; MRS: magnetic resonance spectroscopy; NAA: N-acetyl aspartate; SPECT: single photon emission computed tomography; Tc: technetium.

III. 4.4.2. FDG-PET

FDG is the most widely used PET tracer in oncological imaging. The basic principle resides in the increased uptake of (deoxy)glucose by malignant cells by the upregulation of glycolytic enzymes and glucose transporters. The FDG is phosphorylated by hexokinase and is trapped, as it is not further metabolised. Therefore, there is an accumulation of FDG in neoplastic cells. However, the (radio)biological significance of the amount of FDG uptake is not yet fully understood. The uptake of FGD by neoplastic cells has been positively correlated to the proliferative activity [80], the blood flow and microvessel density in the tumour, and to hypoxia (due to hypoxia-induced increase in glucose metabolism). However, other authors found a negative correlation between tumour perfusion or cellular proliferation and FDG uptake [81]. Differences in tumour models might be partially responsible for these discrepancies.

Another limitation of FDG is that it is far from a specific tracer, as there is also uptake of (deoxy)glucose in normal cells (brain, inflammatory cells, active muscle,…). In some cases, therefore, it is impossible to differentiate between malignant tissue and inflammation. Interpretation of FDG-PET images should therefore best be done in conjunction with anatomical imaging, like CT. Furthermore, a careful assessment of patient history and clinical examination are of utmost importance.

An important drawback of FDG-PET is the poor spatial resolution, being around 5 to 8 mm. If the source of positron emission (i.e. the tumour) is smaller than twice this value, the FDG activity will be underestimated, due to a partial volume effect, eventually leading to a false-negative interpretation. Clearly, if FDG-PET is used for the delineation of the tumour, this limitation should be kept in mind, as superficial extension of the tumour will not be indicated as such by FDG-PET [73].

III. 4.4.3. Rationale for the use of FDG-PET in IMRT

Despite the use of conformal techniques like IMRT, the majority of relapses in HNC patients who receive primary radio-(chemo-)therapy occurs within the GTV [82-84]. This relapse pattern suggests that doses of 65 to 70 Gy are insufficient to kill all clonogenic tumour cells. A logical approach to this would be to escalate the dose to the GTV, or another (better) volume that contains those tumour cells that are most likely to survive the standard dose. However, Fowler *et al* found that altered fractionation and dose escalation is limited due to acute (mucosal) toxicity [61]. Their data were all based on studies using conventional radiotherapy techniques, in which relatively large volumes are treated to these higher doses. With IMRT, it is possible to limit the volume treated to a higher dose, and thus, the maximal values found by Fowler *et al* might be irrelevant to IMRT-based dose escalation, which is also reported by the authors [61]. In a planning study, Zhou *et al* [85] showed that, using 9 co-planar intensity modulated beams, it was possible to escalate dose to the GTV up to 76-82 Gy without major influence on the dose to the surrounding CTV and OARs. It seems obvious that the volume to which the dose escalation will be directed, should fulfil the following two criteria: (1) the volume should contain the most radio-resistant cells, i.e. the origin of a possible subsequent relapse, and (2) the volume should be as small as possible, in order to avoid an excess of toxicity.

Biological imaging, like FDG-PET, MRI and magnetic resonance spectroscopy; could provide 3D maps of radiobiologically important parameters within the tumour [74]. To date, it is unknown which biological imaging modality provides the most valuable information to the radiation oncologist (probably, it will be a combination of several imaging techniques). At GUH, a dose escalation trial was initiated, in which the escalation is guided by FDG-PET. The design of the study is shown in publication V.1, Figure 6. Despite of its known limitations, we choose FDG-PET mainly because of two reasons: (1) high FDG uptake in the tumour correlates with worse local control and disease-free survival [75;86] , and (2) FDG-

PET based delineation of the target volume correlates better with the macroscopic extent of the tumour than current CT- and MRI-based delineation [73]. Moreover, FDG-PET based target delineation results in smaller volumes than CT-based target volumes [73;87].

➔ **The use of biological imaging in target delineation and in dose escalation using IMRT is presented in publications V. 1 (p. 62) and V. 4 (p. 108)**

III. 4.4.4. Image segmentation of FDG-PET images

By segmentation of images, we understand the process of identification and localization of each region of interest (CTVs and OARs). This can be done by manual delineation, but for biological imaging, other techniques are being developed, mainly for two reasons. First, and most important, the interpretation of the biological image – and therefore the delineation - strongly depends on the level and window settings. By using an automated image segmentation tool, this problem is largely obviated (i.e. the inter-observer variation is minimized). Second, the manual delineation is a time-consuming activity, certainly when multiple imaging modalities are used (e.g. planning CT, MRI and PET).

The majority of (semi)automated image segmentation tools use an edge detection. An example is given in Figure 10. In the case of FDG-PET, of course, the difficulty is to find a threshold so that the obtained volume matches the tumour as closely as possible. Daisne et al. [88] developed a methodology for image segmentation, based on the source-to-background ratios. A phantom, filled with 6 spheres (with a known volume, ranging from 0.55 to 17.15 ml) was used. Each of the spheres was filled with 2-3 μCi of ^{18}F. The phantom itself then was filled with increasing concentration of ^{18}F, in order to obtain source-to-background ratios ranging from 1.5 to 8.7. PET scans were acquired, and an threshold-based image segmentation was performed, with increasing thresholds (expressed as a percentage of the maximal activity in the spheres). The threshold resulting in a segmented volume closest to the true volume of the sphere was retained. These data points were fitted to an inverse function.

Limitations of the described method are overestimation of small tumour volumes, and the fact that the phantom measurements are PET-camera specific, and therefore not easily exportable. Also, it is not certain if the methodology that was elaborated on spheres, will hold for irregularly shaped tumours. However, the same group applied this image segmentation technique to a group of patients with a laryngeal cancer, and found a better correlation between the macroscopic tumour (after laryngectomy) and the PET-volume, than with CT or MRI [73].

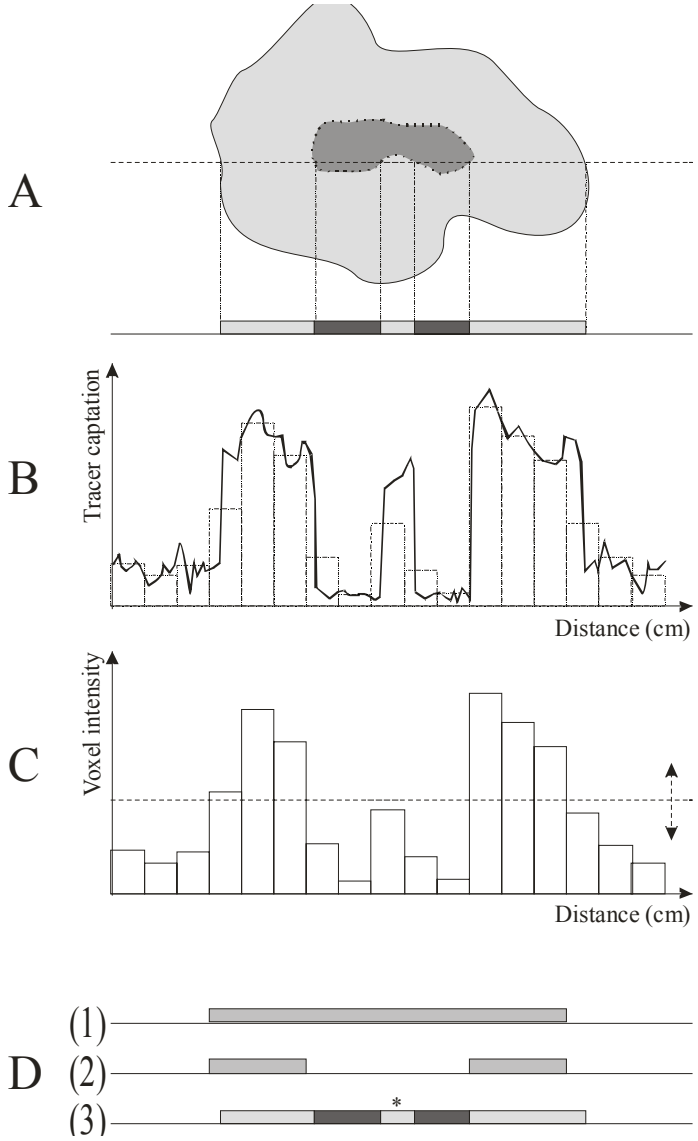

Figure 10: Segmentation of a biological image. In (A), a transverse section through a tumour is shown in light grey, with a zone of necrosis in dark grey. A one-dimensional projection along the dashed line is also shown below.
(B) shows the concentration of the tracer (e.g. FDG) throughout the tumour, along the one-dimensional projection in (A). In the necrotic part of the tumour, there is nearly no tracer uptake, resulting in very low concentrations.
(C) shows the voxel intensities, as obtained from (B). The dashed line represents a threshold value, used for automatic segmentation. Several methods exits for the determination of this threshold value. Voxels will be assigned as "in" or "out" of the volume.
(D) are 1-D representations of segmented volumes, obtained by two different methods (D1 and D2), compared to the true tumour volume (D3). In D1, "holes" (like for necrosis) are not taken in account, while this is the case in D2. Note that in D2, the small part of tumour with tracer uptake (* in D3), is not delineated due to the partial volume effect.

Another approach is to directly use the information of the biological imaging modality into the planning, thus bypassing the step of image segmentation [89]. Here, a hypothetical relationship between the voxel intensity and the intended dose is made. The most simple example is a linear relationship between an arbitrarily defined minimum and maximum voxel intensity. Once the voxel intensities are translated to intended doses, this new planning objective is added to the optimization algorithm. This direct incorporation of biological information seems promising, but more work is needed to establish the relationship between signal intensity – biological significance – intended dose.

IV Intensity modulated arc therapy

IV. 1. Introduction

Arc therapy is not a novel delivery technique in radiation oncology. It has been used on cobalt machines for deep seated tumours (and was then rather called rotation therapy), compensating the lack of high energy photons. A major advantage of all forms of rotational radiotherapy is the infinite number of beam directions, resulting in more degrees of freedom, and possibly better planning results than those obtained with a limited number of beam directions. The first intensity-modulated rotational (or arc) therapy should be attributed to Proimos [90], who obtained modulation of the beam intensity by hanging gravity-oriented attenuating blocks on the radiation machine. As the gantry rotated, the OARs were shielded by the blocks. Due to the rather confined nature if the intensity modulation, however, dose to the target volume was not very uniform. The production of the blocks was also labour-intensive, and the technique has never been widely applied. With the introduction of MLC-based IMRT, it has been abandoned [91].

Tomotherapy using the NOMOS® MIMiC MLC was the first widespread delivery method for IMRT [92], and was introduced in 1993. In this sequential tomotherapy approach, the linac gantry, to which the MIMiC MLC is attached, rotates around the patient and the binary position of the leaves (open or closed) are adjusted at every 0.5 degrees of gantry rotation. After one pair of slices (there are two banks of leaves) is treated, the table moved longitudinally with 2 or 4 cm (the length of one leaf position was adjustable to 1 or 2 cm), and the next pair of slices is irradiated. This process is repeated until the whole target volume is covered. Patient immobilization and a perfect couch control are of the utmost importance in this approach. Moreover, even assuming a perfect control of the couch position and no intra-fraction patient motion, both under- and overdosages can be created by the use of small arcs [93]. Another approach consists of helical tomotherapy, in which the patient is moved longitudinally through a slit-collimated fan beam [94]. A clear disadvantage of tomotherapy (serial and helical) is the need for a dedicated delivery system. Intensity modulated arc

therapy (IMAT) using MLC-equipped linacs was first proposed in 1995 by Yu as an alternative to tomotherapy [95]. IMAT is a form of rotational therapy, but has the advantage that it can be implemented on widely installed linacs equipped with an MLC. Instead of using a slit beam, a conventional MLC is used to form the field apertures. Both the gantry and the MLC leaves move during radiation. The modulation of the intensity originates from overlapping arcs, each arc consisting of "beams" with a flat intensity on their own. IMAT differs from conformal arc therapy in the fact that, in the latter, the field aperture covers the whole PTV, while in the former, field apertures of (some) arcs will only cover parts of the PTV. Some characteristic features of different radiation techniques are given in Table 4.

Gantry	**Static**		**Dynamic**		
	3D-CRT	**IMRT**	**CAT**	**OSAMAT**	**IMAT**
Leaves	static	static or dynamic	dynamic	dynamic	dynamic
Intensity modulation	none	temporal superposition of segments	none	none	temporal superposition of arcs
Segment outline	whole PTV	part of PTV	whole PTV	part of PTV	part of PTV
Indications	convex PTV	concave PTV (small inner radius)	convex PTV	convex PTV	concave PTV (large inner radius)

Table 4: Some characteristic features of the most prevalent MLC-based conformal radiotherapy techniques. *Abbreviations:* 3D-CRT = three-dimensional conformal radiotherapy; IMRT = intensity modulated radiation therapy; CAT = conformal arc therapy; OSAMAT = optimized segment aperture mono-arc therapy; IMAT = intensity modulated arc therapy; PTV = planning target volume.

IV. 2. Indications for IMAT

IV. 2.1. Concave PTV around an OAR with large radius.

We hypothesized that IMAT might have both planning and delivery advantages over static-gantry IMRT in some clinical cases. More specifically, it was presumed that IMAT would obtain better planning results than IMRT in those cases where the PTV is wrapped concavely around an OAR with a "large" radius. The modulation of the intensity is needed in order to create a concave dose distribution, while the large radius of the concavity demands a high number of beam directions. Still, the higher the number of beam directions used, the longer

the treatment will take for delivery. Arc therapy represents an infinite number of beam incidences, and certainly is the most efficient way for delivery when a large number of beam incidences is desirable. IMAT combines these two features.

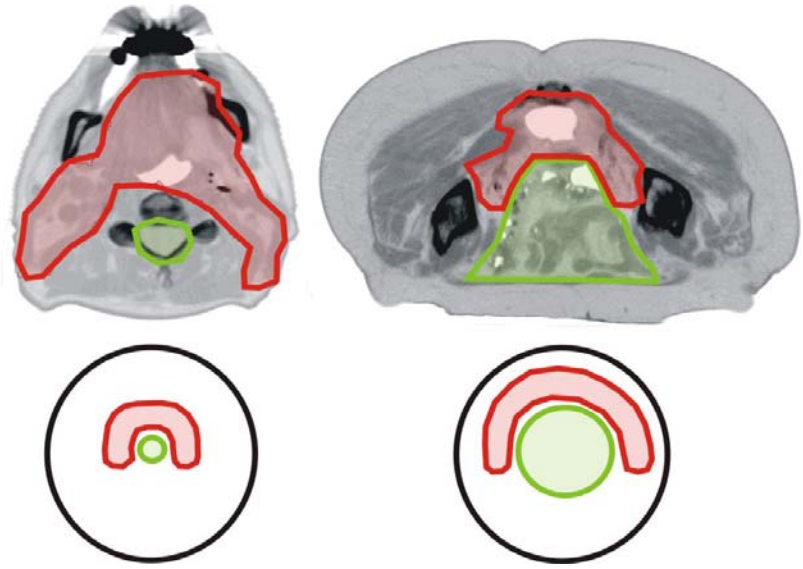

(A) (B)

Figure 11: Examples of two distinct planning situations, showing the planning CT scan, with the delineated PTV and OAR (upper row), and their abstract representation (lower row). In the left column (A), a head and neck case is represented, while in the right column (B), a case of rectal cancer is shown. In both cases, the OAR lies within the concavity formed by the PTV, and they only differ in the radius of the OAR (and, logically, also the inner radius of the concave PTV).

A planning experiment was done to support this hypothesis. We considered two cases (A and B) with a concave PTV, having an OAR within this concavity (Figure 11). In one case (A), the OAR has a small radius, and so is the inner radius of the PTV. This situation is typically found in the irradiation for a HNC. In the other case (B), the OAR's radius (and the PTV's inner radius) is relatively large. Again, for this latter situation, there are several clinical examples, of which rectal cancer irradiation is the one depicted here. Both distinct clinical cases were than simplified in a cylindrical phantom, depicted in Figure 11. For each of these phantoms, three plans were made. The first plan consisted of 3 intensity-modulated beams, while the second plan used 7 intensity-modulated beams. The last plan consisted of an IMAT plan using 4 arcs. All plans were optimized in order to deliver a median dose of 50 Gy to the PTV (the dose is chosen arbitrarily). The same PTV homogeneity requirements were used for all plans. A hard constraint was set on the maximal dose to the OAR of 30 Gy, while a soft constraint was used in order to minimize the mean dose to the OAR and the dose to the

surrounding tissue, in order to avoid hot spots outside the PTV. The dose distributions and the DVHs for all three plans for both case A and B are shown in Figure 12.

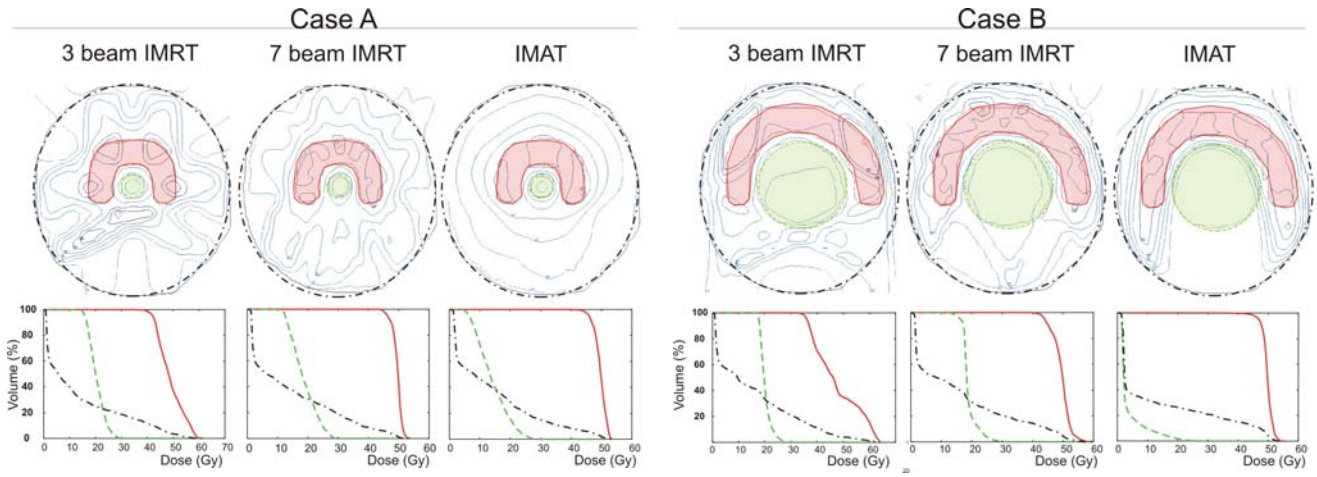

Figure 12: planning results for case A (left) and B (right), represented by dose distributions (upper row) and DVHs (lower row). An arbitrary end dose of 50 Gy was chosen. The DVHs are shown for the PTV (red, full lines), the OAR (green, dashed lines) and the total phantom volume (black, dashed-dotted lines).

For case A, the 3 beam IMRT plan is unable to produce a homogeneous dose in the PTV for the given OAR dose constraint. Also, the use of only three beam directions results in hot spots outside the PTV. These problems can be solved by increasing the number of beam directions. The 7 beam IMRT indeed results in a homogeneous PTV irradiation, with no overdosage in the surrounding tissue, and only at the cost of a larger volume of surrounding tissue receiving low doses (and a longer treatment time). The IMAT plan results in a comparable PTV dose homogeneity, with a slightly better sparing of the OAR. The DVHs for the three plans for case A are summarized in Figure 13

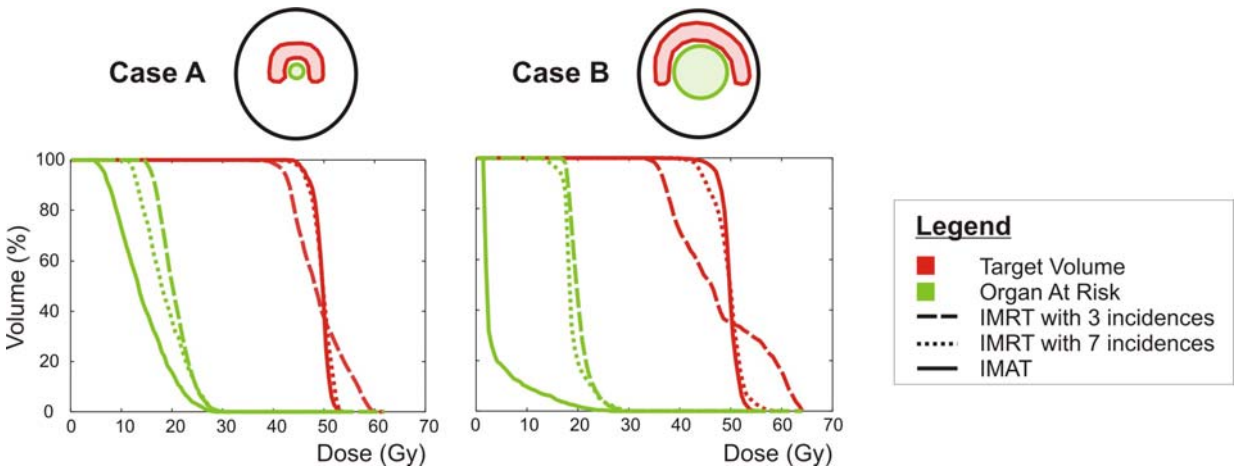

Figure 13: summary of the planning results for both cases

For case B, the use of three beams results in a larger inhomogeneity in the PTV than for case A. The use of more beam directions largely settles this inhomogeneity problem. The IMAT plan, however, results in an even better PTV dose homogeneity and a major decrease in dose to the OAR. These results are summarized in Figure 13b. This experiment thus confirms the hypothesis that a higher number of beam directions is needed to obtain the same planning results (= PTV dose homogeneity and OAR sparing) as the inner radius of the concave PTV is larger. This hypothesis is also discussed in [96] (see publication V. 5, p. 122). It is of note that the number of intensity levels is less for the IMAT plan than for the static-gantry IMRT plans. Still, planning results are more favourable for the IMAT plans, indicating that the limited number of intensity levels is compensated for by the infinite number of beam directions. This was also suggested by other investigators [95].

IV. 2.2. IMAT for the delivery of biological imaging guided radiotherapy

The integration of biological imaging in radiotherapy (section III. 4.4) will lead to the fragmentation of PTVs in multiple regions, possibly all with different dose prescriptions. Although it has been suggested by Zhou *et al* [85] that there was no additional benefit – for dose escalation - by increasing the number of beam directions (from 9 to 15), this was only done on one patient. Moreover, in his study, there was only one dose peak. This does – however – not reflect the situation in which several regions, to which a higher dose is prescribed, exist. In these cases, a large concave target volume exists, within which reside multiple (mostly convex) islands of target subvolumes. For convex dose distributions, it is obvious that conformal arc therapy will create the steepest dose gradient when considered over the whole target contour. IMAT has the possibility to combine both features of intensity modulation and arc therapy, and therefore has advantages over static-gantry IMRT for these cases.

IV. 3. IMAT delivery issues on Elekta linacs at GUH

The radiation therapy desktop (RTD) from Elekta is the computer system that controls the linac. In this RTD, both the linac and the MLC are controlled. However, IMAT is – at the moment – not yet possible on the RTD. Therefore, IMAT has to be delivered using prototype linac control software, using the “Javelin” control cabinet. In Javelin, the linac (gantry and collimator angle, beam quality, dose rate) and the MLC are controlled separately, both driven

by the monitor unit (MU) counter. The dynamic (both gantry angle and MLC) delivery is executed as described hereafter [19]. A prescription of an IMAT plan consists of both a prescription file for the linac controller (manual input), and a prescription file for the MLC controller (transferred over the network).

The main elements in the linac prescription file consist of a start and stop gantry angle, a collimator angle, the beam quality and the number of MUs to be delivered. Other non-field related parameters, like table top rotation, are also specified here. Although some investigators were able to specify the nominal dose rate (MU/min) [95], we were unable to do so without eliminating important safety locks. The nominal dose rate is automatically selected from a set of discrete values (32, 65, 130, 260 and 520 MU/min) and is chosen in such a way, that the gantry speed is as close as possible to 157.5°/min, with a possible range in gantry speed between 105°/min and 210°/min (see Figure 14). The gantry rotational speed within one arc is kept proportional to the (slightly fluctuating) nominal dose rate. Therefore, the angular delivery rate (ADR), expressed in MUs/°, is constant within one arc.

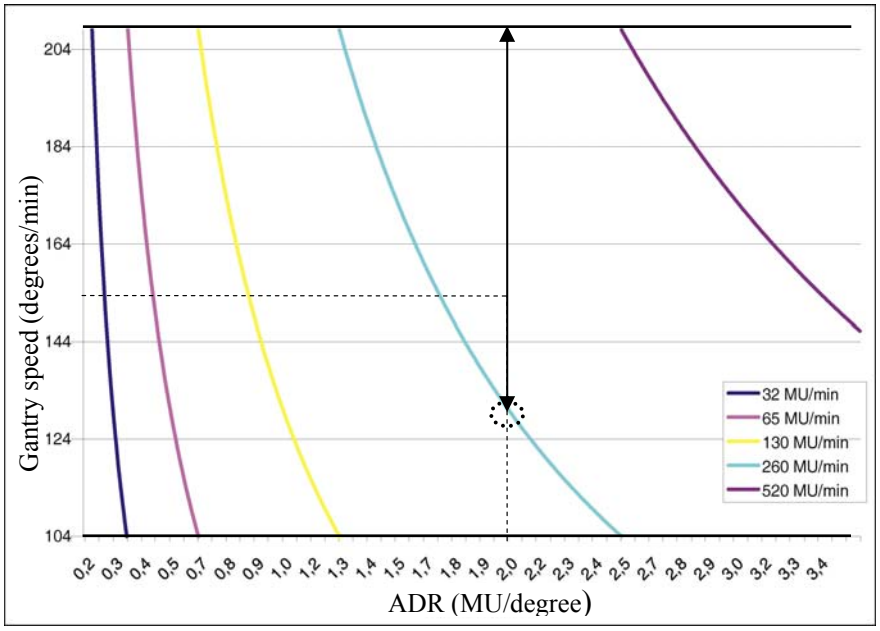

Figure 14: Graph showing the relation between the angular delivery rate (ADR), which is the number of MUs that have to be delivered per degree (abscissa), the gantry speed (in °/min; ordinate), and the nominal dose rate, selected by the linac controller software. An example is indicated by the dashed lines and the arrows: for an arc with a length of 100° and 200 MUs to deliver (= 2 MUs/°), the linac controller software will pick a nominal dose rate of 260 MUs/min, and the gantry speed will be 130 °/min.

The MLC prescription file contains a sequence of control points (CPs), in which a CP defines a machine state (MS, defined by the gantry and collimator angle, leaf and diaphragm positions …) and the cumulative MU count that has to be delivered at reaching the actual CP. The transition from one CP to the next one is steered by the MU counter. The value of each parameter (like leaf position, diaphragm position, gantry angle, collimator angle) that changes between two successive CPs is linearly interpolated as a function of the MU count. All machine parameters are constantly monitored during radiation. For the Elekta MLC, the actual leaf positions are monitored using a camera in the linac head. When the difference between an actual machine parameter, like the position of a leaf, and the prescribed value (or the value obtained by interpolation) exceeds a preset tolerance range, the radiation is interrupted. The parameter is adjusted until it is within tolerance, and the radiation is resumed. When the interruption lasts longer than 5 seconds, the beam is terminated, and an operator intervention is needed to finish the remaining arc.

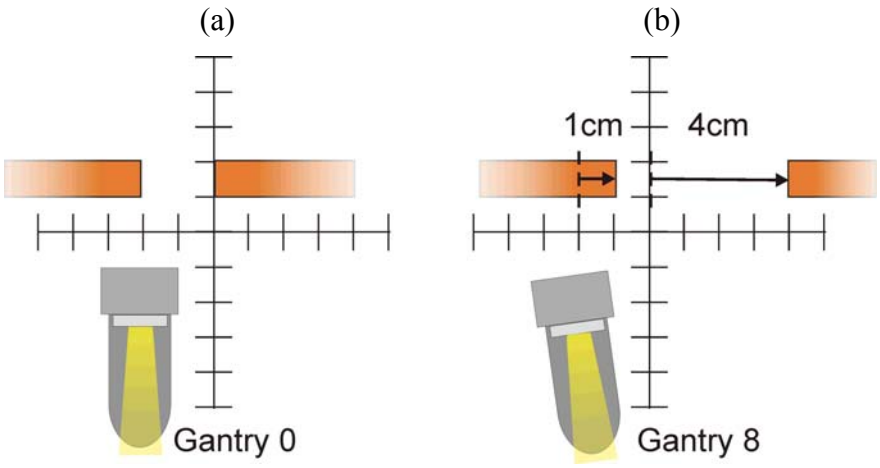

Figure 15: Illustration of the maximal leaf speed constraint. The coordinate system from the beam's eye view (BEV) is shown, with the origin through the central axis. A pair of leaves is shown at the first control point (CP) (a), and at the next CP (b). The gantry positions at each CP (0° and 8°) are also depicted in the left lower corner. The difference in position for the left leaf is only 1 cm, while it is 4 cm for the right leaf. If we would assume the maximal gantry speed of 210°/min, the time needed for the transition between the two CPs is 2.3 seconds. The requested leaf speed would thus be 1.75 cm/sec, exceeding the maximal leaf speed of 0.92 cm/sec. Thus, this prescription has a high probability of causing a termination of the arc delivery.

Any premature termination during IMAT delivery is highly unwanted, as the operator interventions needed to complete the prescribed arc considerably extend the treatment time and – even more important - are prone to human error. Therefore, they should be avoided, in the first place, by making "executable" prescriptions. It is obvious that the dynamic delivery

is restricted by the physical constraints imposed by the linac hardware characteristics. The gantry speed and the dose rate are automatically set by the linac controller software, and are always within the limits. The requested leaf speed, however, depends on the difference in the position of that leaf between two CPs (Figure 15). De Gersem found a relationship between the requested leaf speed, and the number of beam terminations (Werner De Gersem, personal communication), and the maximal leaf speed (MLS) in arc mode was set to 0.92 cm/s for planning purposes. This is a value that is obtained empirically, which, if respected in the planning, will not lead to treatment interruptions due to leaf lag. The same reasoning is valid for the jaws that move orthogonally to the leaves, for which a maximal speed of 1.5 cm/s is proposed.

IV. 4. IMAT planning issues

In the planning process, an arc is approximated by a large number of static "beams" (as mentioned earlier, these are called machine states), interspaced with an equal gantry angle. Typically, these MSs are created using a gantry angle interval of 5-10°. It was shown by others [97] and also by our group [98], that the size of the angular spacing between consecutive MSs does only minimally influence the obtained dose distributions. When the angular spacing was varied between 5° and 20°, dose to the central axis nor target dose coverage changed [97]. We examined the influence of the angular spacing in a rectal cancer IMAT plan. An IMAT plan was optimized and calculated using 8° interspaced MSs. The resulting prescription parameters were duplicated at the end of the planning process, and additional MSs were created every 2° by interpolating the parameters (gantry angles, leaf and jaw positions) of the existing MSs. Then, a dose calculation was done for both (the original and the "interpolated") plans, and both dose grids were compared using dose distributions and DVHs. No clinically relevant differences were found for the dose to the target volume. In the low dose regions, dose folds appear as a consequence of the coarse 8°-discretization of the arc. These ripples in the low-dose regions can be explained by the gaps in overlap near the surface. However, in most cases, these dose ripples are of no clinical significance [98].

At GUH, we chose a gantry angle interval of 8°, which represents a compromise between a better approximation of arcs, and available time for planning. As for static-gantry IMRT, two planning approaches exist for IMAT: inverse and forward (or better: anatomy-based)

planning. Here, we will discuss the anatomy-based planning. Inverse planning for IMAT will be discussed later in Section IV. 4.2 (p. 57).

IV. 4.1. Anatomy-based planning for IMAT (the GUH approach)

After the delineation of all relevant target structures and OARs, and after the generation of optimization structures [96;98;99], the first step in an IMAT plan is the positioning of an isocenter. This is done in such a way, that it lies at the center of mass of the PTV. For large volumes, like in WAPRT, the position of the isocenter can be critical with regard to the maximal aperture of the MLC, and has to be chosen with care. The IMAT planning procedure, as it is developed and used at GUH, is shown in Figure 16.

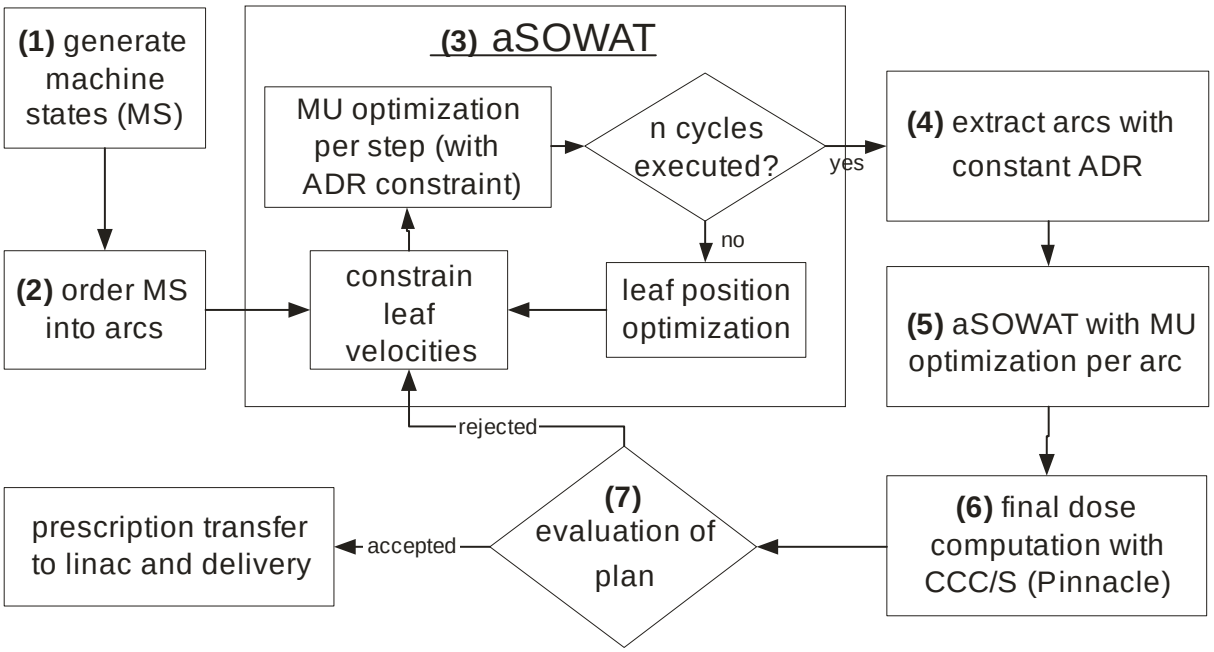

Figure 16: Planning process for IMAT. Abbreviations: ADR = angular delivery rate; aSOWAT = arc-therapy adapted segment outline and weight adaptation tool; MU = monitor unit; CCC/S = collapsed cone convolution/superposition dose calculation algorithm; MS = machine state. A MS is defined as a set of machine parameters (gantry angle, position of the leaves, photon beam quality). A step is defined as the transition from one MS to the next. More details about all steps are provided in the text, according to the numbers in the figure.

(1) **Generation of MSs:** MSs are generated every 8° using ABST in a pre-defined range of gantry angles. This range of possible gantry angles depends on the specifications of the treatment couch. The range of usable gantry angles is restricted by the need to avoid that beams would traverse metal components of the couch before entering the patient. The Elekta table top for the SL*i*18 has two metal C-arms, which can be swung down in steps of 30°. The

largest range of gantry angles was obtained by setting the C-arms on 120° or 150° (with their most lateral position being 0°). Aside from the table top structure, the range of possible gantry angles also depends on the PTV geometry and the relative position of the isocenter (and the PTV as a whole) to the table. For WAPRT, the range of gantry angles was from -128° to 128° [96], while this was from -136° to 136° for rectal cancer cases [98]. For the WAPRT cases, this limited range of useable gantry angles, in conjunction with the geometry of the PTV, urged the need for an additional posterior sliding window beam. Recently, the Elekta table top has been replaced by a carbon-fibre table top, called Mastercouch® (Sinmed BV, Reeuwijk, The Netherlands), as was suggested earlier [96]. It was shown that the use of the Mastercouch® table top allowed more beam incidences, due to the absence of metallic elements in its design [100]. Since the implementation of the carbon-fibre, MSs are generated in a broader range, being from -176° to 176°.

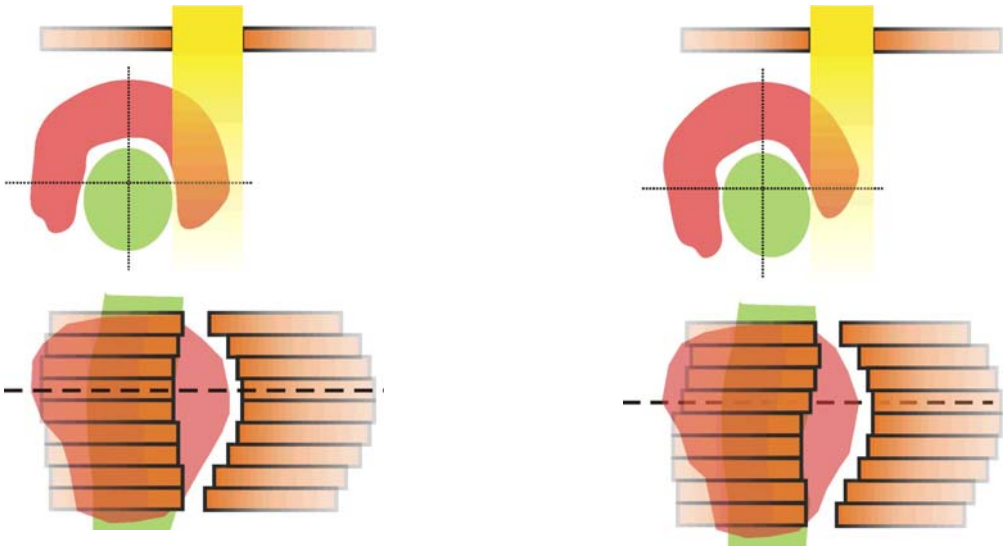

Figure 17: Smooth transition between two adjacent machine states, interspaced with 8 degrees of gantry angel rotation. In the upper row, an axial projection is shown, while the BEV can be seen in the lower row. The leaf motion from the first machine state to the next is limited, and complies with the constraint of the maximal leaf speed.

One of the most important prerequisites for a fluent IMAT delivery is the compliance with the MLS constraint. This is largely secured by ABST, as the change in the beam's eye view (BEV) projection of the PTV between two adjacent MSs of the same type will be small (Figure 17). Theoretically, the largest leaf motion between two 8°-interspaced MSs is 3.5 cm for volumes within 20 cm of the longitudinal axis (20 cm is the maximal aperture of the Elekta MLC), thus violating the MLS constraint. However, this only happens in the worst

case, and an additional planning tool (a leaf velocity constrainer (LVC), see point 3a for more details) was developed to deal with this situation. For a typical case with one PTV and one OAR (that is used as segmentation structure), the parameters for ABST are set in such a way that they result in 4 MSs per gantry angle: one MS covering the part of the PTV at the left of the OAR, one covering the PTV portion at the right of the OAR, and then, again at each side of the OAR, a MS covering a small part of the PTV close to the OAR.

(2) **Ordering of MSs into arcs:** In this step, MSs are linked to each other to form arcs. The MSs are stratified per type (e.g. all MSs covering the part of the BEV projection at the left side of the OAR), and ordered on base of the gantry angle. As the gantry cannot rotate over the 180° position, the arcs start at -176° and end at 176° (or inversely). If, at a certain gantry angle, no MS of a certain type is created (due to the specific anatomical situation), this will result in the ending of this arc (Publication V. 7, Figure 2). Thus, if there are 4 MSs per gantry angle, this ordering will result in 4 arcs. These provisional arcs will then be used as starting point for the optimization.

(3) **aSOWAT optimization:** The optimization procedure for IMAT consists of a user-defined number (=n) of cycles, in which one cycle executes three distinct processes: (a) the LVC; (b) MU optimization, with ADR constrainer, and (c) LPO.

a) The optimization starts with the LVC tool (L. Olteanu and W. De Gersem, method unpublished). The LVC checks if the constraints for the minimal separation between opposed leaves, diagonally opposed leaves, and opposed jaws is met. This is done for all collimating leaves per CP. If the criteria for minimal separation are not met, a force F_1 is calculated by multiplying the surplus distance (minimal separation minus actual separation; in cm) with a constant (1 N/cm). In addition to this, the LVC also examines the maximal leaf travel between two CPs. The maximal leaf travel (between two CPs) can be obtained from the MLS, the gantry speed and the angular separation between two CPs. If the maximal leaf travel constraint is violated, a force F_2 is calculated using the same approach, in which the surplus distance (actual leaf travel minus maximal leaf travel) is multiplied by a constant (1 N/cm). For each leaf, the applied correction (= distance in cm) is calculated by multiplying (F_1+F_2) with a constant 0.5 cm/N. The whole procedure is repeated until all leaves are within the constraints. Then, a fast dose calculation algorithm (the same as used in the LPO tool) will calculate the difference in dose between the original and the adapted CPs. The dose grids that are used for the further optimization are adapted accordingly.

b) The second step consists of MU optimization. Here, it is the number of MU per step that is optimized, in which a step is defined as the transition from one CP to the next. As the number of MUs per step varies due to this optimization, this will result in an arc with a variable ADR. As explained earlier, this is – at present – not deliverable on the Elekta linac. Finally, the IMAT plan must consist of (deliverable) arcs with a constant ADR. These arcs will be extracted from the preliminary arcs (see point 4: "arc extraction"). This arc extraction procedure is a manual operation, and in order to facilitate this, a constraint is imposed in order to minimize too large differences between the number of MUs assigned to one adjacent step. In fact, this constraint acts like a smoothing tool on the ADR graph (Figure 18b).

c) The LPO is the same algorithm as used in static-gantry IMRT (see p. 26). Thus, during this step, the MLS constraint is not considered. If the LPO would result in a violation of the constraint, this will be solved by the next LVC execution.

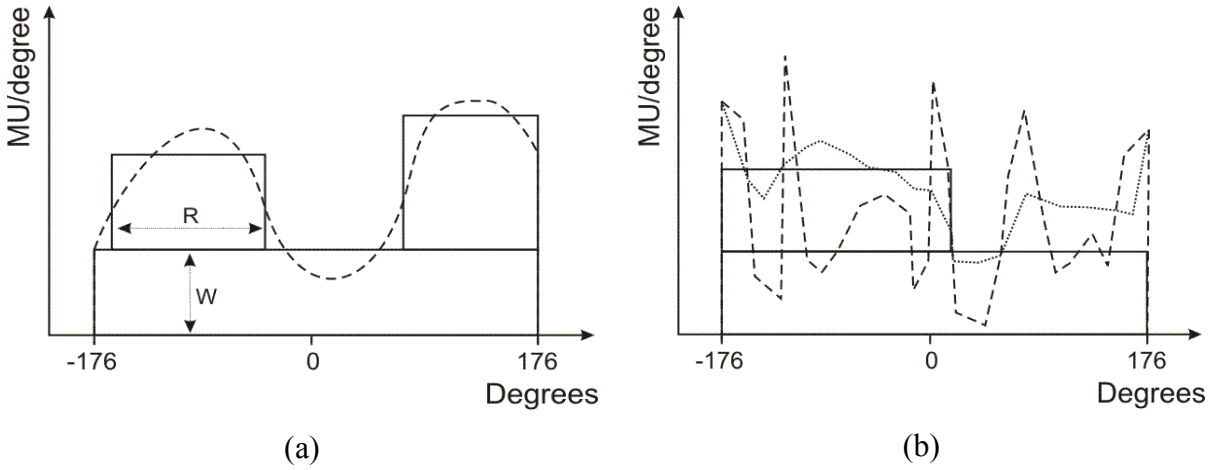

Figure 18: Illustration of the angular delivery rate (ADR) and the process of the extraction of deliverable arcs from preliminary arcs with variable ADR. On the x-axis, the gantry angle (in degrees) is shown, while the y-axis gives the number of monitor units that have to be delivered per degree of rotation. (a) Theoretical case, with the ADR of one preliminary arc (dashed line). As the Elekta linac is not capable of delivering an arc with a variable ADR, this preliminary arc has to be split into several arcs, each with a constant ADR. These deliverable arcs are depicted by the full line rectangles, and approximate the original ADR curve. The range (R) of the deliverable arcs is thus selected manually, and can be "optimized" by trial-and-error. The final (constant) ADR, that can also be viewed as the relative "weight" (W), of the deliverable arcs is further optimized by the optimization algorithm. (b) A clinically encountered example of an ADR graph, obtained after optimization without (dashed line) or with the ADR constrainer (dotted line). The rectangles show the deliverable arcs, derived from the dotted ADR graph.

(4) **Arc extraction (Figure 18):** After aSOWAT, the IMAT plan consists of the preliminary arcs, of which the apertures and the MU/step are optimized. As in conventional radiotherapy, some beam directions (or, for arc therapy: some arc segments) are more favourable than others. This is directly reflected by the variable ADR. Arc segments with a low ADR might reflect these parts of the arc, where primary dose to the OAR cannot be avoided. Still, these arcs are still not deliverable, and have to be split into arcs with a constant ADR per arc. This decomposition problem could be compared with the leaf sequencing procedure (see p. 19 and also Figure 4) converting optimized fluence maps to deliverable segments. In the clinical example in Figure 18b, it is easy to appreciate the difficulty of decomposing the ADR graph as obtained after optimization without ADR constrainer. The optimization of the MU per step operates in a very large search space. For an example with 4 preliminary arcs spanning from over the full range, there are 4x44=176 steps to optimize. This large "freedom" results in the spiked ADR graph, as shown. The ADR constrainer results in a smoother graph, that is easier to decompose [98]. The extraction of deliverable arcs from the preliminary arc is not a one-step procedure, as this would result in a very rough discretization. Rather, each arc is split off separately. After the isolation of each deliverable arc, the MUs of all deliverable arcs are (shortly) optimized (over the whole arc, and not per step), as well as the remnant MUs of the preliminary arc (here, MUs are optimized per step). By an additional factor in the optimization algorithm, the number of MUs in the original arc is downforced, in favour of the MUs of the deliverable arcs. In order to keep the IMAT delivery time-efficient, care is taken to keep the number of deliverable arcs low. The extraction procedure for one preliminary arc is finished when the remaining number of MUs in the original arc is negligible. The range of the deliverable arcs can be optimized by the planner by trial-and-error, which is a very time-consuming activity.

(5) **aSOWAT with MU optimization per arc:** As the optimized original arc is discretized by several arcs with a constant ADR, the quality of the IMAT plan deteriorates by this procedure. Again, this closely resembles the deterioration in inverse IMRT planning due to the conversion from optimized fluence maps to deliverable segments. Therefore, an additional aSOWAT cycle is necessary, in order to counteract this decline. The only difference between the previous aSOWAT optimization resides in the MU optimization, which is now done per arc instead of per step. This guarantees a constant ADR and thus deliverable arcs.

(6) **Final dose calculation:** A final dose calculation is done with an external (= not a part of the in-house developed planning software) dose calculation engine. Until now, the

collapsed cone convolution/superposition algorithm from Pinnacle® was used. The software to convert beam data to the Pinnacle® station was developed in our department. However, other dose calculation engines, like Monte Carlo based dose calculations algorithms, might be used as well. As for the planning and delivery stage, dose distributions of arcs are approximated by calculating the dose delivered by the 8°-interspaced MSs. In order to calculate the dose distribution, a number of MUs has to be assigned to each MS. The first and last MS receive a number of MUs equal to the total number of MUs for that arc, divided by twice the number of steps. The MUs assigned to the other MSs is equal to the total MU count for that arc, divided by the number of steps. A final optimization of the weights per arc is done, using the results of the final dose calculation.

(7) **Plan evaluation:** The evaluation of the plan is done as described earlier (p. 35). If the plan does not fulfil the goals, the planning process is re-entered at point 3, 4 or 5, depending on the extent of the deviation of the preset goal. If all goals are reached, or no further improvements can be made, the plan is finalized, and the prescription is entered into the linac controller. The IMAT prescription is then evaluated by executing a dummy run, in order to prevent any possible problem at the delivery.

IV. 4.2. Inverse IMAT planning

This anatomy-based approach, as described above, differs substantially from the inverse planning method that was initially proposed by Yu *et al* [95]. Yu used a commercial TPS (PEACOCK, NOMOS), and adapted it to suit the IMAT needs. An intensity-modulated beam is generated every 5°, and after optimization of the fluence map per gantry angle, the 2D intensity distribution is segmented into multiple one-dimensional intensity profiles. Each one-dimensional intensity profile is than translated into a number of “subfields”. Arcs are then formed by picking one subfield from the stack of subfields at each beam angle in a top-down order. The decomposition pattern of a given beam angle is compared to the finalized decomposition pattern of the previous beam angle. Once a decomposition pattern is found that meets the constraint of the maximal leaf travel, it is accepted. If none of the decomposition patterns meet this criterion, a less stringent criterion is set, resulting in longer leaf travels between two gantry angles, and thus a lower dose rate (and subsequently gantry speed) is set (which we were unable to do on our linac!). In this method, the outlines of the arcs are thus established in a unidirectional way. The inverse planning method was illustrated for a simple

phantom geometry [95], but was – to our knowledge - never clinically implemented. Other centers who developed IMAT also applied the anatomy-based approach [101-103].

IV. 5. Dosimetry for IMAT

In terms of the requirements asked from the linac and MLC control system, as well as from the TPS, IMAT is a demanding technique. Due to the dynamic character of the delivery, both concerning the MLC leaves and the gantry, quality assurance for IMAT is not a trivial task. The comparison of measured and calculated dose distributions occupies a central position in the quality assurance of conformal irradiation techniques [5]. The approach that was used to validate IMAT for clinical use consisted of mimicking the whole treatment chain on an anthropomorphic phantom. The major advantage of this policy is that it validates the planning and delivery procedure as a whole. The apparent drawback of this method is the difficulty to dissect any deviation that is found between the measured and calculated dose.

Different dosimeters have been used for IMAT, such as ionization chambers (1D dosimetry) and radiographic films (2D dosimetry) [97;104]. However, as IMAT treatments typically result in highly 3D-sculpted dose distributions, a dosimeter capable of measuring in 3D is desirable. For the moment, only polymer gel dosimetry (PGD) is capable to combine 3D measurements with high spatial accuracy [105]. At GUH, a longstanding and extensive experience in PGD is available [106-108]. For these reasons, we selected PGD for the IMAT dose measurements. The basis of PGD is the radiation-induced polymerization of (vinyl) monomers dispersed in a hydrogel structure [109]. The polymerization reaction is initiated by reactive radicals, which are formed by radiolysis during irradiation of the gel. The amount of polymer formed is related to the absorbed dose. The polymer alters the nuclear magnetic resonance spin-spin relaxation rate R2 of the water protons. This enables the quantification of the polymerisation reaction (and thus of the absorbed dose) by MRI. IMAT typically is indicated for the irradiation of large volumes, and the dosimeter itself should have a large volume to enable the measurement of all relevant dose regions. This prerequisite represents a specific challenge to PGD due to technical reasons concerning MRI measurements. [110]. A review of the history, principles and implementation of PGD is given elsewhere [108].

For the two classes of IMAT treatment (WAPRT and rectal cancer), a PGD verification was performed [96;98]. A PGD experiment is executed as follows:

(1) The relevant region of the Rando phantom (Alderson Research Laboratories, Stamford, CT, USA) is selected, and a 4mm thick Barex cast is vacuum moulded over it. Care is taken to hermetically close the Barex cast from air, as oxygen would inhibit the response of the gel dosimeter. Full scatter condition is obtained by placing three supplemental Rando slices at the cranial and caudal side of the Barex phantom during CT acquisition and irradiation.

(2) The gel-filled Barex phantom is positioned within the treatment room, and laser lines are delineated on the phantom in a transverse, coronal and sagittal plane, defining a reference point. Fiducial markers, that are readily visible on both CT and MRI, are placed on these laser lines for future registration. The phantom is then transferred to a CT scanner that is also equipped with calibrated positioning lasers, and positioned according to the delineated lines.

(3) The CT scan is imported in the planning system, and the delineated structures (PTV, OARs and optimization structures) of a selected patient are transferred to the phantom CT scan. If necessary, small modifications are done to the delineated structures. An IMAT plan is made as described earlier. The prescription is rescaled in order to obtain a fraction of 7.5 Gy as a median dose to the PTV. This ensured the maximal response range of the gel, while avoiding saturation effects.

(4) The gel-filled phantom is positioned on the treatment couch, using the laser lines and fiduciary markers and is subsequently irradiated. Afterwards, a series of gel-filled test tubes were irradiated to known doses for gel calibration purposes.

(5) The phantom and the test tubes are scanned together in the MRI scanner [110], and a dose-R2 relationship is established using the calibration tubes. The R2 maps of the phantom are translated to a 3D dose distribution, using the calibration curve. The gel-measured dose distribution was registered with the calculated dose distribution as follows: on both the planning CT and the MRI, the gel was automatically contoured. Then, the centre of volume of both gel-contours was identified, and positioned onto each other. Rotations between the two data sets were minimized by the laser line positioning system on both the CT scan and the MRI scan, and were assumed to be negligible, which was checked by visual inspection).

(6) The comparison between the measured and the calculated dose distributions was done by visual inspection of both dose distributions and their subtraction image. Also, DVHs were computed for all relevant structures, truncated to the gel-volume, both for the measured and the calculated dose maps. Additionally, a γ-index [111] was calculated in 3D.

➔ The use of PGD for the dosimetrical validation of IMAT is described in publications V. 5 and V. 7 , and in [112].

V Publications

V. 1. Intensity-modulated radiation therapy for head and neck cancer.

Authors: W. De Neve and W. Duthoy.

Journal: Expert Review of Anticancer Therapy 2004; 4(3):425-434

Acknowledgements: The Conformal Radiotherapy Ghent University Hospital project is supported by the Belgische Federatie tegen Kanker and by grants from the Fonds voor Wetenschappelijk Onderzoek Vlaanderen (grants FWO G.0049.98, G.0039.97), the Ghent University (GOA 12050401, BOF 01112300, 011V0497, 011B3300) and the Centrum voor Studie en Behandeling van Gezwelziekten.

Key issues discussed in this paper:

- IMRT is a new technique to fine tune the radiation dose distribution, with the aim to reduce the dose to sensitive organs, while delivering a higher prescription dose to the tumour.
- IMRT was performed for oral cavity, pharyngeal and laryngeal cancer with functional sparing of salivary glands and reduction of xerostomia, and without increased incidence of recurrences near the spared region.
- In sinonasal cancer, IMRT allows avoiding dry-eye syndrome and optic neuropathy but cannot reverse the high failure rates in T4b disease.
- IMRT allows dose escalation to reduced volumes by concomitant boost techniques.
- Progress in biological imaging, based mainly on positron emission tomography, may allow us to identify recurrence-prone regions inside the tumour as targets for dose escalation.

Intensity Modulated Radiation Therapy for Head and Neck Cancer

Wilfried De Neve, M.D., Ph.D. and Wim Duthoy, M.D.

Department of Radiotherapy, Ghent University Hospital (GUH), Belgium

Abstract

In head and neck cancer, intensity-modulated radiation therapy (IMRT) makes the use of electron beams for irradiation of the posterior neck obsolete, inherently performs missing tissue compensation and allows concave and intentionally non-homogeneous dose distributions. By clinical use of these physical characteristics, salivary or lacrimal glands, optic pathway or auditory structures can be selectively under-dosed and good evidence of decreased radiation toxicity is available. Evidence for increased local control is still lacking. Recurrences are mainly located in the high dose-prescription regions (macroscopic disease, tumour bed), suggesting the need for higher doses in these regions. Image-aided design of IMRT dose distributions is an area of intense research. New positron emission tomography and magnetic resonance imaging developments might allow definition of volumes inside the tumor where treatment failure is most likely to occur. If these volumes are small, focused dose escalation of large magnitude can be attempted and the hypothesis of improved local control by IMRT can be tested.

Introduction

Within a year of discovery, more than a century ago, x-rays were used therapeutically. Over time, many technological developments took place that aimed to improve the delivery of radiation to the tissues where it is wanted and that reduced the radiation to normal tissues. This aim, for which the modern implementations are called conformal radiotherapy, is obviously as old as radiotherapy itself. For many decades, improvements in radiotherapy were hampered by inability to determine accurately the geometrical location of tumors. In so-called conventional radiotherapy, bony landmarks, air-soft tissue edges, skin-topography or contrast (liquid, surgical clips) related to the location of the tumor were used to define roughly shaped fields. With the development of medical CT-scanners, progress in radiotherapy was boosted. The 3-dimensional (3D) information given by CT was further fine-tuned by magnetic resonance and functional imaging. In conformal radiotherapy, fields from which the aperture was conformed to the edges of the tumor replaced roughly shaped fields. Gantry-based linear accelerators and isocentric pedestal treatment couches offered a large window of possible beam orientations in space. Conformal radiotherapy became the issue of tightening the dose distribution to the target shape in 3D.

Treatment machines were designed to deliver flat (unmodulated: the radiation fluence is practically the same over the whole cross-sectional area of the beam) and later also wedged beams. Spatial combinations of flat and wedged beams collimated to the projection of the target create a convex high-dose volume (i.e. it cannot create high-dose volumes with concave surfaces). Using flat beams, the treatment of tumor volumes with concave surfaces would overdose sensitive tissues in the concavities. In the 80s, Brahme demonstrated the unique potential intensity modulated (IM) beams to create homogeneous concave dose distributions [1]. Inside IM-beams, the radiation fluence (intensity) was not equal but had a value that was function of its geometrical location inside the cross section of the beam [2]. The concept of inverse planning was proposed by Brahme as a possible strategy to make the design of IM-beams feasible [3]. In inverse planning, computer optimization technology is used to convert a (medically) desired dose distribution into instruction files of the (robotized) treatment machine. Execution of the instruction files by the machine leads to a dose deposition in the patient that is as close as possible to the desired dose distribution.

IMRT remained a research topic in physics laboratories until, in 1993, Carol proposed an integrated planning and delivery system (NOMOS MiMiC) capable of clinical IMRT tomotherapy [4]. Since 1993, much happened. The major vendors of linear accelerators developed multileaf collimator (MLC) technology capable of delivering IMRT. Smaller companies developed micro-MLCs for IMRT. IMRT research is intense and clinical results have been published for various tumor sites including prostate, head and neck and base of skull. A variety of methods to plan and deliver IMRT are available. Now, the field of IMRT application is not only the generation of concave dose distributions but includes almost any clinical situation in which precise control of the dose distribution, inside as well as outside the tumor volume, is required.

IMRT for head and neck cancer was pioneered by investigators from the University of Michigan in Ann Arbor [5, 6]. Several other groups have recently reported on the use IMRT for head and neck cancer [7, 8, 9, 10, 11]. A PubMed search on February 25, 2004 using IMRT and head and neck neoplasms as keywords yielded 88 publications, mostly dealing with treatment planning and physics-related issues. Reports of clinical outcome of IMRT are scarce. Results from randomized trials testing the hypothetical benefit of IMRT over un-modulated beam techniques are inexistent. Conclusions about efficacy and toxicity have to be derived from small case series in single institutions (level of evidence III). In most series, the IMRT techniques have changed during the studies. Nevertheless, some pertinent conclusions can be drawn. This review will discuss i) the rationale for using IMRT in the head and neck region, ii) the benefit obtained by IMRT according to clinical data, iii) the need for improvement of the clinical results and iv) the present and future directions of research.

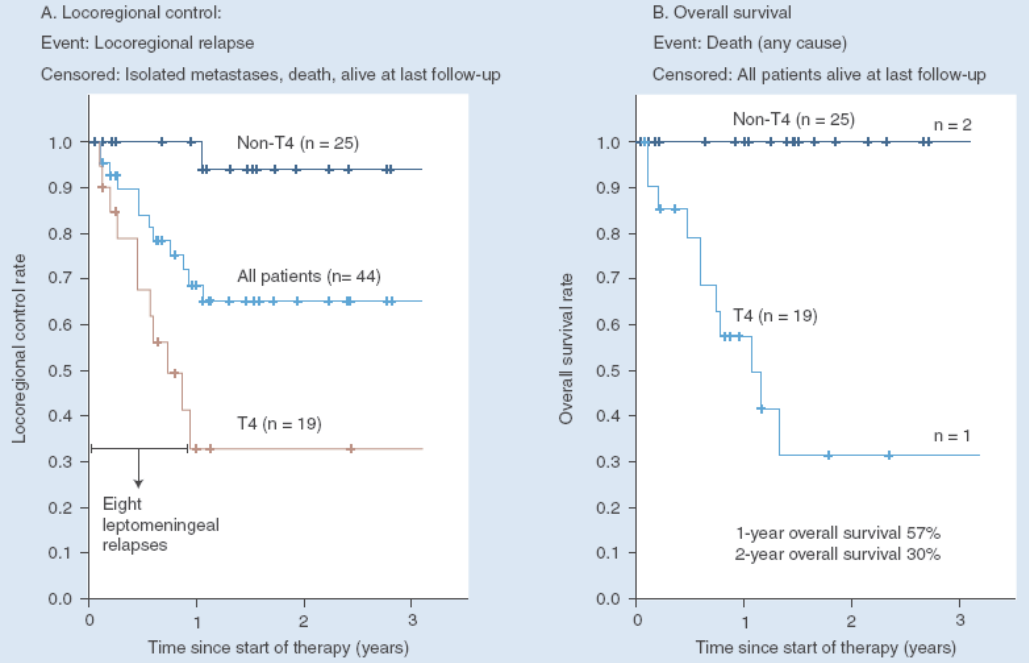

Figure 1: Locoregional control and survival in 44 sinonasal tumors.

Rationale for IMRT in head and neck cancer

Six major head and neck cancer sites can be distinguished: paranasal sinus, oral cavity, pharynx (naso-, oro- and hypopharynx), larynx, salivary gland and thyroid gland. The anatomical challenges for safe delivery of radiotherapy are site dependent and increase with T-stage.

In head and neck cancer, IMRT has been advocated for its ability to create concave dose distributions [12, 13] in order to spare organs at risk (OAR) including spinal cord, salivary glands, optical pathway structures; to avoid photon-electron beam matching planes [13] and to facilitate prescription of intentionally inhomogeneous dose distributions as in case of simultaneous application of multiple dose levels [13, 14].

Beautiful examples of concave PTVs are found in each of the 3 subsites of pharyngeal cancer [15]. The pharynx is located anteriorly and antero-laterally from the brain stem and spinal cord. The pharynx is spaced (distance 1-2.5 cm) from these nervous structures by the sphenoidal body (corpus ossis sphenoidalis) and the cervical vertebral bodies and their pre-vertebral muscles. Brainstem and/or spinal cord are the posteriorly located organs at risk (OARs) in the irradiation of pharyngeal cancers. Superiorly (cranially), various other central nervous system (CNS) structures form a corona of OARs (brain, pituitary, chiasma opticum, optical nerves) that give rise to planning problems especially for nasopharyngeal tumors. Antero-superiorly, the eyes and accessory structures restrict access to incoming or outgoing beam trajectories. Left and right lateral OARs are mandibular bone and parotid glands for nasopharynx and oropharynx sub-sites. Pharyngeal cancers show a high incidence of sub-clinical or macroscopic lymph node metastases to many areas of the cervical lymphatic drainage system. Lymph node area II is of special concern to the radiotherapy planner when parotid sparing is a treatment objective [16].

Tumors that invade the lateral pharyngeal recesses or the para-pharyngeal space pose a dosimetrical challenge. The matching plane between electron and photon beams, used in conventional irradiation techniques to spare the spinal cord, typically transects through gross tumor. Because of a rapidly widening of the electron beam penumbra with depth, the conventional technique carries substantial risk for

under-dosage of the anatomical structures located at the deep portion of the matching plane at the electron beam side. Photon IMRT-techniques allow avoidance of under-dosage at the lateral pharyngeal recesses and the parapharyngeal space.

For paranasal sinus tumours, concave dose distributions are needed to spare optic pathway structures [17]. For oral cavity and pharyngeal tumours, the advantages of IMRT are most prominent if irradiation of the primary tumour and cervical lymph node chains is prescribed, especially if sparing of the parotid is attempted [5]. For most head and neck sites, planning studies show an improved target coverage compared to conventional techniques [19, 20, 21, 22, 23]. For paranasal sinus, improved dose reduction to OARs at equal target coverage was reported [24].

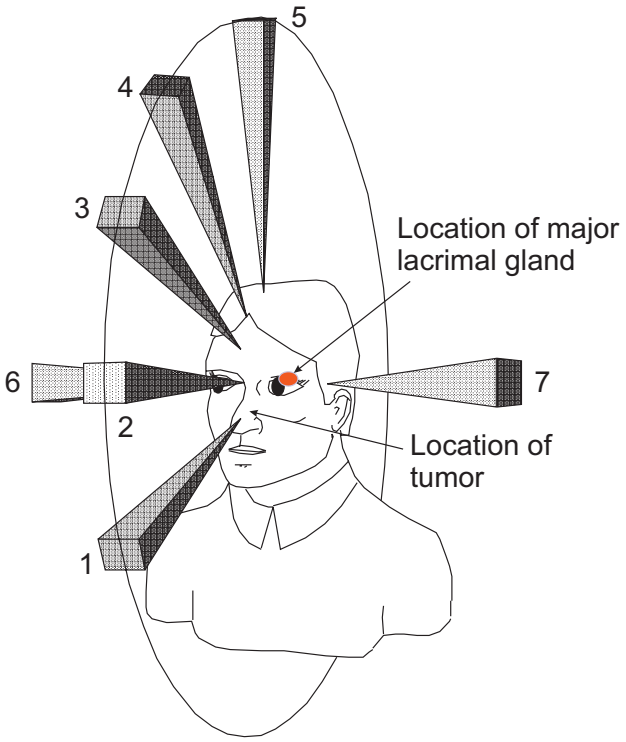

Figure 2: Directions of the 7 beams used at Ghent University Hospital to treat N0 sinonasal tumours. In most patients, the major lacrimal glands and the lateral parts of the tarsal and accessory glands are not exposed to primary radiation from beams 1, 2 and 3.

Clinical results

Typical for the achievements of IMRT in head and neck tumors are the results from Eisbruch [25] and Dawson [26] of University of Michigan for oral cavity, oropharyngeal, hypopharyngeal and laryngeal tumours; from Lee [27] of University of California at San Francisco for nasopharyngeal tumours; from Claus [17] of Ghent University Hospital for sinonasal sites and from Chao [28] of Washington University for all sites except salivary and thyroid gland. The study of Chao also included cancers of unknown primary (CUP).

Oral cavity, oropharyngeal, hypopharyngeal and laryngeal tumours

Eisbruch reported on the outcome of 88 patients irradiated with parotid sparing 3D-CRT or IMRT. Saliva flow rates before and after radiotherapy were measured for 152 parotid glands. From these data a dose/volume/function relationships was obtained that showed that a parotid mean dose < 26 Gy was consistent with preservation of salivary gland function [29]. None of the recurrences in 12 of 58 patients were observed nearby the spared parotid glands [26]. The main conclusions were that parotid function sparing may be achieved without increased risk for relapses adjacent to the spared area and that failures occur mainly in the high-dose area. Amosson et al. showed that IMRT allowed dosimetric sparing of the parotid, which resulted in less subjective feeling of xerostomia [30].

Sinonasal cancer

The report on IMRT for sinonasal cancer [9] was updated in 2003 (De Neve: teaching course at ECCO 12, Copenhagen, 21-25 Sept 2003). A summary of the update is presented here. Between 1999 and 2002, 44 patients received R0 surgery for ethmoid sinus (n=33), maxillary sinus (n=6) or nasal cavity (n=5) cancer. PTV prescription dose was 60 Gy with a maximum dose constraint of 50 Gy to the optic nerves and chiasm for the first 4 patients, 66 Gy for next 4 patients and 70 Gy for the remaining 36 patients. In one patient no dose constraint was implemented for the

Table 1: Complications of post-operative radiation therapy for ethmoid sinus tumors.

Period	Radiation therapy	Number of patients	Grade 4 optic neuropathy	Dry-eye syndrome*
1985-1994	2D	19	0	5
1995-1998	3D	11	2	2
1999-2002	IMRT	33	1†	0

* Chronic conjunctivitis and keratitis,visus drop to < 20 of visus before RT. Enucleation in 1 patient. †No dose constraint was applied to the left optic nerve damaged by tumor. A dose of 70 Gy to the optic nerve resulted in blindness of the left eye.

left optic nerve because of a pre-existing severe drop in visual acuity caused by tumour extension. This patient developed full blindness of the left eye. For the optic nerves and chiasm of the remaining 39 patients, the structures were expanded by 2 mm and a maximum dose constraint of 60 Gy was implemented. None of these patients developed blindness. Loco-regional control and survival are shown in figure 1. Median duration of follow-up in surviving patients is 14 months. Loco-regional control was excellent for patients with T1-T3 stage but poor in T4 stage. All patients with T4b developed local or lepto-meningeal relapses within 8 months after treatment.

Table 1 gives a summary of optic pathway injury for the subgroup of patients with ethmoid sinus primary tumours. A comparison with historic controls was performed. During the period 1985-1994, most patients were treated using anterior and ipsilateral wedged fields, sometimes complemented with an opposed lateral field. Of 19 patients, receiving prescription doses of 54-66 Gy (1.8 Gy/fraction), 5 patients developed severe dry-eye syndrome. During the period 1995-1998, 3D-conformal non-coplanar techniques were used. Of 11 patients, receiving prescription doses of 60-70 Gy (2 Gy/fraction), grade 4 optic neuropathy was observed in 2 patients and severe dry-eye syndrome in another 2 patients. For the 33 patients treated by IMRT during the period 1999-2002, grade 4 optic neuropathy was seen in the one patient where optic nerve sparing was not attempted. For this group of patients, the duration of follow-up is too short to draw conclusions regarding optic pathway injury. With regard to dry-eye syndrome, relevant conclusions can be drawn since patients who develop severe dry-eye syndrome are symptomatic within months after radiotherapy. None of the patients developed severe dry-eye syndrome and this observation can be explained by the IMRT beam arrangement used at GUH (figure 2) rather than by beam modulation itself. The major lacrimal glands are located at the upper-lateral corner of the orbit while the other (accessory and tarsal) lacrimal glands are located in the upper eyelid. The BEV-projection of 3 or more of the 7 beams, used by the GUH class solution (figure 2), excludes most of the lacrimal apparatus. In addition, most of glandular tissue is located less than 5-7 mm below the skin, in the build-up region of many of the beams. By this beam arrangement, most of the lacrimal gland apparatus typically receives a dose well below 30 Gy, which seems consistent with functional sparing (figure 3).

Nasopharyngeal tumors

Lee [27] reported the results of 67 patients with non-keratinizing (n=34) or undifferentiated (n=33) stage I-IV nasopharyngeal cancer treated with IMRT (combined with chemotherapy in most patients) between April 1995 and October 2000. IMRT given by compensators, MLC or MIMiC was used to treat head region, conventional fields were used to treat the neck. With a median follow-up of 31 (range 7-72) months, loco-regional control was obtained in all but 2 patients; one with a local relapse and one with a failure in the neck. The 4-year actuarial overall survival was 88% and the 4-year actuarial distant metastasis-free rate was only 66%. The authors pointed out that xerostomia was less than would have been expected with conventional radiotherapy. The high local-regional control rate suggests that IMRT provided good tumor target coverage.

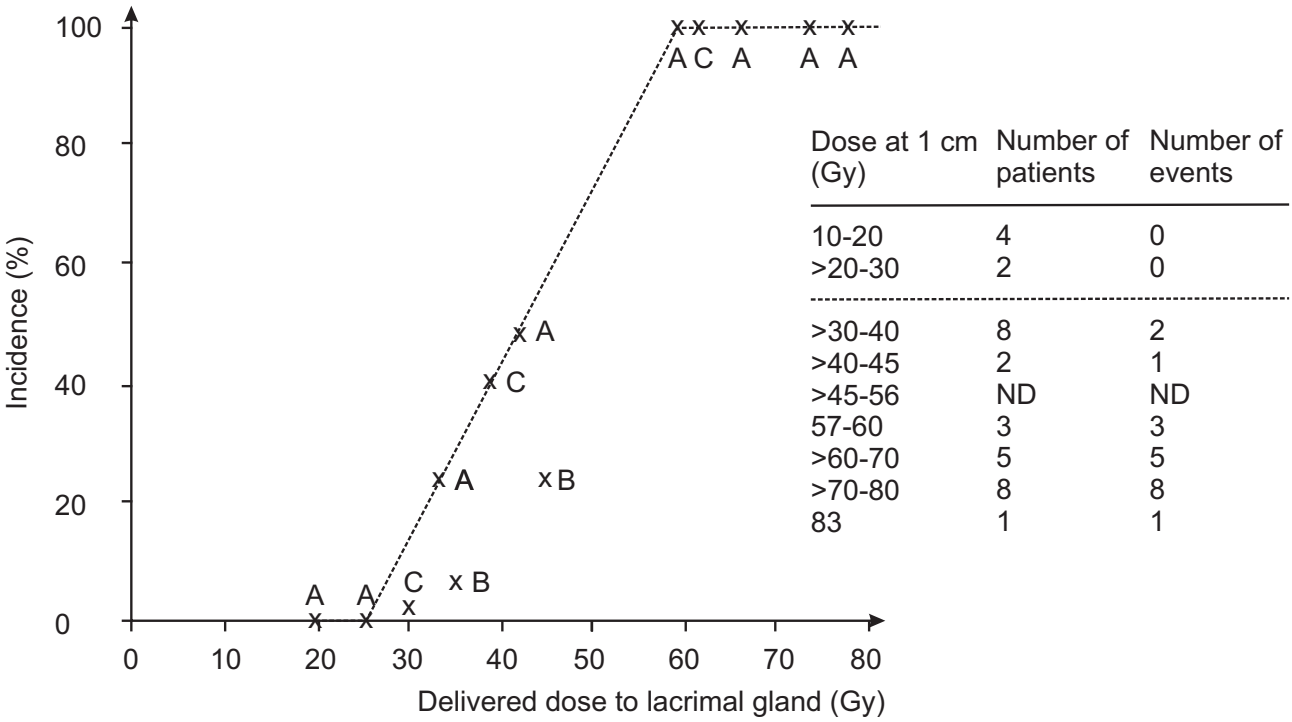

Dose at 1 cm (Gy)	Number of patients	Number of events
10-20	4	0
>20-30	2	0
>30-40	8	2
>40-45	2	1
>45-56	ND	ND
57-60	3	3
>60-70	5	5
>70-80	8	8
83	1	1

Figure 3: Dose-effect relationship for severe dry-eye syndrome. With doses of less than 30 Gy to the lacrimal apparatus, induction of severe dry-eye syndrome was a rare event. A: [42] B: [43] C: [44] D: [45].

Various sites and CUP

Chao described the clinical outcome, with a median follow-up of 26 months, of IMRT for 165 head and neck cancer patients from which a subgroup of 126 patients were treated for primary tumours [28]. IMRT was given for upper neck and head and conventional AP photon beams for the lower neck. Of the 17/126 patients who had loco-regional relapse or progression, the site of failure was gross tumour and/or adjacent sites in 10 patients (1 patient had also a relapse in the lower neck region). In 3 patients the site of failure was the electively irradiated site (n=1) or marginal to the electively irradiated site (n=2) while in 4 patients isolated failure occurred in the conventionally treated lower neck. The main conclusion was that the predominant tumor failure occurred within clinical target volume at high prescription dose.

These and other published data provide good evidence that IMRT can reduce side effects in head and neck cancer. However, most loco-regional relapses still occur in the region that was selected to receive the highest prescription dose. Chao pointed out that this may imply the need to identify patients with radio-resistant tumor sub-volumes (such as hypoxic regions) within the tumor [28].

Directions for further improvements

Two main arguments were used in favour of IMRT. Selective dose-reduction to radiation-sensitive organs would result in less toxicity. Alternatively, reduction of the dose to OARs relative to the tumour prescription dose would open a window for dose escalation with the aim to improve local control. Table 2 shows that in the abovementioned IMRT studies [28, 17, 26, 29] conventional levels of prescription doses were used and that dose escalation was not attempted. In fact, dose prescription to gross tumour or elective sites was performed as in conventional radiation therapy. A homogeneous dose was prescribed at different dose levels for sub-regions of the PTV. By using IMRT, the dose could be lowered to selected OARs like parotid glands, lacrimal glands, optic pathway structures, middle ear or tem-

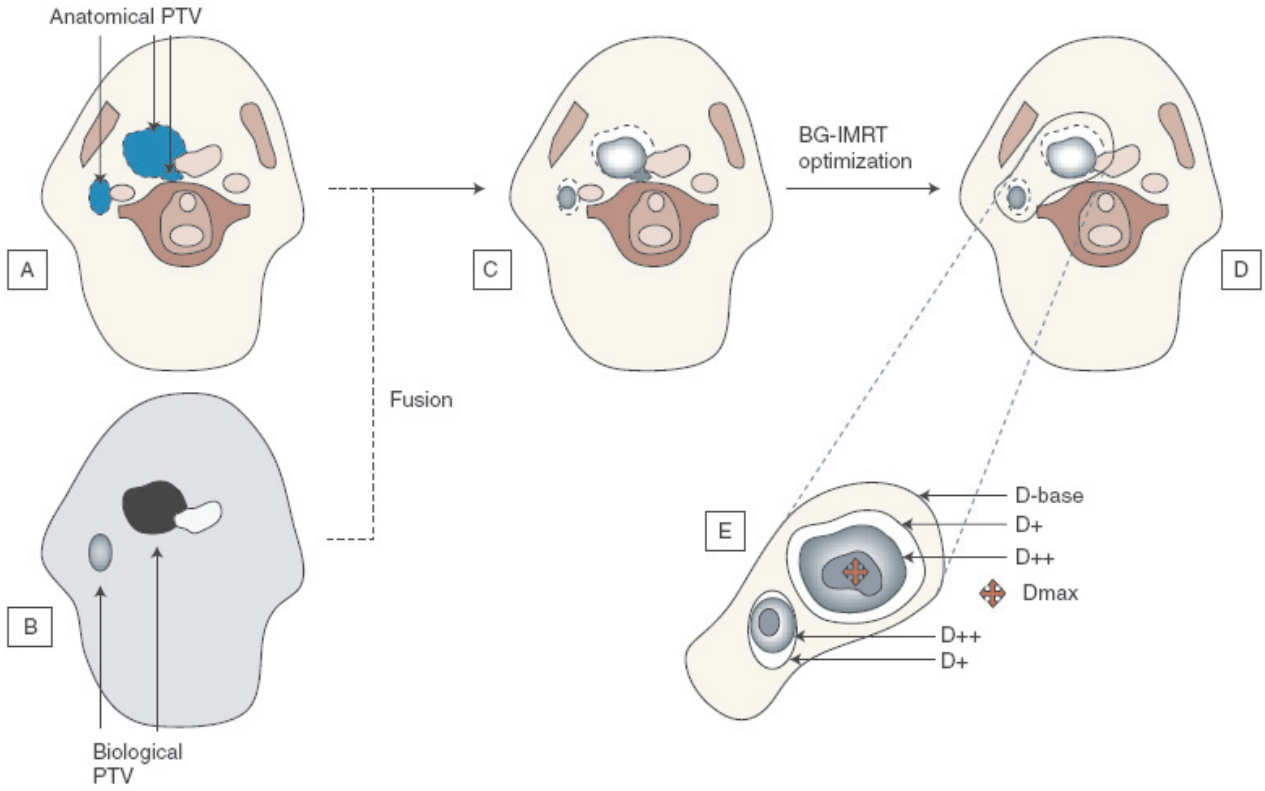

Figure 4: Biological image-guided intensity-modulated radiation therapy (BG-IMRT) optimization. (A) Anatomical information remains the basis for conventional PTV definition. (B) Biological imaging provides radiobiological information as a SI to voxels that is proportional to a radiobiological parameter. (C) Fusing provides an image where each voxel has a Hounsfield value and SI. (D) BG-IMRT optimization requires the development of a transformation engine that secures a spatial dose variation in the anatomical PTV (E) as a function of SI in the PET imaging. D-base: Conventionally applied dose level that encompasses the anatomical PTV; D+/D++/Dmax: Dose escalation (limited to intra-PTV regions as function of SI values); PTV: Planning target volume; SI: Signal intensity.

Table 2: Prescription doses (Gy) of intensity-modulated radiation therapy in head and neck cancer.

Clinical target volume	Elective		Ref.
	1^{st}	2^{nd}	
70.4	61.2	50.4	[26, 29]
60-70	50-60	-	[27]
60-70	-	-	[17]
70	56		[28]

poral lobes. This resulted in a reduction of the severity of a specific side effect but the window for dose escalation remained small, if not inexistent, because of the presence of the remaining dose-limiting structures like cartilage, connective tissues, nerve tissues, bone, the swallowing apparatus or the lymphatic system in the large volume treated at high-dose. With the risk of over-simplification, we could state that the high-dose volumes are too large for a strategy of homogeneous dose escalation. We hypothesize that dose escalation focused to small sub-volumes of the PTV is feasible. The hypothesis is supported by theoretical considerations [14], by results of feasibility trials using a simultaneous boost technique at Baylor College [31] and at Virginia Commonwealth University [32] and by experience obtained with com-

bining high-dose or accelerated external beam radiotherapy or radio-chemotherapy with stereotactic radiosurgery [33] or with brachytherapy [34, 35].

It seems self-evident to direct foci of dose escalation to the regions inside the tumour that are supposed to be the most radiation resistant [36]. Novel biological imaging techniques, mostly based on PET, MRI and MRS may have the potential to construct three-dimensional maps of radio-biologically relevant parameters [37, 38, 39]. These maps can be fused with high-resolution CT and MRI for treatment design and optimisation with a strategy of small-volume focused dose escalation to radiation resistant foci. The strategy for clinical trials of focused dose escalation at GUH involves the flow of procedures given in figure 4. Anatomical (CT) information remains the basis for conventional PTV definition. Biological (PET) imaging provides radiobiological information as a signal intensity (SI) to voxels that is proportional to a radiobiological parameter like hypoxia, proliferation, intrinsic radiation sensitivity. Fusing provides an image where each voxel has a Hounsfield value (for computation of absorbed dose) and a SI (for intra-tumour guidance of the dose distribution). Bio-image guided-IMRT optimisation requires the development of a transformation engine that secures a spatial dose variation in the anatomical PTV as function of SI in the PET imaging. The D-base indicates a conventionally applied dose level that encompasses the anatomical PTV. Dose escalation (D+, D++, Dmax) is limited to intra-PTV regions as function of SI values.

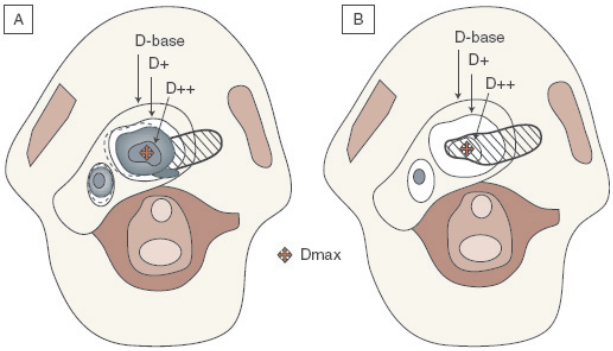

Figure 5: Biological image-guided optimization. (A) Based on biological and anatomical imaging immediately before the onset of radiotherapy. This results in a treatment where the high-dose peaks are accurately focused to the regions of the tumor that showed the highest signal intensity. This treatment plan may be appropriate to deliver focused dose escalation as long as the anatomical and biological image geometry remains unchanged (e.g., during the 1st week of treatment). (B) Tumor response observed at the 4th week of treatment illustrates that the patient cannot be considered unchanged for the whole duration of treatment. The planned dose deposition would focus dose escalation into the oropharyngeal cavity, which is obviously useless.
D-base: Conventionally applied dose level that encompasses the anatomical planning target volume (PTV); D+/D++/Dmax: Dose escalation (limited to intra-PTV regions as function of signal intensity values).

The fourth dimension

The current state of the art for planning and evaluation of irradiation treatment of cancer patients is to work in three dimensions (3D) and to consider the patient as unmoving and unchanging, that is, images that are made once prior to therapy are considered representative for the whole course of treatment. As a result, the precision of treatment is compromised by anatomical changes during treatment even if patient immobilization and positioning can be done accurately.

The problem is illustrated in figure 5. Suppose that the dose distribution was optimised using pre-treatment anatomical and biological imaging. This dose distribution may be suitable in the beginning of the treatment course. However, after 4 weeks of treatment when the tumour has regressed, one of the intended dose peaks coincides with the air of the oropharyngeal cavity, clearly unlikely to host radiation resistant cells. Figure 5 illustrates that an IMRT plan based on biological image information can be applied only during a brief time period. After that period, both re-imaging and re-planning need to be performed. This is not trivial since neither the methods for re-imaging nor the technology to re-optimise the plan taking into account a delivered dose on a changing anatomy are available. Therefore we reasoned that a strategy of focused dose escalation might be

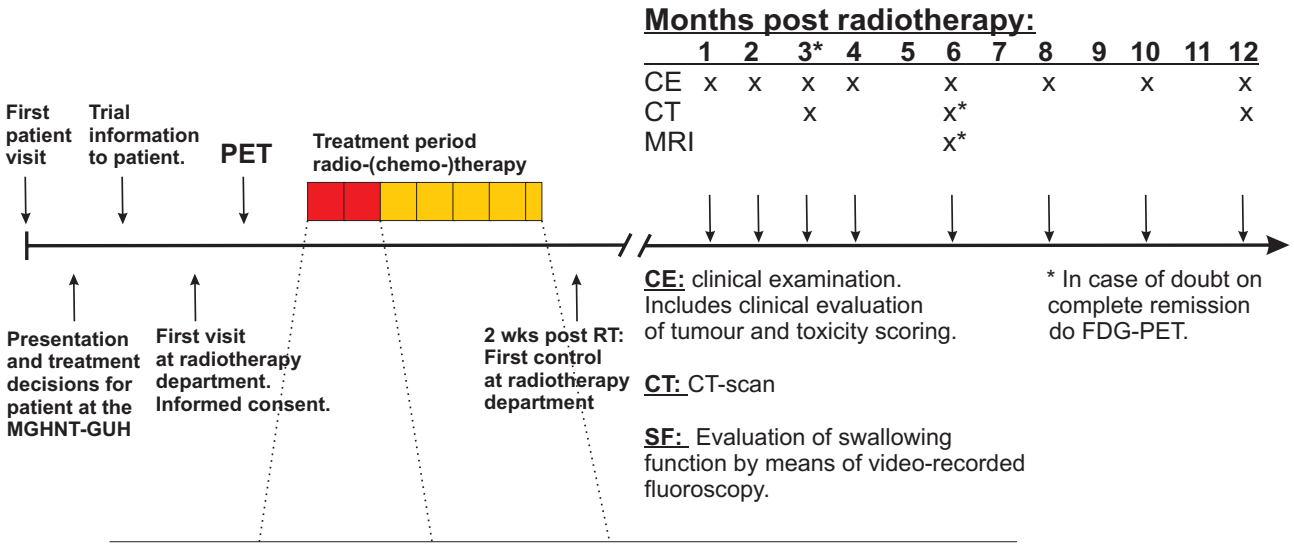

PTV based on CT/MRI	Phase I 10 fractions (Gy/fraction)	Phase II 22 fractions (Gy/fraction)	Total physical dose (Gy)	Total dose (2 Gy equivalent)
PTV-PET	2.50	2.16	72.5	74
PTV-70Gy	2.16	2.16	69.1	70
PTV-62Gy	1.94	1.94	62.1	62
PTV-55Gy	1.75	1.75	56.0	55

Figure 6: Design of the pilot study: first level of focused dose escalation. Table shows that focused dose escalation to PTV-PET is performed at 2.5 Gy/fraction during the 2 weeks of Phase I treatment. Abbreviations: MGHNT-GUH: Multidisciplinary Group on Head and Neck Tumours-Ghent University Hospital; PTV-PET: planning target volume obtained by a 3 mm isotropical expansion of the automatically contoured lesion defined by FDG-PET. PTV-70Gy, PTV-62Gy, PTV-55Gy: different planning target volume based on CT and MRI imaging with prescription doses of respectively 70, 62 and 55 Gy biological (2 Gy equivalent) dose. Inserted table shows that focused dose escalation to the PTV-PET is performed at 2.5 Gy/fraction during the 2 weeks of phase I of the treatment.

applicable for a short time period immediately after imaging. This reasoning was incorporated in a pilot study described below.

Pilot study of focused dose escalation

The purpose of this study was to apply focused dose escalation to the GTV in patients with histological proof of carcinoma of the oropharynx, hypopharynx or larynx who were referred for primary radiotherapy or radio-chemotherapy. The design of the study is shown in figure 6. The radiation treatment was divided in 2 phases: a first phase of 10 fractions followed by a second phase of 22 fractions. FDG-PET image information is used in plan optimisation for the first phase only. During the second phase of treatment a conventional IMRT treatment is applied. At the first level of dose escalation, a simultaneous boost was delivered to a PTV-PET. The PTV-PET was a 3 mm expansion of a GTV-PET that had been automatically delineated based on signal to background ratio in the FDG-PET image. The technology had been developed by Grégoire and co-workers [40]. They have shown that this GTV-PET correlated much better with the macroscopic surgical specimen than expert-contoured GTVs based on CT or MRI images (Grégoire, personal communication).

The GTV-PET was also much smaller than the

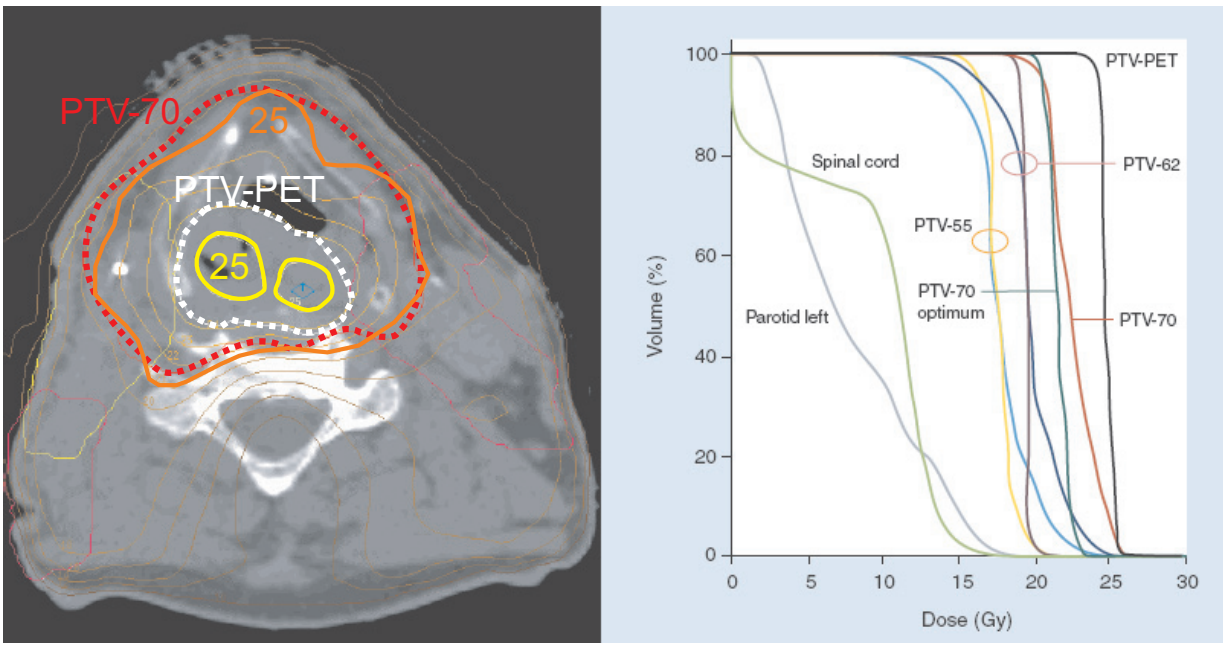

Figure 7: Phase I plan: transverse dose distribution and dose-volume histogram. Due to isotropic expansion of the respective clinical target volumes, PTV-70, -62 and -55 Gy reach close to the skin surface and are mutually overlapping. For optimization purposes, subvolumes are created for each of these PTVs In the dosevolume histogram plots, two histograms are shown for each PTV, one for the whole PTV, the other for the subvolume. The subvolume is equal to the PTV minus the part of the PTV that is closer than 6 mm to the skin and minus the overlap region with the PTV planned at a higher dose level. The use of subvolumes for intensity-modulated radiation therapy optimization and reporting is described elsewhere [41]. PET: Positron emission tomography; PTV: Planning target volume.

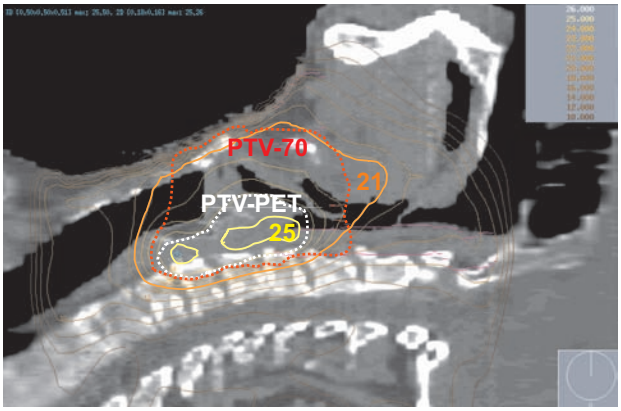

Figure 8: Sagittal dose distribution: mid-sagittal section. PET: Positron emission tomography; PTV: Planning target volume.

expert-contoured GTVs but still larger than the macroscopic tumour volume as derived from the surgical specimen. We hypothesized that the PET-based GTV could be a volume suitable for focused dose escalation. A typical dose distribution and DVH applied during the first phase of IMRT is shown in figures 7 and 8. Fifteen patients have been included at the first level of dose escalation. For the second level of dose escalation, a second PTV-PET will be defined using a higher PET-signal to background ratio. Optimisation aiming at a dose of 3.0 Gy per fraction for the 10 fractions of treatment phase 1 will is planned.

Expert opinion:

Bilateral neck IMRT was performed for oral cavity, pharyngeal and laryngeal cancer with functional sparing of salivary glands, reduction of xerostomia and without increased incidence of recurrences nearby the spared region. Low rates of recurrences were

observed in elective nodal sites indicating that PTV definition and prescription doses were adequate for elective neck irradiation. Recurrences were mainly located in the high dose-prescription regions (GTV, tumor bed), suggesting the need for a selective delivery of higher doses to these regions. In sinonasal cancer, IMRT avoids dry-eye syndrome and may be used to reduce the incidence of optic neuropathy but it could not reverse the high failure rates in T4b disease. For all head and neck sub-sites, planning studies show equal or improved coverage with IMRT. In clinical IMRT studies, substantial dose escalation was not achieved and improved local control by using IMRT for head and neck cancer cannot be demonstrated. Progress in biological imaging, mostly based on PET, may allow us to identify recurrence-prone regions inside the GTV as targets for focused dose escalation. With focused dose escalation, the PTV cannot be considered as spatially invariant during a long treatment course. Re-planning will be required which remains a technological challenge.

Five-year view

Radiotherapy with curative intent for head and neck cancer will gradually be replaced by concurrent radio-chemotherapy. To limit the toxicity of radio-chemotherapy while increasing the efficacy of radiation, the high-dose radiation volume will have to be reduced. Progress in biological imaging, mostly based on PET and MRS, together with IMRT will allow limiting the high dose volume to the recurrence-prone regions inside the tumor. Biological image-guided IMRT requires resources and an assembly of multidisciplinary skills of a magnitude that will not be present in most cancer centers in Europe. For imaging and IMRT planning, we expect that the patient will have to travel to expert centers. The IMRT plans, developed in these centers, will be sent by network to the referring radiotherapy department as machine instruction files for robotized equipment. The actual IMRT treatment can then be performed in a radiotherapy center close to the patients home.

References

[1] Brahme A, Roos JE, Lax, I. Solution of an integral equation encountered in rotation therapy. *Phys.Med.Biol.* 27, 1221-1229 (1982).

[2] Lax I, Brahme A. Rotation therapy using a novel high-gradient filter. *Radiology* 145, 473-478 (1982).

[3] Eklof A, Ahnesjo A, Brahme A. Photon beam energy deposition kernels for inverse radiotherapy planning. *Acta Oncol*. 29, 447-454 (1990).

[4] Carol M, Grant WH III, Pavord D, *et al*. Initial clinical experience with the Peacock intensity modulation of a 3-D conformal radiation therapy system. *Stereotact. Funct. Neurosurg.* 66, 30-34 (1996).

[5] Eisbruch A, Ship JA, Martel MK, *et al*. Parotid gland sparing in patients undergoing bilateral head and neck irradiation: techniques and early results. *Int. J. Radiat. Oncol. Biol. Phys.* 36, 469-480 (1996).

[6] Eisbruch A, Marsh LH, Martel MK, *et al*. Comprehensive irradiation of head and neck cancer using conformal multisegmental fields: assessment of target coverage and noninvolved tissue sparing. *Int. J. Radiat. Oncol. Biol. Phys.* 41, 559-568 (1998).

[7] Teh BS, Mai WY, Grant WH III, *et al*. Intensity modulated radiotherapy (IMRT) decreases treatment-related morbidity and potentially enhances tumor control. *Cancer Invest* 20, 437-451 (2002).

[8] Chao KS, Low DA, Perez CA, Purdy JA. Intensity-modulated radiation therapy in head and neck cancers: The Mallinckrodt experience. *Int. J. Cancer* 90, 92-103 (2000).

[9] Claus F, Boterberg T, Ost P, De Neve W. Short term toxicity profile for 32 sinonasal cancer patients treated with IMRT. Can we avoid dry eye syndrome? *Radiother. Oncol.* 64, 205-208 (2002).

[10] Lee N, Xia P, Fischbein NJ, Akazawa P, Akazawa C, Quivey JM. Intensity-modulated radiation therapy for head-and-neck cancer: the

UCSF experience focusing on target volume delineation. *Int. J. Radiat. Oncol. Biol. Phys.* 57, 49-60 (2003).

[11] Verellen D, Linthout N, Storme G. Target localization and treatment verification for intensity modulated conformal radiation therapy of the head and neck region. The AZ-VUB experience. Akademisch Ziekenhuis-Vrije Universiteit Brussel. *Strahlenther. Onkol.* 174 Suppl 2, 19-27 (1998).

[12] Cozzi L, Fogliata A. IMRT in the treatment of head and neck cancer: is the present already the future? *Expert. Rev. Anticancer Ther.* 2, 297-308 (2002).

[13] De Neve W, Claus F, Van Houtte P, Derycke S, De Wagter C. [Intensity modulated radiotherapy with dynamic multileaf collimator. Technique and clinical experience]. *Cancer Radiother.* 3, 378-392 (1999).

[14] Mohan R, Wu Q, Manning M, Schmidt-Ullrich R. Radiobiological considerations in the design of fractionation strategies for intensity-modulated radiation therapy of head and neck cancers. *Int. J. Radiat. Oncol. Biol. Phys.* 46, 619-630 (2000).

[15] De Neve W, De Gersem W, Derycke S, *et al*. Clinical delivery of intensity modulated conformal radiotherapy for relapsed or second-primary head and neck cancer using a multileaf collimator with dynamic control. *Radiother. Oncol.* 50, 301-314 (1999).

[16] Claus F, Duthoy W, Boterberg T, *et al*. Intensity modulated radiation therapy for oropharyngeal and oral cavity tumors: clinical use and experience. *Oral Oncol.* 38, 597-604 (2002).

[17] Claus F, De Gersem W, De Wagter C, *et al*. An implementation strategy for IMRT of ethmoid sinus cancer with bilateral sparing of the optic pathways. *Int. J. Radiat. Oncol. Biol. Phys.* 51, 318-331 (2001).

[18] Tsien C, Eisbruch A, McShan D, Kessler M, Marsh R, Fraass B. Intensity-modulated radiation therapy (IMRT) for locally advanced paranasal sinus tumors: incorporating clinical decisions in the optimization process. *Int. J. Radiat. Oncol. Biol. Phys.* 55, 776-784 (2003).

[19] Penagaricano JA, Papanikolaou N. Intensity-modulated radiotherapy for carcinoma of the head and neck. *Curr.Oncol. Rep.* 5, 131-139 (2003).

[20] Teh BS, Woo SY, Butler EB. Intensity modulated radiation therapy (IMRT): a new promising technology in radiation oncology. *Oncologist* 4, 433-442 (1999).

[21] Dogan N, Leybovich LB, King S, Sethi A, Emami B. Improvement of treatment plans developed with intensity-modulated radiation therapy for concave-shaped head and neck tumors. *Radiology* 223, 57-64 (2002).

[22] Hunt MA, Zelefsky MJ, Wolden S, *et al*. Treatment planning and delivery of intensity-modulated radiation therapy for primary nasopharynx cancer. *Int. J. Radiat. Oncol. Biol. Phys.* 49, 623-632 (2001).

[23] Cozzi L, Fogliata A, Bolsi A, Nicolini G, Bernier J. Three-dimensional conformal vs. intensity-modulated radiotherapy in head-and-neck cancer patients: comparative analysis of dosimetric and technical parameters. *Int. J. Radiat. Oncol. Biol. Phys.* 58, 617-624 (2004).

[24] Mock U, Georg D, Bogner J, Auberger T, Potter R. Treatment planning comparison of conventional, 3D conformal, and intensity-modulated photon (IMRT) and proton therapy for paranasal sinus carcinoma. *Int. J. Radiat. Oncol. Biol. Phys.* 58, 147-154 (2004).

[25] Eisbruch A, Dawson LA, Kim HM, *et al*. Conformal and intensity modulated irradiation of head and neck cancer: the potential for improved target irradiation, salivary gland function, and quality of life. *Acta Otorhinolaryngol. Belg.* 53, 271-275 (1999).

[26] Dawson LA, Anzai Y, Marsh L, *et al*. Patterns of local-regional recurrence following parotid-sparing conformal and segmental intensity-modulated radiotherapy for head and neck cancer. *Int. J. Radiat. Oncol. Biol. Phys.* 46, 1117-1126 (2000).

*** Recurrences did not occur in the regions**

of the parotid glands functionally spared by IMRT.

[27] Lee N, Xia P, Quivey JM, *et al*. Intensity-modulated radiotherapy in the treatment of nasopharyngeal carcinoma: an update of the UCSF experience. *Int. J. Radiat. Oncol. Biol. Phys.* 53, 12-22 (2002).

[28] Chao KS, Ozyigit G, Tran BN, Cengiz M, Dempsey JF, Low DA. Patterns of failure in patients receiving definitive and postoperative IMRT for head-and-neck cancer. *Int. J. Radiat. Oncol. Biol. Phys.* 55, 312-321 (2003).

[29] Eisbruch A, Ten Haken RK, Kim HM, Marsh LH, Ship JA. Dose, volume, and function relationships in parotid salivary glands following conformal and intensity-modulated irradiation of head and neck cancer. *Int. J. Radiat. Oncol. Biol. Phys.* 45, 577-587 (1999).

[30] Amosson CM, Teh BS, Van TJ, *et al*. Dosimetric predictors of xerostomia for head-and-neck cancer patients treated with the smart (simultaneous modulated accelerated radiation therapy) boost technique. *Int. J. Radiat. Oncol. Biol. Phys.* 56, 136-144 (2003).

[31] Butler EB, Teh BS, Grant WH III, *et al*. Smart (simultaneous modulated accelerated radiation therapy) boost: a new accelerated fractionation schedule for the treatment of head and neck cancer with intensity modulated radiotherapy. *Int. J. Radiat. Oncol. Biol. Phys.* 45, 21-32 (1999).
*** Demonstrates the feasibility of simultaneous boost to small volumes by IMRT. Provides in the discussion section a review of the clinical experience with fraction sizes larger than 2 Gy.**

[32] Wu Q, Mohan R, Morris M, Lauve A, Schmidt-Ullrich R. Simultaneous integrated boost intensity-modulated radiotherapy for locally advanced head-and-neck squamous cell carcinomas. I: dosimetric results. *Int. J. Radiat. Oncol. Biol. Phys.* 56, 573-585 (2003).

[33] Tate DJ, Adler JR Jr, Chang SD, *et al*. Stereotactic radiosurgical boost following radiotherapy in primary nasopharyngeal carcinoma: impact on local control. *Int. J. Radiat. Oncol. Biol. Phys.* 45, 915-921 (1999).

[34] DeNittis AS, Liu L, Rosenthal DI, Machtay M. Nasopharyngeal carcinoma treated with external radiotherapy, brachytherapy, and concurrent/adjuvant chemotherapy. *Am. J. Clin. Oncol.* 25, 93-95 (2002).

[35] Rudoltz MS, Perkins RS, Luthmann RW, *et al*. High-dose-rate brachytherapy for primary carcinomas of the oral cavity and oropharynx. *Laryngoscope* 109, 1967-1973 (1999).

[36] Gregoire, V. [Target-volume selection and delineation in the cervico-maxillo-facial region: beyond the concepts of the ICRU]. *Cancer Radiother.* 6 Suppl 1, 29s-31s (2002).

[37] Ling CC, Humm J, Larson S, *et al*. Towards multidimensional radiotherapy (MD-CRT): biological imaging and biological conformality. *Int. J. Radiat. Oncol. Biol. Phys.* 47, 551-560 (2000).
**** Review of the present and the future of biological imaging for radiotherapy treatment design.**

[38] Van de Wiele C, Lahorte C, Oyen W, *et al*. Nuclear medicine imaging to predict response to radiotherapy: a review. *Int. J. Radiat. Oncol. Biol. Phys.* 55, 5-15 (2003).

[39] Chao KS, Bosch WR, Mutic S, *et al*. A novel approach to overcome hypoxic tumor resistance: Cu-ATSM-guided intensity-modulated radiation therapy. *Int. J. Radiat. Oncol. Biol. Phys.* 49, 1171-1182 (2001).

[40] Daisne JF, Sibomana M, Bol A, Cosnard G, Lonneux M, Gregoire V. Evaluation of a multimodality image (CT, MRI and PET) coregistration procedure on phantom and head and neck cancer patients: accuracy, reproducibility and consistency. *Radiother. Oncol.* 69, 237-245 (2003).

[41] De Neve W, Duthoy W, Claus F, *et al*. Dose conformation in IMRT for head and neck tumors: which solution to apply? *Cancer Radiother.* 6 Suppl 1, 32s-36s (2002).

[42] Parsons JT, Bova FJ, Fitzgerald CR, Mendenhall WM, Million RR. Severe dry-eye syndrome

following external beam irradiation. *Int. J. Radiat. Oncol. Biol. Phys.* 30(4), 775-780 (1994)

[43] Bessel EM, Henk JM, Whitelocke RA, Wright JE. Ocular morbidity after radiotherapy of orbital and conjunctival lymphoma. *Eye* 1(Pt 1), 90-96 (1987)

[44] Letschert JG, Gonzalez Gonzalez D, Oskam J *et al*. Results of radiotherapy in patients with stage I orbital non-Hodgkin's lymphoma. *Radiother. Oncol.* 22(1), 36-44 (1991)

[45] Morita K, Kawabe Y. Late effects on the eye of conformation radiotherapy for carcinoma of the paranasal sinuses and nasal cavity. *Radiology* 130(1), 227-232 (1979)

V. 2. Intensity modulated radiation therapy for oropharyngeal and oral cavity tumors: clinical use and experience.

Authors: F. Claus, W. Duthoy, T. Boterberg, W. De Gersem, J. Huys, H. Vermeersch and W. De Neve.

Journal: Oral Oncology 2002; 38(6):597-604

Acknowledgements: The project ‘‘Conformal Radiotherapy Ghent University Hospital’’ is supported by the Belgische Federatie tegen Kanker and by grants of the Fonds voor Wetenschappelijk Onderzoek Vlaanderen (grants FWO G.0049.98, G.0039.97), the University of Ghent (BOF 01112300, 011V0497, 011B3300), the Sportvereniging tegen Kanker and the Centrum voor Studie en Behandeling van Gezwelziekten. F. Claus and W. Duthoy are Research Assistants of the FWO. The Ghent University Hospital is a member of the Elekta IMRT Consortium.

Key issues discussed in this paper:

- IMRT was first implemented for re-irradiation of locoregional relapse of HNC, and later on for the primary treatment of patients with a HNC arising from the oropharynx or oral cavity.
- The delineation and planning strategies are presented. For the group of patients who were treated with IMRT as primary radiotherapy, two consecutive phases were used.
- Acute toxicity and treatment outcome are reported for the two separate groups of patients. The possibility of parotid sparing was explored and confirmed.
- The importance of clear delineation guidelines is emphasized, as this can have a large impact on the possibility of sparing of OARs, like the parotid gland.

Intensity modulated radiation therapy for oropharyngeal and oral cavity tumors : clinical use and experience

Filip Claus[1]*, M.D., Wim Duthoy[1], M.D., Tom Boterberg[1], M.D., PhD.,
Werner De Gersem[1], Ir., John Huys[1], M.D., PhD., Hubert Vermeersch[2], M.D.
and Wilfried De Neve[1], M.D., PhD.

[1]Division of Radiotherapy, Ghent University Hospital, Belgium
[2]Department of Head and Neck Surgery, Ghent University Hospital, Belgium

Abstract

Background and purpose : Intensity modulated radiation therapy (IMRT) offers an opportunity to generate dose distributions highly conformal to the target volume. Head and neck cancer patients, referred for radiotherapy, may be good candidates to benefit from IMRT. This paper discusses the clinical implementation of IMRT for oropharyngeal and oral cavity tumors, and reports the clinical results of the 14 patients treated with this technique at Ghent University Hospital (GUH).
Patients and Methods : Between May 1999 and May 2001, 14 patients were treated with IMRT at GUH for oropharyngeal or oral cavity tumors. Two groups of patients can be distinguished. The first group consists of 8 patients re-irradiated with IMRT for a locoregional relapse. The second group of 6 patients were treated with IMRT for a primary tumor. For the first group, IMRT was used to treat the relapse by generating a concave dose distribution, i.e. to combine a homogeneous target re-irradiation with a dose to the spinal cord as low as possible. For the second group, IMRT was applied in order to achieve a more homogeneous dose distribution inside the PTV and to preserve parotid gland function.
Results : The majority of the patients of group 1 (6/8) relapsed in field within 4 months after the end of the re-irradiation, with a median overall survival of 7 months. For group 2, two patients died shortly after the end of the IMRT treatment, the other 4 patients are free of tumor relapse with a median follow-up of 5 months (1-13 months). The acute toxicity due to radiation was acceptable for both patient groups. Dysphagia and pain was more present in group 1. Regarding late complications for the group of re-irradiations (group 1), no myelitis, carotid rupture or cranial nerve palsy was observed. One patient of group 1 developed osteoradionecrosis of the mandible and feeding tube dependency was present for another patient. No fatal late complications were observed in this group. For the first two patients of group 2, sparing of the parotid function was not a treatment objective. For the other patients of group 2, the mean dose to the contralateral parotid gland ranged from 17 to 25 Gy, which resulted in a decrease of subjective symptoms of xerostomia compared to patients treated with conventional radiotherapy.
Conclusions : The implementation of IMRT for oropharyngeal and oral cavity tumors results in a homogeneous target irradiation and allows to re-irradiate locoregional relapses with acceptable adverse effects. Sparing of the parotid gland by IMRT is feasible, although this may be significantly influenced by the delineation method of the elective lymph node regions.

Introduction

Head and neck cancer patients may be good candidates to benefit from intensity modulated radiation therapy (IMRT). IMRT offers the opportunity to improve the planning target volume (PTV) dose homogeneity by omitting photon-electron matchplanes, and in selected cases, to decrease xerostomia by sparing one or more of the major salivary glands. However, due to the complexity of implementing IMRT for this region, few clinical results are reported yet, and most of the data consist of very small patient series [1][3][8][9][10][13][16][22]. IMRT is often delivered in combination with conventional techniques [15], or its use is restricted to a boost to the primary tumor region [21].

By May 2001, 85 head and neck patients were treated with IMRT at Ghent University Hospital (GUH). Initially, IMRT was the treatment modality of choice to re-irradiate locoregional relapses or second primary head and neck cancers [10]. In a second phase, IMRT was applied as primary treatment. For pharyngeal and oral cavity tumors, the rationale to use IMRT was to increase the dose homogeneity inside the target volume and to preserve parotid function.

This paper discusses a clinical implementation of IMRT for oropharyngeal and oral cavity tumors.

Patients and Methods

Between May 1999 and May 2001, 14 patients were treated with IMRT at GUH for oropharyngeal or oral cavity tumors. Two groups of patients can be distinguished. The first group consists of 8 patients re-irradiated with IMRT for a locoregional relapse. The second group of 6 patients was treated with IMRT for a primary tumor.

group 1 : IMRT for locoregional relapses

Treatment objectives

For all patients, the dose to the spinal cord by the first radiotherapy treatment ranged between 40 and 50 Gy, delivered by 2 Gy fractions (5 days/week). IMRT was used to treat the relapse by generating a concave dose

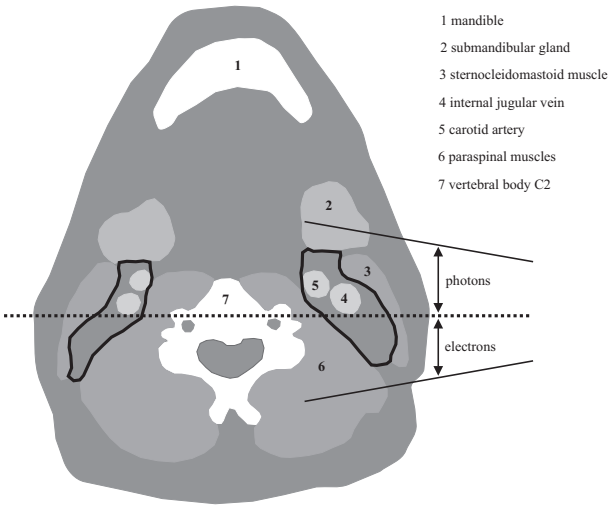

Figure 1: Drawing of a transverse section through the bottom level of the second cervical vertebral body, illustrating the photon-electron match line (black dotted line), located in the middle of the upper jugular lymph node chain, outlined in solid black.

distribution, i.e. to combine a homogeneous target re-irradiation with a dose to the spinal cord as low as possible.

The maximal dose to the spinal cord imposed by the IMRT plan was 15 Gy. The PTV dose prescription ranged between 64 and 70 Gy. For the dose homogeneity within the PTV, the ICRU (International Commission on Radiation Units and Measurements) guidelines were followed, i.e. a maximal underdosage of 5 % and maximal overdosage of 7 %. In case of overlap or close vicinity of the PTV and the spinal cord, the dose constraint to the spinal cord was respected, at the cost of the PTV dose homogeneity. Dose to the mandible was penalized by plan optimization, but no dose constraints were specified upfront as treatment objectives.

Planning strategy

Our IMRT planning strategy for locoregional relapses of head and neck cancer is previously reported [9][10]. The IMRT plans consisted of six non-opposed coplanar 6 MV photon beams, for which the individual multileaf collimated beamparts (segments) were optimized by adapting leaf positions and segment weights [7], using a biophysical cost func-

Table 1: Selection and dose prescription of lymph node target volumes

lymph node region	selection criterion	ipsi-bilateral	dose (Gy)
Ia	if evidence clinical invasion floor of mouth or region Ib	ipsilateral*	60
Ib	target in all cases	ipsilateral*	60
II	target in all cases	bilateral	60
III	target in all cases	bilateral	50-60**
IV	target in all cases	bilateral	50-60**
V	if clinical evidence invasion regions II or III or IV	ipsilateral	60
retropharyngeal	target in all cases	bilateral	60

* : bilateral if tumor crosses the midline

** : 60 Gy if first elective station, 50 Gy if second or third elective station

tion [11]. Treatments were delivered within a time slot of 15 minutes on an Elekta Sli-plus accelerator.

group 2 : IMRT as primary radiotherapy

Treatment objectives

Conventional radiotherapy for elective node irradiation of head and neck cancer patients at GUH consisted of two lateral fields and an anterior supraclavicular field, delivered with a single isocenter technique [20]. At a dose of 44 Gy, the spinal cord was blocked, and the target region not covered by the photon beams was boosted with electron beams. Figure 1 shows the location of the matchplane (dotted line) between a lateral photon and electron beam in a transverse plane through the body of the second cervical vertebra. The matchplane is situated in the middle of the upper jugular lymph node chain. Initially, IMRT was used to avoid electron-photon matching. In a second phase, preservation of the parotid gland function was also intended.

For the part of the PTV that is located outside build-up regions and outside regions where PTV overlaps with organs at risk (OARs), the ICRU guidelines for dose homogeneity were followed. The region of the PTV that extends close to the skin in the build-up region, is carefully analyzed. If underdosage is clinically unacceptable, bolus material is used. A clinical decision is also made regarding overlap areas of PTV and OARs. If the OAR function is to be preserved, a PTV underdosage restricted to the overlap zone which is consistent with OAR function preservation, is accepted. When parotid gland function had to be preserved, the mean dose to the contralateral parotid gland was limited to 26 Gy. This dose threshold was based on previous data published by Eisbruch et al. [12].

Current planning strategy

Entrance criteria for patients included

Since December 2000, following entrance criteria are specified to include patients for IMRT. For oropharyngeal cancer, stages T1-3 N0-2b M0 are included, for oral cavity cancer, the stages T1-T4 N0-2b M0. The expected median survival has to exceed 1 year, and the Karnofsky performance status has to be more than 50.

Treatment protocol

Table 1 specifies the selection of lymph node target volumes, and the prescribed dose to these volumes, as used for the IMRT plans. The terminology for lymph node regions as proposed by Robbins et al. [19] is used in the table.

The clinical target volume is 3D-isotropically expanded with a margin of 3 mm to a PTV, to take into account setup-inaccuracies during treatment delivery. A reduced PTV, excluding the region within a distance of 6 mm from the skin outline, is used for plan optimization and dose prescription. By excluding the build-up region from the PTV, conflicts during plan

Table 2: Group 1 : patients treated with IMRT for locoregional relapses

case	age* (y)	subsite primary	TNM primary	histology grade (G)	surgery /chemo	start radiation	dose** (Gy)	subsite relapse	TNM relapse	surgery /chemo	start IMRT	dose** (Gy)
1	56	floor of mouth	pT4pN0M0	SCC G3	y / n	01/10/97	50	soft palate	r cT4cN0M0	n / n	18/05/99	66
2	51	retromolar area	pT3pN0M0	SCC G2	y / n	23/10/98	60	retromolar area, tongue, tonsil	r cT4cN0M0	n / y	13/12/99	64
3	51	floor of mouth, tongue	cT2cN0M0	SCC G3	n / n	24/01/99	65	retromolar area, submandibular nodes	r pT4pN2bM0	y / n	21/12/99	64
4	52	uvula	cT1cN0M0	SCC G3	n / n	01/03/99	70	cranial jugular nodes, retropharyngeal nodes	r cTxcN3M0	n / n	27/01/00	66
5	55	floor of mouth	pT1pN0M0	SCC G1	y / y	03/05/96	56	floor of mouth, tonsil, cranial jugular nodes	r cT4cN3M0	n / y	10/03/00	66
6	40	cheek mucosa	pT4pN0M0	muco-epidermoid carcinoma	y / n	08/04/99	60	cheek mucosa, posterior wall, submandibular nodes	pT4pN1M0	y / n	13/03/00	70
7	59	floor of mouth	cT1cN0M0	SCC G2	n / n	07/07/99	84***	floor of mouth, tonsil, retromolar area, tongue	r pT4pN0M0	y / n	05/09/00	70
8	49	floor of mouth, tongue	pT2pN0M0	SCC G3	y / n	27/09/99	50	floor of mouth, tongue	r cT3cN2cM0	n / n	19/03/01	70

Abbreviations: *y*: year; SCC: squamous cell carcinoma

* at time of analysis (July 2001) **dose to the primary tumor site ***includes brachytherapy dose

optimization and a potential impossibility to achieve the ICRU guided PTV dose homogeneity are avoided. Dose is reported for the complete as well as for the reduced PTV.

Before December 2000, dose prescriptions were made on a patient-individual basis (patients 1-4 in table 3). Since December 2000, a treatment protocol was applied.

Three PTVs with corresponding dose prescriptions are specified :

PTV-70 :

- the primary tumor and lymph nodes containing clinical or radiological evidence of disease, treated to 70 Gy
- the median PTV-70 dose is used for dose prescription
- the tolerated dose range inside this PTV-70 is 66 to 75 Gy
- the 3D-maximum dose has to be located inside this PTV-70

PTV-60 :

- elective lymph node regions treated to a dose of 60 Gy
- the selection criterium is specified in table 1
- the median PTV-60 dose is used for dose prescription
- the tolerated dose range inside this PTV-60 is 57 to 65 Gy

PTV-50 :

- elective lymph node regions treated to a dose of 50 Gy
- the selection criterion is specified in table 1
- the minimum PTV-50 dose is used for dose prescription (i.e the minimum PTV-50 dose is 50 Gy)

When we elected to spare a parotid gland, it was a planning goal to keep its mean dose below 26 Gy [12]. The dose constraints for the spinal cord and brainstem were respectively set to 50 and 60 Gy, with a maximum daily fraction size of 2 Gy.

The IMRT treatment is delivered in two consecutive phases. The first phase consists of 27 fractions of 1.85 Gy to PTV-50 and 2.22 Gy to PTV-60 and PTV-70. In a second phase, 5 fractions of 2 Gy were delivered to PTV-70.

The beam setup consists of six non-opposed coplanar 6 MV photon beams, for which the individual multileaf collimated segments are computer-generated [6] and optimized by adapting leaf positions and segment weights [7], using a biophysical cost function [11]. Treatments are delivered within a time slot of 15 minutes on an Elekta Sli-plus accelerator.

Patients

Table 2 and 3 list the 14 patients. All of them were treated with curative intent.

Results

Table 4 reports the clinical results for the 14 patients. The follow-up was recorded from the end of the IMRT treatment till the time of analysis (July 2001).

The first 6 patients of group 1 relapsed in field within 4 months after the end of the re-irradiation. For patients 4 and 5, residual disease was present at the end of the IMRT treatment. Patients 7 and 8 of group 1 are still free of disease. The median overall survival for the patients of this group (measured as the time after the end of the treatment) is 7 months.

For group 2, two patients (patient 1 and 2) died shortly after the end of the IMRT treatment. Patient 1 died one month after the end of the concomittant chemo-radiotherapy treatment, due to a candida sepsis. Patient 2 developed a tumor relapse in the contralateral lymph node region II, which was not treated by the previous radiotherapy (the patient was treated before December 2000, and thus not according to the current IMRT treatment protocol). He died four

Table 3: Group 2 : patients treated with IMRT for primary lesions

case	age* (y)	subsite primary	TNM staging primary	histology grade (G)	surgery / chemo	start date radiotherapy	dose** (Gy)	parotid sparing treatment goal
1	43	tonsil, posterior wall	cT4cN2cM0	SCC G2	n / y	24/12/1999	70	no
2	58	retromolar area	pT2pN2bM0	SCC G3	y / n	03/02/2000	60	no
3	53	tonsil, tongue	cT3cN2bM0	SCC G1	n / n	17/03/2000	70	yes
4	47	tonsil	pT2pN1M0	SCC G3	y / n	06/11/2000	66	yes
5	67	tonsil, soft palate	pT3pN1M0	SCC G1	y / n	14/12/2000	70	yes
6	61	tonsil	pT2pN1M0	SCC G2	y / n	20/03/2001	70	yes

* at time of analysis (July 2001) **dose to the primary tumor site

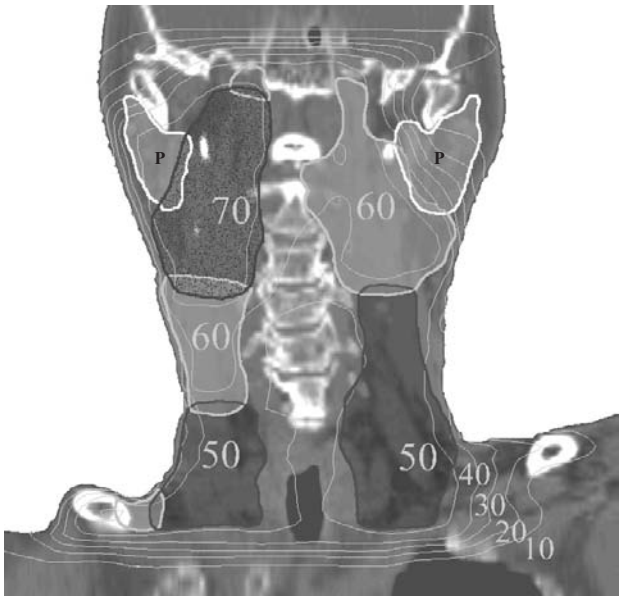

Figure 2: Dose distribution in a coronal plane of the IMRT treatment plan for patient 6 of the second group, illustrating the intended sparing of the left parotid gland. The isodose lines, expressed in Gy, represent the cumulative dose for the two treatment phases. The PTV-50 is coloured in transparent dark grey, the PTV-60 in transparent light grey and the PTV-70 in black speckles. The parotid glands are outlined in white and designated with the capital P.

months after the end of the radiation treatment. Patients 3-6 are free of tumor relapse, with a median follow-up of 5 months (1-13 months).

To score the acute toxicity due to radiation, the Common Toxicity Criteria (CTC) of the NIH (The US National Institutes of Health) were used (information on http://ctep.info.nih.gov/CTC3). Weight loss was less than 10 % for all patients, except for the second patient of group 1 (15 %). Radiation dermatitis was mild (dry desquamation) to moderate (patchy moist desquamation) for 13 patients, and confluent moist for the first patient of group 1. Pain due to radiation was more present in group 1. Pain due to radiation was mild and not interfering with function for 2 patients, moderate for 8 patients and severe (interfering with activities of daily living) for 4 patients. Mucositis was mild (erythema) for only 2 patients, patchy pseudomembranous for 6 patients and confluent pseudomembranous for 6 patients. Pharyngeal dysphagia was mild (patient could eat regular diet) to moderate (requiring predominantly pureed, soft, or liquid diet) for 12 patients. Two patients suffered from severe dysphagia, requiring feeding tube and IV hydratation.

Regarding late complications for the group of reirradiations (group 1), no myelitis, carotid rupture or cranial nerve palsy was observed. Patient 7 of group 1 developed osteoradionecrosis of the mandible. Feeding tube dependency was present for patient 7. All patients had neck fibrosis and two of them suffered from hearing loss. No fatal late complications were observed in this group.

For the first two patients of group 2, sparing of the parotid function was not a treatment objective. For patients 3-6, the mean dose to the contralateral parotid gland ranged from 17 to 25 Gy, which resulted in a decrease of subjective symptoms of xerostomia compared to patients treated with conventional radiotherapy. No functional tests or saliva flow measurements were performed. Figure 2 shows the dose distribution in a coronal plane of the treatment

Table 4: Results of the IMRT treatments for group 1 and 2

category	**group 1 : relapses**								**group 2 : primaries**					
case	1	2	3	4	5	6	7	8	1	2	3	4	5	6
common toxicity criteria : peak score (grade)														
weight loss	0	2	0	1	0	1	1	0	1	1	1	1	1	0
radiation dermatitis	1	1	2	1	1	2	1	2	3	2	1	1	3	2
pain due to radiation	3	3	3	3	2	2	2	2	2	2	1	1	2	2
mucositis due to radiation	1	3	3	2	2	2	2	2	3	3	2	1	3	3
dysphagia due to radiation	2	3	2	2	2	2	3	1	2	1	1	1	2	1
(second) relapse / survival														
relapse	yes	yes	yes	yes	yes	yes	no	no	no	yes	no	no	no	no
in field relapse	yes	yes	yes	yes	yes	yes	no	no	no	no	no	no	no	no
time to relapse (months)	1	2	4	0*	0*	4	/	/	/	1	/	/	/	/
cancer-related death	yes	yes	yes	yes	yes	yes	no	no	no	yes	no	no	no	no
non-cancer-related death	no	no	no	no	no	no	no	no	yes	no	no	no	no	no
time to death (months)	12	3	11	7	7	7	/	/	1	4	/	/	/	/

* : residual disease

plan for patient 6 of group 2, illustrating the intended sparing of the left parotid gland.

Discussion

As previously reported [5], the overall survival for high dose re-irradiations of head and neck cancer remains poor, and is associated with a lower rate of local tumor control compared to tumors of similar stage treated with primary radiotherapy. Although re-irradiations for locoregional relapses are associated with a poor prognosis, IMRT is a good technique to combine a high tumor dose with acceptable toxicity grades. The osteoradionecrosis of the mandible observed in patient 7 of group 1, may be explained by the high cumulative dose (154 Gy) of both treatment plans and the use of brachytherapy for the first radiation treatment.

For primary radiotherapy, IMRT allows a higher dose homogeneity inside the PTV by avoiding photon-electron matching. Another advantage is the possibility and feasibility of IMRT to preserve uni- or bilateral parotid gland function [12][4][23].

A strategy to treat 3 dose prescription levels with 2 consecutive treatment phases reduces the planning workload and results for the macroscopically invaded regions and the first elective lymph node stations in a radiobiological advantage, because of a higher fraction size (2.22 Gy) with shortening overall time [17].

The use of a fixed beam-setup and a fixed set of parameters for beam segmentation and plan optimization, allows to automate the generation of IMRT plans and guarantees a plan deliverable within a specified time slot.

The bottle-neck of the treatment planning process is the delineation of the clinical target volumes. The implementation of IMRT for head and neck cancer has lead to an increased interest in guidelines for delineation of lymph node regions. Especially the definition to outline lymph node region II may affect, or even determine the feasibility to preserve the parotid function by conformally irradiating this lymph node region. Figure 3 displays the difference in delineation guidelines for this region in a transverse plane, as proposed by Gregoire et al. [14] (solid white line) and Nowak et al. [18] (dashed white line). In a coronal plane, the difference is even more striking, as illustrated by figure 4.

The cranial border of lymph node region II, as defined by Gregoire, is the bottom edge of the body of the first cervical vertebra (C1), whereas Nowak defines the cranial border as the cranial CT-slice (in a transverse plane) through C1. These differences in contouring may affect cure rates of the radiation treat-

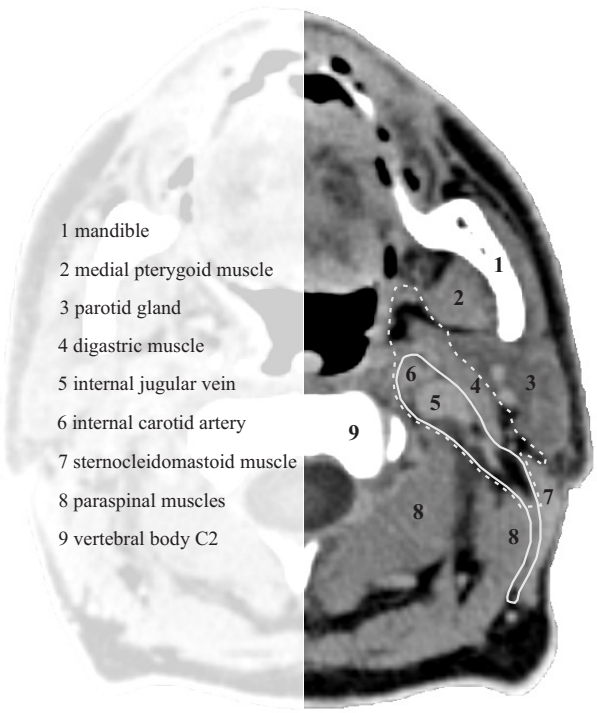

Figure 3: Transverse CT-slice through the second cervical vertebral body illustrating two different approaches to delineate lymph node region II. In white solid line the delineation as defined by Gregoire et al., in white dashed line the guidelines proposed by Nowak et al.

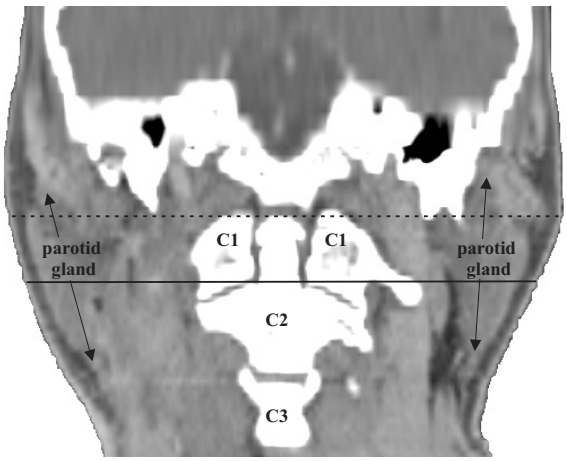

Figure 4: A coronal reconstructed CT-image through the cervical vertebral bodies 1, 2 and 3 (C1,C2,C3). The black lines represent the cranial edge of the target volume for lymph node region II, as respectively defined by Gregoire et al. (solid line) and Nowak et al. (dashed line). The black solid lines with arrows indicate the craniocaudal extent of the parotid glands.

ment, but certainly affect the plantechnical feasibility to limit dose to a certain volume of the parotid gland. The validity of the two proposed guidelines needs to be confirmed in larger patient series. For our IMRT implementation, we follow the guidelines proposed by Gregoire, except for the cranial border of lymph node region II, which we define at the middle of the body of C1.

Dawson et al. [4] reported the patterns of locoregional recurrence following parotid-sparing radiotherapy. This sparing was achieved by limiting the dose to the contralateral parotid gland. The superior extent of the contralateral lymph node region II, was defined as the axial CT image in which the posterior belly of the digastric muscle crosses the jugular vein. This corresponds to the superior extent of a radical neck dissection. The ipsilateral superior extent was set at the base of the skull. They examined 58 patients, and the eligibility criteria for the parotid-sparing protocol were patients who required radiotherapy to the primary tumor and bilateral neck lymph nodes. Patients with suspicion of contralateral neck disease were included as long as the jugulodigastric and higher neck nodes did not contain metastases. The median time from treatment to follow-up was 27 months. They found that the majority of locoregional relapses after parotid-sparing radiotherapy were in-field, and none of the relapses occurred in the contralateral high level of lymph node region II. These data support a rationale to implement IMRT to preserve salivary gland function by sparing the contralateral parotid gland.

Chao et al. [2] reported 27 patients treated with IMRT, most of them nasopharyngeal and oropharyngeal cases. Bilateral sparing of the parotid glands was a treatment objective, and the average dose to the parotid gland was 28 Gy for the postoperative cases and 30 Gy for the patients receiving IMRT as definitive treatment. The jugular chain (level II-IV) was target volume for all cases, but there was no specification with regard to their lymph node delineation method. Disease free survival rates were not reported.

In conclusion, the implementation of IMRT for oropharyngeal and oral cavity tumors results in a homogeneous target irradiation and allows to re-irradiate locoregional relapses to high doses with acceptable adverse effects. Sparing of the parotid gland by IMRT is feasible, although this may be significantly influenced by the delineation method of the elective lymph node regions. Sparing of the ipsilateral gland remains a topic of debate.

References

[1] Butler EB, Teh BS, Grant WH, Uhl BM, Kuppersmith RB, Chiu JK, Donovan DT, Woo SY. Smart (simultaneous modulated accelerated radiation therapy) boost: a new accelerated fractionation schedule for the treatment of head and neck cancer with intensity modulated radiotherapy. Int. J. Radiat. Oncol. Biol. Phys. 1999;45(1):21-32.

[2] Chao KS, Deasy J, Markman J, Haynie J, Perez CA, Purdy JA, Low DA. A prospective study of salivary function sparing in patients with head-and-neck cancers receiving intensity-modulated or three-dimensional radiation therapy: initial results. Int. J. Radiat. Oncol. Biol. Phys. 2001;49:907-916.

[3] Chao KS, Low DA, Perez CA, Purdy JA. Intensity-modulated radiation therapy in head and neck cancers: The Mallinckrodt experience. Int J Cancer 2000;90(2):92-103.

[4] Dawson LA, Anzai Y, Marsh L, Martel MK, Paulino A, Ship JA, Eisbruch A. Patterns of local-regional recurrence following parotid-sparing conformal and segmental intensity-modulated radiotherapy for head and neck cancer. Int. J. Radiat. Oncol. Biol. Phys. 2000;46(5):1117-1126.

[5] Dawson LA, Myers LL, Bradford CR, Chepeha DB, Hogikyan ND, Teknos TN, Terrell JE, Wolf GT, Eisbruch A. Conformal re-irradiation of recurrent and new primary head-and-neck cancer. Int. J. Radiat. Oncol. Biol. Phys. 2001;50(2):377-385.

[6] De Gersem, W., Claus, F., De Wagter, C. and De Neve, W. An anatomy based beam segmentation tool for intensity modulated radiation therapy and its application to head and neck cancer. Int. J. Radiat. Oncol. Biol. Phys. (accepted for publication).

[7] De Gersem, W., Vakaet, L., Claus, F., Remouchamps, V., Van Duyse, B. and De Neve, W. MLC leaf position optimization using a biophysical objective function. Radiother. Oncol. 2000;56(suppl.1):S96-S97 abstract 348.

[8] De Neve W, Claus F, Van Houtte P, Derycke S, De Wagter C. Intensity modulated radiotherapy with dynamic multileaf collimator. Technique and clinical experience. Cancer Radiother 1999;3(5):378-92.

[9] De Neve W, De Wagter C, De Jaeger K, Thienpont M, Colle C, Derycke S, Schelfhout J. Planning and delivering high doses to targets surrounding the spinal cord at the lower neck and upper mediastinal levels: static beam-segmentation technique executed by a multileaf collimator. Radiother Oncol 1996;40:271-279.

[10] De Neve W, De Gersem W, Derycke S, De Meerleer G, Moerman M, Bate MT, Van Duyse B, Vakaet L, De Deene Y, Mersseman B, De Wagter C. Clinical delivery of intensity modulated conformal radiotherapy for relapsed or second-primary head and neck cancer using a multileaf collimator with dynamic control. Radiother Oncol 1999;50:301-314.

[11] De Neve, W., De Gersem, W., De Meerleer, G., Claus, F. and De Wagter, C. Reduction of target dose inhomogeneity in IMRT treatment planning using biological objective functions. Int. J. Radiat. Oncol. Biol. Phys. 2001;49:1519-1520.

[12] Eisbruch A, Ten Haken RK, Kim HM, Marsh LH, Ship JA. Dose, volume, and function relationships in parotid salivary glands following conformal and intensity-modulated irradiation of head and neck cancer. Int. J. Radiat. Oncol. Biol. Phys. 1999;45:577-587.

[13] Fraass BA, Kessler ML, McShan DL, Marsh LH, Watson BA, Dusseau WJ, Eisbruch A, Sandler HM, Lichter AS. Optimization and clinical use of multisegment intensity-modulated radiation therapy for high dose conformal therapy. Semin Radiat Oncol 1999;9(1):60-77.

[14] Gregoire V, Coche E, Cosnard G, Hamoir M, Reychler H. Selection and delineation of lymph node target volumes in head and neck conformal radiotherapy. Proposal for standardizing terminology and procedure based on the surgical experience. Radiother Oncol 2000;56(2):135-150.

[15] Hunt MA, Zelefsky MJ, Wolden S, Chui CS, LoSasso T, Rosenzweig K, Chong L, Spirou SV, Fromme L, Lumley M, Amols HA, Ling CC, Leibel SA. Treatment planning and delivery of intensity-modulated radiation therapy for primary nasopharynx cancer. Int. J. Radiat. Oncol. Biol. Phys. 2001;49(3):623-632.

[16] Kuppersmith RB, Greco SC, Teh BS, Donovan DT, Grant W, Chiu JK, Cain RB, Butler EB. Intensity-modulated radiotherapy: first results with this new technology on neoplasms of the head and neck. Ear Nose Throat J 1999;78(4):238, 241-6, 248 passim.

[17] Mohan R, Wu Q, Manning M, Schmidt-Ullrich R. Radiobiological considerations in the design of fractionation strategies for intensity-modulated radiation therapy of head and neck cancers. Int. J. Radiat. Oncol. Biol. Phys. 2000;46(3):619-630.

[18] Nowak PJ, Wijers OB, Lagerwaard FJ, Levendag PC. A three-dimensional CT-based target definition for elective irradiation of the neck. Int. J. Radiat. Oncol. Biol. Phys. 1999;45(1):33-39.

[19] Robbins KT, Medina JE, Wolfe GT, Levine PA, Sessions RB, Pruet CW. Standardizing neck dissection terminology. Arch Otolaryngol Head Neck Surg 1991;117:601-605.

[20] Sohn JW, Suh JH, Pohar S. A method for delivering accurate and uniform radiation dosages to the head and neck with asymmetric collimators and a single isocenter. Int. J. Radiat. Oncol. Biol. Phys. 1995;32(3):809-813.

[21] Sultanem K, Shu HK, Xia P, Akazawa C, Quivey JM, Verhey LJ, Fu KK. Three-dimensional intensity-modulated radiotherapy in the treatment of nasopharyngeal carcinoma: the University of California-San Francisco experience. Int. J. Radiat. Oncol. Biol. Phys. 2000;48(3):711-22.

[22] Verellen D, Linthout N, van den Berge D, Bel A, Storme G. Initial experience with intensity-modulated conformal radiation therapy for treatment of the head and neck region. Int. J. Radiat. Oncol. Biol. Phys. 1997;39(1):99-114.

[23] Wu Q, Manning M, Schmidt-Ullrich R, Mohan R. The potential for sparing of parotids and escalation of biologically effective dose with intensity-modulated radiation treatments of head and neck cancers: a treatment design study. Int. J. Radiat. Oncol. Biol. Phys. 2000;46(1):195-205.

V. 3. Postoperative intensity modulated radiotherapy in sinonasal carcinoma: clinical results in 39 patients.

Authors: W. Duthoy, T. Boterberg, F. Claus, P. Ost, L. Vakaet, S. Bral, F. Duprez, M. Van Landuyt, H. Vermeersch and W. De Neve.

Journal: Cancer 2005; 104(1):71-82

Acknowledgements: The project "Conformal Radiotherapy Ghent University Hospital" is supported by the Belgische Federatie tegen Kanker and by grants from the Fonds voor Wetenschappelijk Onderzoek (FWO) Vlaanderen (G.0183.03), the University of Ghent (GOA 12050401, BOF 01112300, 011VO497, 011B3300), and the Centrum voor Studie en Behandeling van Gezwelziekten. Werner De Gersem is acknowledged for his help in analyzing the dosimetric data. Wim Duthoy is a research assistant (aspirant) of the FWO.

Key issues discussed in this paper:

- A group of 39 consecutive patients with sinonasal carcinoma was treated with post-operative IMRT using a standard class solution. A detailed description of symptoms and patient and tumour characteristics is given.
- Dosimetrical analysis of the IMRT plans is given, using DVHs compiled from the whole group.
- Both acute toxicity and chronic toxicity are assesses and analysed.
- Local control, disease-free survival and overall survival are analysed for the IMRT group, and prognostic factors are identiefied. The IMRT results are compared with a historical cohort of sinonasal cancer patients, treated with conventional techniques or 3D-CRT.
- A literature review on elective lymph node irradiation in sinonasal is presented.

Post-operative intensity-modulated radiation therapy (IMRT) in sinonasal carcinoma: clinical results in 39 patients.

Wim Duthoy, M.D.[1], Tom Boterberg, M.D., Ph.D.[1], Filip Claus, M.D., Ph.D.[1,2], Piet Ost[1], Luc Vakaet, M.D., Ph.D.[1], Samuel Bral, M.D.[1], Frederic Duprez, M.D.[1], Marianne Van Landuyt, M.D.[1], Hubert Vermeersch, M.D., Ph.D.[3] and Wilfried De Neve, M.D., Ph.D.[1]

1. Department of Radiotherapy, Ghent University Hospital, De Pintelaan 185, 9000 Ghent, Belgium;
2. Present address: Department of Radiology, Memorial Sloan-Kettering Cancer Center, New York, NY 10021, USA;
3. Department of Head and Neck Surgery, Ghent University Hospital, De Pintelaan 185, 9000 Ghent, Belgium

Abstract

Purpose: Carcinoma of the paranasal sinuses is rare. Standard therapeutic modalities consist of surgery and radiotherapy (RT). Because of the often advanced stage and the vicinity of optic structures, RT-induced ocular toxicity is a feared side effect of conventional RT. Intensity-modulated radiation therapy (IMRT) is a relatively new radiation technique, which is implemented with the hypothesis that, compared with conventional RT, it would result in a lower rate of ocular toxicity for an equal local control (LC).

Methods and Materials: Between 1998 and 2003, 39 consecutive patients received postoperative irradiation by means of IMRT for an adenocarcinoma (n=31) or squamous cell carcinoma (n=8) of the paranasal sinuses (n=36) or nasal cavity (n=3). T-classification was T2 in 41%, T3 in 15%, T4a in 23% and T4b in 21% of patients. Invasion through the cribriform plate was seen in 11 patients. Orbital invasion was present in 36% of patients. The delivered dose ranged from 60 Gy to 70 Gy (median 70 Gy). The authors compared the overall survival (OS) and LC with a historical cohort (HC) (n=30), treated with conventional or 3-dimensional conformal RT.

Results: The median follow-up was 31 months. Actuarial OS rates were 68% at 2 years and 59% at 4 years. Actuarial LC rates were 73% at 2 years and 68% at 4 years. Invasion through the cribriform plate was a significant prognostic factor for LC and OS, with a median time to local disease recurrence of 7 months if present, and a 2-year LC rate of 90% if not present. In the comparison between the IMRT and the HC groups, no significant differences were found for LC and OS. Acute toxicity was mild. Two patients developed a decreased vision after RT. No RT-induced blindness was observed.

Conclusion: Postoperative IMRT for sinonasal carcinoma resulted in good LC, with a low acute toxicity and no RT-induced blindness.

Introduction

Carcinoma of the paranasal sinuses or the nasal cavity is a rare disease, representing 5% of all head and neck tumours, and less than 1% of all malignancies in Flanders in 1998 [1]. The treatment options for sinonasal carcinoma consist of combinations of surgery, radiotherapy (RT) and chemotherapy. The most applied strategy consists of extensive surgery, followed by RT [2, 3]. The reported 5-year overall survival (OS) rate varied from 30% to 79% [4, 5]. The wide range in reported treatment results might rather be a consequence of patient selection, than of the applied treatment strategy, and hinders the comparison between various treatment regimens. A major concern in the irradiation of sinonasal carcinoma is chronic toxicity to the optic pathways. The incidence of RT-induced blindness can be as high as 37% [6, 7, 8], and depends (among other factors) on irradiated volume, total dose and dose per fraction [9, 10, 11]. Intensity-modulated radiation therapy (IMRT) is a relatively new radiation technique, offering the possibility to create concave dose distributions [12]. This allows better sparing of the optic structures without compromising the dose in the target volume (Fig. 1). . Since July 1998, IMRT has been the standard treatment for sinonasal carcinoma at Ghent University Hospital (GUH; Ghent, Belgium) [13]. The hypothesis for the implementation of IMRT for sinonasal carcinoma was that it would result in a decrease in ocular toxicity, without compromising local control (LC). First, we report on the outcome results and acute and chronic toxicity in a group of patients who received post-operative RT by means of IMRT. Second, we compared patients with an adenocarcinoma of the ethmoid sinuses, treated postoperatively with IMRT, with patients treated with conventional RT.

Patients and Methods

Between July 1998 and August 2003, 39 consecutive patients were treated postoperatively for a histologically proven adenocarcinoma or squamous cell carcinoma (SCC) of the sinonasal cavities by means of IMRT at GUH. Median age at diagnosis was 62 years (range 30-78 years). The reported symptoms at the time of diagnosis were nasal obstruction in 26 patients, epistaxis in 14 patients, ocular symptoms in 6 patients, swelling of the cheek in 5 patients, and neurological symptoms in 3 patients. A history of occupational wood exposure was present in 24 patients, all of whom had an adenocarcinoma. Two patients were treated for a recurrence of an earlier tumour of the paranasal sinuses (1 with ethmoid sinus carcinoma and 1 with maxillary sinus carcinoma). These two patients were treated with surgery alone at the time of the first diagnosis. The (sub)site of the tumour was defined from the epicenter of the tumour mass, as observed on computed tomography (CT) and/or magnetic resonance imaging (MRI). In 30 patients, the subsite of origin was the ethmoidal sinus, the maxillary sinus in 6 patients and the nasal cavity in 3 patients. Histologic diagnosis was obtained in all patients, and showed adenocarcinoma in 31 patients and SCC in 8 patients. All patients were (partly retrospectively) staged using the 2002 TNM classification system [14]. A cross-tabulation among site, histology and T-classification is shown in Table 1. Of the patients classified with T4b tumours, all had invasion of the dura and/or brain. In the group of patients classified with T4a tumours, 4 patients had tumour extension through the cribriform plate (CP) with minimal invasion of the anterior cranial fossa. Macroscopic extension (with invasion of the external ocular muscles) into the orbital content was seen in 4 patients. Moderate orbital invasion (invasion of orbital fat, without muscle invasion) was present in 7 patients. Invasion of the lamina papyracea was seen in 3 patients, while bulging (without invasion) of the medial orbital wall was seen in another 3 patients. One patient had cervical lymph nodes for which he received a bilateral neck dissection. In this patient, the neck was included in the clinical target volume (CTV). All patients were free of distant metastasis at the time of diagnosis. The mean time between surgery and the start of RT was 48 days (range 25-89 days). The type of surgery was broad resection (via lateral rhinotomy) in 22 patients, maxillectomy in 5 patients, functional endoscopic resection in 4 patients, and craniofacial resection in 8 patients. Three patients underwent an orbital exenteration as part of

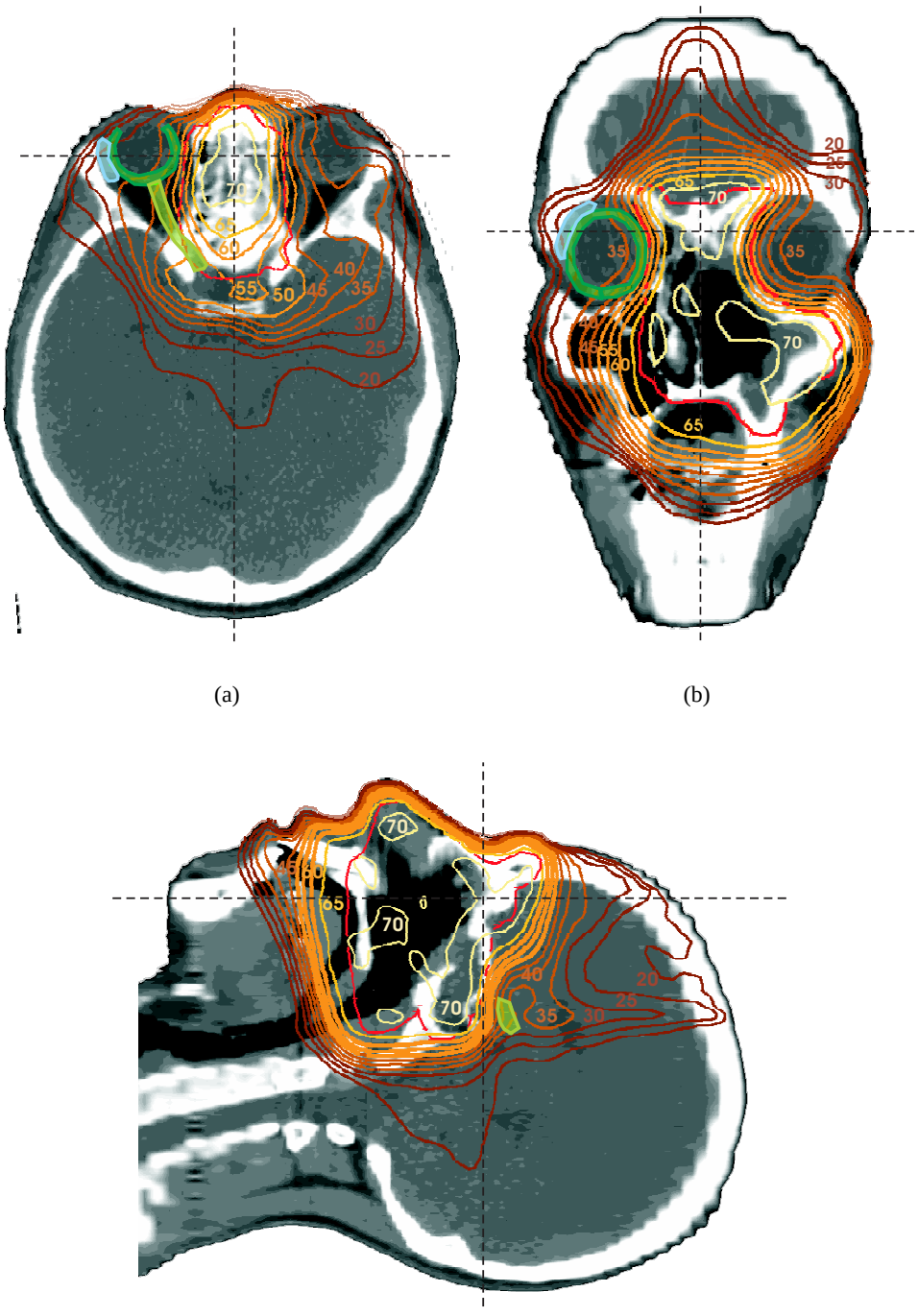

Figure 1: Dose distributions of a typical intensity-modulated radiation therapy plan for an ethmoid sinus carcinoma. Dose distributions are shown in a (a) transverse, (b) coronal and (c) sagittal plane. The planning target volume (PTV) is shown in red. For clarity, the right-sided retina (dark green), optic nerve (light green), and major lacrimal gland (blue) are depicted in panel (a) and (b). The optic chiasm (light green) is shown in (c). The dashed lines represent the level at which the other planes are shown. Isodose lines are in gray (Gy).

Table 1: T-classification per subsite and per histological type.

	Ethmoid sinus				Maxillary sinus			Nasal cavity			
Histology	T2	T3	T4a	T4b	T2	T3	T4a	T2	T3	T4	**Total**
Adeno	13	3	5	7	-	-	-	3	-	-	31
SCC	-	-	1	1	-	3	3	-	-	-	8
Total	13	3	6	8	-	3	3	3	-	-	39

Abbreviations: Adeno: adenocarcinoma; SCC: squamous cell carcinoma

the surgical procedure. Unless stated differently, all results presented in the "Results" section concern the 39 patients described above.

The historical cohort (HC) consisted of 30 patients, who were irradiated postoperatively for an adenocarcinoma of the ethmoid sinus between September 1985 and July 1998 at GUH. Clinical characteristics, treatment details and outcome of this group have been reported in more detail elsewhere [15]. The 1997 TNM classification [16] was used, and all patients diagnosed before 1997 were staged retrospectively. In the HC, there were 2 patients with a T1, 8 with a T2, 9 with a T3 and 11 patients with a T4 tumour. Three patients had cranial invasion. This HC was then compared with all patients with an adenocarcinoma of the ethmoid, treated with IMRT (n=28). The 1997 T-classification for the IMRT group was: T1= 0; T2= 13; T3= 4 and T4= 11. In the IMRT group, all T4 patients (n=11) had invasion through the CP.

Radiotherapy details

All patients were irradiated using IMRT during the entire RT treatment. The development and clinical implementation of IMRT for paranasal sinus carcinoma has been described earlier [13]. The CTV consisted of the resection cavity plus all paranasal sinuses which were (partially) invaded or neighbored invaded cavities. In case of minimal or moderate orbital invasion, the medial part (up to the rectus medialis muscle) of the orbit was included in the CTV. No elective irradiation of the cervical lymph nodes (ELNI) was performed. A 3-mm isotropic margin was used for the expansion from CTV to planning target volume (PTV). The optic structures, like retina, optic nerve and optic chiasm, were delineated on planning CT scans and expanded to a planning risk volume (PRV) with a margin of 2 mm. In regions where the PTV and the PRVs overlap, an underdosage of the PTV was tolerated, in order to fulfill the constraints for the optic structures [13]. Prescribed end-dose was 60 Gy in 4 patients and 66 Gy in 6 patients. For all subsequent patients, the prescribed end-dose was 70 Gy (median dose to the PTV), delivered in 35 fractions. Prescribed dose was not reached in 2 patients. Of these, 1 patient died after 21 fractions from complications of the craniofacial resection, and in 1 patient, RT was stopped after 26 fractions because of the histological diagnosis of liver metastases from a (rapidly evolving) small cell lung cancer (SCLC).

In the HC, 19 patients were irradiated using a conventional beam setup (one anterior beam, and two lateral wedged beams) up to doses of 61 to 70 Gy (median 65 Gy), with a fraction dose of 1.8 Gy. In 11 patients, a 3D conformal technique with non-coplanar beams was used. The prescribed dose in this group ranged from 54 to 66 Gy (median 66 Gy), and was delivered in 2 Gy fractions.

Follow-up (IMRT group)

During RT, patients were evaluated clinically at least weekly. Acute toxicity scoring was done using the Common Toxicity Criteria (CTC, version 2) of the US National Institutes of Health (NIH) (information on http://ctep.cancer.gov/reporting/ctc.html). For the first 16 patients, no prospective scoring was done, and only the presence of grade 2 toxicity or higher was reported in the patient files. Therefore, a distinction between grade 0 (no symptoms) and grade 1 (mild symptoms) could not be made. For conjunctivitis, dry eye, tearing, mucositis, dysphagia and radioder-

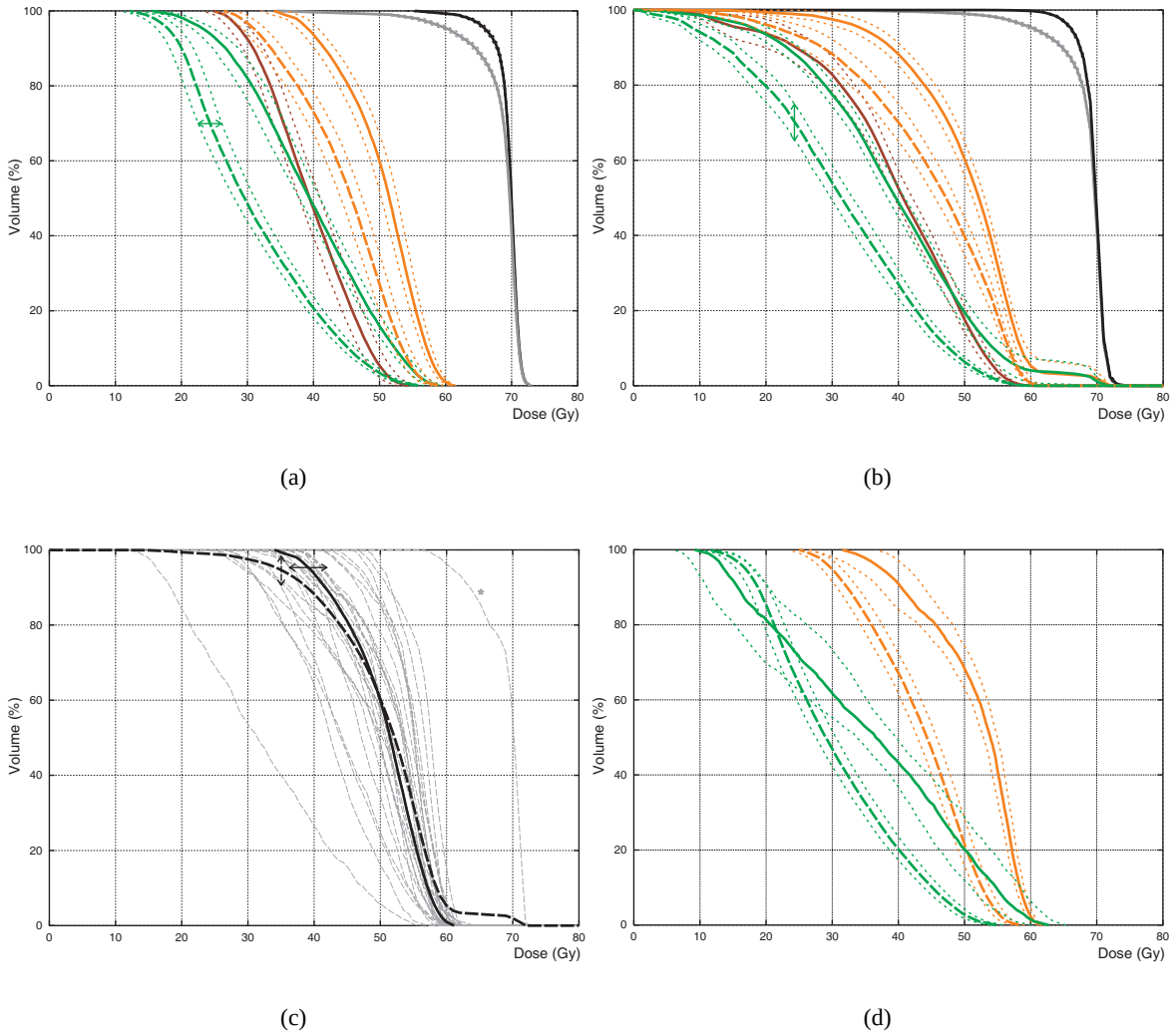

Figure 2: Compiled dose volume histograms (DVHs).
(a,b) Compiled DVHs for the following structures: clinical target volume (CTV; black), planning target volume (PTV; grey), optic chiasm (brown), ipsilateral (full line) and contralateral (dashed line) optic nerve (orange), and ipsilateral and contralateral retinae (green). All data concerning optic structures are for the expanded optic structures. DVHs are compiled from the data from the 29 patients that were planned to a dose of 70 Gy. As one of these patients underwent an ipsilateral orbital exenteration, the data for the ipsilateral optic nerve and retina are averaged over 28 patients. For each structure, the mean (bold line) and the standard error of the mean (SEM; dotted thin lines) are shown. In (a), the dose at every 1% volume level was calculated for each structure and for all patients. For each of these volume levels, the mean and the SEM over all 29 patients were calculated. The direction in which the spread around the mean value should be read is indicated by the arrow. The median, maximal and minimal dose, averaged over the 29 patients whom were planned to 70 Gy, can be read from this graph. In (b) the volume percentiles at every 1 Gy dose level were calculated for the same structures as in (a). The mean and the SEM over the 29 patients were calculated for each of the dose levels. Here, the spread around the mean should be read vertically (as indicated by the arrow). This graph shows the relative volume receiving a specified dose or more (e.g. on average, 6% $\pm$ 1% of the contralateral retina receives a dose > 50 Gy). (c) Graph showing all individual DVHs (thin grey lines) for the ipsilateral optic nerve. The full black DVH is calculated as in (a), while the dashed black line is calculated as in (b). This graph clarifies how these two ways of calculating a compiled DVH yield different results. The DVH indicated with an asterisk ($\star$) represents Patient 2 (see Table 5), for whom no attempt was made to spare the ipsilateral optic nerve. (d) Compiled DVHs for the optic nerves (orange) and the retinae (green) with (full lines) or without (dashed lines) chronic toxicity. DVHs are compiled for all patients without preexisting ocular disease, who completed their treatment course, and who had > 6 months of follow-up (n=33). DVHs are calculated according to the method described in (a).

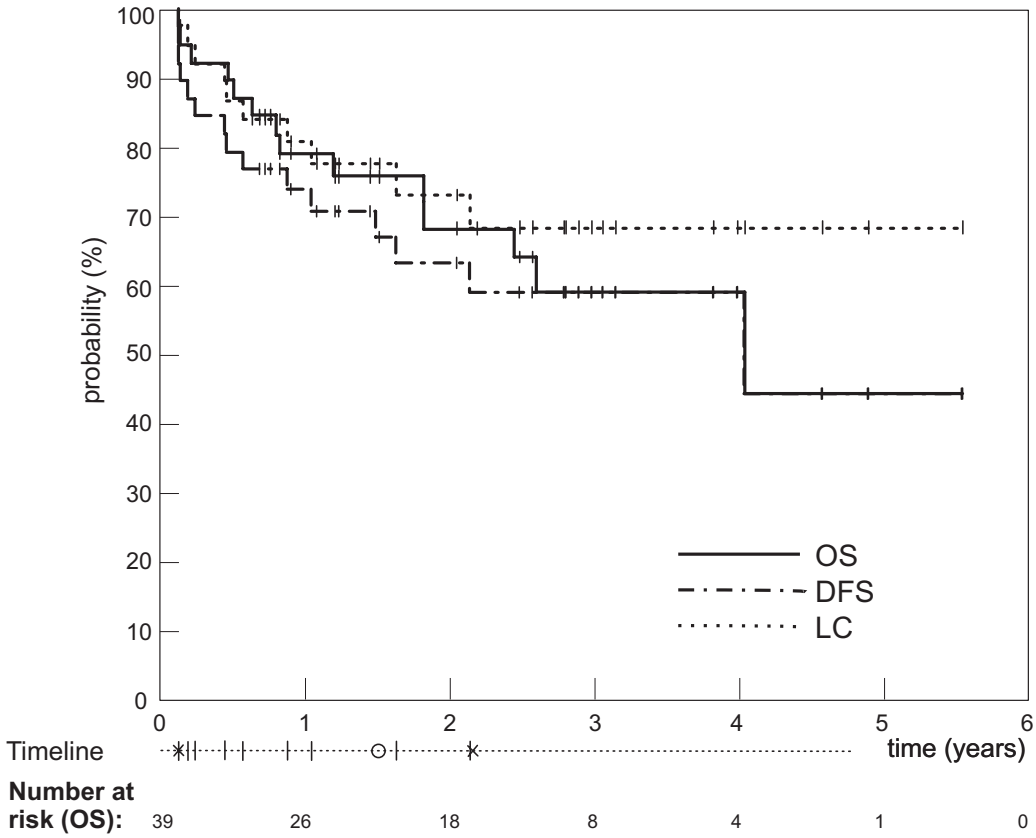

Figure 3: Overall survival (OS), Disease-free survival (DFS) and local control (LC) for all patients. A timeline is shown, indicating the time of local (|), regional (◯) and distant (×) recurrence.

mitis, a grade 1 score was assigned if no information was found concerning the specified symptom. For the subsequent 24 patients, a prospective scoring was done using a standard form. After completion of RT, patients were evaluated 1 month after the end of RT, and then every 3-4 months during the first 2 years and twice a year thereafter. Chronic ocular toxicity was prospectively scored according to the Lent/Soma scale [17]. In case of ocular symptoms, the patient was sent to an ophthalmologist for further investigation. Furthermore, a routine ophthalmologic examination was performed in 60% of patients without symptoms of chronic ocular toxicity. Patients who did not receive the prescribed radiation dose (n=2), or with a follow-up of less than 6 months (n=2) were excluded from the chronic toxicity analysis. No patient was lost to follow-up.

Statistical analysis

Overall survival (OS), disease-free survival (DFS), disease-specific survival (DSS) and local control (LC) were determined using the the Kaplan-Meier actuarial method. All analyses were calculated from the first day of RT. Events were defined as follows: OS: death from any cause; DFS: disease recurrence (local, regional or distant) or death from any cause (whatever came first); DSS: death due to cancer progression (local, regional or distant) and LC: local disease recurrence. Differences between subcategories were calculated using the log-rank test. A p-value <0.05 was considered statistically significant. For all statistical analyses, a standard software package (SPSS Inc., Chicago, IL) was used.

Table 2: Summary of the DVH data.

		Mean	SEM
PTV			
D_{med}	(Gy)	69.7	0.0
$V_{>95\%}$	(%)	87.3	0.9
CTV			
D_{med}	(Gy)	70.0	0.0
$V_{>95\%}$	(%)	95.2	0.6
Optic chiasm			
D_{med}	(Gy)	39.4	1.6
D_{max}	(Gy)	54.2	1.5
Optic nerve (ipsilateral)			
D_{med}	(Gy)	51.5	1.2
D_{max}	(Gy)	61.1	0.5
$V_{>60Gy}$	(%)	5.3*	3.4
Optic nerve (contralateral)			
D_{med}	(Gy)	45.8	1.6
D_{max}	(Gy)	58.8	0.9
$V_{>60Gy}$	(%)	0.6	0.2
Retina (ipsilateral)			
D_{med}	(Gy)	39.4	1.6
D_{max}	(Gy)	59.0	0.8
$V_{>55Gy}$	(%)	8.9*	3.3
Retina (contralateral)			
D_{med}	(Gy)	29.6	1.6
D_{max}	(Gy)	55.9	0.8
$V_{>55Gy}$	(%)	1.5	0.4

Abbreviations: D_{med}: median dose; $V_{>95\%}$: relative volume of the specified structure, receiving at least 95% of the prescribed dose; D_{max}: maximal dose; $V_{>60Gy}$: relative volume of the specified structure receiving more than 60 Gy.

*: This is due to one patient (Table 5, Patient 2). When omitting the patient, the $V_{>60Gy}$ for ipsilateral optic nerve is $1.9 \pm 0.6\%$, and the $V_{>55Gy}$ for the ipsilateral retina is $5.9 \pm 1.3\%$.

Results

IMRT planning results

Typical dose distributions for an IMRT plan are shown in Figure 1. The conformal avoidance of the optic nerves and retinae is readily visible in panel (a) and (b). The ability to create concave dose distributions is best illustrated in panel (b). In a sagittal plane (panel c), the relative underdosage of the optic chiasm is evident. Figure 2 shows the dosimetrical data on the patients treated with an end-dose of 70 Gy. The contralateral optic structures (retina and optic nerve) received a lower dose than the optic structures ipsilateral to the tumour. The underdosage in the PTV (on average, 12.7% of the PTV received less than 95% of the prescribed dose) is partly due to build-up, and partly due to the overlap of the PTV with the PRVs of the optic structures. A summary of these DVH data is given in Table 2.

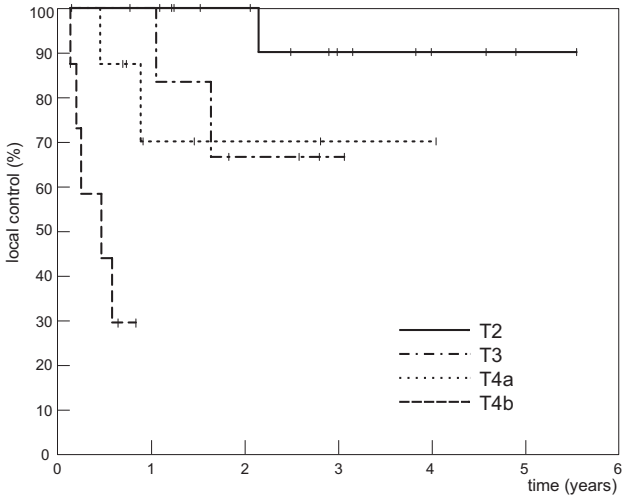

Figure 4: Local control by T-classification for all patients.

Survival and local control

IMRT group

The median follow-up in survivors was 31 months (range 9-67 months). The 2 and 4-year actuarial OS rates were 68% and 59%, respectively. The 2 and 4-year actuarial DFS rates were 63% and 59%, respectively. The corresponding LC rates were 73% and 68%. Actuarial OS, DFS and LC curves are shown in Figure 3. DSS rate was 74% at 2 years and 64% at 4 years. According to T-classification, the LC rate at 2 years was 100% for T2, 67% for T3 and 70% for T4a. For T4b lesions, the median duration of local control was 6 months. LC per T-classification is shown in Figure 4 . There was no statistically sig-

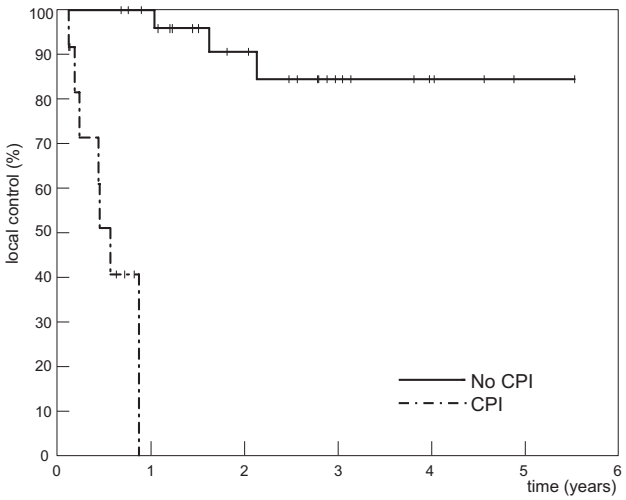

Figure 5: Local control in function of the presence of invasion through the cribriform plate (CP).

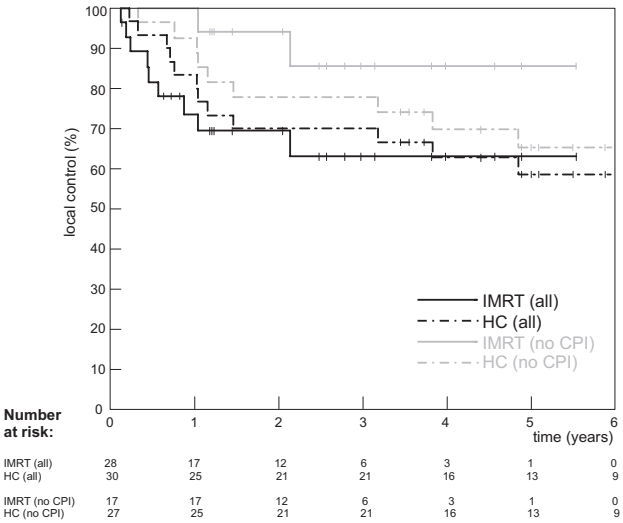

Figure 6: Local control for the patients treated with IMRT (solid lines) and the historical cohort (dashed lines). The black lines represent the data for all patients, while the grey lines represent the group of patients without invasion of the cribriform plate (="no CPI").

nificant difference in LC between T2, T3 and T4a lesions. Patients with a T4b tumour had a significantly worse LC than patients with a T2 ($p<0.001$), a T3 ($p=0.013$) and a T4a ($p=0.021$) lesion. Figure 5 shows the LC in function of the presence of invasion through the CP (with minimal extension into the anterior cranial fossa). CP invasion was a significant prognostic factor for both LC ($p<0.001$) and for OS ($p<0.001$). When only those patients without extension through the CP (n=27) were considered for analysis, the LC rate was 90% at 2 years, and 84% at 4 years. For patients who presented with extension of their tumour through the CP, the median time to local disease recurrence was 7 months.

At the time of analysis, 25 patients were alive. Eleven patients had died due to progression of the sinonasal carcinoma, and three had died due to other causes: one by complications of the craniofacial resection, one by intercurrent disease (exacerbation of chronic obstructive pulmonary disease) and one by a second primary cancer (SCLC). Of the 11 patients who died from sinonasal carcinoma progression, 2 patients died from distant metastasis, but were locally free of disease. For one patient, the diagnosis of bone metastasis was made at the end of the RT course, while in the other patient, brain metastases were diagnosed. This was 3 months after retreatment for a local disease recurrence. One patient died from disease due to isolated lymph node recurrence. Eight patients died due to local disease progression. The timing of local, regional and distant metastasis is shown in Figure 3. In total, ten patients developed a local disease recurrence during the follow-up period. The characteristics of these 10 patients are summarized in Table 3.

Comparison between IMRT group and HC

The median follow-up for survivors in the HC was 83 months. OS rates at 2 and 4 years were 65% and 58% for the IMRT group, and 83% and 66% in the HC ($p=0.25$). LC rates at 2 and 4 years were 69% and 63% for the IMRT group, and 70% and 63% for the HC ($p=0.72$). The LC in the HC and IMRT groups is shown in Figure 6. In the subselection of patients without extension through the CP, the 2 and 4-year OS rates were both 94% for the IMRT group, and 93% and 73% in the HC. This was not significantly different ($p=0.29$). For the same subselection, the LC rates at 2 and 4 years in the IMRT group were 94% and 86%, and in the HC, this was 78% and 70%, respectively ($p=0.28$).

Table 3: Tumour and local disease recurrence characteristics.[a]

	T-stage	CPI	Surgery	disease recurrence	Location
1	T4b	+	CFR	OF	temporal meninges
2	T3		LR	BF	bottom of orbita
3	T4b	+	CFR	IF	frontal lobe
4	T4b	+	CFR	BF	optic chiasm
5	T3		LR	-[c]	orbit, ethmoid, frontal lobe
6	T2		LR	IF	sphenoid and maxilla
7	T4a	+	ER[b]	IF	cranial to CP
8	T4b	+	CFR	-[c]	CNS invasion (clinically)
9	T4b	+	CFR	BF	frontal lobe
10	T4a	+	LR	IF	cranial to CP

Abbreviations: CPI: invasion of cribriform plate (CP); CFR: craniofacial resection; LR: lateral rhinotomy; ER: endoscopic resection; OF: out-of-field disease recurrence; BF: border-of-field disease recurrence; IF: in-field disease recurrence; CNS: central nervous system.

[a] Patients are sorted chronologically on the date of start of radiotherapy.

[b] Intraoperative tearing of the dura.

[c] Not evaluable.

Table 4: Highest acute toxicity during radiotherapy.

CTC-scaling	grade 0	grade 1	grade 2	grade 3
conjunctivitis	0 (0)	23 (59)	15 (38)	1 (3)[b]
dry eye	0 (0)	36 (92)	3 (8)	0 (0)
tearing	5 (13)	24 (62)	9 (23)	1 (3)[b]
blurred vision	34 (87)	-[a]	4 (10)	1 (3)[b]
photophobia	35 (90)	-[a]	3 (8)	1 (3)[b]
keratitis	36 (92)	-[a]	3 (8)	0 (0)
mucositis	0 (0)	21 (54)	11 (28)	7 (18)
dysphagia	7 (18)	21 (54)	11 (28)	0 (0)
radiodermitis	0 (0)	25 (64)	12 (31)	2 (5)

The percentages are given between brackets.

[a] For blurred vision, photophobia and keratitis, there is no definition of grade 1 in the CTC v2.

[b] This patient received amiodarone during radiotherapy

Acute toxicity

Acute toxicity scores are summarized in Table 4. One patient had grade 3 ocular toxicity (symptomatic conjunctivitis, tearing and photophobia, interfering with activities of daily living). For this patient, IMRT treatment had to be interrupted for 2 weeks. Twenty-one (54%) patients had any ocular grade 2 (symptomatic, not interfering with activities of daily living) as highest toxicity during RT treatment, and the remaining 17 patients (44%) had only grade 1 or lower ocular toxicity. Conjunctivitis and tearing were the most frequent ocular grade 2 toxicities seen during RT, in 38% and 23% of the patients, respectively. In 23 patients (58%), tearing was already present before the start of RT. The presence of keratitis, blurred vision or photophobia was only seen in 8%, 13% and 11% of the patients, respectively. None of these three

symptoms was seen in 30 (77%) patients. One patient (Table 5, Patient 3) had a retinal detachment 1 month after the end of RT. Even after maximal therapy for this retinal detachment, vision remained impaired. It is unclear if there is a relation between the RT course and this event. For the analysis of the chronic toxicity, it was considered as induced by RT.

No grade 3 dysphagia was seen. Mucositis was seen in all patients, but grade 2 and 3 were seen in < 50% of all patients. The most common site for mucositis was the hard palate, as this is the lower border of the nasal cavity, and as such included in the CTV (Figure 1). Grade 3 radiodermitis was seen in 2 patients (of which one was patient 3 from Table 5).

Chronic toxicity

Vision

Before the start of RT, three patients had a preexisting ocular disease. One patient had known retinitis pigmentosa, 1 had preexisting severe hypertensive retinopathy, and 1 patient with tumour-induced blindness (Patient 2 from Table 5). The patient with hypertensive retinopathy had no decrease of vision (DV) over baseline at 15 months after RT, and the patient with retinitis pigmentosa had a significant DV (from grade 2 bilaterally before RT to grade 3 11 months after RT). In these patients, it is not clear if the deterioration of the visual acuity is caused by the effects of the radiotherapy course, or by the progression of the underlying ocular disease and, therefore, they were excluded from this analysis for visual impairment. In the remaining 33 patients, no RT-induced blindness was seen. Table 6 summarizes data on 5 patients (15%) who developed vision impairment. Figure 2d shows the compiled DVHs for optic nerves and retinae with or without RT-induced damage, resulting in vision impairment .

Dry eye and pain

Dry eyes were seen in 10 patients. In three patients, this caused no pain at all, and was only noted by the ophthalmologist. In two patients, the dry eyes caused minimal pain (grade 1). Three patients had grade 2 pain (intermittent and tolerable), and two patients had grade 3 (Table 5, Patient 2) persistent pain due to dry eyes. Although these two patients required permanent analgesic therapy, no enucleation was required to control the pain.

Other ocular toxicity

Twenty patients (50%) had any grade of chronic tearing. This was grade 1 in 9 patients, grade 2 in 7, and grade 3 in the other 4 patients. In all but one patient, tearing was also present during RT. When compared with tearing during the RT period, the chronic tearing was worse in 3 patients, unchanged in 16 patients, and was better in 1 patient. Cataracts were seen in 15 patients during the follow-up period. Of these 15 patients, 8 patients already had cataracts before RT, and it worsened after RT in 1 patient. Three patients had surgery for their cataract, with a normal vision after the treatment. This was at 9 months, 4.8 and 5.4 years after the end of RT.

Non-ocular chronic toxicity.

Brain necrosis was seen in 2 patients. In 1 patient, it was shown on MRI and histologically confirmed. In the other patient, the localization and the time of onset, which was synchronous with optic nerve toxicity, suggested the diagnosis of brain necrosis (Table 5, Patient 1; Figure 7). Both patients are alive at the time of analysis. Grade 2 xerostomia (partial but persistent dryness) was present in 5 patients. Grade 2 taste alteration was seen in 6 patients. No chronic mucosal lesions were noted. Although not scored, more than half of the patients had nasal crusts, which were treated by daily nasal irrigations with a physiologic solution.

Discussion

IMRT has been used increasingly in many centers throughout the world. However, for head and neck carcinoma, there are only few reports on the clinical long-term outcome obtained with IMRT. In the present report, prospectively collected long-term results are given for a homogeneous patient group, all of which were postoperatively irradiated for an adenocarcinoma or SCC of the paranasal sinuses. With

Table 5: Clinical data of three patients with accumulated chronic toxicity.[a]

Patient	subsite	T-stage	Clinical course
1	ethmoid	pT2	Brain necrosis (see Figure 7) and grade 3 visual impairment due to radiovasculitis
2	ethmoid	pT4b	Unilateral blindness due to orbital tumour invasion. No attempt was made to spare ipsilateral orbit. Relapsed at optic chiasm. Bilateral blindness due to tumour invasion of chiasm. Grade 3 ocular pain after RT.
3	ethmoid	pT4a	Receipt of amiodarone until one week before RT. Grade 3 acute toxicity (radiodermitis and mucositis) and retinal detachment one month after RT, causing grade 3 visual impairment.

[a] Patients are sorted chronologically on the date of start of radiotherapy. RT: radiotherapy

Table 6: Patients with a radiation-induced decrease of vision.[a]

Pt.	Grade	Side	Time of onset	Visual acuity	Cause
1	2	bilateral	29	8/10	optic neuropathy
2	2	ipsilateral	6	8/10	optic neuropathy
3	2	ipsilateral	8	8/10	optic neuropathy
4	3	ipsilateral	1	2/10	retinal detachment
5	3	ipsilateral	24	2/10	radiovasculitis + neovascular glaucoma

[a] Time of onset (in months) was measured from the first day of radiotherapy.

a median follow-up of 31 months, this series is mature enough to report 2-year LC and survival rates. The results obtained in other series are summarized in Table 7. The 2-year OS ranges between 47% and 83%, but most series report a 2-year OS rate of approximately 70%, which is comparable to the OS rate observed in the present series. It remains very difficult to compare results between different series. As it is a very rare disease, paranasal sinus cancer series are mostly composed of a multitude of histologies, and data are often collected retrospectively. Even the comparison of the treatment results with an HC from the same institution remains difficult to interpret. When considering all patients, both OS and LC are slightly (not statistically significant) lower for the IMRT group, than for the HC. However, there might have been a patient selection bias since the introduction of IMRT. As the observed acute toxicity with IMRT was low, patients with a very advanced stage of sinonasal carcinoma were treated to high dose, whereas they would have been treated with a strictly palliative intention in the pre-IMRT era. Moreover, in the process of retrieving data on the HC group, it was clear that the majority of patients who were deemed to be inoperable in the period from 1985 to 1997 would nowadays undergo surgery followed by RT. Most probably, this is the reason for the unequal distribution of the number of patients with invasion through the CP, which was shown to be an important prognostic factor. If only those patients without extension through the CP were compared, IMRT resulted in a (statistically not significant) higher OS and LC. However, the follow-up is much shorter for the IMRT group, and no definitive conclusions can yet be drawn from this historical comparison.

Invasion through the CP with extension into the anterior cranial fossa was shown to be an important prognostic factor for both LC and OS. A median time to local disease recurrence of 7 months and a median survival of 8 months was observed in these patients. In none of these patients, local control was achieved. In our opinion, these poor results do not

Table 7: Literature review on treatment results and chronic toxicity.

Series	N	Period	Site	Treatment	Techn.	Dose (Gy)	FU	OS	RIB (%)	MD;ON (n)	Enucl. (n)
Shukovsky [6]	30	'60-'69	E;NC	RT	2D	70-75	-	-	30%	7;3	-
Ellingwood [7]	32	'64-'75	E;NC	RT	2D	63-66	-	83	28%	3;0	6
Katz [8]	78	'64-'98	NC;E	RT;S→RT	2D	65	-	75	37%*	-;-	0
Jiang [18]	34	'69-'93	E	S→RT;RT	2D	60-63	64	65	9%	1;1	-
Karim [19]†	45	'70-'85	E	S→RT	2D‡	64-70	-	70	4%	3;6	-
Tiwari [20]†	50	'75-'94	E	S→RT	2D‡	65	-	77§	2%	8	0
Waldron [21]	29	'76-'94	E	RT;RT→S	2D	60	48	53	15%	7	-
Jansen [3]	73	'77-'96	-	S→RT;RT	2D‡	66	66	70	21%$^{||}$	3;3	3
Roa [22]	39	'86-'92	M	S→RT;RT	3D	56-68	54	60	0%	0	0
Padovani [23]	25	'95-'01	E	S→RT;RT	3D	64-70	25	47	0%	0;1	0
HC	30	'85-'98	E	S→RT	2D;3D	66 (60-70)	83	83	10%	0;2	1
IMRT	39	'98-'03	E	S→RT	IMRT	70 (60-70)	31	69	0%	2;3	

Abbreviations: N= number of patients. Site: most prevalent subsite(s) in the series, with E: ethmoid sinuses, NC: nasal cavity and M: maxillary sinus. Treatment: most prevalent treatment strategies, with RT: radiotherapy, S: surgery, C: chemotherapy; an arrow (→) indicates that one modality was followed by the other. Techn.: radiation technique, with 2D: conventional technique (mostly one anterior beam and two, lateral wedged fields); 3D: conformal radiotherapy, in which the shape of the field is based on CT-based target delineation and IMRT: intensity-modulated radiotherapy. Dose: median (or range) of target dose. FU: Median follow-up (in months); OS: 2-year overall survival. RIB: radiation induced blindness, expressed as percent of all patients in the series. MD;ON: radiation-induced maculo-retinal degeneration (MD) or optic neuropathy (ON). Enucl.: enucleation due to radiation-induced toxicity (e.g. severe dry eye). "-": not specified;

*percentage calculated on the number of evaluable patients (n=60).

†represent data from the same center.

‡shielding of uninvolved part of the orbita.

§ disease-specific survival

$^{||}$include both patients with blindness and severe visual impairment (not reported separately).

justify the further use of our current treatment policy (craniofacial resection and post-operative IMRT) for this subset of patients. Patients should be thoroughly informed about the grim prognosis, and the possible benefit of a treatment should be weighted against the risk of adverse effects. Besides the current approach, the patient should be offered the choice between an experimental treatment strategy within a clinical (multicentric) trial, or a strictly palliative treatment. In an investigational treatment approach, craniofacial resection could be replaced by tumour debulking using a lateral rhinotomy approach. This surgical procedure carries less morbidity than the craniofacial approach, and cannot cause surgical tumour spill in the subarachnoidal space. In our experience, all recurrences in the patients with invasion through the CP were intracranially, suggesting a pattern of meningeal spread [15]. There were two patients with a recurrence at the border of the PTV, and one patient with a meningeal disease recurrence outside the PTV (Table 3). This indicates the need for a broader target volume definition, and we would propose to delineate an additional CTV including the subarachnoidal space over the frontal lobes and the anterosuperior part of the temporal lobes. This second CTV could than be irradiated to an elective dose. Three patients relapsed inside of the PTV, but only cranial to the cribriform plate. This might indicate the need for an even higher dose to the PTV that is constructed around (the surgical bed of) the primary

tumour. This hypothesis and treatment approach is a purely radiotherapeutic one, and other approaches and/or modalities, like systemic [24] or topical [5] chemotherapy might be indicated. To our knowledge, this clinical problem has not yet been fully addressed.

At our institution, for paranasal sinus cancer, the cervical lymph nodes are only treated when they are clinically (palpation and CT) invaded. In this series of 39 patients, only one patient presented with cervical lymph node metastases at the time of diagnosis. Of the 38 remaining patients, only one patient (with a squamous cell carcinoma of the maxillary sinus) developed a regional lymph node metastasis. Thus, none of the 31 patients in whom an adenocarcinoma was diagnosed, developed a lymph node recurrence, while this was 1 out of 8 (13%) for squamous cell carcinoma. This is consistent with data found in literature, summarized in Table 8. The prevalence of positive cervical lymph nodes at time of diagnosis varies between 0% and 15% [19, 20, 22]. When pooling all patients from the five first series (predominantly ethmoid sinus cancer, called group I), only 2% (4/197) had positive cervical lymph nodes at diagnosis, whereas this was 12% (32/278) in the five series with mainly maxillary sinus cancer (further called group II). The percentage of patients suffering from a lymph node recurrence during follow-up was 7% (14/194) in group I, and 12% (33/274) in group II. For isolated lymph node recurrences, these numbers were 2% (3/147) and 5% (14/274) for group I and group II, respectively. It is well described that lymph node recurrence is associated with a bad prognosis, despite salvage treatment [3, 4, 26, 27]. These considerations made us change our treatment policy, and we included elective lymph node irradiation (ELNI) for T3-4 maxillary sinus carcinoma, as was proposed by Le *et al* [26]. An ELNI should include the ipsilateral level Ib and II, as most lymph node recurrences are located in these lymph node regions [26, 27]. In ethmoid sinus cancer, and most of all in adenocarcinoma of the ethmoid sinuses, the incidence of lymph node recurrence is so low that there is no indication for ELNI.

Chronic toxicity data were prospectively scored and collected, and showed visual impairment in 5 of 33 evaluable patients (15%). Three of these were

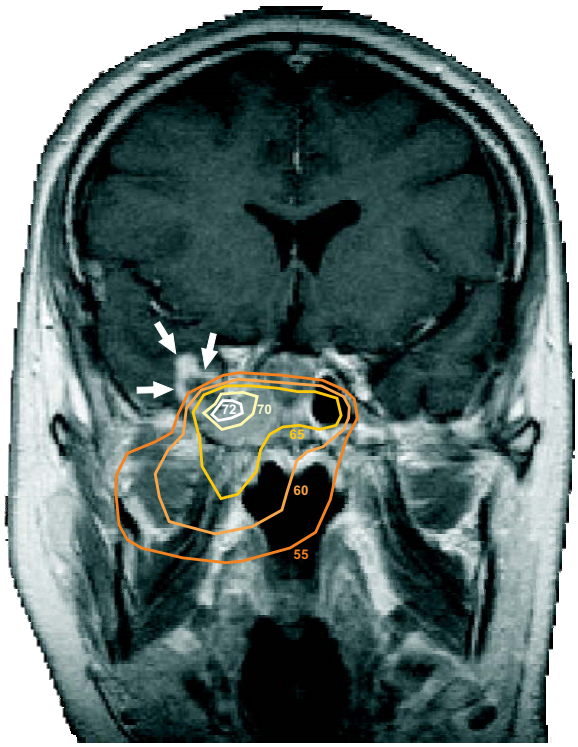

Figure 7: Coronal view of a magnetic resonance image (MRI) showing the zone of brain necrosis (white arrows) in patient 1 from Table 5. The MRI was acquired two years after the end of radiotherapy. The planning CT was matched to the MRI, and the dose distributions were transferred to the MRI. All isodoses are in Gy.

grade 2 (with a visual acuity score of 8/10), and the diagnosis of the underlying optic neuropathy was based on ophthalmologic examination (fundoscopy, visual evoked potentials and perimetry) rather than on symptomatic decrease in vision. Two patients had grade 3 (decrease in central vision) vision impairment at the ipsilateral eye. Of these, 1 patient was chronologically the first patient treated with IMRT, and the IMRT plan was made with a simple optimization tool, resulting in an inhomogeneous dose to the PTV. Moreover, in this first patient, the delineated optic structures were not expanded to account for possible setup errors. The combination of both resulted in a high dose region near to the optic structures (Figure 7). Until now, no radiation induced blindness was observed. However, follow-up was relatively short.

Table 8: Literature review on lymph node recurrence.

Series	N	Site (%) E/NC/M	Histol (%) Ad/SCC/O	Initial N+	ELNI	Lnn recurr.	Isolated Lnn recurr
Tiwari [20]	50	100/0/0	58/18/24	0 (0%)	(no)	2/50 (4%)	-
Waldron [21]	29	100/0/0	31/41/28	2 (7%)	no	5/29 (17%)	1/29 (3%)
Jiang [18]	34	100/0/0	26/24/50	1 (3%)	2/33	3/31 (10%)*	0/34 (0%)
This series	39	77/8/15	79/21/0	1 (3%)	no	1/39 (3%)	1/39 (3%)
Karim [19]	45	(E+NC)	51/27/22	0 (0%)	no	3/45 (7%)	1/45 (2%)
Roa [22]	39	23/26/59†	10/41/62†	6 (15%)	10/33	3/39 (8%)	2/39 (5%)
Budihna [4]	46	17/2/81	4/87/9	4 (9%)	no	5/46 (11%)	0/46 (0%)
Lavertu [25]	54	11/0/89	0/100/0	7 (13%)	no	6/54 (11%)	1/54 (2%)
Le [26]	97	0/0/100	4/60/36	11 (11%)	26/86	8/97 (8%)	7/97 (7%)
Paulino [27]	42	0/0/100	0/100/0	4 (10%)	no	11/38 (29%)*	4/38 (11%)
Porceddu [28]	60	-	42/53/5	5 (8%)	no	7/60 (12%)	1/60 (2%)
Jansen [3]	73	-	19/55/26	8 (11%)	no	8/73 (11%)	5/73 (7%)

The series are ordered and grouped by the percent of patients whose tumour originates from the ethmoidal sinus complex. *Abbreviations:* N: number of patients. Site: subsite of primary tumour, with E = ethmoid sinus; NC = nasal cavity and M = maxillary sinus; Histol = Histology of primary tumour, with Ad = adenocarcinoma; SCC = squamous cell carcinoma and O = other histologies. Initial N+: number of patients with positive lymph nodes at the time of diagnosis. ELNI: elective lymph node irradiation; the denominator is the number of patients without positive lymph nodes at the time of diagnosis. Lnn recurr.: lymph node recurrence. "-": not specified

* the denominator indicates all patients who did not have positive lymph nodes at the time of diagnosis, and who did not undergo ELNI.

† The sum is not 100 (error in original publication?)

Optic neuropathy typically develops between 2 and 4 years after the end of radiotherapy, but can occur up to 14 years after treatment [9]. Comparably, radiation induced retinopathy develops within a period of 1.4 to 5 years after radiotherapy [11]. Data about ocular toxicity after high dose radiotherapy for sinonasal cancer are summarized in Table 7. In the patient series in which a large part of the orbital cavity or the optic nerve was irradiated to high doses, the incidence of radiation induced blindness ranges between 15% and 40% [6, 7, 8, 21]. Karim *et al* [19] showed that irradiation of the whole orbit was unnecessary in case of minimal to moderate orbital extension. They found a low incidence of radiation induced blindness (4%) by applying a shrinking field technique, thus excluding the ocular structures from the high dose regions. These results were confirmed by a later series of the same center [20]. Two series report on the results obtained by 3D conformal irradiation of sinonasal cancer. Roa *et al* [22] and more recently Padovani *et al* [23] did not find any radiation induced blindness. Finally, in the HC, 7 patients developed a decrease of the vision, accompanied by chronic conjunctivitis. In 1 patient, enucleation of the eye was necessary to control the pain caused by a dry eye. One patient developed unilateral blindness due to optic neuropathy, and 1 patient suffered bilateral blindness. In total, 3 out of 30 patients (10%) lost vision at at least one eye in the HC. In conclusion, the data on LC and ocular toxicity support our hypothesis that IMRT results in a higher uncomplicated local control in sinonasal carcinoma.

Conclusion

For sinonasal carcinoma, IMRT results in equal local control and survival features as conventional or conformal RT techniques. Both acute and chronic ocular toxicity were low, and no radiation-induced blindness was observed. Invasion through the cribriform plate was an important prognostic factor.

References

[1] Van Eyken E, editor. Kankerincidentie in Vlaanderen, 1997-1999. [Cancer incidence in Flanders,1997-1999]. VLK. Brussels: Vlaams kankerregistratienetwerk, 2002

[2] Dulguerov P, Jacobsen M, Allal A, Lehmann W, Calcaterra T. Nasal and paranasal sinus carcinoma: are we making progress? A series of 220 patients and a systematic review. *Cancer* 2001;92:3012-3029

[3] Jansen E, Keus R, Hilgers J, Haas R, Tan I, Bartelink H. Does the combination of radiotherapy and debulking surgery favor survival in paranasal sinus carcinoma? *Int J Radiat Oncol Biol Phys* 2000;48:27-35

[4] Budihna M, Smid L. Carcinoma of the paranasal sinuses: results of treatment and some prognostic factors. *Strahlenther Onkol* 1992;168(6):322-327

[5] Knegt P, Ah-See K, vd Velden L, Kerrebijn J. Adenocarcinoma of the ethmoidal sinus complex: surgical debulking and topical fluorouracil may be the optimal treatment. *Arch Otolaryngol Head Neck Surg* 2001;127(2):141-146

[6] Shukovsky L, Fletcher G. Retinal and optic nerve complications in a high dose irradiation technique of ethmoid sinus and nasal cavity. *Radiology* 1972;104(3):629-634

[7] Ellingwood K, Million R. Cancer of the nasal cavity and ethmoid/sphenoid sinuses. *Cancer* 1979;43(4):1517-1526

[8] Katz T, Mendenhall W, Morris C, Amdur R, Hinerman R, Villaret D. Malignant tumors of the nasal cavity and paranasal sinuses. *Head Neck* 2002;24(9):821-829

[9] Parsons J, Bova F, Fitzgerald C, Mendenhall W, Million R. Radiation optic neuropathy after megavoltage external-beam irradiation: analysis of time-dose factors. *Int J Radiat Oncol Biol Phys* 1994;30(4):755-763

[10] Jiang G, Tucker S, Guttenberger R, *et al*. Radiation-induced injury to the visual pathway. *Radiother Oncol* 1994;30(1):17-25

[11] Takeda A, Shigematsu N, Suzuki S, *et al*. Late retinal complications of radiation therapy for nasal and paranasal malignancies: relationship between irradiated-dose area and severity. *Int J Radiat Oncol Biol Phys* 1999;44(3):599-605

[12] De Neve W, De Wagter C, De Jaeger K, *et al*. Planning and delivering high doses to targets surrounding the spinal cord at the lower neck and upper mediastinal levels: static beam-segmentation technique executed with a multileaf collimator. *Radiother Oncol* 1996;40:271-279

[13] Claus F, De Gersem W, De Wagter C, *et al*. An implementation strategy for IMRT of ethmoid sinus cancer with bilateral sparing of the optic pathways. *Int J Radiat Oncol Biol Phys* 2001;51:318-331

[14] Sobin LH, Wittekind C, editors. UICC TNM classification of malignant tumours 6th ed. New York: Wiley-Liss, 2002

[15] Claus F, Boterberg T, Ost P, *et al*. Postoperative radiotherapy for adenocarcinoma of the ethmoid sinuses: treatment results for 47 patients. *Int J Radiat Oncol Biol Phys* 2002;54(4):1089-1094

[16] Sobin L, Wittekind C, editors. UICC TNM classification of malignant tumours 5th ed. New York: Wiley-Liss, 1997

[17] Lent Soma Scales for all anatomic sites. *Int J Radiat Oncol Biol Phys* 1995;31:1049-1091

[18] Jiang G, Morrison W, Garden A, *et al*. Ethmoid sinus carcinomas: natural history and treatment results. *Radiother Oncol* 1998;49(1):21-27

[19] Karim A, Kralendonk J, Njo K, Tabak J, Elsenaar W, van Balen A. Ethmoid and upper nasal cavity carcinoma: treatment, results and complications. *Radiother Oncol* 1990;19(2):109-120

[20] Tiwari R, Hardillo J, Tobi H, Mehta D, Karim AB, Snow G. Carcinoma of the ethmoid: results of treatment with conventional surgery and post-operative radiotherapy. *Eur J Surg Oncol* 1999;25(4):401-405

[21] Waldron J, O'Sullivan B, Warde P, *et al*. Ethmoid sinus cancer: twenty-nine cases managed with primary radiation therapy. *Int J Radiat Oncol Biol Phys* 1998;41(2):361-369

[22] Roa W, Hazuka M, Sandler H, *et al*. Results of primary and adjuvant CT-based 3-dimensional radiotherapy for malignant tumors of the paranasal sinuses. *Int J Radiat Oncol Biol Phys* 1994;28(4):857-865

[23] Padovani L, Pommier P, Clippe S, *et al*. Three-dimensional conformal radiotherapy for paranasal sinus carcinoma: clinical results for 25 patients. *Int J Radiat Oncol Biol Phys* 2003;56(1):169-176

[24] Brasnu D, Laccourreye O, Bassot V, Laccourreye L, Naudo P, Roux F. Cisplatin-based neoadjuvant chemotherapy and combined resection for ethmoid sinus adenocarcinoma reaching and/or invading the skull base. *Arch Otolaryngol Head Neck Surg* 1996;122:765-768

[25] Lavertu P, Roberts J, Kraus D, *et al*. Squamous cell carcinoma of the paranasal sinuses: the Cleveland Clinic experience 1977-1986. *Laryngoscope* 1989;99(11):1130-1136

[26] Le Q, Fu K, Kaplan M, *et al*. Lymph node metastasis in maxillary sinus carcinoma. *Int J Radiat Oncol Biol Phys* 2000;46(3):541-549

[27] Paulino A, Fisher S, Marks J. Is prophylactic neck irradiation indicated in patients with squamous cell carcinoma of the maxillary sinus? *Int J Radiat Oncol Biol Phys* 1997;39(2):283-289

[28] Porceddu S, Martin J, Shanker G, *et al*. Paranasal sinus tumors: Peter MacCallum Cancer Institute experience. *Head Neck* 2004;26(4):322-330

V. 4. Positron emission tomography (PET) guided dose escalation with intensity modulated radiotherapy in head and neck cancer.

Authors: W. Duthoy, W. De Gersem, X. Geets, M. Lonneux, B. Vanderstraeten, V. Grégoire and W. De Neve.

Submitted to: Radiotherapy and Oncology.

Acknowledgements: The project "Conformal Radiotherapy Ghent University Hospital" is supported by the Belgische Federatie tegen Kanker (grants 51AC8904, FBC2003/2006 and ZKB2747) and by grants from the Fonds voor Wetenschappelijk Onderzoek (FWO) Vlaanderen (G.0183.03), the University of Ghent (GOA 12050401, BOF 01112300, 011VO497, 011B3300), and the Centrum voor Studie en Behandeling van Gezwelziekten.
Barbara Vanderstraeten and Wim Duthoy are Research Assistants (Aspirant) of the FWO.

Key issues discussed in this paper:

- Despite advanced conformal techniques, like IMRT, local relapse in HNC is still frequent, and mostly develops in the high-dose region. This urges for focused dose escalation to the regions within the GTV at highest risk for relapse.
- Biological imaging, like FDG-PET, correlates better to tumour macroscopy than CT- and MRI-based delineation, and might indicate tumour regions with a higher intrinsic radioresistance, needing higher doses.
- FDG-PET data were used both in the delineation of the target volumes and in guiding the dose escalation. The latter was done using 2 phases, with the dose escalation embedded in the first ten fractions.
- The use of FDG-PET information led to changes in the CTV in 7 out of 20 patients. The GTV, delineated on FDG-PET was significantly smaller than the CT-based GTV.
- The dose escalation to the FDG-PET positive lesion did not result in more complex plans, nor in higher doses to the surrounding targets and OARS.

Positron emission tomography guided dose escalation with intensity-modulated radiation therapy in head and neck cancer

Wim Duthoy, M.D.[1], Werner De Gersem, Ir.[1], Xavier Geets, M.D.[2],
Max Lonneux, M.D., Ph.D.[3], Barbara Vanderstraeten, Ir.[1],
Vincent Grégoire, M.D., Ph.D.[2] and Wilfried De Neve, M.D., Ph.D.[1]

(1) Department of Radiotherapy, Ghent University Hospital, De Pintelaan 185, 9000 Ghent, Belgium
(2) Department of Radiotherapy, and (3) Department of Nuclear Medicine, Cliniques Universitaires Saint-Luc, UCL Medical school, Avenue Hippocrate 10, 1200 Brussels, Belgium

Abstract

Background and Purpose: In head and neck cancer, the majority of relapses occur in the gross tumor volume (GTV). This relapse pattern suggests the need for selective delivery of higher doses to the GTV. 2-^{18}fluoro-2-deoxy-glucose positron emission tomography (PET) appears to be more accurate for GTV definition than computed tomography (CT) or magnetic resonance imaging. This report describes the implementation and planning results of PET-guided intensity-modulated radiation therapy (IMRT) with a dose escalation, focused on a PET-based GTV (GTV_{PET}).

Materials and Methods: Twenty patients with head and neck cancer were included in a dose escalation trial. All patients had a planning CT and a PET in treatment position. All target volumes were first delineated on CT without PET data. Then, CT and PET were fused, and GTV_{PET} was automatically segmented. If needed, target volumes were enlarged according to PET findings. All target subvolumes were grouped according to various prescription dose levels. The IMRT treatment ($IMRT_{escal}$) aimed at a selective dose escalation to the PTV_{PET} up to 72.5 Gy, and consisted of 10 fractions of phase 1 (containing the dose escalation) and 22 fractions of phase 2. The $IMRT_{escal}$ was evaluated using median dose (D_{med}) and indices for range for PTVs and dose constraints for organs at risk (OARs). The selectivity of dose escalation for the PTV_{PET} was evaluated by comparing the $IMRT_{escal}$ to a virtual "conventional" IMRT treatment ($IMRT_{conv}$), which consisted of 32 fractions of phase 2 plan.

Results: GTV_{PET} was 45% smaller than the CT-based GTV (GTV_{CT}). PET resulted in an adaptation of target volumes in 7 patients. The multiple dose levels, prescribed as D_{med} to the various PTVs, could be planned within 0.5 Gy in nearly all patients. Comparing $IMRT_{escal}$ with $IMRT_{conv}$ showed that selectivity of dose escalation was secured with respect to OARs and PTVs.

Conclusions: The use of PET had an impact on target volumes in one third of the patients. Dose escalation of GTV_{PET} to 72.5 Gy using two phases was feasible on planning and delivery, and was highly selective since it did not increase dose to the OARs.

Introduction

In conformal radiotherapy, like intensity-modulated radiation therapy (IMRT), three-dimensional (3D) imaging is directly used to shape beam outlines and sometimes to modulate beam intensity as function of 3D anatomical information. Clinical use of conformal radiotherapy serves 2 main objectives. First, selective reduction of the dose to radiation-sensitive organs may result in less toxicity and results of case series indeed suggest that conformal avoidance of radiation-sensitive structures like parotid or lacrimal glands, optic or auditory pathways has resulted in less morbidity [10]. Reduction of dose to sensitive organs relative to the tumor prescription dose could be exploited to reach the second objective: improved loco-regional control by dose escalation [10]. Case studies of conformal radiotherapy show that the majority of relapses occur in the gross tumor volume (GTV) or tumor bed receiving the highest prescription dose, and less often in electively irradiated areas [2, 6]. This pattern of relapse suggests that target definition and prescription doses are appropriate for electively irradiated regions to which prescription doses of 40-50 Gy, 50-60 Gy and 60-70 Gy are typically applied for low, intermediate and high probability of microscopic invasion respectively. Prescription doses to the region of the GTV are of the same order or slightly higher than for the high-risk elective regions. For some tumor sites, the feasibility and safety of dose escalation has been demonstrated using brachytherapy [16], stereotactic radiosurgery [19] and IMRT simultaneous boost techniques [20]. In all these techniques, dose was escalated to small volumes. Neither the criteria to define the boost volume, nor the dose/volume/toxicity relationships for boosting small volumes are known. We decided to use 2-^{18}fluoro-2-deoxy-glucose positron emission tomography (FDG-PET, further referred to as PET) imaging for the definition of the boost volume. Daisne et al showed that in pharyngo-laryngeal squamous cell cancer, the GTV that had been automatically delineated based on the FDG-PET data (GTV_{PET}), correlated better with the macroscopic surgical specimen than expert-contoured GTVs based on computed tomography (CT) or magnetic resonance imaging (MRI) scans [5]. We reasoned that this PET lesion might be a suitable target subvolume for dose escalation inside the expert-contoured highest-dose planning target volume (PTV).We clinically implemented focused dose escalation, based on PET, and report on the planning results of the first escalation step.

Table 1: T- and N-stage for the 20 patients, according to the UICC TNM classification [18].

	T2	T3	T4a	T4b	**All**
N0	1	2	1	-	**4**
N1	1	4	-	-	**5**
$N2_b$	1	2	-	-	**3**
$N2_c$	2	-	1	3	**6**
N3	-	2	-	-	**2**
All	**5**	**10**	**2**	**3**	**20**

Materials and Methods

Patient description

Twenty patients were enrolled in the first level of this dose escalation trial. Inclusion criteria for the trial were: (1) histological diagnosis of a squamous cell carcinoma (SCC) arising from the hypopharynx, the oropharynx or the larynx (for larynx, only T_{3-4} N_0 or T_{any} N_+ were included); (2) the patients did not undergo surgery of the primary tumor as a part of their treatment; (3) the patients were free of lung metastases (assessed by CT). Patients who had previously been irradiated in the head and neck region were excluded from the trial. All patients gave their written informed consent to enter the study protocol, which was approved by the local ethics committee. Of the twenty patients included in the trial, 8 patients had a SCC of the larynx, 6 patients had a tumor arising from the hypopharynx and another 6 patients had an oropharyngeal tumor. All patients were staged according to the UICC TNM classification [18](see Table 1).

Delineation of target volumes and organs at risks (OARs)

Planning CT and PET scan were both acquired in treatment position, immobilized with a thermoplas-

tic mask. All anatomical structures were delineated on the CT before PET information was made available. A summary of target structure definitions is given in Table 2. The GTV was delineated based on the planning CT (GTV_{CT}), using complementary diagnostic imaging (CT and/or MRI) but not PET. The clinical target volume (CTV) containing the microscopic extension locally around the GTV_{CT} was manually delineated based on the idea of compartmental tumor spread [13], resulting in the primary CTV ($pCTV_{CT}$). All lymph node regions (LNRs) were contoured separately [12].

The PET acquisition was done on a Siemens Exact HR+ camera (CTI-Siemens, Knoxville, USA), operating in 3D-mode, i.e. septa retracted. Imaging began 60 minutes after iv injection of 185-259 MBq (5-7 mCi) FDG. Emission scans were first obtained at two bed positions, with a 3.9-cm overlap, covering an axial field of view of 26,675 cm. The duration of the emission scans was 10 minutes each. Transmission scans (5 min each) were then obtained. The data were transferred to a dedicated workstation and reconstructed using a fully 3D iterative algorithm (attenuation-weighted-OSEM), without rebinning of the data. Images were reconstructed with correction for random, normalization, scatter and attenuation. Pixel size in the final image was 2.5, 2.5 and 2.4 mm in the x, y and z direction, respectively. The PET lesion (GTV_{PET}) was automatically segmented based on the source-to-background ratio [4]. The CT and PET transmission scan were coregistered using Pinnacle (Philips Medical Systems, Milpitas, CA). After the CT/PET fusion and the segmentation of the GTV_{PET}, a final GTV_{union} was made by the addition of GTV_{CT} and GTV_{PET}. The pCTV was composed from the $pCTV_{CT}$ and - if needed - extended to encompass the GTV_{union} with a margin for microscopic extension.

CTV subvolumes (pCTV and all the separate LNRs) were grouped according to the dose prescription levels in CTV_{69}, CTV_{66}, CTV_{62} and CTV_{56}, as explained in Table 2. A 3 mm margin was applied for the expansion from CTV to PTV for all CTV volumes and for the expansion of GTV_{PET} to PTV_{PET}.

In order to avoid ambiguous demands to the optimization algorithm, subvolumes of each PTV were

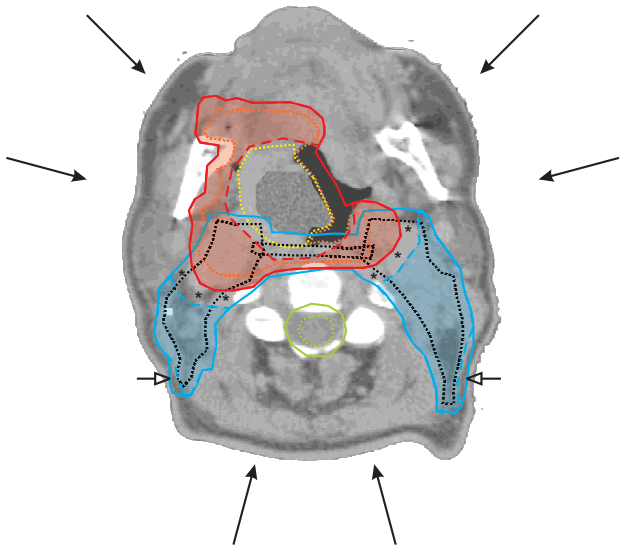

Figure 1: Transverse plane of planning CT from a patient with a tumor originating from the oropharynx. The automatically delineated PET lesion (GTV_{PET}) is indicated by the speckled area. Dotted lines represent manually delineated structures, with gross tumor volume (GTV_{CT}) in yellow, the clinical target volume around the GTV_{CT} ($pCTV_{CT}$) in orange, lymph node regions (LNRs) in black and spinal cord in green. Full lines represent the expanded structures, with the PTV_{69} in red, the PTV_{56} in blue and the expanded spinal cord in green. The dashed lines and shaded areas represent the optimization structures $PTV_{69,optim}$ (red) and $PTV_{56,optim}$ (blue). $PTV_{56,optim}$ results from PTV_{56} using the subtraction of a 6 mm build-up region (indicated by the hollow arrows) and excluding the PTV_{69} with a margin of 6 mm (shown by the asterisks). In the same way, $PTV_{69,optim}$ is made by subtracting the PTV_{PET} (not shown) from PTV_{69} with the same margin. The beam directions are indicated by the six arrows.

Table 2: Overview of target structure definition.

Structure Name	Description
GTV_{CT}	GTV as delineated on the planning CT without PET information
GTV_{PET}	GTV, automatically segmented on PET based on the source-to-background ratio
GTV_{union}	GTV constructed by the addition of GTV_{CT} and GTV_{PET}.
pCTV	CTV containing GTV_{union} and microscopic extension locally around GTV_{union}
CTV_{69}	CTV consisting of CTV subvolumes with macroscopic tumor: pCTV and LNRs with clinically positive and unresected lymph nodes
CTV_{66}	CTV containing resected LNRs with pathologically positive lymph nodes with capsular rupture
CTV_{62}	CTV containing resected LNRs with pathologically positive lymph nodes without capsular rupture
CTV_{56}	CTV containing elective LNRs: no clinical evidence of disease but at risk for microscopic invasion

Abbreviations: GTV: gross tumor volume; CT: computed tomography; PET: positron emission tomography; CTV: clinical target volume; LNR: lymph node region.

constructed using in-house developed software [9]. From each PTV_D (D = prescription dose for a given PTV), a $PTV_{D,whbu}$ (whbu: without build-up) was created by subtraction of a 6 mm build-up region. All PTVs to which a dose higher than D Gy was prescribed were subtracted from $PTV_{D,whbu}$ with a margin of 6 mm. The part of $PTV_{D,whbu}$, which remains after the subtraction procedure(s) is called $PTV_{D,optim}$. This procedure secures priority ranking for the PTVs to which the highest dose was prescribed. The method of delineation and creation of target subvolumes is illustrated in Fig. 1. The contoured OAR set consisted of spinal cord, brainstem, parotid glands, mandible and thyroid cartilage. Spinal cord was expanded with a 5 mm margin, while a 3 mm margin was used for brainstem. The other OARs were not expanded.

Planning procedure

The treatment consisted of 2 consecutive phases for which separate plans were made. Dose escalation to the PTV_{PET} was embedded in the phase 1 plan. Ten fractions were delivered according to this phase 1 plan. The phase 2 plan, without dose escalation, was given for 22 fractions. Both plans were IMRT plans, using multiple prescription dose levels simultaneously for the different target volumes. The technique is referred to as simultaneous integrated boost (SIB) [20, 15]. Details about dose prescription per plan are given in Table 3. These doses represent the median dose (D_{med}) to a $PTV_{D,optim}$ that was requested from the optimization algorithm. In practice, both the phase 1 plan and the phase 2 plan were optimized to 69.1 Gy to the $PTV_{69,optim}$ (this is as if the plan would virtually be given 32 fractions), and rescaled to 1 fraction (see Table 3). This strategy enabled us to use the same biological optimization parameters for OARs for both plans.

A class solution, consisting of 6 coplanar predefined beam directions, was used for all patients. For each beam direction, segments were generated by the anatomy-based segmentation tool [7]. Segment outlines and weights were optimized based on a bio-physical cost function [8]. Several cycles of optimization were executed, until the planning goals/constraints were reached/respected. For all $PTV_{D,whbu}$, the partial volume receiving less than 95% of the prescribed dose ($V_{<95\%}$) had to be less than 5%. For the PTV to which the highest dose was

prescribed (for the phase 1 plan, this was PTV_{PET}, while for phase 2 plan, this was PTV_{69}), the partial volume receiving more than 107% of the prescribed dose ($V_{>107\%}$) had to be less than 5%. The inhomogeneity factor $U_{98/2} = 100\,x\,\frac{D_2 - D_{98}}{D_{med}}$, with D_2 the 2^{nd} percentile dose and D_{98} the 98^{th} percentile dose, had to be less than 12% for PTV_{PET} and for $PTV_{69,optim}$. For all PTVs with a lower prescription dose (66 Gy, 62 Gy and 56 Gy), the maximal homogeneity depends on the dose prescriptions and constraints to neighbouring structures. For this reason, we choose not to impose a homogeneity criterium to PTV_{66}, PTV_{62} and PTV_{56} or their respective optimization subvolumes.

The partial volume of the expanded spinal cord receiving more than 50 Gy ($V_{>50Gy}$) had to be less than 5%. If there was a conflicting situation between PTV underdosage ($V_{<95\%}$) and the $V_{>50Gy}$ for spinal cord, priority was given to the latter. Sparing of the contralateral parotid was only performed in those cases were the contralateral LNR II and III were free of lymph nodes that were clinically suspect for tumoral invasion. Fourteen patients fulfilled this criterium (7 left and 7 right parotids). The planning goal for parotid sparing was a D_{med} less than 27 Gy.

Evaluation endpoints

The volumes of the following structures were recorded: i) the GTV_{CT} ii) the GTV_{PET}, iii) the mismatch volume $GTV_{PET-only}$, which is the partial volume of the GTV_{union} that is only contoured using PET and iv) the mismatch volume of $GTV_{CT-only}$, which is the part of the GTV_{union} that is only contoured by the expert. Also, the influence of the PET information on the CTVs was recorded.

Statistics regarding the number of segments and the monitor unit (MU) efficiency of the phase 1 and the phase 2 plans were computed. MU efficiency was calculated per patient by dividing the number of MUs needed for one fraction by the prescription dose (i.e. 250 cGy for phase 1 plans and 216 cGy for phase 2 plans).

The effect of dose escalation to the PTV_{PET} on the other subvolumes and on the OARs was evaluated by comparing clinically relevant indices between the summed plans ($IMRT_{escal}$) and the conventional IMRT treatment ($IMRT_{conv}$). The $IMRT_{escal}$ was made by summing 10 fractions of phase 1 plan with 22 fractions of phase 2 plan. The hypothetical $IMRT_{conv}$ was composed of 32 fractions of phase 2 plan, which is the plan without dose escalation. For each target volume PTV_D , the D_{med}, $V_{<95\%}$, $U_{98/2}$, the minimal dose (D_{min}) and the maximal dose (D_{max}) were evaluated. The 98^{th} and 2^{nd} dose percentile were used as surrogate for D_{min} and D_{max}, respectively [20]. For the expanded spinal cord, the $V_{>50Gy}$ and the D_{max} were reported, while for the parotid glands the D_{med} and the $V_{>27Gy}$ are given. Results are presented as the mean $\pm$ standard deviation. For all statistical comparisons, a paired Student *t* test was used. All tests were two-tailed. A p-value < 0.05 was considered significant.

Dose-volume histograms (DVHs) of phase 1 and phase 2 plans were compiled for the whole group of patients using the following method: for all patients, the volume percentiles at every 2 cGy dose level between 0 and 270 cGy were computed from the calculated fraction dose distribution for the relevant anatomical structures. For each of these dose levels, the mean and standard error of the mean (SEM) over all the patients were calculated. Compiled DVHs were then plotted using this mean volume percentile and SEM value.

Results

Target volume adaptations

The mean GTV_{CT} volume was 17.4 $\pm$ 13.8 cc, while for the GTV_{PET}, this was 9.7 $\pm$ 8.4 cc (p = 0.026). When looking at the regions covered by GTV_{PET} but not by GTV_{CT}, the mean absolute volume of $GTV_{PET-only}$ was 2.7 $\pm$ 2.6 cc (19.3 $\pm$ 14.9% of GTV_{union} volume). The reverse mismatch structures $GTV_{CT-only}$ had a mean volume of 10.4 $\pm$ 9.8 cc, representing 45.7 $\pm$ 25.6% of the volume of GTV_{union}. The volume of the GTV_{PET} was larger than that of the GTV_{CT} in 6 patients. The average volume of the pCTV was 104.9 $\pm$ 41.2 cc. In 8 patients, PET imaging gave

Table 3: PTV dose prescription levels.

	phase 1 plan	phase 2 plan	TPD (Gy)	NID_{2Gy} (Gy)
PTV_{PET}	2.50 [80.0]	2.16 [69.1]	72.5	78.3
$PTV_{69,optim}$	2.16 [69.1]	2.16 [69.1]	69.1	72.5
$PTV_{66,optim}$	2.06 [65.9]	2.06 [65.9]	65.9	67.2
$PTV_{62,optim}$	1.94 [62.1]	1.94 [62.1]	62.1	60.9
$PTV_{56,optim}$	1.75 [56.0]	1.75 [56.0]	56	51.1

Numbers represent dose (in Gy) per fraction. Numbers between square brackets represent the dose (in Gy) to which the plans were optimized. TPD: Total physical dose (in Gy) represents the dose that was actually delivered to the patients, which consists of 10 fractions according to phase 1 plan, and 22 fractions according to the phase 2 plan. The several PTVs are explained in the text and in Table 2. NID_{2Gy}: Normalized Iso-effective Dose (in Gy) for 2 Gy fractions, calculated according to Lee et al [14] with α/β=10 Gy, β=0.035 Gy^{-2} and a potential doubling time of 4 days. Treatment time was estimated as $\frac{7n}{5}$ with n the number of fractions.

additional information about the tumor extent. In one patient with a pathologically enlarged retropharyngeal lymph node on CT, a second retropharyngeal lymph node at the contralateral side was found by PET. As the retropharyngeal LNR was already included in the CTV_{69}, this additional finding did not alter the target volumes. In the 7 other patients, PET information led to adaptations of the CTV. In 3 of these, the pCTV was only marginally adapted after PET information was available. However, in one patient, PET imaging showed FDG activity at the contralateral side of the tumor imaged on CT and seen at endoscopy. This finding was confirmed on repeated endoscopy. The average volume of the $pCTV_{CT}$ in these 4 patients was 117.8 $\pm$ 46.3 cc, while, using the PET information, the pCTV became 138.3 $\pm$ 34.1 cc. In the 3 other patients, additional lymph nodes were seen on PET scan that were not suspect by previous diagnostic interventions. One patient shifted from cN0 to cN1, another patient reached cN2b instead of cN1. In the third patient, a lymph node that was suspect on CT but negative on fine needle aspiration cytology was clearly positive on PET scan.

Planning results for $IMRT_{escal}$

The planning results of $IMRT_{escal}$ are summarized in Table 4. The achieved D_{med} to the PTVs were all within acceptable range around the D_{med} that was required from the optimization. The underdosage constraint for PTV_{PET} and $PTV_{69,whbu}$ were met in all but one patient. In this patient, the PTV_{PET} was partly lying in the build-up region ($V_{<95\%}$ for $PTV_{PET,whbu}$ was 0%). For $PTV_{69,optim}$, the planning did not fulfill the constraint for avoiding underdosage in 2 patients ($V_{<95\%}$ of 5.3% and 5.8%). The $V_{<95\%}$ constraint for $PTV_{56,optim}$ was not met in half of the patients. No overdosages were seen in the PTVs.

Comparison $IMRT_{conv}$ vs $IMRT_{escal}$

Results of the comparison between $IMRT_{conv}$ and $IMRT_{escal}$ are summarized in Table 4. Dose escalation to the PTV_{PET} results in a higher dose to the surrounding PTV_{69}, but did not significantly affect dose to other structures. No statistically significant differences were found for spinal cord, parotid gland (spared and unspared) and mandible. For thyroid cartilage, the D_{mean} was 65.8 $\pm$ 3.6 Gy for $IMRT_{conv}$ and 66.6 $\pm$ 4.1 Gy for $IMRT_{escal}$ (p = 0.508), while the D_{max} was 69.7 $\pm$ 1.5 Gy and 71.7 $\pm$ 2.5 Gy (p = 0.347). For the subselection of the patients with a primary tumor of the larynx or hypopharynx (n = 14), the D_{max} of the thyroid cartilage was significantly higher in the $IMRT_{escal}$ (72.6 $\pm$ 0.7 Gy) than in $IMRT_{conv}$ (70.1 $\pm$ 0.4 Gy) (p < 0.001). The D_{mean} for thyroid cartilage in this group of patients

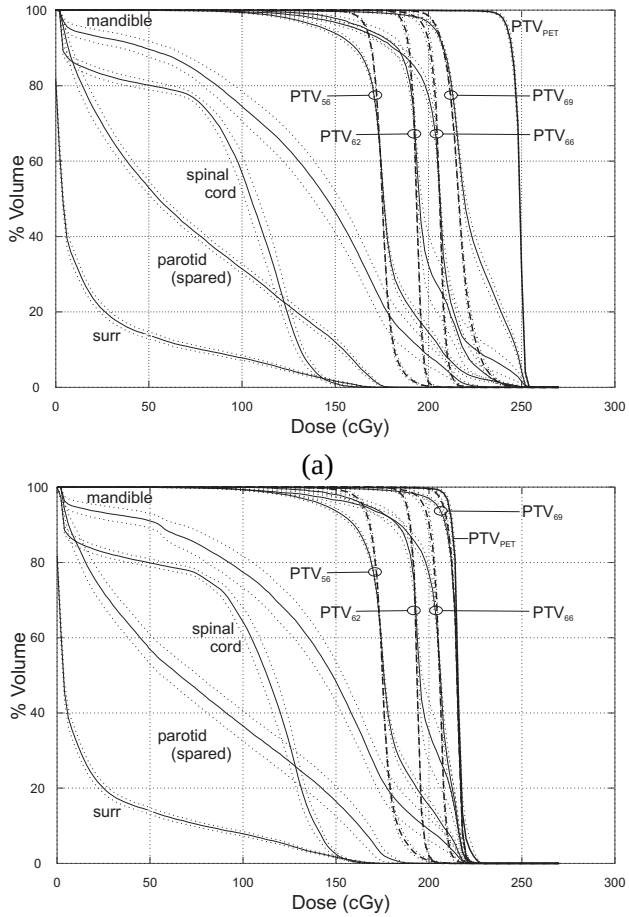

Figure 2: DVHs compiled from the data of the whole patient group for phase 1 plan (a) and phase 2 plan (b). The method of the DVH compilation is described in the Materials and Methods section. The represented dose (in cGy) is the dose given per fraction. For each structure, the mean $\pm$ the standard error of the mean (dotted lines) of the relative volumes is represented. For each target structure, except for PTV_{PET}, both the PTV_D (solid thin lines) and the $PTV_{D,optim}$ (dashed bold lines) are shown. The DVHs for PTV_{66} and PTV_{62} are compiled from the 6 and 4 patients respectively for whom this PTV dose level existed. The data for the spared parotid are compiled over the 14 "spared" parotids. The surr structure is the region at least 30 mm away from PTV_{69} and at least 20 mm from PTV_{56}.

was not significantly different, being 67.3 $\pm$ 1.6 Gy for $IMRT_{conv}$ and 68.4 $\pm$ 2.1 Gy for $IMRT_{escal}$ (p = 0.158).

Comparison of the phase 1 and the phase 2 plans

The phase 1 IMRT plans were not more complex than the phase 2 IMRT plans. The average number of segments, used in the final plan, was 40.2 $\pm$ 7.1 for phase 1 plans and 37.3 $\pm$ 6.3 for phase 2 plans (p = 0.180). The total number of MUs for the delivery of one fraction was 481.5 $\pm$ 81.0 for phase 1 plans and 407.0 $\pm$ 37.5 for phase 2 plans (p < 0.001). However, the MU efficiency for phase 1 plans (1.92 $\pm$ 0.32 MU/cGy) and phase 2 plans (1.88 $\pm$ 0.17 MU/cGy) was not significantly different (p = 0.616).

A comparison of the compiled DVHs between the phase 1 and phase 2 plans is shown in Fig. 2. Besides the (intended) difference for PTV_{PET}, and the subsequent higher doses in the parts of the other PTVs that lie in vicinity of the PTV_{PET}, no major differences are visible between phase 1 plan (Fig. 2a) and phase 2 plan (Fig. 2b). The $V_{>105\%}$ for $PTV_{69,whbu}$ was 36.0 $\pm$ 14.7% in phase 1 plan. For $PTV_{69,whbu}$, there was a significant correlation between the ratio of the volume of PTV_{PET} over the volume of $PTV_{69,whbu}$ and the $V_{>105\%}$ for $PTV_{69,whbu}$ (product-moment coefficient of correlation R^2 = 0.818, p < 0.001).

Fig. 3 shows the dose distributions of phase 1 plan for a patient with a tumor of the oropharynx.

Discussion

IMRT offers a high control over the distribution of dose within the patient. It enables the conformal sparing of OARs on the one side, and the escalation of dose to the target volume on the other side. The different fraction sizes within one plan offer a combination of radiobiological advantages over conventional radiotherapy, like higher/lower dose per fraction to the tumor/OARs, and result in (slightly) accelerated treatments [20]. Theoretically, IMRT allows dose es-

Table 4: Summary of the dose volume histogram (DVH) data showing averages ± SD.

		$IMRT_{conv}$	$IMRT_{escal}$	Constr. violation	p-value
PTV_{PET} (volume: 25 ± 16 cc)					
D_{med}	(Gy)	69.0 ± 0.6	72.4 ± 0.4	2/20	<0.001
D_{min}	(Gy)	66.8 ± 2.1	70.3 ± 2.1	-	<0.001
D_{max}	(Gy)	70.5 ± 0.9	73.6 ± 0.6	-	<0.001
$U_{98/2}$	(%)	5.4 ± 3.4	4.6 ± 3.0	1/20	0.468
$V_{<95\%}$	(%)	0.7 ± 1.6	0.6 ± 1.5	1/20	0.728
$PTV_{69,whbu}$ (volume: 202 ± 76 cc)					
D_{med}	(Gy)	68.8 ± 0.1	69.6 ± 0.6	-	<0.001
D_{min}	(Gy)	65.7 ± 1.1	65.9 ± 0.8	-	0.456
D_{max}	(Gy)	70.5 ± 0.5	73.0 ± 0.4	-	<0.001
$U_{98/2}$	(%)	7.0 ± 2.0	10.2 ± 1.2	2/20	<0.001
$V_{<95\%}$	(%)	2.2 ± 1.9	1.9 ± 1.4	0/20	0.463
$PTV_{69,optim}$ (volume: 140 ± 64 cc)					
D_{med}	(Gy)	68.8 ± 0.1	69.0 ± 0.2	0/20	<0.001
D_{min}	(Gy)	65.7 ± 1.0	65.6 ± 0.8	-	0.652
D_{max}	(Gy)	70.3 ± 0.4	71.1 ± 0.6	-	<0.001
$U_{98/2}$	(%)	6.6 ± 1.9	8.0 ± 1.4	0/20	0.016
$V_{<95\%}$	(%)	2.2 ± 2.1	2.4 ± 1.8	2/20	0.743
$PTV_{56,whbu}$ (volume: 372 ± 132 cc)					
D_{med}	(Gy)	56.9 ± 1.4	56.9 ± 1.4	-	0.920
D_{min}	(Gy)	51.9 ± 2.1	52.4 ± 1.5	-	0.395
D_{max}	(Gy)	69.1 ± 0.9	70.1 ± 1.6	-	0.016
$U_{98/2}$	(%)	30.2 ± 4.3	31.1 ± 4.3	-	0.504
$V_{<95\%}$	(%)	5.2 ± 4.6	4.0 ± 3.2	6/20	0.339
$PTV_{56,optim}$ (volume: 272 ± 102 cc)					
D_{med}	(Gy)	56.0 ± 0.3	56.0 ± 0.2	2/20	0.579
D_{min}	(Gy)	51.5 ± 2.3	52.0 ± 1.6	-	0.385
D_{max}	(Gy)	61.2 ± 2.2	60.8 ± 1.7	-	0.568
$U_{98/2}$	(%)	17.3 ± 7.5	15.6 ± 5.5	-	0.439
$V_{<95\%}$	(%)	6.8 ± 5.8	5.2 ± 4.0	10/20	0.341
spinal cord					
$V_{>50Gy}$	(%)	0.9 ± 1.4	0.5 ± 0.8	0/20	0.232
D_{max}	(Gy)	45.8 ± 3.9	45.3 ± 3.8	-	0.673
parotid (sparing)					
D_{med}	(Gy)	20.2 ± 10.6	19.5 ± 8.5	1/14	0.838
D_{mean}	(Gy)	24.1 ± 7.5	23.3 ± 5.7	-	0.780
$V_{>27Gy}$	(%)	42.6 ± 15.5	41.2 ± 13.0	-	0.795
parotid (no sparing)					
D_{med}	(Gy)	55.1 ± 8.7	54.5 ± 8.8	-	0.817
$V_{>27Gy}$	(%)	86.4 ± 15.5	86.4 ± 15.9	-	0.995
mandible					
$V_{>60Gy}$	(%)	14.2 ± 17.1	13.7 ± 17.1	-	0.931
D_{max}	(Gy)	63.3 ± 6.0	63.0 ± 6.1	-	0.881

$IMRT_{conv}$: total treatment without dose escalation (32 fraction of phase 2 plan). $IMRT_{escal}$: total treatment with dose escalation (10 fractions of phase 1 plan + 22 fractions of phase 2 plan). Constr. violation: number of patients for whom a specified constraint was violated in the $IMRT_{escal}$ treatment.

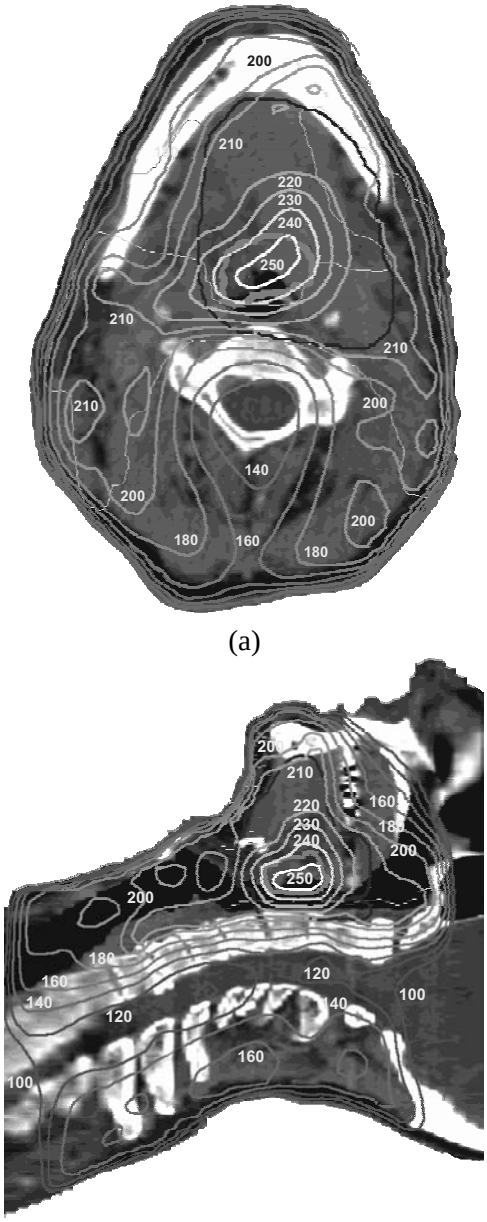

Figure 3: Fraction dose distribution for a patient with a tumor of the oropharynx in a transverse (a) and sagittal (b) view. The PTV_{PET} is indicated by a thick grey line, while the PTV_{69} is shown in a black line. Isodose lines are in cGy.

calation up to $\pm$ 80 Gy (as a maximal dose) to the GTV without major influence on the dose to the surrounding structures [21]. The boost volume should ideally reflect that part of the tumor with the highest intrinsic radio-resistance. The macroscopic tumor - approximated on CT by the GTV_{CT} - is very heterogeneous with respect to radiobiological properties, like clonogenic cell density, proliferation rate and hypoxia. FDG uptake might express some of these biological properties. It has been shown that patients with a head and neck tumor showing a higher uptake of FDG have a worse local control than the patients with a lower FDG uptake [1]. In conclusion, there are two main reasons to select FDG-PET in order to determine the boost volume: (1) high FDG uptake correlates with worse local control; (2) FDG-PET-based target delineation correlates better with tumor macroscopy than CT-based delineation and results in smaller volumes. The use of FDG-PET scans for the delineation of the tumor volume in head and neck has been investigated by several authors. Ciernik *et al* [3] used coregistered PET/CT in the radiotherapy treatment planning of 12 head and neck patients. In their report, the GTV (including possible lymph nodes) changed by more than 25% in 6 out of 12 patients. Moreover, the inter-observer variability of the GTV delineation significantly decreased by the use of PET. Geets *et al* [11] found a reduction of 40% in GTV by FDG-PET when compared to CT-based GTV delineation. In the present report, we found a GTV_{PET} that was 45% smaller than the GTV_{CT}, confirming the data of Geets *et al*. Scarfone *et al* [17] studied the influence of FDG-PET scan on the target volumes in 6 head and neck cancer patients. In their series, the GTV (as defined on CT only) was adapted in 5 out of 5 analyzable patients after coregistered PET/CT data were available and nearly 20% of the GTV_{PET} was located outside of the GTV_{CT}.

The dose escalation to the PTV_{PET} in the IMRT planning did not increase the complexity of the IMRT plans. The same class solution with 6 beam directions could be used, and the number of segments did not significantly increase. Except for thyroid cartilage in the patients with laryngeal and hypopharyngeal tumors, dose escalation to the PTV_{PET} did not alter the dose to the surrounding OARs. Wu *et*

al [20] reported on a dose escalation study in which the dose was escalated to the GTV, as defined on CT. They found that dose escalation, using a simultaneous integrated boost IMRT technique was feasible, and did not hamper parotid sparing. They found a homogeneity of $\pm$ 7% in the GTV, which is comparable to the $U_{98/2}$ of 4.6% we observed. In the report by Wu *et al*, boost dose was integrated over the whole treatment, by giving a higher dose/fraction every fraction. Although we also used the SIB planning technique (with different fraction sizes for different target structures), we choose to give the dose escalation during the first 10 fractions. Current state of the art planning systems are designed to use invariant anatomy for a treatment plan. Images used for planning are considered representative for the entire duration of treatment for which the plan was made. However, anatomical changes during fractionated treatment schedules of several weeks for head and neck cancer are known to occur frequently. These changes may involve tumor as well as OARs but the common practice of delineation and dose prescription seems robust against changing anatomy. In conventional radiotherapy, homogeneous doses are prescribed to PTVs that contain generous margins around known or suspected disease. Thereby, the risk for tumor to move out of the PTV margin is low, especially if the tumor is regressing during the course of treatment and the dosimetric effects of motion inside the PTV are low when dose homogeneity is high. However, when using a conformal dose distribution inside the PTV, like dose escalation to a subvolume, motion may seriously affect the tumor dose. In our application of focused dose escalation, any motion of the tumor tends to lower the dose it receives. For these reasons, we elected to use a focused dose escalation plan only for the 1^{st} phase of treatment. For the 2^{nd} phase of treatment, it appears logical to perform re-imaging and re-planning. The re-planning however, is not a trivial task if anatomy has changed since it has to take into account a previously given non-homogeneous dose, delivered to a different anatomy. None of our planning systems is capable to secure dose integration of two or more plans with a changing anatomy in-between. For these reasons, we used the pre-treatment imaging for the planning of both phases of treatment, the 1^{st} phase involving focused dose escalation while for the 2^{nd} phase a more robust conventional IMRT plan with homogeneous prescription doses to large (pre-treatment) volumes was made. "Biological imaging" (BI)-guided IMRT is a relatively new research area for improving treatment results of radiotherapy. Although it has been shown to be feasible, several improvements can be made on different levels. A closer integration of the biological image into the planning system seems a logical next step for BI-guided IMRT. The dose escalation in this study was applied to a contour that was generated by clipping on a certain PET signal value. PET signal values within the GTV_{PET} can still vary substantially. We are currently investigating the feasibility of direct incorporation of the PET signal intensity into the planning procedure.

In conclusion, twenty patients were treated within a dose escalation protocol. The use of PET information altered the target volumes in approximately one third of the patients. The GTV defined on PET was significantly smaller than the GTV that was delineated using CT only. Dose escalation to the PTV_{PET} was performed in the first 10 fractions, and resulted in a total physical dose of 72.5 Gy to the PTV_{PET}. This dose escalation did not influence the complexity of the IMRT treatment and was highly selective to PTV_{PET}, as the dose to the other PTVs and organs at risk was not significantly higher due to the escalation.

References

[1] Allal AS, Dulguerov P, Allaoua M, *et al*. Standardized uptake value of 2-[(18)F] fluoro-2-deoxy-D-glucose in predicting outcome in head and neck carcinomas treated by radiotherapy with or without chemotherapy. *J Clin Oncol* 2002;20:1398-404

[2] Chao K, Ozyigit G, Tran B, Cengiz M, Dempsey J and Low D. Patterns of failure in patients receiving definitive and postoperative IMRT for head-and-neck cancer. *Int J Radiat Oncol Biol Phys* 2003;55:312-321

[3] Ciernik I, Dizendorf E, Baumert B, *et al*. Radiation treatment planning with an integrated positron emission and computer tomography (PET/CT): a feasibility study. *Int J Radiat Oncol Biol Phys* 2003;57:853-63

[4] Daisne JF, Sibomana M, Bol A, Doumont T,Lonneux M and Gregoire V. Tri-dimensional automatic segmentation of PET volumes based on measured source-to-background ratios: influence of reconstruction algorithms. *Radiother Oncol* 2003;69:247-50

[5] Daisne JF, Duprez T, Weynand B *et al*. Tumor volume in pharyngolaryngeal squamous cell carcinoma: comparison at CT, MR imaging, and FDG PET and validation with surgical specimen. Radiology 2004;233(1):93-100

[6] Dawson L, Anzai Y, Marsh L, *et al*. Patterns of loco-regional recurrence following parotid-sparing conformal and segmental intensity-modulated radiotherapy for head and neck cancer. *Int J Radiat Oncol Biol Phys* 2000;46:1117-1126

[7] De Gersem W, Claus F, De Wagter C and De Neve W. An anatomy-based beam segmentation tool for intensity-modulated radiation therapy and its application to head-and-neck cancer. *Int J Radiat Oncol Biol Phys* 2001;51:849-859

[8] De Gersem W, Claus F, De Wagter C, Van Duyse B and De Neve W. Leaf position optimization for step and shoot IMRT. *Int J Radiat Oncol Biol Phys* 2001;51:1371-1388

[9] De Neve W, Duthoy W, Claus F, *et al*. Dose conformation in IMRT for head and neck tumors: which solution to apply? *Cancer/Radiotherapie* 2002;6 (Suppl. 1):32-36

[10] De Neve W and Duthoy W. Intensity-modulated radiation therapy for head and neck cancer. *Expert Rev Anticancer Ther* 2004;4:425-34

[11] Geets X, Daisne JF, Grégoire V, Hamoir M and Lonneux M. Role of 11-C-methionine positron emission tomography for the delineation of the tumor volume in pharyngo-laryngeal squamous cell carcinoma: comparison with FDG-PET and CT. *Radiother Oncol* 2004;71:267-73

[12] Grégoire V, Coche E, Cosnard G, Hamoir M and Reychler H. Selection and delineation of lymph node target volumes in head and neck conformal radiotherapy. Proposal for standardizing terminology and procedure based on the surgical experience. *Radiother Oncol* 2000;56:135-150

[13] Harnsberger HR. Handbook of Head and Neck Imaging. 2nd edition, St. Louis: Mosby. 1995

[14] Lee S, Leu M, Smathers J, McBride W, Parker R and Withers H. Biologically effective dose distribution based on the linear quadratic model and its clinical relevance. *Int J Radiat Oncol Biol Phys* 1995;33:375-389

[15] Mohan R, Wu Q, Manning M and Schmidt-Ullrich R. Radiobiological considerations in the design of fractionation strategies for intensity-modulated radiation therapy of head and neck cancers. *Int J Radiat Oncol Biol Phys* 2000;46:619-630

[16] Rudoltz M, Perkins R, Luthmann R, *et al*. High-dose-rate brachytherapy for primary carcinomas of the oral cavity and oropharynx. *Laryngoscope* 1999;109: 1967-1973

[17] Scarfone C, Lavely W, Cmelak A, *et al*. Prospective feasibility trial of radiotherapy target definition for head and neck cancer using 3-dimensional PET and CT imaging. *J Nucl Med* 2004;45:543-52

[18] Sobin LH, Wittekind C, editors. UICC TNM classification of malignant tumours 6th ed. New York: Wiley-Liss, 2002

[19] Tate D, Adler J, Chang S, *et al*. Stereotactic radiosurgical boost following radiotherapy in primary nasopharyngeal carcinoma: impact on local control. *Int J Radiat Oncol Biol Phys* 1999;45:915-921

[20] Wu Q, Mohan R, Morris M, Lauve A and Schmidt-Ullrich R. Simultaneous integrated boost intensity-modulated radiotherapy for locally advanced head-and-neck squamous cell carcinomas. I: dosimetric results. *Int J Radiat Oncol Biol Phys* 2003;56:573-585

[21] Zhou J, Fei D and Wu Q. Potential of intensity-modulated radiotherapy to escalate doses to head-and-neck cancers: what is the maximal dose? *Int J Radiat Oncol Biol Phys* 2003;57:673-82

V. 5. Whole abdominopelvic radiotherapy (WAPRT) using intensity-modulated arc therapy (IMAT): First clinical experience.

Authors: W. Duthoy, W. De Gersem, K. Vergote, M. Coghe, T. Boterberg, Y. De Deene, C. De Wagter, S. Van Belle and W. De Neve.

Journal: International Journal of Radiation Oncology Biology Physics 2003; 57(4):1019-1032

Acknowledgements: The project "Conformal Radiotherapy Ghent University Hospital" is supported by the Belgische Federatie tegen Kanker and by grants from the Fonds voor Wetenschappelijk Onderzoek (FWO) Vlaanderen (G.0183.03), the University of Ghent (GOA 12050401, BOF 01112300, 011VO497, 011B3300), and the Centrum voor Studie en Behandeling van Gezwelziekten. Wim Duthoy is a Research Assistant (Aspirant) of the FWO. Yves De Deene is Post-Doctoral Research Fellow of the FWO.

Key issues discussed in this paper:

- Theoretically, IMAT is indicated in these anatomical situations in which a PTV is wrapped concavely around an OAR with a large radius.
- The anatomy-based approach for segmentation, developed at GUH, has favorable characteristics for the transition from IMRT to IMAT.
- An IMAT class solution was developed for whole abdominopelvic radiotherapy, and clinically implemented for ovarian carcinoma.
- A PGD experiment on an anthropomorphic phantom showed good agreement between the calculated and measured dose distributions for the PTV. All clinically imposed constraints were met in the PGD-measured dose distribution for the PTV and OARS.
- Compared to the best available 3D plan, IMAT resulted in a higher homogeneity in the PTV, and a lower mean and median dose the kidneys (dose-limiting OARS).

Whole abdominopelvic radiotherapy (WAPRT) using Intensity Modulated Arc Therapy (IMAT): first clinical experience.

Wim Duthoy, M.D.[1], Werner De Gersem, Ir.[1], Koen Vergote, M.Sc.[1],
Marc Coghe, Lic.[1], Tom Boterberg, M.D., PhD.[1], Yves De Deene, M.Sc., PhD.[1],
Carlos De Wagter, Ir., PhD.[1], Simon Van Belle , M.D., PhD.[2], and Wilfried De Neve, M.D., PhD.[1]

1. Division of radiotherapy and 2. Department of Medical Oncology,
Ghent University Hospital, De Pintelaan 185, 9000 Ghent, Belgium

Abstract

Purpose: Whole abdominopelvic radiation therapy (WAPRT) is a treatment option in the palliation of patients with relapsed ovarian cancer. With the conventional techniques, kidneys and liver are the dose and homogeneity limiting organs. We developed a planning strategy for intensity modulated arc therapy (IMAT) and report on the treatment plans of the first five treated patients.

Materials and methods: Five consecutive patients with histologically proven relapsed ovarian cancer were sent to our department for WAPRT. The target volumes and organs at risk (OAR) were delineated on 0.5 cm thick CT slices. The clinical target volume (CTV) was defined as the total peritoneal cavity. CTV and kidneys were expanded with 0.5 cm. In a preset range of 8° interspaced gantry angles, machine states were generated with an anatomy based segmentation tool. Machine states of the same class were stratified in arcs. The optimization of IMAT was done in several steps, using a biophysical objective function. These steps include weight optimization of machine states, leaf position optimization adapted to meet the maximal leaf speed constraint, and planner-interactive optimization of the start and stop angles. The final control points (machine states plus associated cumulative monitor unit counts) were calculated using a collapsed cone convolution/superposition algorithm. For comparison, two conventional plans (CONV) were made, one with two fields (CONV2), and one with four fields (CONV4). In these CONV plans, dose to the kidneys was limited by cerrobend blocks. The IMAT and the CONV plans were normalized to a median dose of 33 Gy to the planning target volume (PTV). Monomer/polymer gel dosimetry was used to assess the dosimetric accuracy of the IMAT planning and delivery method.

Results: The median volume of the PTV was 8306 cc. The mean treatment delivery time over four patients was 13.8 minutes. A mean of 444 monitor units was needed for a fraction dose of 150 cGy. The fraction of the PTV volume receiving more than 90% of the prescribed dose (V_{90}) was 9% higher for the IMAT plan than for the CONV4 plan (89.9% vs 82.5%). Outside a build-up region of 0.8 cm and 1 cm away from both kidneys, the inhomogeneity in the PTV was 15.1% for the IMAT plans and 24.9% for the CONV4 plans (for CONV2 plans, this was 34.9%). The median dose to the kidneys in the IMAT plans was lower for all patients. The 95^{th} percentile dose for the kidneys was significantly higher for the IMAT plans than for the CONV4 and CONV2 plans (28.2 Gy vs 22.2 Gy and 22.6 Gy for left kidney, respectively). No relevant differences were found for liver. The gel-measured dose was within clinical planning constraints.

Conclusion: IMAT was shown to be deliverable in an acceptable time slot and to produce dose distributions that are more homogeneous than those obtained with a CONV plan, with at least equal sparing of the OARs.

Introduction

The treatment options for most patients with relapsed ovarian cancer are palliative. For patients who relapse within 12 months after platinum-based schedules, second or third line chemotherapy is often used, but the response rates average between 10% and 30% [1].

A difficult problem to palliate is bowel obstruction. Surgery may be attempted but the disease is often multifocal making palliative resection impossible. In reports of Redman [2] and Krebs [3] , 10% to 15% of patients died within 8 weeks after surgery and 35% to 38% had no clinical benefit. The results of chemotherapy for bowel obstruction are disappointing. In a report by Abu-Rustum [4] , a response was observed in only one of 18 patients treated with chemotherapy for bowel obstruction. Radiation therapy seems to compare favorably to second or third line chemotherapy, with symptom response rates between 63% and 79% with a median duration between 4 and 9 months [5, 6, 7]. Given the pattern of spread of ovarian cancer, whole abdominopelvic radiation therapy (WAPRT) could be the radiation technique of choice, eventually with a boost to sites of gross tumor.

Maximum tolerated dose levels to the whole kidney are often set to 20 Gy or less. When the kidneys are blocked from radiation, conventional techniques result in underdosage of the peritoneal regions in the blocked areas.

We investigated the potential of Intensity Modulated Radiation Therapy (IMRT) to spare kidneys and liver. For reasons described in the discussion section, we selected Intensity Modulated Arc Therapy (IMAT) [8] as the most appropriate IMRT-technique for WAPRT.

This paper describes the results of the translational research that was performed to bring IMAT into the clinic for WAPRT. We report on treatment planning and delivery for the first five patients treated with IMAT-WAPRT. The clinical results of the phase I study will be reported elsewhere.

Materials and methods

Delineation of target volumes and OARs

Between November 2001 and October 2002, 5 patients with a relapse of a histologically proven adenocarcinoma of the ovary were treated by IMAT. All patients signed informed consent for IMAT to the whole abdomen. A planning CT-scan was performed with the patient lying supine, with both arms resting under the head. The upper border of the scanned volume was located 10 cm cranial to the diaphragm, while the lower border was defined as 10 cm caudal to the obturator foramina. 0.5 cm thick sequential CT-slices were acquired without contrast enhancement. Clinical Target Volume (CTV) was defined as the total peritoneal cavity, with the inclusion of iliac and paraaortic lymph node regions. A 0.5 cm rim of liver, adjacent to the peritoneum, was also included into the CTV. The upper CTV boundary was defined by the highest CT-slice on which the diaphragmatic dome was visible, and the most caudal drawing of the CTV was on the level of the bottom of the obturator foramina. A Planning Target Volume (PTV) was made by a 3D expansion of the CTV with a margin of 0.5 cm in all directions. The kidneys and the liver (further called OARs: organs at risk) were drawn as visualized on CT, and the kidneys were expanded with 5 mm (kidney_exp_5mm), to account for setup inaccuracy and organ motion. PTV and OARs overlap, which would result in a conflicting requirement from the optimization algorithm. A similar problem arises with those parts of the PTV in the build-up region. Both problems were solved by defining subvolumes inside the PTV which are used as optimization volumes (PTV_optim). PTV_optim was nowhere closer than 0.8 cm to the skin surface or 0.5 cm to the expanded kidneys. A surrounding structure was made by subtracting the PTV from the total scanned volume of the patient. This structure (sur_0cm) was used to avoid hot spots outside of the PTV. A general description of the use of PTV subvolumes and surrounding structures for IMRT plan optimization is found elsewhere [9].

Table 1: Details about the IMAT treatments.

	isocenters	arcs	control points	monitor units	delivery time (min.)
Patient 1	1	11	73	568	< 20
Patient 2	1	7 + 1 SW	110	387	11.6 ± 2.5
Patient 3	1	7 + 1 SW	78	378	15.3 ± 3.6
Patient 4	2	7 + 1 SW	99	528	18.1 ± 3.6
Patient 5	1	6 + 1 SW	148	359	13.5 ± 1.3

For the first patient, no systematic measurements were done concerning the delivery time. The monitor units are for one fraction of 150 cGy. SW= Sliding Window.

IMAT planning procedure

Generation of machine states by ABST

An anatomy based segmentation tool (ABST) was developed at our institution to create segments for step-and-shoot IMRT [10]. For IMAT planning ABST is used to create an initial set of segments, which we will call machine states. A machine state is described by a set of machine parameters that uniquely define the beam incidence, aperture and photon beam quality. After definition of the isocenter location and with the collimator, table top and isocenter rotations at zero degrees, ABST generated machine states per 8° of gantry rotation. Restriction of the range of gantry angles was needed to avoid beams traversing metal components of the couch before entering the patient. The couch on the linear accelerator (Elekta, Crawley) used for the IMAT treatments has two C-arms, which can be positioned at one of the 30° discrete angles. The largest range of possible gantry angles was obtained by setting the arms at 120°, measured from their lateral position (Fig. 1). For patients 2, 3 and 5, a class solution was used, implying that the initial machine states were generated using a fixed set of parameters, including start and stop gantry angles, widths of the segments and conformal avoidance structure. The arcs used by the class solution are shown in figure 1. For patient 4, where the cranio-caudal extend of the PTV was 42 cm, a second isocenter was defined 12 cm from the first isocenter in caudal direction. Only a longitudinal table shift is required to perform the transition between the two isocenters. An additional "pelvic arc" was made around a structure called PTV_pelvis, with the L5-S1 intervertebral space as the upper border. The collimator was rotated by 90°, to have the leaf movements in the cranio-caudal direction and allow for feathering in the junction region [11].

For each gantry angle, ABST generates multiple machine states which only differ by apertures of the multileaf collimator (MLC). Each beam's-eye-view (BEV) projection of a MLC aperture covers a part of the PTV at one side of the anatomical structure that is to be avoided. A margin of 0.8 cm around the PTV is used to account for penumbra. For each gantry angle, the machine states differ from each other by the degree of coverage of the BEV projection of the PTV. For a detailed description of ABST, we refer to De Gersem et al. [10]. These machine states are useful to create intensity levels that increase with decreasing distance to the anatomical structure that is to be spared. It was shown by Brahme and others [12, 13] that such intensity profiles are useful to create homogeneous dose distributions to a concave PTV which conformally avoid anatomical structures at risk. The machine states were stratified in classes, the first class consisting of machine states with the largest area of MLC aperture; the second class consisting of machine states with the second largest area of MLC aperture and so on. Due to the algorithm inside ABST which creates MLC apertures avoiding anatomical structures with -in this case- smooth surfaces, MLC apertures, which belong to the same class of machine states, do not differ much from one gantry angle to the next, their angular separation being only 8°. Hence, the leaf travel required when moving from one gantry angle to the next is small for machine states of the same class which is preferable for dynamic transitions as in IMAT.

For patients 2-5, an additional posterior "sliding window" intensity modulated beam with a 90° col-

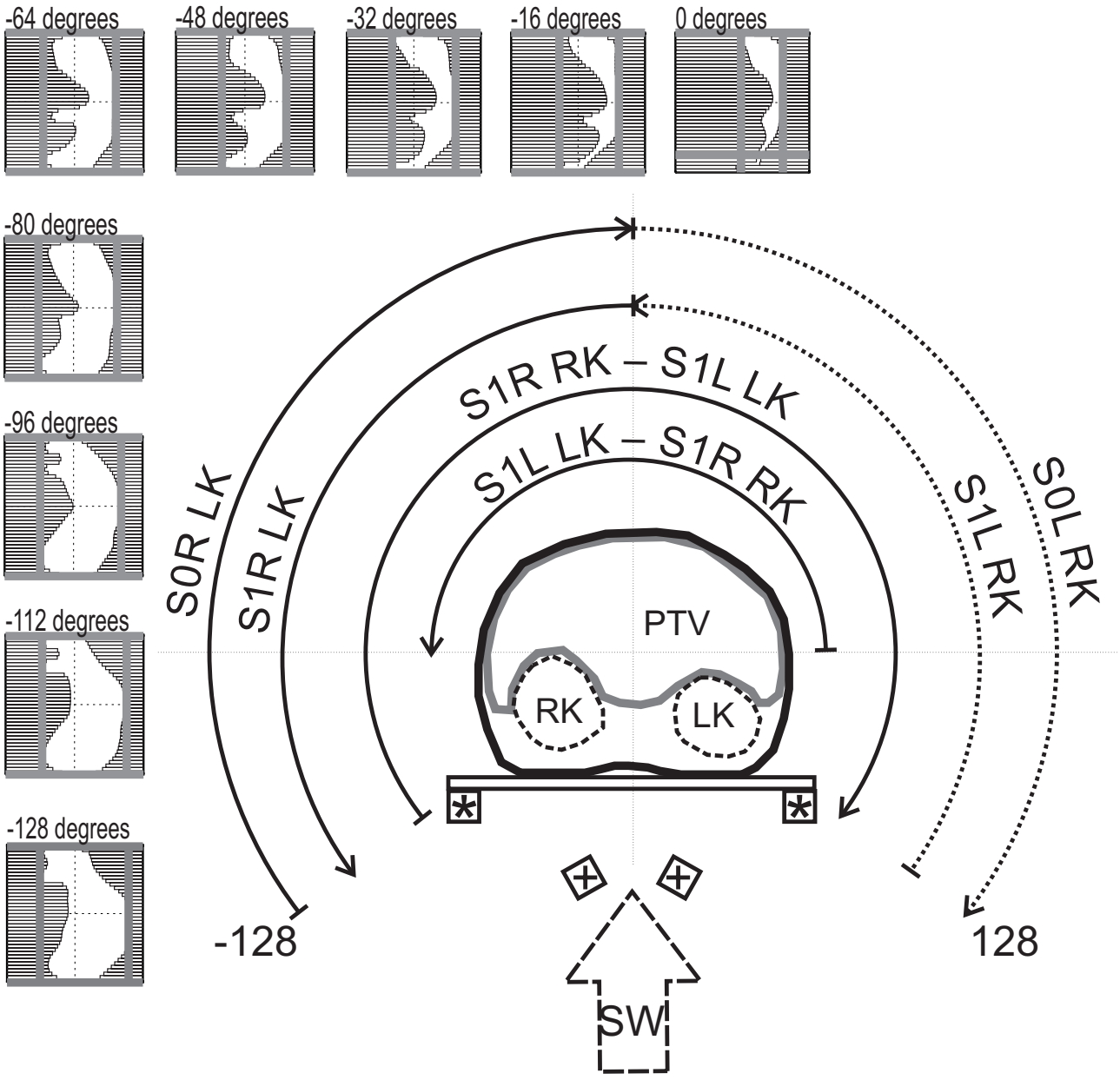

Figure 1: Class solution for the IMAT plan. A transverse plane through the patient can be appreciated, with the PTV, the left kidney (LK) and the right kidney (RK). The arcs are depicted by circle segments. Abbreviations: S0R LK: Arc composed by the machine states covering the total BEV projection of the PTV passing the right side of the LK. S0L RK: Arc composed by the machine states covering the total BEV projection of the PTV passing the left side of the RK. S1R LK: Arc composed by the machine states covering a 3 cm wide area of the PTV at the right side of the LK. S1L RK: Arc composed by the machine states covering a 3 cm wide area of the PTV at the left side of the RK. The metal C-arms are shown as the grey squares, respectively in their most lateral position (asterisk) for the sliding window, and in their 120° position (+ sign). The large dashed arrow represents the beam direction for the delivery of the sliding window (SW). Machine states for one arc (S0R LK) are shown every 16°, from -128° to 0°. The thick grey lines represent the jaw position, each small white bar stands for one leaf.

limator rotation was used. For this beam, the table bars were put on their most lateral position. Due to the position of these metal bars, and the impossibility to prescribe arcs traveling over the 180° gantry point, the range for posterior arcs is very limited. Therefore, a sliding window IM-beam with static gantry angle was preferred to boost the most posterior region of the PTV. The control points for this sliding window were made manually. For patient 4, the most caudal isocenter was selected for this sliding window beam.

Creation and optimization of control points

The machine instruction file to deliver arc therapy with dynamic MLC consists of a sequence of control points (Fig. 1). A control point is defined as a machine state plus a monitor unit count (MUC) value. Delivery of a sequence of control points implies that the prescribed machine state has to be reached at the MUC value for each control point. The transition from a control point to the next is slaved by the MU counter, each parameter (leaf positions, jaw positions and gantry angle) that changes between two control points is linearly interpolated as function of the MUC value. The beam is paused if the control software detects that a machine parameter is outside tolerance to the (linearly interpolated) position prescribed by the machine state. Control point optimization involves the machine states - and more precisely the leaf positions - as well as the MUC values and is done by a Segment Outline and Weight Adapting Tool (SOWAT) [14], modified for IMAT purposes (SOWAT-IMAT). The main difference between SOWAT and SOWAT-IMAT resides in the maximal leaf velocity (MLS) constraints. After the control point generation and after each leaf position optimization cycle, a leaf velocity constrainer (LVC) adapts leaf positions of all control points to obey maximum leaf speeds, minimum distances to opposed and diagonally opposed leaves and maximum leaf position extends (method unpublished). MUCs are optimized for each step, a step being defined as the transition from one control point to the next. The objective function on which the optimization is done is a biophysical model and has been described and discussed elsewhere [15, 16].

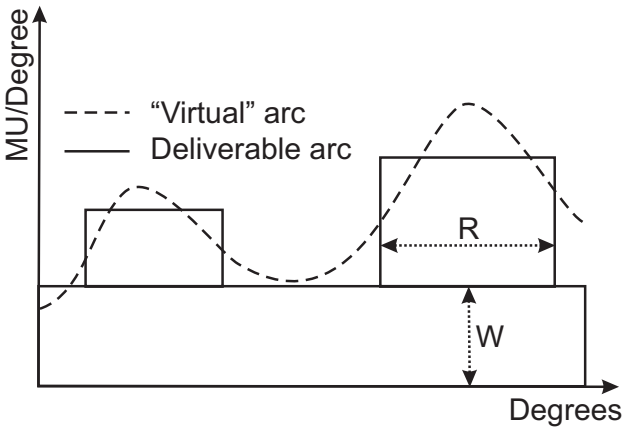

Figure 2: Picture representing the angular delivery rate. One "virtual" arc (dashed line) as well as three deliverable arcs (solid lines) are shown. The "virtual" arc is not deliverable on the Elekta linac. The deliverable arcs approximate the optimized virtual arc. The final angular delivery rate (W) of the deliverable arcs is optimized as described in the text.

Transformation to deliverable arcs

As a result of SOWAT-IMAT, n machine states and n-1 weights are obtained. These weights are numbers of monitor units that have to be delivered while the machine moves from one control point to the next. Apart from leaf and jaw travel, such motion involves a 8° gantry rotation. Because the Elekta SL-series of linear accelerators was designed to deliver arcs with a gantry rotation speed directly proportional to the dose rate, the number of monitor units delivered per degree (angular delivery rate) must remain constant over the whole arc. This condition is not secured by SOWAT-IMAT. In fact, the (requested) angular delivery rate may be different for each 8°-sector of gantry rotation. This problem is solved by splitting each arc which features a variable angular delivery rate into multiple overlapping arcs each with a constant angular delivery rate (Fig. 2). This procedure also provides the start and stop angles of the delivered arcs. The plan is finalized by a SOWAT-IMAT optimization cycle which involves optimization of leaf positions and the angular delivery rate (equal for all sectors of the arc in order to keep the angular delivery rate constant within each arc).

Dose prescription and computation

The prescribed dose was 33 Gy (median dose in the PTV), given in 22 fractions. Except for the first patient, IMAT plans were accepted using the following clinical criteria: less than 5% of the PTV volume was allowed to receive more than 107% of the prescribed dose, and more than 95% of the volume of PTV_optim had to receive more than 90% of the prescribed dose; less than 5% and 20% of the kidneys_exp_5mm should receive more than 30 Gy and 25 Gy, respectively, while the median dose had to be lower than 18 Gy; the median liver dose was constrained to 30 Gy. After clinical constraints were met by the optimization procedure, a final dose computation was performed for 18 MV with the collapsed cone convolution/superposition algorithm from Pinnacle [Philips Medical Systems, Best, The Netherlands]. A final optimization of the MUs of all arcs was done using the results of this dose computation. The value of a MU is such that 100 MUs correspond to 1 Gy at reference depth (5 cm for 6 MV and 10 cm for 18 MV) for a 10x10 cm field and a source-detector distance of 100 cm.

IMAT treatment delivery

For each arc, a prescription file containing the sequence of control points and related monitor units is generated and networked to an SLiPlus 18 MV linear accelerator (Elekta, Crawley, UK). The IMAT treatment is delivered in local service mode using prototype dynamic control software (Elekta, Crawley, UK), operating as described before [17]. Delivery of dynamic prescriptions is not possible in clinical mode on the Elekta linear accelerators. The local service mode is operated in the same interlock class as in clinical mode. Thereby, tolerances used by the linac's control system are the same as for clinical mode.

Conventional plans

For each patient, two different conventional (CONV) plans were made. The first plan was the widely used "AP/PA" technique, using an anterior and a posterior field (CONV2). A second plan used 4 beams (CONV4), anterior, posterior and two lateral fields. The field margins were drawn with a 1 cm margin around the PTV in all directions. Kidney blocks covered the BEV projection of the kidneys with a margin of 0.5 cm. For the CONV2 plans, the posterior field was duplicated in 2 segments, an open segment and a segment where kidney blocks were inserted. Respectively, 6 MV and 18 MV photons were used for the anterior and posterior field. For the CONV4 plans, all four fields were duplicated in 2 segments each, an open segment and a segment with kidney blocks. Here, 18 MV photons were used for all fields.

Optimization of the relative segment weights was done by the planner, to reach a median dose to the expanded kidneys between 18 and 20 Gy. Median dose to the liver was constrained to 30 Gy. Dose computation was done with the same collapsed cone convolution/superposition algorithm.

Treatment evaluation.

Delivery time, defined as the time between the start of the first arc and the end of the last arc or sliding window, was measured for patients 2-5. Additionally, the setup time was measured from the entrance of the treatment room by the patient to the start of the first arc. This includes the time necessary to acquire portal images and correction of the patient position.

Comparison of dose distributions obtained with the CONV2, CONV4 and the IMAT plan were done after normalizing the median dose of the PTV to 33 Gy. To evaluate the dose homogeneity in the target volumes, an inhomogeneity factor $U_{95/5}$ was defined as the difference between the 95^{th} percentile dose (D_{95}) and the 5^{th} percentile dose (D_5), divided by the median dose (D_{med}). We preferred to use the D_{95} and the D_5 above the maximum and minimum dose, because an underdosage was allowed in the region close to the kidneys. Other endpoints for the target volumes were the first percentile dose (as a surrogate for minimum dose), the 99^{th} percentile dose and the ratio of volume of the target structure receiving more than 95% of the prescribed dose (V_{95}) over the total volume. For the parallel-element organs kidney and liver, the D_{med} was used. The DVHs were reconstructed for the 5 patients, by calculating the mean dose and the standard error of the mean at every 5% volume level. The paired Student t-test was used. All

tests were two-tailed and $p < 0.05$ was considered as a statistically significant difference.

Dosimetric verification of the IMAT treatment.

Monomer/polymer gel dosimetry was used for 3D dose verification of the whole IMAT procedure. A de-oxygenated hydrogel infused with acrylic monomers forms the basis for this dosimetric technique [18]. Highly reactive radicals, formed by radiolysis during irradiation of the gel, initiate a polymerization reaction. The amount of polymer formed is related to the absorbed dose. Formation of polymer clusters in the water-equivalent gel increases the local spin-spin relaxation rate (R2), a typical magnetic resonance (MR) contrast parameter. Therefore, MR imaging (MRI) can be used to visualize the amount of polymer formed and subsequently the dose distribution in the gel. With monomer/polymer gel dosimetry, it is possible to obtain absorbed dose information in 3D with high spatial accuracy [19]. For a more detailed review on this subject, the reader is referred to De Deene et al. [20].

A Barex (Cifra, Chateau Thierry, France) cast was vacuum molded on the abdominal region of the Rando phantom (Alderson Research Laboratories, Stamford, CT). At our laboratory, the maximum amount of monomer/polymer gel that can be produced in one batch is 10 liter. Hence, the entire volume irradiated with IMAT can not be verified by one gel dosimetry experiment. We chose to limit the phantom geometry to that part of RANDO containing the (dosimetrically most interesting) region around the kidneys. Supports on the cranial and caudal side, marker lines and placement of fiduciary markers (Medtronic, Louisville, USA) on the surface facilitated a reproducible positioning of the gel phantom during CT scanning, IMAT delivery and MRI (Fig. 3). Three supplemental Rando slices were placed alongside the phantom on the cranial and caudal side during CT scanning and treatment delivery, to ascertain full scatter conditions in the gel upon irradiation. Spiral CT scans (Siemens Somatom Plus 4, Erlangen, Germany) of the gel-filled phantom were transferred to the planning system. Volumes of interest (kidneys, liver and PTV) from the first patient were transferred to the CT data set. For this setup, an IMAT plan was made by using the methods as described above. This resulted in a plan with 6 arcs and one sliding window. To cover the maximum response range of the gel while avoiding gradient dependent non-linearities in dose response [21], the monitor units were multiplied with a factor five, thus giving a median dose of 7.5 Gy to the PTV. For calibration purposes, gel-filled test tubes were irradiated to known doses (0 - 10 Gy, every 1 Gy) to

Figure 3: Adapted Rando phantom as used for the gel dosimetry. At each side of the Barex cast, three Rando slices were added to obtain full scatter conditions. Tape is attached to the phantom to draw laser lines in transverse, sagittal and coronal reference planes. Seven markers are attached to the phantom on the laser lines to facilitate positioning. The transverse plane indicated in the middle of the barex phantom is 13.5 cm cranial to the treatment isocenter. A barex screw is used to close the phantom at the place where the gel was inserted, visible left to the sagittal plane.

establish a dose-R2 relationship. The gel dosimeter and test tubes were scanned together in the body coil of a 1T MR system (Expert, Siemens, Erlangen, Germany). A 26-spin-echo sequence was applied with a (Carr-Purcell Meiboom-Gill) CPMG RF pulse encoding scheme and equidistant echo spacing (TE = 40 - 1080 ms). The phantom was scanned in 33 adjacent transverse slices, each with a slice thickness of 5 mm. A field-of-view of 320 mm and image resolution of 128×128 resulted in an in-plane resolution of 2.5 mm. Ideally, a homogeneous unirradiated gel phantom should produce identical R2 readings throughout the entire volume when scanned with MRI. A homogeneity study was done on the IMAT phantom filled with a blank gel and the MRI protocol was adjusted to minimize R2 variations related to temperature deviations and radiofrequent inhomogeneities.

A linear regression was used to describe the dose-R2 relationship. The gel-measured dose grid was transferred to the planning system and scaled to the prescription dose (33 Gy), which allowed the comparison of measured and computed DVHs of the different structures inside the abdominopelvic phantom, truncated to the volume of the gel-phantom. Low's γ-index [22] was calculated in 3D (dose difference criterion = 7.5%, distance-to-agreement = 5 mm), as a guide to pinpoint significant deviations between the computed and measured dose matrix. A γ-index above 1 indicates that the specified tolerances are not met.

Results

The median volume of the PTV in the five patients was 8306 cc (range 5717 - 9054 cc), and the median of the cranio-caudal length which had to be covered was 36 cm. Details on the treatment plans and delivery times are shown in table 1. Mean delivery time over patients 2-5 was 13.8 minutes (range 9.5 - 24.5 minutes). Less than 30% of the given fractions had a delivery time exceeding 15 minutes. Of these, 50 % were seen in patient 4, who had two isocenters, necessitating entrance of the treatment room to perform a cranial shift of the patient. For one patient (chronologically the last), the setup-time was measured over all the fractions, and showed a mean of 8 $\pm$ 2.9 minutes. Though actively asked for, no patient complained about the rotating gantry. As an example, the obtained intensity profiles for patient 5 are shown in figure 4.

Dose Volume Histogram analysis and dose distributions

The DVH data for the five patients are summarized in Table 2 and graphically displayed in figure 5. For both the CONV4 and IMAT plans, there is a large variation in minimal dose (represented by D_1) in the PTV (range 0.2 - 26.1 Gy), resulting from the PTV extending outside the skin in one patient. When considering the PTV without a build-up region of 8 mm (PTV_whbu), the very low doses that are the result of the ICRU PTV definition rather than of the planning technique, are eliminated (range of D_1: 19.5 - 26.9 Gy). The homogeneity in the PTV_whbu is better for the IMAT plan than for the CONV4 plan ($U_{95/5}$ is 20 % and 32% respectively; p = 0.01). Due to the strong dose constraint to the expanded kidneys, and due to the possibility to generate concave dose distributions, we expected an underdosage in the PTV in the region around the kidneys. For the PTV_optim, the mean (and the standard deviation) of the V_{95} was 78.4% ($\pm$ 2.2%) for the CONV4 plan, and 88.9% ($\pm$ 5.1%) for the IMAT plan (p = 0.01). For the V_{90}, these values were 87.7% ($\pm$ 3.0%) and 95.8% ($\pm$ 3.5%) for the CONV4 and the IMAT plan, respectively (p = 0.02). The comparison between the IMAT plan and the CONV2 plan (Table 1) shows a significant increase in homogeneity (expressed by $U_{95/5}$) for the PTV as well as for PTV_optim by the IMAT plans.

The median dose to the kidneys was lower for the IMAT plan in all patients, when compared to both CONV plans. The maximal doses to the kidneys were significantly higher for the IMAT plan than for the CONV plans, as can be seen in figure 5. For the liver, no significant differences were found between the IMAT and the CONV plans. The higher homogeneity by the use of lateral beams in the CONV4 plans yielded a higher dose to the liver.

Dose distributions for the first patient are shown in figure 6. The sparing of the kidneys by the IMAT

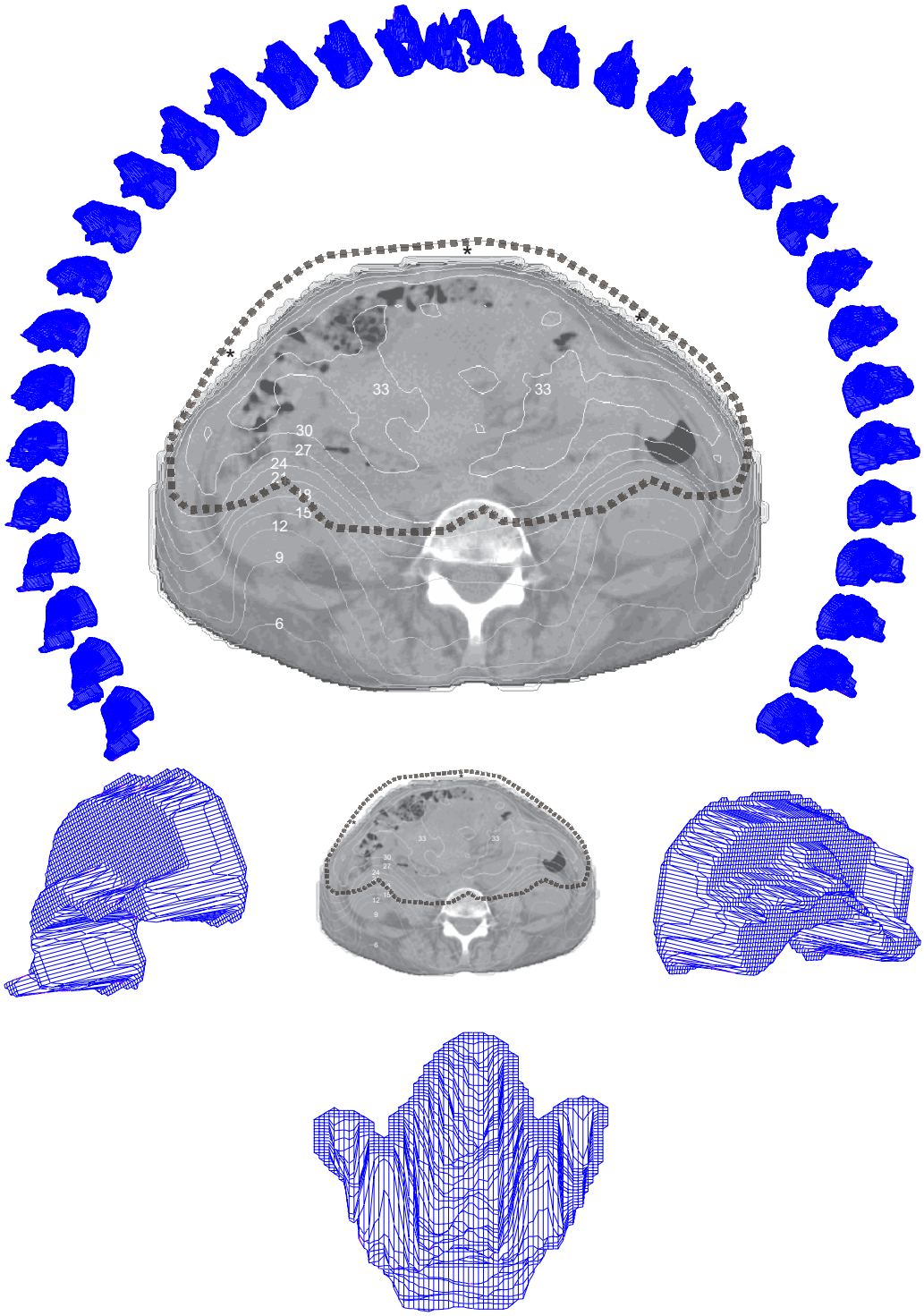

Figure 4: (a) Intensity profiles (rescaled) for the delivered plan of patient 2. The CT slice through the isocentric plane is shown, with the dose distribution in Gy. The PTV (dotted line) extends outside the scanned volume (asterisks). (a) Intensity profiles, generated at a range of gantry angles from -128° to 128°, are plotted around the CT-slice. (b) Intensity profiles for the gantry at -104°, 104° and for the posterior beam, delivered as a sliding window (180°).

Table 2: Summary of the DVH data showing averages $\pm$ standard deviations.

	IMAT	CONV2	p-value	CONV4	p-value
PTV					
V_{95} (%)	82.2 ± 6.5	76.8 ± 5.2	0.11	73.6 ± 5.9	0.01
V_{90} (%)	89.9 ± 5.7	80.1 ± 4.6	0.01	82.5 ± 6.1	0.01
V_{107} (%)	2.7 ± 3.4	6.4 ± 3.3	0.18	7.2 ± 4.41	0.05
D_1 (Gy)	19.0 ± 10.8	16.4 ± 9.1	0.09	16.6 ± 9.3	0.10
D_{99} (Gy)	35.8 ± 0.9	36.1 ± 0.6	0.53	36.5 ± 0.9	0.02
$U_{95/5}$ (%)	28.1 ± 15.8	42.3 ± 7.9	0.03	34.4 ± 10.9	0.10
PTV_optim					
D_1 (Gy)	27.0 ± 2.8	21.7 ± 0.9	0.02	24.5 ± 1.2	0.12
$U_{95/5}$ (%)	15.1 ± 5.8	34.9 ± 2.5	< 0.01	24.9 ± 4.1	0.01
Left kidney (expanded)					
D_{med} (Gy)	16.1 ± 3.6	19.9 ± 0.6	0.11	19.4 ± 0.4	0.11
D_{95} (Gy)	28.2 ± 1.3	22.6 ± 0.8	< 0.01	22.2 ± 0.4	< 0.01
Right kidney (expanded)					
D_{med} (Gy)	13.6 ± 3.9	19.3 ± 1.5	0.02	18.6 ± 1.1	0.02
D_{95} (Gy)	26.0 ± 2.9	22.8 ± 1.0	0.02	22.2 ± 1.0	0.08
Liver					
D_{med} (Gy)	24.4 ± 6.3	22.8 ± 10.1	0.44	29.2 ± 2.0	0.09

Abbreviations: IMAT: Intensity modulated arc Therapy; CONV2: conventional plan with an antero-posterior and a postero-anterior field; CONV4: conventional plan with 4-field technique; PTV: planning target volume; PTV_optim: PTV without build-up region of 0.8 cm and with the exclusion of the expanded kidneys with an extra margin of 5 mm;V_{95}, V_{90} and V_{107}: the partial volume (percent) receiving more than 95%, 90% and 107% of the prescribed dose; D_{99} and D_1: Dose given to 99% and 1% of the volume, respectively; $U_{95/5}$: inhomogeneity factor, defined as $\frac{(D_{95}-D_5)}{D_{med}}$, with D_{95} the 95^{th} percentile dose; D_5 the 5^{th} percentile dose andD_{med} the median dose.

plan does not produce underdosages in the cone of the PTV lying anteriorly to the kidney, in contrast to the CONV2 plan (Fig. 6b and 6e). This underdosage is largely, but not completely, resolved in the CONV4 plan, at the cost of higher liver dose (Fig. 6c and 6f). The dose distributions also illustrate that the maximal doses to the kidneys were higher in the IMAT plans than in the CONV plans, as there is a steep circular gradient around the kidneys.

Dosimetric verification.

Volumes of total and truncated structures are compared in table 3.

The DVHs for the truncated structures of both the computed plan and the results of the dosimetric measurements are shown in figure 7a. The median gel-measured dose in the PTV was 1% lower compared to the calculations. The median gel-measured dose for the liver was 16% higher (18.9 Gy compared to 16.4 Gy). For the right kidney, median measured dose was 13% lower than predicted by the dose calculations. All planning constraints were met in the measured dose distribution (Fig. 7a). A volume histogram was made using the computed γ-indexes for the total measured volume and for each relevant (truncated) structure (Fig. 7b). The γ-index was higher than 1 for 8.1% of the total measured volume (Table 3). The γ-index for the left and right expanded kidneys was higher than unity in 8.3% and 19.6% of the volumes respectively. Dose was outside tolerance in 1.9% volume of the liver part within the gel phantom. For

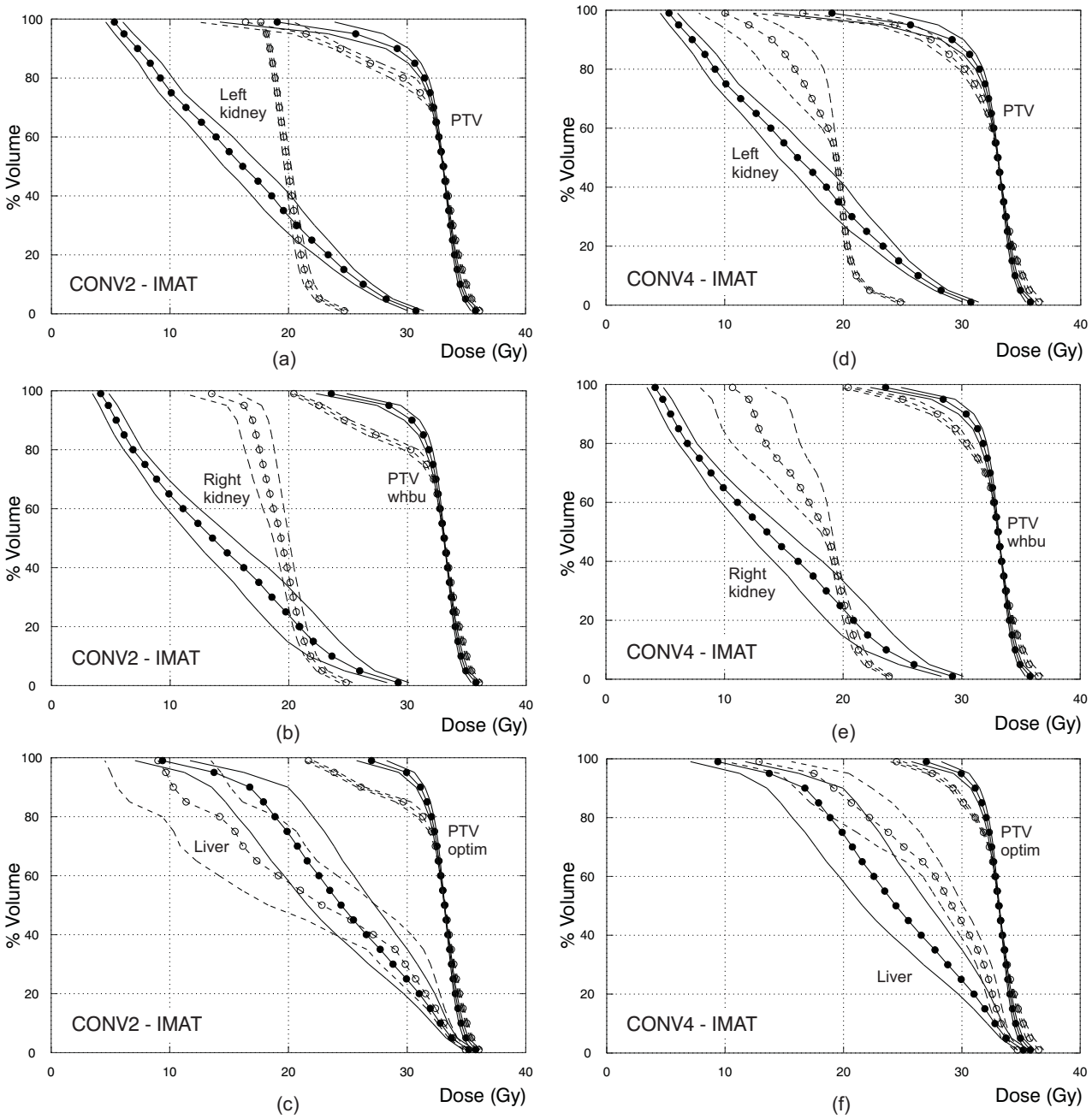

Figure 5: DVHs compiled from the data of the five patients. Solid lines and bold dots represent the IMAT plans (mean $\pm$ standard error of the mean). Dashed lines and circles represent the 2D plans. (a-c) DVHs of the IMAT and CONV2 plans. (d-f) DVHs of the IMAT and CONV4 plans. (a) + (d) DVHs of PTV and expanded left kidney. (b) + (e) DVHs for PTV_whbu and expanded right kidney. (c) + (f) DVHs of PTV_optim and liver.

PTV, 1.2% of the volume had a γ-index above 1. An example of a computed and a measured dose distribution is shown in figure 8a and 8b, respectively, together with a the iso-γ line at value 1 (Fig. 8c).

Discussion

Intensity modulation gives the possibility to generate concave dose distributions. This is a major ad-

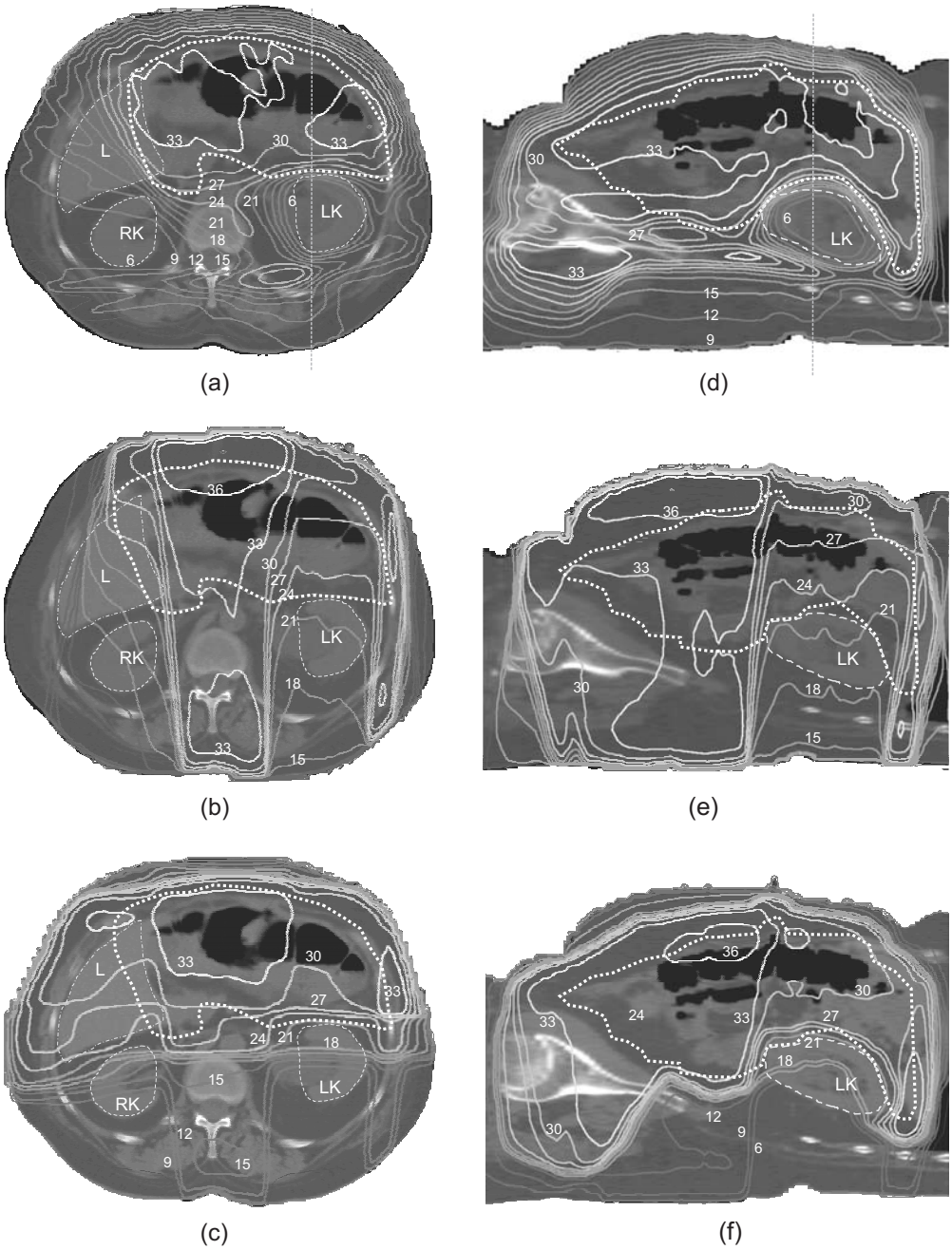

Figure 6: Dose distributions for patient 1, showing the delivered IMAT plan in a transverse (a) and sagittal (d) plane, and the conventional comparison plans in (b) + (e) for the CONV2 and (c) + (f) for the CONV4 plan. Isodose values are in Gy. The PTV is delineated with a dotted line. The kidneys (LK: left kidney and RK: right kidney) are delineated by dashed lines, while the liver (L) is circled by a dashed-dotted line. The dotted straight line in (a) and (d) indicates the transection planes in (d-f) and (a-c), respectively.

vantage in the treatment of cases where the PTV is wrapped around a dose limiting OAR, e.g. in the head and neck region. For planning cases where the radius of curvature of the concavity of the intended iso-

Table 3: Total volumes of contoured structures, volumes of the parts of these structures inside the gel phantom and relative volumes of these parts. Percentage volumes of the truncated structures that have a γ-index above unity are shown in the last column.

Structure	Volume (cc)	Volume in gel-phantom (cc)	Partial volume in gel-phantom (%)	Volume($\gamma > 1$) (%)
PTV	6943.2	2060.9	29.7	1.2
PTV_optim	6574.8	1907.9	29.0	0.4
Left kidney (expanded)	370.8	337.5	91.0	8.3
Right Kidney (expanded)	283.6	254.4	89.7	19.6
Liver	1471.6	1459.0	99.1	1.9
Scanned volume	18653.8	8330.7	44.7	8.1

dose lines is rather small, a beam setup with a limited number of incidences is sufficient. Stein et al. [23] demonstrated this for prostate cancer where the dose distribution concavity is generated around the rectum. However, when the internal radius is increasing with equal distance to OAR(s) inside the concavity, an increasing number of beam incidences is needed to avoid underdosage in parts of the PTV while maintaining the same OAR sparing, as demonstrated in figure 9. The fastest way to deliver a very large number of incidences is arc therapy. Therefore, IMAT was selected in our department as a delivery method only for those situations where intensity modulation is needed together with sparing of OARs of medium and large sizes. Next to WAPRT, the same planning problem can be encountered in e.g. rectal cancer (and more broadly in pelvic irradiation), malignant pleural mesothelioma and breast cancer.

We compared the planning results of the IMAT plan with a 2-field and a 4-field conventional plan. By applying IMAT, we could improve homogeneity ($U_{95/5}$) by 49% in the PTV_whbu in comparison with the CONV2 plan, and by 37% compared to CONV4. Furthermore, the median dose to the kidneys was lower in all patients. A recent report found that functionality defects (estimated using static scintigraphy) were correlated with the dose and volume of the irradiated kidney [24]. In that dose-effect curve, the risk of any scintigraphic changes for an irradiation of 10 to 30% of the renal volume to doses between 20 and 30 Gy is estimated to be between 10 and 40%. The five patients described in our report were all in this range (Fig. 5). However, in their series, no patient had clinical symptoms of nephrotoxicity nor any rise in serum creatinine levels. Considering the dose distribution to the liver, no relevant differences were found between IMAT and CONV.

The doses measured with gel dosimetry were within clinical planning constraints, although large differences can be seen on the DVHs (Fig. 7) for the right kidney and the liver. For the kidney, a lower dose was measured than computed, while for liver the opposite was seen. Only a small part (1.9%) however of the liver had a γ-index above one. For PTV, DVHs of measured and computed dose distributions showed no relevant differences. Also only a low volume part of the PTV had a γ-index more than one (1.2%). Both results validated the IMAT delivery in the PTV. The relatively large fractions of left and right kidney with a γ-index more than one (8.3% and 19.6%, respectively) can have multiple reasons. As the kidneys are most of the time shielded by leaves only and not by the backup diaphragms, calculation errors of leaf transmission have a high impact on the computed doses to these structures. Inaccuracy of computed output factors of fields with high offsets, setup errors both at the irradiation of the gel and at the dose acquisition by MR further can contribute to differences seen between measurements and calculations and will be investigated.

Hong et al. [11] describe the planning results for WAPRT using static gantry IMRT with five incidences. The delineation of the target volumes and OARs were quite similar to those described in this report. Their treatment planning goal differs by the use of the unexpanded kidneys as OARs. The mean

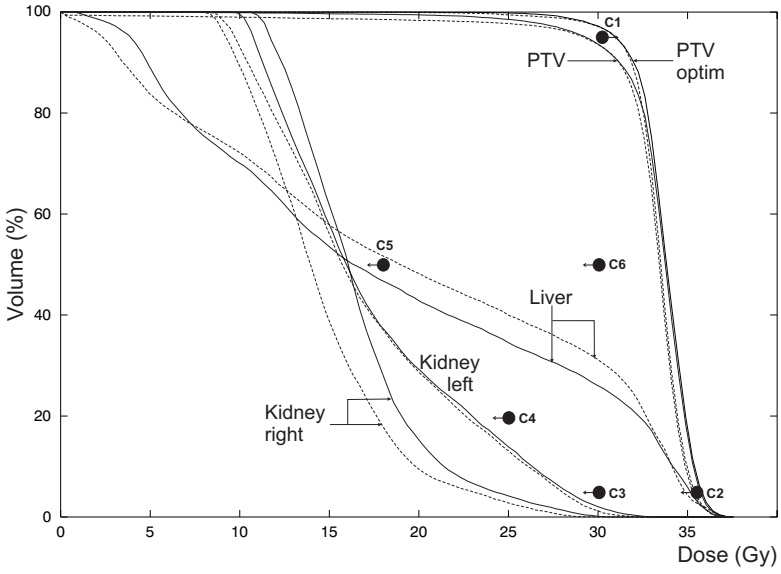

(a)

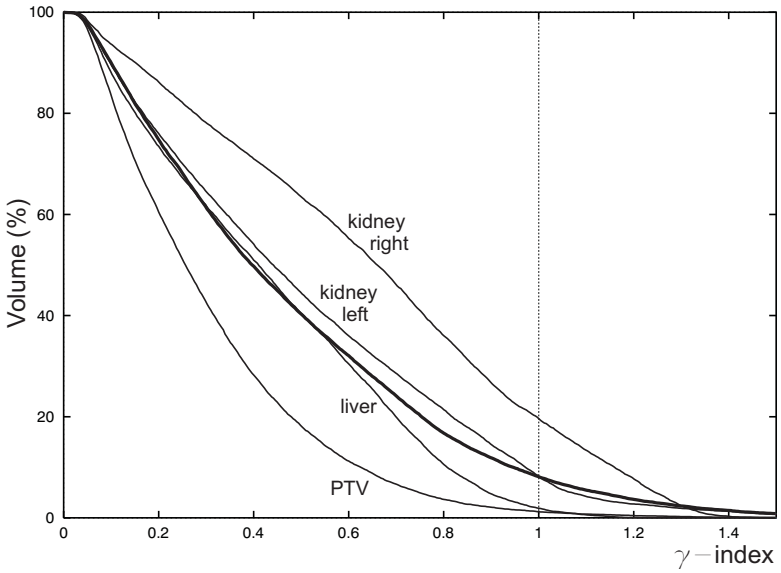

(b)

Figure 7: (a) Dose volume histograms of the computed (solid lines) and gel-measured (dashed lines) dose for the contoured volume inside the gel. C1-6: clinical constraints, with C1: more than 95% of the volume of the PTV_optim has to receive more than 90% of the prescribed dose; C2: less than 5% of the PTV may receive more than 107% of the prescribed dose; C3: less than 5% of the expanded kidneys may receive more than 30 Gy; C4: less than 20% of the expanded kidneys may receive more than 25 Gy; C5: median dose to the expanded kidneys should be lower than 18 Gy and C6: median dose to the liver should be lower than 30 Gy. (b) Volume histogram using the computed γ-index. The thick line represents the total measured volume.

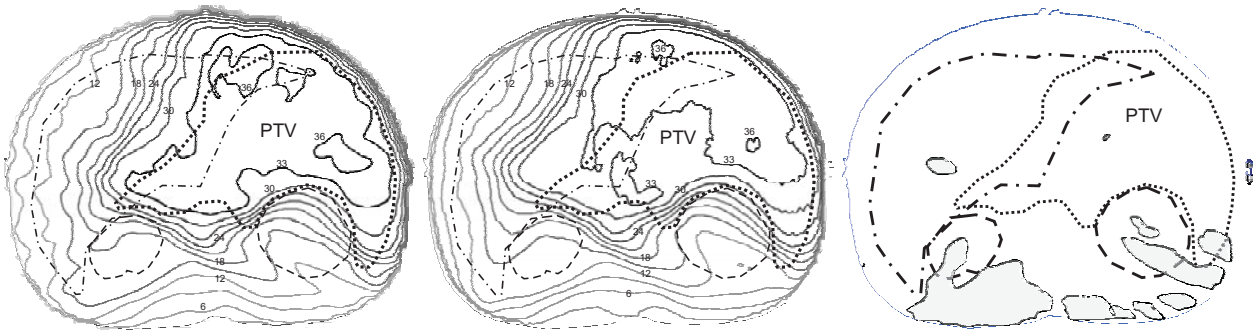

(a) (b) (c)

Figure 8: Dose distributions in the middle transverse plane of the Barex cast (figure 3) for the IMAT plan, (a) as calculated with the collapsed cone convolution/superposition algorithm from Pinnacle and (b) as measured by monomer/polymer gel dosimetry. For (a) and (b) isodoses are shown at 3 Gy intervals. (c) Iso-γ line for γ = 1. PTV: planning target volume (dotted line). The liver is indicated with a dashed-dotted line, the kidneys with a dashed line.

V_{95} of the PTV was 83.5% for the static IMRT, while it was 82.2% in our study. However, in the report by Hong et al., the overlap with the kidneys was excluded from the PTV. When we look at the PTV_optim, which also excludes the overlap region, the mean of the V_{95} was 88.9%. These data reflect that the dose homogeneity in the PTV is similar for both planning techniques. The mean dose to the kidneys is also in the same range in both reports. In the report of Hong et al., a mean of 1442 MUs was needed for a fraction of 150 cGy, where IMAT resulted in 444 MUs on average for the same dose. Due to the design of the Varian MLC for which Hong's implementation was intended, a split of the intensity modulated fields was necessary, which gives rise to a higher number of MUs. Hong did not report on delivery time.

IMAT with dynamic multileaf collimation was first described by Yu [8]. Yu initially reported on an IMAT planning methodology using inverse planning (Peacock by NOMOS Corporation). Optimized beam fluences were "decomposed" to multiple superimposing fields. In the inverse planning strategy described by Yu, the intend is to generate control points that are compliant with the MLS-constraint with regard to the previous control point of the arc. If such a decomposition can't be found, Yu described a softening of the MLS-constraint with selection of a lower nominal dose rate. The Elekta SL*i*-18 picks a nominal dose rate from a set of discrete values (32, 65, 130, 260 or 520 MU/minute) so that the gantry speed is as close as possible to 156°/minute (range: 104 - 208°/minute). We were unable to apply Yu's method as we could not influence the selection of this nominal dose rate without elimination of safety interlocks. In our implementation, the MLS-constraint is handled using a combination of anatomy-based segmentation and the LVC. For volumes of interest at maximum 12.5 cm of a cranio-caudal axis through the isocenter, it can be proven that the lateral position of their projected outlines in BEV between two adjacent incidences, interspaced by eight degrees, can in the worst case only differ 2.0 cm when beam divergence is not taken into account. As the Elekta MLC has a possible overtravel distance up to 12.5 cm for all leaves, and leaf speeds are sufficient to move 2.0 cm each 8 degrees of arc rotation, the conformal avoidance of OARs within the above-mentioned regional constraint is always possible. For volumes of interest as the PTV that do not fit within the 12.5 cm cylinder, anatomical boundaries in BEV can have higher lateral shifts. For volumes within 20.0 cm of the longitudinal axis, this can amount up to 3.5 cm, which is however only obtained in the worst case scenario.

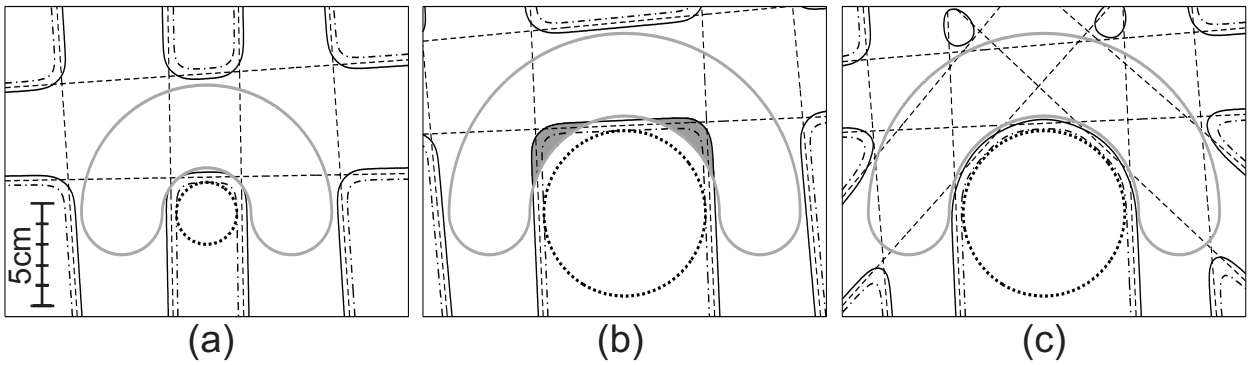

Figure 9: Demonstration of the need for more incidences as the inner radius of a concave PTV is increasing, if the same homogeneity and OAR sparing is wanted and for the same distance between PTV and OAR. The concave PTV is shown in a solid grey line, the circular OAR in dotted black line, the borders of the beams in dashed fine black lines, the 70% dose level in solid black line and the 30% dose level in a dashed-dotted black line. These dose levels were defined relative to the maximum dose of one beam. The isocenter is located in the middle of the OAR. Beam weights were set equal, and attenuation was not taken into account. The profile function used was described earlier [14]. (a) A concave PTV with a small internal radius. Three beams (gantry angles $0°$, $90°$ and $180°$) are sufficient to obtain a 40% dose difference between the PTV and the OAR. (b) The same beam setup for a PTV with a larger internal radius and the same distance between OAR and PTV, with equal sparing of the OAR, produces underdosages (grey areas) in the PTV.(c) This can be avoided by the increase of incidences ($45°$ and $135°$). Note that due to the higher number of beam portals, beam aperture could be reduced without PTV underdosage.

By beam divergence, larger lateral shifts can occur. Where the MLS-constraint would be violated in the process of machine state generation, it was resolved by the LVC. Recently, the first clinically delivered planning results of IMAT were published [25][26]. In both reports, a planning strategy was used in which the outlines of the machine states were based on patient anatomy. The initial reports, using anatomy based segmentation could indicate that the inverse planning method described by Yu [8] is hard to implement in clinical practice. To deal with the problem of MLS, they had to insert a wedge in (some) arcs in order to increase the number of MU per degree of arc rotation [26]. In our opinion, wedges are superfluous in IMAT planning, as this procedure decreases MU-efficiency and as the leaf speed problem can be solved by optimization methods.

The clinical implementation of IMAT for this site was a challenge for other than plan-technical reasons too. The setup procedure was strongly influenced by the combination of the large target volume and the limitations of the Elekta table. The C-arms can only be set in a non-horizontal position ($120°$) if the table is sufficiently extended longitudinally towards the gantry drum. The distance in caudal direction between the isocenter and metal components of the support system in this extended position is maximally 26.4 cm. As the PTV has a median height of 36 cm, repositioning range in cranio-caudal direction using the table shift possibility was restricted. This is a problem that however equally occurs when a static incidence technique would be used, unless care is taken to only generate segments that can be delivered with the bars in either the most lateral or medial position. For a PTV of the above-mentioned sizes, this will in practice lead to a restriction of possible gantry angles, or delivery of the treatment in two parts (one for each bar position). During the planning process, the maximal arc range was used, taking a 2 cm margin between table bars and field aperture in lateral direction into account. Repositioning using the motorized table shift system in this direction was therefore restricted to an uncommonly small range. As a consequence, the table had to be set to predefined lateral

and longitudinal positions, after which the first positioning is done by shifts of the patient relative to the table. The support system capabilities were used to correct for the last millimeters of the patient setup. A shorter setup time could be achieved by use of a appropriately designed carbon fiber table top.

To implement IMAT (8 patients so far) in the same routine clinical practice as IMRT (in total 362 patients, 120 in 2002, which is $\pm$ 10 % of our patientload), further automation is necessary on several points. The transition of virtual to deliverable arcs is a time-consuming manual operation. Although a class solution can aid the planner towards a final arc setup, constraints on the modulation of the angular delivery rate during optimization would reduce the problem. Full automation of this procedure would be optimal. Start and stop angle optimization can fine-tune converted arcs. The conversion of arcs with a non-constant angular delivery rate could be avoided by a variable gantry speed. This could enhance planning quality, reduce the number of arcs and the delivery time, together with a decrease of planning complexity by elimination of the conversion and elimination of local minima induced by the discretization. Although the Elekta linac has by its rotation mechanism excellent mechanical possibilities to achieve this, Elekta was not yet able to implement a variable angular delivery rate for IMAT.

Conclusion

We clinically applied five IMAT treatment plans for WAPRT. IMAT was validated dosimetrically and was shown to be deliverable in an acceptable time slot and to produce dose distributions that are significantly more homogeneous at the PTV than those obtained with a CONV plan. Our anatomy based segmentation strategy offered a feasible solution in view of the leaf speed constraint. Although the planning is still time consuming, we think this can be solved by adaptations to the patient couch, the control software of the linear accelerator and the planning software, intervention of which each has the potential to improve the quality of the IMAT plans.

References

[1] Hogberg T, Glimelius B, Nygren P. A systematic overview of chemotherapy effects in ovarian cancer. *Acta oncologica* 2001;40:340-360

[2] Redman CW, Shafi MI, Ambrose S, *et al.* Survival following intestinal obstruction in ovarian cancer. *Eur J Surg Oncol* 1988;14:383-386

[3] Krebs HB, Goplerud DR. Surgical management of bowel obstruction in advanced ovarian carcinoma. *Obstet Gynecol* 1983;61:327-330

[4] Abu-Rustum NR, Barakat RR, Venkatraman E, *et al.* Chemotherapy and total parenteral nutrition for advanced ovarian cancer with bowel obstruction. *Gynecol Oncol* 1997;64:493-495

[5] May LF, Belinson JL, Roland TA. Palliative benefit of radiation therapy in advanced ovarian cancer. *Gynecol Oncol* 1990;37:408-411

[6] Tinger A. Effective palliative radiation therapy in advanced and recurrent ovarian carcinoma. *Int J Radiat Oncol Biol Phys* 2001;51:1256-1263

[7] Corn BW, Lanciano RM, Boente M, *et al*. Recurrent ovarian cancer. Effective radiotherapeutic palliation after chemotherapy failure. *Cancer* 1994;74:2979-2983

[8] Yu C. Intensity-modulated arc therapy with dynamic multileaf collimation: an alternative to tomotherapy. *Phys Med Biol* 1995;40:1435-1449

[9] De Neve W, Duthoy W, Claus F, *et al.* Dose conformation in IMRT for head and neck tumors: which solution to apply. *Cancer Radiother* 2002;6 (Suppl. 1):32s-36s

[10] De Gersem W, Claus F, De Wagter C, *et al.* An anatomy-based beam segmentation tool for intensity-modulated radiation therapy and its application to head-and-neck cancer. *Int J Radiat Oncol Biol Phys* 2001;51:849-859

[11] Hong L, Alektiar K, Chui C, *et al.* IMRT of large fields: whole-abdomen irradiation. *Int J Radiat Oncol Biol Phys* 2002;54:278-289

[12] Brahme A, Roos J-E, Lax I. Solution of an integral equation encountered in rotation therapy. *Phys Med Biol* 1982;27:1221-1229

[13] De Neve W, De Wagter C, De Jaeger K, *et al.* Planning and delivering high doses to targets surrounding the spinal cord at the lower neck and upper mediastinal levels: static beam-segmentation technique executed with a multileaf collimator. *Radiother Oncol* 1996;40:271-279

[14] De Gersem W, Claus F, De Wagter C, *et al.* Leaf position optimization for step and shoot IMRT. *Int J Radiat Oncol Biol Phys* 2001;51:1371-1388

[15] De Gersem W, Derycke S, De Wagter C, *et al.* Optimization of beam weights in conformal radiotherapy planning of stage III non-small cell lung cancer: effects on therapeutic ratio. *Int J Radiat Oncol Biol Phys* 2000;47:255-260

[16] Vaarkamp J, Krasin M. Reduction of target dose inhomogeneity in IMRT treatment planning using biologic objective functions. *Int J Radiat Oncol Biol Phys* 2001;49:1518-1520

[17] De Neve W, De Gersem W, Derycke S, *et al.* Clinical delivery of intensity modulated conformal radiotherapy for relapsed or second-primary head and neck cancer using a multileaf collimator with dynamic control. *Radiother Oncol* 1999;50:301-314

[18] Maryanski MJ, Gore JC, Kennan RP, *et al.* NMR relaxation enhancement in gels polymerized and cross-linked by ionizing radiation: a new approach to 3D dosimetry by MRI. *MRI* 1993;11:253-258.

[19] De Deene Y, De Wagter C, Van Duyse B, *et al.* Validation of MR-based polymer gel dosimetry as a preclinical three-dimensional verification tool in conformal radiotherapy. *Magnet Reson Med* 2000;43:116-125.

[20] De Deene Y. Gel dosimetry for the dose verification of intensity-modulated radiotherapy treatments. *Z Med Phys* 2002;12:77-88.

[21] De Deene Y, Reynaert N, De Wagter C. On the accuracy of monomer/polymer gel dosimetry in the proximity of a high-dose-rate 192Ir source. *Phys Med Biol* 2001;46:2801-2825

[22] Low DA, Harms WB, Mutic S, *et al.* A technique for the quantitative evaluation of dose distributions. *Med Phys* 1998;25:656-661

[23] Stein J, Mohan R, Wang XH, *et al.* Number and orientations of beams in intensity-modulated radiation treatments. *Med Phys* 1997;24:149-160

[24] Kost S, Dorr W, Keinert K, *et al.* Effect of dose and dose-distribution in damage to the kidney following abdominal radiotherapy. *Int J Radiat Biol* 2002;78:695-702

[25] Yu C, Li XA, Ma L, *et al.* Clinical implementation of intensity-modulated arc therapy. *Int J Radiat Oncol Biol Phys* 2002;53:453-463

[26] Ma L, Yu CX, Earl M, *et al.* Optimized intensity-modulated arc therapy for prostate cancer treatment. *Int J Cancer* 2001;96:379-384

V. 6. Definition and delineation of the clinical target volume for rectal cancer.

Authors: S. Roels[†], W. Duthoy[†], K. Haustermans, F. Penninkx, V. Vandecaveye, T. Boterberg and W. De Neve

[†]Both authors contributed equally to the manuscript.

Submitted to: International Journal of Radiation Oncology Biology Physics (conditionally accepted)

Acknowledgements: Supported by a grant from the "Stichting tegen Kanker" (University of Ghent: No 51AC8904; Universite Catholique de Louvain (UCL) FBC:2003/2006; Katholieke Universiteit Leuven: No ZKB 2747)

Key issues discussed in this paper:

- The implementation of conformal radiation techniques necessitates a definition for the CTV. For rectal cancer, only guidelines for 2D portals exist. There is a need for a true 3D definition and according delineation guidelines
- A systematic literature review was performed, and 17 articles were retained, giving information on the pelvic localization of the tumour spread and/or tumour recurrence.
- Several pelvic subsites were defined, aiming at the greateste common denominator. The lymph node regions were also defined.
- A CT and MRI-based atlas is presented in order to facilitate the CTV delineation in rectal cancer, and thus to implement 3D-CRT, IMRT and/or IMAT for rectal cancer.

Definition and delineation of the clinical target volume for rectal cancer.

Sarah Roels, M.D.[1], Wim Duthoy, M.D.[2], Karin Haustermans, M.D., Ph.D.[1]
Freddy Penninckx, M.D., Ph.D.[3], Vincent Vandecaveye, M.D., Ph.D.[4],
Tom Boterberg, M.D., Ph.D.[1], Wilfried De Neve, M.D., Ph.D.[1]

1. Department of Radiotherapy, University Hospital Gasthuisberg, Leuven, Belgium
2. Department of Radiotherapy, Ghent University Hospital, Gent, Belgium
Departments of 3. Surgery and 4. Radiology, University Hospital Gasthuisberg, Leuven, Belgium

Abstract

Purpose: Optimization of radiation techniques to maximize local tumour control and minimize small bowel toxicity in rectal cancer requires proper definition and delineation guidelines for the clinical target volume (CTV).

Materials and methods: Seven reports were analysed to assess the incidence and predominant location of local recurrences in rectal cancer. The distribution of lymphatic spread was analysed in another 10 reports in order to record the relative frequency and location of metastatic lymph nodes in rectal cancer, according to the stage and level of the primary tumour.

Results: The mesorectal (MS), posterior (PPS) and inferior pelvic subsite (IPS) are mostly at risk for local recurrences, while lymphatic tumour spread proceeds mainly in three directions: upward along the superior rectal artery to the inferior mesenteric nodes, lateral into the internal iliac lymph nodes and in a few cases downwards into the external iliac and inguinal lymph nodes. The risk for recurrence or lymph node involvement is related to the stage and the level of the primary lesion, resulting in more IPS recurrences and lateral lymphatic seeding in low seated tumours and increased risk of lateral lymphatic spread in advanced stage malignancy. According to the results, we propose guidelines for inclusion of the tumour, the MS and the PPS into the CTV in all cases. The IPS is at risk if 1) the surgeon aims a sphincter saving procedure and the tumour is located within +/- 6 cm from the anal margin or 2) the tumour invades the anal sphincter and an abdominoperineal resection (APR) is necessary. Concerning the lymph node regions, the mesorectal lymph nodes and the lateral lymph nodes are mostly at risk and should be included into the CTV for all patients. We did not find solid evidence to include the external iliac nodes in the target volume, except in these cases where anterior organ involvement is highly suspected. The inguinal lymph node group is not at risk in rectal cancer patients.

Conclusion: Definition and delineation guidelines are necessary to optimize radiation treatment and define the best therapy according to the primary tumour characteristics. Based on a review of articles reporting on the incidence and predominant location of local recurrences and the distribution of lymphatic spread in rectal cancer, we defined guidelines for inclusion of the most critical pelvic subsites and lymph node regions.

Introduction

Since the introduction of total mesorectal excision (TME), a significant decrease in local recurrence rate has been observed in resectable rectal cancer [1]. The use of radiotherapy, either pre- or postoperatively, decreases the local recurrence rate and improves survival in locally advanced rectal cancer [2, 3, 4]. Chemotherapy has shown to enhance the efficacy of pelvic radiation [5]. While postoperative radiation allows patient selection based on histopathological tumour characteristics, recent data demonstrate the superiority of preoperative radiation [6]. Moreover, preoperative chemoradiation allows downsizing of low seated rectal tumours which may result in more sphincter preservation [7]. Based on the results of prior randomised trials [3, 8], radiation therapy to a dose of 45-50 Gy in 1.8-2 Gy per fraction, combined with 5-FU chemotherapy is the current standard pre-operative schedule in T3 (and/or positive lymph nodes, further N+) tumours in many European centres.

Indeed, high-risk patients (T3-T4, N+) still suffer from local relapse rates in up to 33% with trimodality treatment [9]. In these selected patients improvement in treatment may be achieved with higher preoperative doses with or without altering the fractionation of radiotherapy, and integrating novel chemotherapeutic and molecular targeted agents with radiosensitizing properties. Mohiuddin et al. [10] treated patients with escalating doses of preoperative radiotherapy, resulting in a global improvement in overall local control and survival. However, further dose escalation is limited due to normal tissue toxicity. Dose limiting toxicities originate mainly from irradiation of the small bowel and the normal rectal tissue resulting in a 15 to 40% grade III-IV diarrhoea, depending on the scoring system, type of surgery, adjuvant chemotherapy, and other factors such as comorbidity [11, 12]. Chronic small bowel radiation toxicity is irreversible and can be life threatening, requiring surgical interventions [13].

In radiotherapy, multiple beam set-up, customized blocking, and the use of a special open table top or belly-board device, shifting the small bowel out of the treatment field can limit the volume of small bowel treated [13]. In rectal cancer, intensity-modulated radiation therapy (IMRT) and intensity-modulated arc therapy (IMAT) can be used to spare the small bowel around which the planning target volume (PTV) is located in a horseshoe shape [14]. However, as these techniques introduce dose gradients close to the PTV (Figure 1), proper definition and delineation of the clinical target volume (CTV) is required to avoid underdosage of regions that could possibly harbour cancer cells. Some studies are published on guidelines to define and delineate the CTV in rectal cancer [15, 16, 17, 18, 19], but they all give recommendations for two-dimensional treatment portals, rather than for three-dimensional (3D) treatments like IMRT or IMAT.

In this paper we analyse reported data on the predominant locations and frequency of local recurrences and lymph node involvement in rectal cancer to propose a definition of the CTV for rectal cancer and guidelines for its delineation.

Materials and Methods

Literature search strategy

Medline (http://www.pubmed.com) was searched for the following title terms:

((rectum or rectal or colorect* or rectosigm* or sigmo*) and (cancer or adenocarcinoma or carcinoma or neoplasm*) and (recurrence or failure or relapse or recurrent or spread or node or lymph or lymphatic) and (local or locoregional or regional or pelvic)) up to September 2005 (note: the "*" depicts a "wildcard").

This yielded 406 hits. A selection was made based on the titles, excluding all articles dealing with prostate cancer, diagnostic techniques for recurrent rectal cancer, treatment of recurrence or follow-up strategies for rectal cancer. Only publications in English, French or German were retained. After this first selection, 114 articles remained, of which the abstracts were read, and only those articles that were expected to give precise anatomical information about the location of the recurrence or pathologic lymph nodes, more detailed than pelvic or local, were retained. This yielded 22 articles. From these 22 articles, the full text version was retrieved, and only 4 of these 22 articles gave satisfactory information

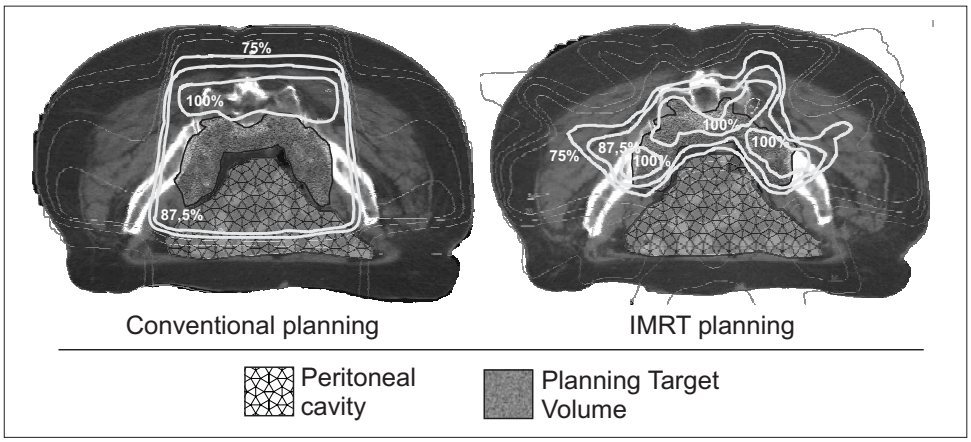

Figure 1: Dose distribution in a transverse plane for a conventional plan (2 lateral wedged beams and 1 posterior beam) at the left side, and an intensity-modulated radiotherapy (IMRT) plan at the right. The ability of IMRT to spare small bowel [14] is clearly visible. Note that the conventional plan is more robust against less accurate delineation of the clinical target volume (CTV) than the IMRT plan. In the latter approach, an erroneous CTV definition will lead to underdosage of regions possibly containing tumour cells.

on the precise location of recurrence and a clear description of the number of patients at risk. By extensive cross-referencing, 18 articles were eventually retained [17;20-36]. Of these, one article [17] was withdrawn from the final analysis in account of less reliable information, based on CT findings only, compared to histologically proven data.

Definitions

In an attempt to compare the results of the remaining 17 articles, we defined the names of the pelvic areas that seemed most at risk for local recurrence or lymph node spread, aiming at the greatest common divisor of all described areas as discussed in the individual articles.

Pelvic region

Five subsites were defined as the predominant areas at risk for local recurrence: the mesorectal subsite (MS), the posterior pelvic subsite (PPS), the lateral pelvic subsite (LPS), the inferior pelvic subsite (IPS) and the anterior pelvic subsite (APS).

- The MS encompasses the mesorectum, defined as the adipose tissue with lymphovascular and neural structures, encapsulated by a fascia, the so-called perirectal fascia (Figure 2d). The MS is cylindrical with cone shaped tips in cranial and caudal direction, starting at the level of the sacral promontory, at the origin of the superior rectal artery (SRA) and ending at the level where the levator ani muscle inserts into the rectal wall.
- The PPS covers mainly the presacral space: a triangular area, posteriorly enclosed by the presacral fascia (Waldeyers fascia), and anteriorly by the perirectal fascia. This volume is best seen on magnetic resonance imaging (MRI), and contains the median and lateral sacral vessels, the lymphatics of the presacral chains, the anterior branches of the sacral nerves and the inferior hypogastric plexus [37].
- The LPS includes the lateral pelvic side walls.
- The IPS consists of the anal triangle of the perineum, containing the anal sphincter complex with the surrounding perianal and ischiorectal space.
- The APS contains all pelvic organs that are located ventrally from the MS.

The results of the different studies were obtained via retrospective analysis [23, 30, 32], follow-up se-

ries [20, 24, 34] and findings at planned second-look operations [21]. Table 1 shows the risk of local recurrence per pelvic subsite. For the IPS, the distribution of recurrences was further subdivided for patients whom underwent an abdominoperineal resection (APR).

Lymph node regions

To assess the risk of lymph node involvement, we analysed all articles discussing the distribution and frequency of pathological lymph nodes at primary diagnosis, based on histopathological examination at primary surgery [22, 25, 26, 27, 28, 29, 31, 33, 35, 36]. Data on lymph node invasion are generally from Japanese studies, as extended pelvic lymphadenectomy evolved to become the standard treatment for low-lying rectal cancer in some centres in Japan [38, 39].

We defined five lymph node regions (LNRs): the mesorectal lymph nodes (MLN), the upward lymph nodes (ULN), the lateral lymph nodes (LLN), the external iliac lymph nodes (ELN) and the inguinal lymph nodes (ILN). Each LNR was chosen in accordance to the main lymphatic drainage pathways of the rectum. The MLN is, similar to the MS, defined as the mesorectal tissue enclosed by the perirectal fascia, containing the perirectal nodes with their afferent and efferent vessels. The ULN encompasses all lymphatic tissue along the SRA and inferior mesenteric artery (IMA). Lymphatic spread to the LLN is defined as involvement of the lymph nodes along the middle rectal, the obturator and the internal iliac vessels. The lymph nodes along the external iliac artery and superficial inguinal lymph nodes are classified as ELN and ILN, respectively. Table 2 shows the risk of lymph node involvement per LNR. For the LLN, the risk of lymph node invasion was analysed according to T-stage and level of the primary tumour. A separate analysis for high and low-seated tumours was also made for the incidence of ELN and ILN involvement.

Results

Pelvic subsites at risk for local recurrence (Table 1)

Mesorectal subsite (MS)

Only two articles report on the incidence of recurrence in the MS in patients that underwent sphincter saving surgery. The first study [30] reports on 46 patients with a local recurrence, initially operated with a low anterior resection in the pre-TME era, where a blunt dissection was performed with a distal tumour free border of at least 2 cm. Thirty-four patients had a recurrence originating from the perirectal tissue and in 7 patients the recurrence was considered as true anastomotic. In the second article [32], the MS was not totally removed in patients that were operated on before 1985, while after this date, diathermy dissection allowed excision of the perirectal fascia. Of all patients that underwent sphincter saving surgery (468 patients, with or without partial or TME), 15 patients developed a recurrence in the MS, with 8 recurrences in the perirectal tissue. The incidence of anastomotic recurrences (as a percentage of locoregional sites involved) ranged between 10 and 21%, depending on the definition of a true anastomotic recurrence [23, 24, 30, 34].

Posterior pelvic subsite (PPS)

For the PPS, data on recurrences in the presacral space [20;23], posterior pelvis [21], or both [34] were considered. The results were merged, as most of the posterior relapses include presacral disease [34]. If all patients from retrospective studies are considered (3 studies, n=254), then 22% of these patients had a recurrence in the PPS. Looking at all patients suffering from a recurrence (5 studies, n=435), 49% had involvement of the PPS. A recent publication reported on the location of recurrent rectal cancer in 123 patients with the help of a CT based 3-D data file system. They also found that local relapse was mainly situated in the PPS [19].

Table 1: Local recurrence per pelvic subsite at risk.

Subsite	Pt. group	Author	Ref.	No. at risk (n)	Any rec. (n)	Rec. in subsite (n)	Risk for rec. (%)	Involv in rec. (%)
PPS	All	Gilbertsen	[20]	89	32	14	16	44
		Mendenhall	[23]	90	40	18	20	45
		Gunderson	[18]	75	48	25	33	52
		Hruby	[34]	-	269	127	-	47
		Wiig	[30]	-	46	27	-	59
	partial sum			**254**	**-**	**57**	**22**	-
	total sum			**-**	**435**	**211**	**-**	**49**
LPS	All	Gilbertsen	[20]	89	32	1	1	3
		Mendenhall	[23]	90	40	4	4	10
		Gunderson	[18]	75	48	13	17	27
		Killingback	[32]	468	34	24	5	70
		Hruby	[34]	-	269	30	-	11
		Wiig	[30]	-	46	25	-	54
	partial sum			**722**	**-**	**42**	**6**	-
	total sum			**-**	**469**	**97**	-	**21**
IPS	All	Gilbertsen	[20]	89	32	5	6	16
		Mendenhall	[23]	90	40	4	4	10
		Gunderson	[18]	75	48	14	19	29
		McDermott	[24]	934	191	30	3	16
		Hruby	[34]	-	269	15	-	6
	partial sum			**1188**	**-**	**53**	**4**	**-**
	total sum			**-**	**580**	**68**	**-**	**12**
	APR	Gilbertsen	[20]	89	-	5	6	-
		McDermott	[24]	100	-	24	24	-
	total sum			**189**	-	**29**	**15**	-
APS	All	Gilbertsen	[20]	89	32	13	15	40
		Mendenhall	[23]	90	40	6	7	15
		Gunderson	[18]	75	48	21	28	44
		McDermott	[24]	934	191	23	2	12
		Hruby	[34]	-	269	29	-	11
		Wiig	[30]	-	46	12	-	26
	partial sum			**1188**	-	**63**	**5**	-
	total sum			-	**628**	**104**	-	**17**

Abbreviations: PPS: posterior pelvic subsite; LPS: lateral pelvic subsite; IPS: inferior pelvic subsite; APS: anterior pelvic subsite; APR: abdominoperineal resection; Pt.: patient; Ref.: reference; rec.: recurrence; Involv: Involvement of specified subsite. The number of patients at risk for a recurrence are listed in the 5^{th} column, and were extracted from the studies who gave enough information on the patient population at risk. The "partial sum" is the sum over these studies, for the patients at risk, the subsite-specific recurrences and the risk for recurrence in the specified subsite.

Table 2: Lymph node involvement per lymph node region.

LNR	Pt. group	Refs.	No. of pts (n)	N+ (n)	N+ at specified LNR (n)	Positive LN at specified LNR (%)	Involv. of LNR in N+ pts. (%)
MLN	All	[22, 26, 27, 33]	1390	706	615	**44**	87
ULN	All	[22, 26, 27, 31, 33]	2135	1033	578	**27**	56
LLN	All	[22, 25, 26, 27, 31, 33]	2230	1043	285	**13**	27
	T1-2	[22, 26, 28, 29, 31, 35]	595	-	28	**5**	-
	T3	[22, 26, 28, 29, 31, 35, 36]	1494	-	203	**14**	-
	T4	[22, 26, 28, 29, 31, 35, 36]	252	-	51	**20**	-
	HS	[22, 26, 27, 31, 33]	759	-	32	**4**	-
	LS-MiS	[22, 25, 26, 27, 28, 29, 31, 33, 35, 36]	2276	-	405	**18**	-
ELN	All	[33]	605	285	25	**4**	9
	HS/AR	[33]	133	-	0	**0**	-
	LS-MiS/APR	[29, 33]	443	-	30	**7**	-
ILN	All	[22, 33]	1028	505	8	**1**	2
	HS	[22, 33]	281	-	0	**0**	-
	LS	[22, 28, 33]	832	-	10	**1**	-

Abbreviations: LNR: lymph node region; Pt(s).: patient(s); Refs.: references; N+: number of patients with positive lymph nodes (in any LNR, unless specified differently). LN: lymph nodes; Involv.: involvement; MLN: mesorectal lymph nodes; ULN: upward lymph nodes; LLN:lateral lymph nodes; ELN: external iliac lymph nodes; ILN: inguinal lymph nodes. HS: high-seated tumours; LS: low-seated tumours; MiS: middle-seated tumours; AR: anterior resection; APR: abdominoperineal resection.

Lateral pelvic subsite (LPS)

The LPS was only vaguely defined in the articles that were reviewed, as lateral pelvic wall or just lateral. For our analysis, both descriptions were considered as locations for recurrences that are related to the lateral pelvic wall. Six percent of all patients in these series had invasion of the LPS as a part of their disease relapse. When only considering patients with a local recurrence (n=469), the LPS was involved in 21% of the patients.

Inferior pelvic subsite (IPS)

Information on IPS recurrence was found in 4 reports, including 1188 patients. All papers were retrospective analyses. The overall risk of developing a recurrence in the IPS was more than 4%. In one study, the risk of IPS recurrence was calculated in relation to the tumour site, being 8% for tumours located less than 6 cm from the anal margin and 3% for tumours located between 6 cm and 11 cm above the anal margin. For tumours located higher than 11 cm from the anal margin, no recurrences were observed in the IPS [24]. When all patients with an APR were considered (2 studies, 189 patients), 15% developed a recurrence in the IPS. Furthermore, IPS involvement was seen in 12% of all patients suffering from a recurrence. Höcht et al. came to a similar conclusion although no absolute numbers were reported in their publication [19]. These data clearly indicate that the IPS is especially at risk for local recurrence in those patients with a low seated tumour and patients that underwent an APR because of a low seated tumour.

Anterior pelvic subsite (APS)

Recurrences involving one of the following organs: vagina, bladder, prostate, seminal vesicles, urethra, uterus were classified as APS recurrences. APS recurrences were found in only 5% of the patients at risk for local recurrence. In patients with a pelvic recurrence, involvement of the APS was observed in 17%.

Lymph node regions at risk (Table 2)

Eight reports on lymphatic spread in patients with rectal cancer were analysed in order to compute the relative frequency and location of metastatic lymph nodes in rectal cancer. We also assessed the sites of lymph node metastases in relation to those aspects of the primary tumour that can be documented before surgery.

Mesorectal lymph nodes (MLN)

In 44% of all available rectal cancer patients, at least one positive node in the MLN was found. The MLN were involved in 87% of the patients with positive pelvic lymph nodes, showing the importance of this group. Information on correlation with T stage was too scarce for analysis. Morikawa et al. [26] provided detailed information on longitudinal perirectal lymphatic spread. In caudal direction, no lymphatic spread was found more than 4 cm away from the tumour. In cranial direction, positive lymph nodes (in the MLN) were found up to 10 cm above the primary tumour (8%), while above 10 cm, the risk was less than 2%.

Upward lymph nodes (ULN)

In two articles, upward spread is defined along the SRA and the IMA, reported as one entity [22;33]. Other authors only classify the lymph nodes along the IMA in this group [27;31]. In one study upward spread is not further specified [26]. Three articles make a distinction between positive lymph nodes along the peripheral and the root of the IMA, the majority being located along the peripheral IMA [27;33]. The incidence of positive lymph nodes in the ULN was found to be 27%. Looking only at patients with positive lymph nodes in any site, 54% of these patients had lymph node metastases in the ULN.

Lateral lymph nodes (LLN)

Throughout the available articles, the definition of the LLN varied, going from lymph nodes along the internal iliac artery [31], to nodes along the internal iliac artery, the middle rectal artery, and the obturator

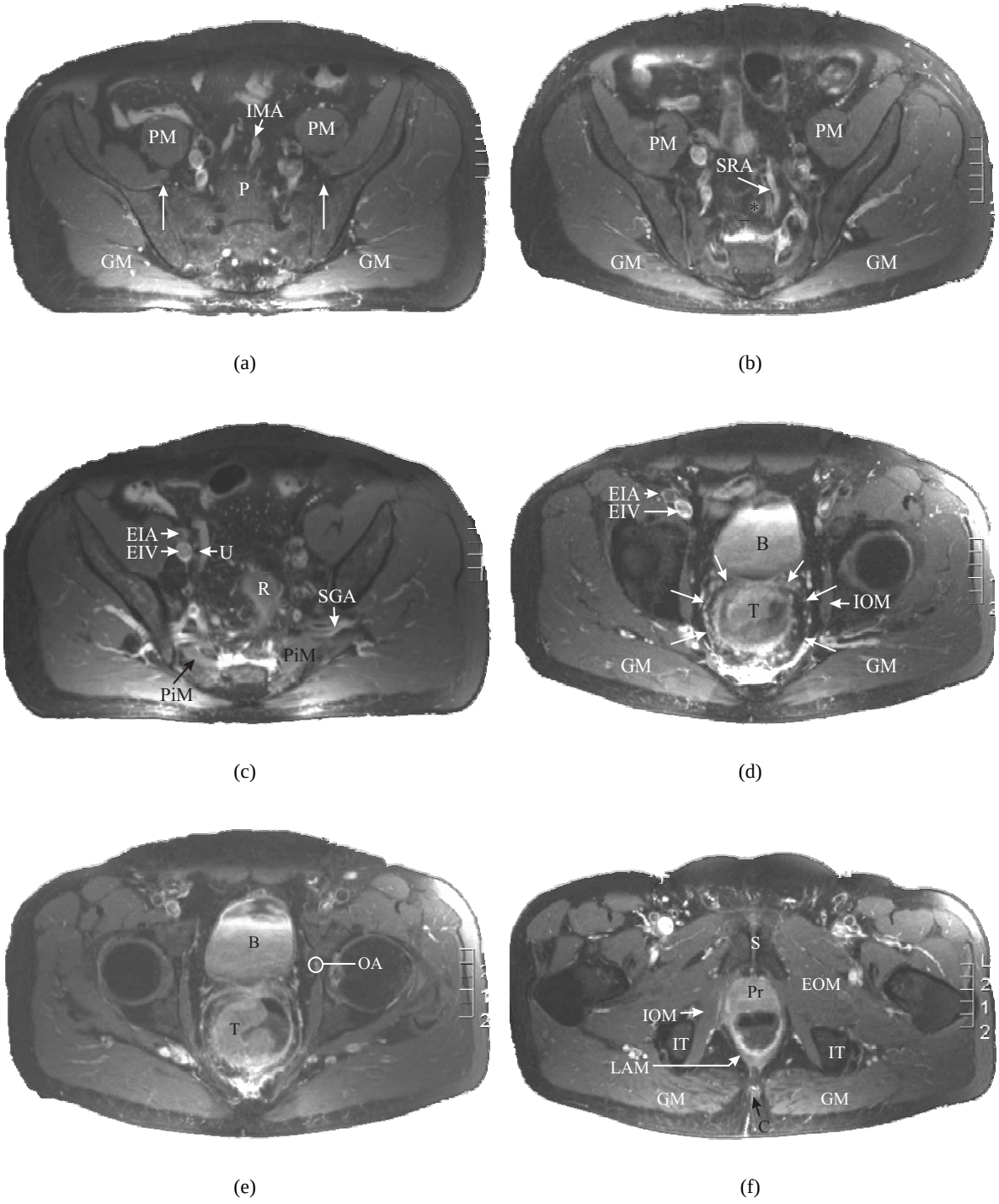

Figure 2: Transverse view through 6 selected levels from cranial (a) to caudal (f) direction. Images are T2 weighted magnetic resonance images. *Abbreviations:* B: bladder; C: coccyx; EIA: external iliac artery; EIV: external iliac vein; EOM: external obturator muscle; GM: gluteus maximus muscle; IMA: inferior mesenteric artery; IOM: internal obturator muscle; IT: ischial tuberosity; LAM: levator ani muscle; OA: obturator artery; P: promontory; PiM: piriform muscle; PM: psoas muscle; Pr: prostate; R: rectum; S: symphysis pubis; SGA: superior gluteal artery; SRA: superior rectal artery; T: tumour; U: ureter. The two arrows in (a) indicate the sacro-iliacal joint. The black asterisk in (b) indicates a suspect lymph node along the SRA.

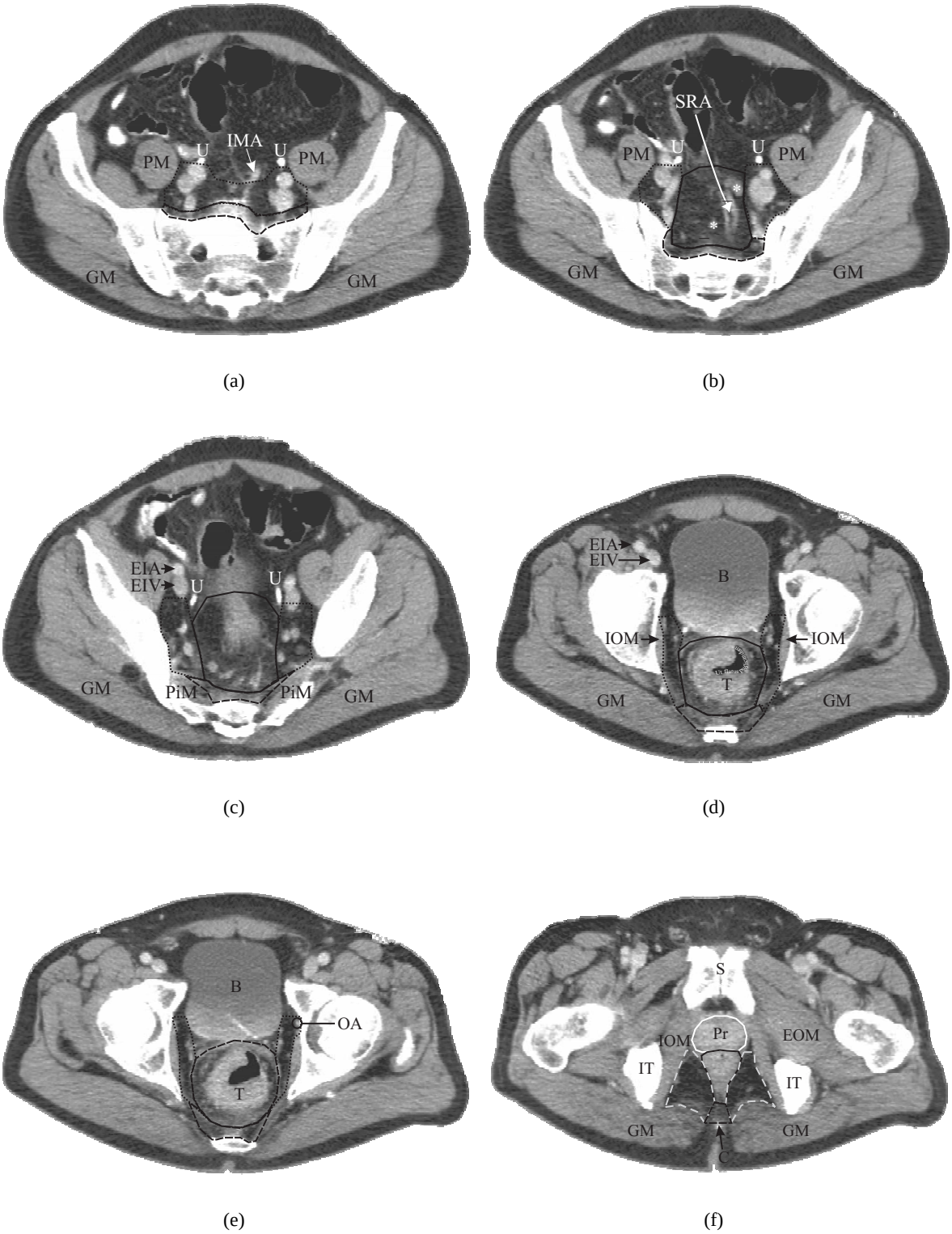

Figure 3: Transverse computed tomography slices through the levels corresponding to those in Figure 2. The abbreviations are explained in the caption of Figure 2. The posterior pelvic subsite (PPS) is indicated by the dashed line. The lymph node regions that are to be included in the clinical target volume (see text for details) are delineated by the dotted lines. The mesorectal subsite (MS) is shown by the full black line, while a grey dashed line indicates the inferior pelvis subsite (IPS; only visible in (f)). In (b), the white asterisks indicate suspect lymph nodes. In (f), the prostate is delineated by the full white line.

artery [22;25;28;33], to even larger groups, including nodes along the common iliac artery [27] and the external iliac artery [29;35;36]. One article did not clearly define the LLN [26].

For all patients at risk (6 studies, n=2230), the incidence of LLN invasion was 13%. When looking at the patients with positive lymph nodes, the risk doubles up to 27%. The main clinical significance is seen in advanced stage and low seated tumours. Six studies give detailed information on T stage, showing 5% positive LLN in T1-T2 tumours, 14% in T3, and 18% in T4 tumours. In high seated tumours, we documented a risk for positive LLN in 4%, whereas in tumours of the middle and lower part of the rectum this risk was up to 18%. Steup et al. [33] reported on a relative large number of positive lymph nodes at the level of the obturator artery (6%), the majority being attributable to tumours located below the peritoneal reflection.

External iliac lymph nodes (ELN) and inguinal lymph nodes (ILN)

Two articles reported on lymph nodes along the ELN. In these retrospective analyses, positive lymph nodes in the ELN were found in 4% when considering the whole patient group, and in 9% when only taking into account the patients with positive lymph nodes. Nearly all positive lymph nodes in this group originate from tumours located close to the anal margin, resulting in a higher percentage for patients with middle or low seated tumours and/or those that underwent an APR (7%, versus non-existing for patients with an anterior resection and/or high seated tumours). Regarding the ILN, 3 articles provide data on 1028 patients, showing only a 1% risk of positive ILN. When looking at the data from Hojo et al. [22] and Steup et al. [33], all positive lymph nodes in the ILN were associated with low seated rectal tumours.

Delineation guidelines (Figures 2 and 3)

Taking into account the results in the Table 1 and 2, we defined delineation guidelines for the CTV for rectal cancer patients, including the most critical subsites and lymph node groups. To decide whether a subsite or lymph node group was critical for inclusion into the CTV, an arbitrary limit was set to 10% overall risk for recurrence or lymph node involvement. Several pelvic subsites partly cover lymph node groups and vice versa. Therefore, we only describe the most relevant subsites and LNRs.

Mesorectal subsite (MS) and mesorectal lymph nodes (MLN)

As this area is highly at risk for lymphatic spread, it must be included in the CTV. Its circumferential boundary (perirectal fascia) is best visualized on MRI (Figure 2d) and can sometimes be identified on CT scan. The lower border is located at the level where the levator ani muscle inserts into the rectal wall. The upper border is situated at the peritoneal fold, where the peritonealized rectum starts and bends anteriorly to form the recto-sigmoid. We propose to take the bifurcation of the IMA into the sigmoid artery and the SRA as the upper limit of the MS [40]. The anterior border is defined by the Denonvilliers fascia. The prostate/seminal vesicles/bladder in men and the posterior vaginal wall/uterus in women define this border. The lateral border below the dentate line is the levator ani muscle, which makes a funnel around the distal rectum. Above the dentate line, the piriform muscle bounds the perirectal fascia on both sides. The retro-rectal fascia forms the anatomical posterior border and lies alongside the PPS.

Posterior pelvic subsite (PPS)

Parallel to the mesorectum, the PPS is highly at risk, independent of tumour location and should therefore always be part of the CTV. The PPS corresponds mainly to the presacral space, a triangular strongly curved volume, which posteriorly faces the sacral concavity. Bounded anteriorly by the perirectal fascia, it extends laterally towards the lateral borders of the sacrum where it encounters the posterior limit of the LLN. Its apex is directed caudally and corresponds to the coccyx, while the sacral promontory delineates its base. The anterior border that coincides with the posterior border of the mesorectal subsite is difficult to spot on CT images. Therefore, we propose to delineate this region by use of MRI or, if not available, take an arbitrary maximal margin of +/- 1

cm ventrally from the sacral bone as anterior border [41]. On the images where there is direct visual connection of the presacral space with the sacral neuroforamina, the CTV should be expanded posteriorly to include the sacral neuroforamina.

Inferior pelvic subsite (IPS)

We suggest including the IPS in the irradiated volume when 1) the surgeon aims a sphincter saving procedure and the tumour is located within +/- 6 cm (depends on the centre) from the anal margin or 2) the tumour invades the anal sphincter and an APR is necessary. This area includes the ischiorectal fossa and the internal and external anal sphincter (Figure 3f), with the penile bulb/vestibular bulb as anterior border. The deeper part of the ischiorectal fossa, located above the transverse septum and bounded laterally by the internal obturator muscle and the ischium, is entirely at risk. We propose to extend this lateral border to the superficial/perianal part of the ischiorectal fossa. The posterior border can be drawn at the level of the gluteal muscle and coccyx. If the IPS is not at risk for subclinical disease, the external and internal sphincter with the surrounding ischiorectal fossa should not be included in the CTV.

Lymph node regions

Table 2 clearly shows that the LNRs at risk depend on the level of the primary lesion. For tumours located in the upper part of the rectum (high seated tumours or more than 10 cm above the anal margin), the lymphatic spread is mainly in the upward direction along the SRA to the nodes along the IMA, while tumours in the middle and lower part of the rectum additionally drain in the lateral direction into the internal iliac nodes. Lesions that extend to the anal canal tend to spread to the inguinal nodes [18]. If the primary tumour spreads beyond the perirectal fascia and invades adjacent structures or organs, nodal drainage extends via the lymphatics of the involved organ (prostate, vagina, uterus, and bladder). This includes the ELN if there is anterior organ involvement and the ILN if the lower third of the vagina is involved [18]. We propose to include the MLN, the ULN and the LLN into the CTV for all patients. Taking into account the results of Steup et al. [33], the obturator nodes can be omitted if the lesion is located more than 10 cm above the anal margin. These guidelines are in correspondence with Arcangeli et al. [15]. We did not find solid evidence to include the ELN in the target volume, except in these cases where anterior organ involvement is highly suspected. The LLN is triangular in shape with the internal iliac artery in the centre, and becomes enlarged caudally around its different visceral branches. The tip is located at the bifurcation of the common iliac arteries (Figure 3a). Anteriorly, the ureter bounds this volume, while the posterior limit reaches the lateral edge of the sacroiliac joint. Inferiorly, we propose to delineate this LNR until the obturator artery enters the obturator canal (Figure 3e). The lateral wall is lined superiorly by the ischium, then by the medial surface of the piriform muscle and the levator ani muscle more caudally. The medial wall of the LLN extends towards the plane of the perirectal fascia. This area contains in the adipose tissue surrounding the internal iliac vessels most of their posterior parietal and visceral branches but also the lymphatic pathways of the middle main pelvic pathway, the proximal part of the posterior presacral pathway, the efferent pelvic nerves of the hypogastric plexus and the origin of the sciatic nerve. The upward spread in rectal cancer runs along the SRA into the nodes along the IMA [37]. The IMA originates from the aorta, 3 to 4 cm cranial to the aortic bifurcation. Considering the whole IMA as CTV is in our opinion unwanted, as it has been shown that para-aortic irradiation to elective doses does not result in an improved disease free survival, and was associated with higher toxicity [42]. We propose to take the promontory as the cranial border for the ULN.

Discussion

In this article, delineation guidelines are defined after a detailed analysis of the literature, combining published data on the frequency and distribution of local recurrences and positive lymph nodes in rectal cancer patients. These guidelines should help the clinical implementation of conformal radiotherapy techniques, like IMRT or IMAT, in rectal cancer.

Some caveats, however, have to be formulated.

Even the selected articles are sometimes difficult to compare in account of diverse, incomplete or even non-existing definitions of pelvic subsites and lymph node groups, obscurity about the surgery performed (definition of curative surgery, the extension of lymphadenectomy (fields and lymph node groups included)), the use of adjuvant therapies, number of patients in studies, collection of data (prospective, retrospective), definition of recurrences, assessment of recurrences (clinical, radiological, histopathological: biopsy or autopsy proven, or findings at second look operations), and differences in the method of recording: number of recurrences versus number of patients with a recurrence per subsite. This problem is reflected in the heterogeneity of the data, as can be seen in Table 1. Therefore, these guidelines should be considered as a starting point, and need to be confirmed by prospective observations.

It should also be noted that a distinction between a nodal and pelvic relapse is difficult to identify in clinical analysis and even in second-look series some of the relapses coded as lateral or posterior were undoubtedly due to relapse within the lymphatics or replaced internal iliac nodes or presacral nodes rather than tumour bed relapse. Two articles [20;30] report on the incidence of local disease recurrence alone without distant metastases, while the other studies record both local recurrence only or in combination with distant relapse [23;24;32;34]. We should, however, realize that once a patient develops distant metastasis, the local disease status is often less carefully verified because of limited therapeutic relevance. Local recurrence in those patients will only be discovered by chance or in case of symptoms, except in the study of Gunderson where initially planned single or multiple second look operations were performed [21;30].

Recurrences in the MS are mostly reported before the introduction of TME. Various articles reported on the importance of the MS as a predominant subsite for local tumour spread, both in lateral and longitudinal direction. Moreover, removing the total mesorectum resulted in a significant improvement of local control. Nevertheless, during preoperative radiotherapy, the mesorectal subsite can hide viable tumour clonogens available for metastasis and should therefore be covered by the CTV. Although difficult to discriminate from a MS recurrence, anastomotic recurrences originate from contamination with cancer cells during operation, while MS recurrences start in remaining circumferential mesorectal tissue (in patients operated with a partial mesorectal excision or in the pre-TME era). In one article, the authors assumed that the recurrence was anastomotic if the tumour volume was larger on the mucosal side than in the perirectal tissue, and, on the other hand, a recurrence starting in the perirectal tissue was assumed to have a relative small volume in the rectal wall [30]. The relative high incidence in some series (Hruby et al. 21%) could be a reflection of a broader definition of a true anastomotic recurrence, but suggest that great care must be taken to avoid peroperative soiling.

The level of the primary tumour is an important factor relative to the mode of spread in rectal cancer. Still, a large variation exists in the definition of low-seated, middle seated and high-seated tumours exist, blurring the analysis. The majority of the authors define the peritoneal reflection as the anatomical boundary between high seated and low seated tumours, based on a biological barrier between lymphatic pathways. The location of the peritoneal reflection has been described in anatomy texts as 7.5 cm from the anal margin in males and 5.5 cm in females. The source of this information was not referenced, but presumably stemmed from cadaveric dissections. Some authors have proposed the anatomic reference of the second rectal valve as the location of the anterior peritoneal reflection [43].

We only found solid evidence of a higher incidence of lymph node involvement in the ELN group in low seated tumours. Data on involvement of the ELN group in tumours that invade adjacent structures are scarce because of the inoperable state of these highly advanced lesions. Nevertheless, it is generally believed that the CTV should include the ELN group in tumours with invasion of adjacent organs on the basis of the lymphatic drainage pattern from those organs.

Conclusion

Definition and delineation guidelines are necessary to optimize radiation treatment and define the best therapy according to the primary tumour characteristics. The CTV should encompass the tumour, the MS and the PPS in all cases. The IPS is at risk if 1) the surgeon aims a sphincter saving procedure and the tumour is located within +/- 6 cm (center-dependent) from the anal margin or 2) the tumour invades the anal sphincter and an APR is necessary. We propose to include the MLN, the ULN and the LLN into the CTV for all patients. We did not find solid evidence to include ELN in the CTV, except in these cases where anterior organ involvement is highly suspected. The ILN are not at risk in rectal cancer patients.

References

[1] Heald RJ, Ryall RD. Recurrence and survival after total mesorectal excision for rectal cancer. Lancet 1986; 1(8496):1479-1482.

[2] Improved survival with preoperative radiotherapy in resectable rectal cancer. Swedish Rectal Cancer Trial. N Engl J Med 1997; 336(14):980-987.

[3] Adjuvant radiotherapy for rectal cancer: a systematic overview of 8,507 patients from 22 randomised trials. Lancet 2001; 358(9290):1291-1304.

[4] Glimelius B. The role of radiotherapy in rectal cancer. Eur J Cancer 2001; 37 Suppl 7:S203-S212.

[5] Krook JE, Moertel CG, Gunderson LL, Wieand HS, Collins RT, Beart RW et al. Effective surgical adjuvant therapy for high-risk rectal carcinoma. N Engl J Med 1991; 324(11):709-715.

[6] Sauer R, Becker H, Hohenberger W, Rodel C, Wittekind C, Fietkau R et al. Preoperative versus postoperative chemoradiotherapy for rectal cancer. N Engl J Med 2004; 351(17):1731-1740.

[7] Gerard JP, Chapet O, Nemoz C, Hartweig J, Romestaing P, Coquard R et al. Improved sphincter preservation in low rectal cancer with high-dose preoperative radiotherapy: the lyon R96-02 randomized trial. J Clin Oncol 2004; 22(12):2404-2409.

[8] Gerard JP, Bonnetain F, Conroy T, Chapet O, Bouche O, Closon-Dejardin MT et al. Preoperative (preop) radiotherapy (RT) +/- 5 FU/folinic acid (FA) in T3-4 rectal cancers: results of the FFCD 9203 randomized trial. Journal of Clinical Oncology 2005; 23(16):247S.

[9] Gunderson LL, Sargent DJ, Tepper JE, Wolmark N, O'Connell MJ, Begovic M et al. Impact of T and N stage and treatment on survival and relapse in adjuvant rectal cancer: a pooled analysis. J Clin Oncol 2004; 22(10):1785-1796.

[10] Mohiuddin M, Ahmad N, Marks G. A selective approach to adjunctive therapy for cancer of the rectum. Int J Radiat Oncol Biol Phys 1993; 27(4):765-772.

[11] Baglan KL, Frazier RC, Yan D, Huang RR, Martinez AA, Robertson JM. The dose-volume relationship of acute small bowel toxicity from concurrent 5-FU-based chemotherapy and radiation therapy for rectal cancer. Int J Radiat Oncol Biol Phys 2002; 52(1):176-183.

[12] Miller RC, Sargent DJ, Martenson JA, MacDonald JS, Haller D, Mayer RJ et al. Acute diarrhea during adjuvant therapy for rectal cancer: a detailed analysis from a randomized intergroup trial. Int J Radiat Oncol Biol Phys 2002; 54(2):409-413.

[13] Letschert JG, Lebesque JV, Aleman BM, Bosset JF, Horiot JC, Bartelink H et al. The volume effect in radiation-related late small bowel complications: results of a clinical study of the EORTC Radiotherapy Cooperative Group in patients treated for rectal carcinoma. Radiother Oncol 1994; 32(2):116-123.

[14] Duthoy W, De Gersem W, Vergote K, Boterberg T, Derie C, Smeets P et al. Clinical implementation of intensity-modulated arc therapy

(IMAT) for rectal cancer. International Journal of Radiation Oncology Biology Physics 2004; 60(3):794-806.

[15] Arcangeli S, Valentini V, Nori SL, Fares C, Dinapoli N, Gambacorta MA. Underlying anatomy for CTV contouring and lymphatic drainage in rectal cancer radiation therapy. Rays 2003; 28(3):331-336.

[16] Lorchel F, Maingon P, Crehange G, Bosset M, Bosset JF. [Cancer of the rectum: target volumes for preoperative radiotherapy]. Cancer Radiother 2002; 6 Suppl 1:93s-99s.

[17] Bagatzounis A, Kolbl O, Muller G, Oppitz U, Willner J, Flentje M. [The locoregional recurrence of rectal carcinoma. A computed tomographic analysis and a target volume concept for adjuvant radiotherapy]. Strahlenther Onkol 1997; 173(2):68-75.

[18] Gunderson LL, Haddock MG, Gervaz PA, Martenson JA, Nelson H. Rectal and anal cancers in conformal radiotherapy planning: selection and delineation of lymph node area tumors. In: Gregoire V, Scalliet P, Ang KK, editors. Clinical target volumes in conformal and intensity modulated radiation therapy. A clinical guide to cancer treatment.1st ed. Heidelberg: Springer-Verlag, 2003: 187-197.

[19] Hocht S, Hammad R, Thiel HJ, Wiegel T, Siegmann A, Willner J et al. Recurrent rectal cancer within the pelvis. A multicenter analysis of 123 patients and recommendations for adjuvant radiotherapy. Strahlenther Onkol 2004; 180(1):15-20.

[20] Gilbertsen VA. Adenocarcinoma of the rectum - incidence and locations of recurrent tumor following present-day operations performed for cure. Ann Surg 1960; 151:340-348.

[21] Gunderson LL, Sosin H. Areas of failure found at reoperation (second or symptomatic look) following "curative surgery" for adenocarcinoma of the rectum. Clinicopathologic correlation and implications for adjuvant therapy. Cancer 1974; 34(4):1278-1292.

[22] Hojo K, Koyama Y, Moriya Y. Lymphatic spread and its prognostic value in patients with rectal cancer. Am J Surg 1982; 144(3):350-354.

[23] Mendenhall WM, Million RR, Pfaff WW. Patterns of recurrence in adenocarcinoma of the rectum and rectosigmoid treated with surgery alone: implications in treatment planning with adjuvant radiation therapy. Int J Radiat Oncol Biol Phys 1983; 9(7):977-985.

[24] McDermott FT, Hughes ES, Pihl E, Johnson WR, Price AB. Local recurrence after potentially curative resection for rectal cancer in a series of 1008 patients. Br J Surg 1985; 72(1):34-37.

[25] Moreira LF, Hizuta A, Iwagaki H, Tanaka N, Orita K. Lateral lymph node dissection for rectal carcinoma below the peritoneal reflection. Br J Surg 1994; 81(2):293-296.

[26] Morikawa E, Yasutomi M, Shindou K, Matsuda T, Mori N, Hida J et al. Distribution of metastatic lymph nodes in colorectal cancer by the modified clearing method. Dis Colon Rectum 1994; 37(3):219-223.

[27] Hida J, Yasutomi M, Fujimoto K, Ieda S, Machidera N, Kubo R et al. Analysis of regional lymph node metastases from rectal carcinoma by the clearing method. Justification of the use of sigmoid in J-pouch construction after low anterior resection. Dis Colon Rectum 1996; 39(11):1282-1285.

[28] Moriya Y, Sugihara K, Akasu T, Fujita S. Importance of extended lymphadenectomy with lateral node dissection for advanced lower rectal cancer. World J Surg 1997; 21(7):728-732.

[29] Ueno H, Yamauchi C, Hase K, Ichikura T, Mochizuki H. Clinicopathological study of intrapelvic cancer spread to the iliac area in lower rectal adenocarcinoma by serial sectioning. Br J Surg 1999; 86(12):1532-1537.

[30] Wiig JN, Wolff PA, Tveit KM, Giercksky KE. Location of pelvic recurrence after 'curative'

low anterior resection for rectal cancer. Eur J Surg Oncol 1999; 25(6):590-594.

[31] Takahashi T, Ueno M, Azekura K, Ohta H. Lateral node dissection and total mesorectal excision for rectal cancer. Dis Colon Rectum 2000; 43(10 Suppl):S59-S68.

[32] Killingback M, Barron P, Dent OF. Local recurrence after curative resection of cancer of the rectum without total mesorectal excision. Dis Colon Rectum 2001; 44(4):473-483.

[33] Steup WH, Moriya Y, van de Velde CJ. Patterns of lymphatic spread in rectal cancer. A topographical analysis on lymph node metastases. Eur J Cancer 2002; 38(7):911-918.

[34] Hruby G, Barton M, Miles S, Carroll S, Nasser E, Stevens G. Sites of local recurrence after surgery, with or without chemotherapy, for rectal cancer: implications for radiotherapy field design. Int J Radiat Oncol Biol Phys 2003; 55(1):138-143.

[35] Koda K, Saito N, Oda K, Takiguchi N, Sarashina H, Miyazaki M. Evaluation of lateral lymph node dissection with preoperative chemo-radiotherapy for the treatment of advanced middle to lower rectal cancers. Int J Colorectal Dis 2004; 19(3):188-194.

[36] Ueno M, Oya M, Azekura K, Yamaguchi T, Muto T. Incidence and prognostic significance of lateral lymph node metastasis in patients with advanced low rectal cancer. Br J Surg 2005; 92(6):756-763.

[37] Lengele B. The lymphatic system. In: Gregoire V, Scalliet P, Ang KK, editors. Clinical target volumes in conformal and intensity modulated radiation therapy. A clinical guide to cancer treatment.1st ed. Heidelberg: Springer-Verlag, 2003: 23-31.

[38] Koyama Y, Moriya Y, Hojo K. Effects of extended systematic lymphadenectomy for adenocarcinoma of the rectum–significant improvement of survival rate and decrease of local recurrence. Jpn J Clin Oncol 1984; 14(4):623-632.

[39] Takahashi T, Ueno M, Asekura K, Ota H. The lymphatic spread of rectal cancer and the effect of dissection: Japanese contribution and experience. In: Soreide O, Norstein J, editors. Rectal Cancer Surgery: Optimisation, Standardisation, Documentation. Berlin: Springer-Verlag, 1997: 165-180.

[40] Canessa CE, Badia F, Fierro S, Fiol V, Hayek G. Anatomic study of the lymph nodes of the mesorectum. Dis Colon Rectum 2001; 44(9):1333-1336.

[41] Oto A, Peynircioglu B, Eryilmaz M, Besim A, Surucu HS, Celik HH. Determination of the width of the presacral space on magnetic resonance imaging. Clin Anat 2004; 17(1):14-16.

[42] Bosset JF, Horiot JC, Hamers HP, Cionini L, Bartelink H, Caspers R et al. Postoperative pelvic radiotherapy with or without elective irradiation of para-aortic nodes and liver in rectal cancer patients. A controlled clinical trial of the EORTC Radiotherapy Group. Radiother Oncol 2001; 61(1):7-13.

[43] Beck DE, Wexner SD. Fundamentals of Anorectal Surgery. 1st ed. New York: McGraw-Hill, 1992.

V. 7. Clinical implementation of intensity-modulated arc therapy (IMAT) for rectal cancer.

Authors: W. Duthoy, W. De Gersem, K. Vergote, T. Boterberg, C. Derie, P. Smeets, C. De Wagter and W. De Neve.

Journal: International Journal of Radiation Oncology Biology Physics 2004; 60(3):794-80

Acknowledgements: The project "Conformal Radiotherapy Ghent University Hospital" is supported by the Belgische Federatie tegen Kanker and by grants from the Fonds voor Wetenschappelijk Onderzoek (FWO) Vlaanderen (G.0183.03), the University of Ghent (GOA 12050401, BOF 01112300, 011VO497, 011F1700), and the Centrum voor Studie en Behandeling van Gezwelziekten. Wim Duthoy is a Research Assistant (Aspirant) of the FWO. Jan Schauvliege from Elekta is acknowledged for fine-tuning the linear accelerator for IMAT purposes. Nucletron is acknowledged for providing the Oncentra Treatment Planning System.

Key issues discussed in this paper:

- In rectal cancer, radiotherapy is standard treatment option. The main dose-limiting organ is the small bowel. Intensity modulation is a possible method to minimize small bowel toxicity. IMAT was selected due to the large inner radius of the PTV.
- An additional IMAT planning tool was implemented, in order to facilitate the extraction of deliverable arcs out of the preliminary arcs with variable ADR.
- An IMAT class solution for rectal cancer was developed, consisting of 3-6 arcs, and resulting in a delivery time of 5 to 10 minutes.
- IMAT was tested against 3D-CRT, and was found to result in a lower dose to the small bowel, at the cost of a slightly larger inhomogeneity in the PTV.
- A series of PGD experiments showed good agreement between measured and calculated dose in the PTV, and confirmed the sparing of the small bowel. IMAT delivery was shown to be as accurate as 3D-CRT delivery.

Clinical implementation of intensity modulated arc therapy (IMAT) for rectal cancer

Wim Duthoy, M.D.[1], Werner De Gersem, Ir.[1], Koen Vergote, M.Sc.[1], Tom Boterberg, M.D., PhD.[1], Cristina Derie[1], Peter Smeets, M.D.[2], Carlos De Wagter, Ir., PhD.[1] and Wilfried De Neve, M.D., PhD.[1]

1. Department of radiotherapy and 2. Department of radiology, Ghent University Hospital, De Pintelaan 185, 9000 Ghent, Belgium

Abstract

Purpose: In rectal cancer, combined radiotherapy and chemotherapy, either pre- or postoperatively, is an accepted treatment. Late small bowel (SB) toxicity is a feared side effect and limits radiation-dose escalation in a volume-dependent way. A planning strategy for Intensity Modulated Arc Therapy (IMAT) was developed and IMAT was clinically implemented with the aim to reduce the volume of SB irradiated at high doses and thus reduce SB toxicity. We report on the treatment plans of the first seven patients, on the comparison of IMAT with conventional 3D planning (3D) and on the feasibility of IMAT delivery.

Methods and Materials: Seven patients, who were referred to our department for pre- (n=4) or postoperative (n=3) radiotherapy for rectal cancer, gave written consent for IMAT treatment. All patients had a planning CT in prone position. The delineation of the clinical target volume was done after fusion of CT and MRI, with the help of a radiologist. For the IMAT plan, arcs were generated using an anatomy-based segmentation tool. The optimization of the arcs was done by weight optimization (WO) and leaf position optimization (LPO), both of which were adapted for IMAT purposes. The 3D plans used one posterior and 2 lateral wedged beams, of which the outlines were shaped to the beam's eye view projection of the planning target volume (PTV). Beam WO was done by constrained matrix inversion. For dose volume histogram analysis, all plans were normalized to 45 Gy as median PTV dose. Polymer Gel Dosimetry (PGD) on a humanoid phantom was used for the validation of the total chain (planning to delivery). IMAT treatments were delivered by an Elekta Sl*i*Plus linear accelerator using prototype software with the same interlock class as in clinical mode.

Results: The IMAT plan resulted in 3 to 6 arcs, with a mean delivery time of 6.3 minutes and a mean of 456 monitor units (MU) for a 180 cGy fraction. The minimal dose in the PTV was not significantly different between 3D and IMAT plans. Inhomogeneity was highest for the IMAT plans (14.1%) and lowest for the 3D plans (9.9%). Mean dose to the SB was significantly lower for the IMAT plans (12.4 Gy) than for the 3D plans (17.0 Gy). The volume of SB receiving less than any dose level was lower for the IMAT plans than for 3D plans. Integral dose was lower in the IMAT plans than for the 3D plans (respectively 244 J and 262 J to deliver 45 Gy). Differences between the PGD measured dose and the calculated dose were as small for IMAT as for 3D treatments.

Conclusion: IMAT plans are deliverable within a 5-10 minute time slot, and result in a lower dose to the SB than 3D plans, without creating significant underdosages in the PTV. PGD showed that IMAT delivery is as accurate as 3D delivery.

Introduction

The use of radiotherapy, either pre- or postoperatively, in addition to systemic chemotherapy, decreases the local recurrence rate and improves survival in rectal cancer [1]. Randomized trials of preoperative radiation and surgery versus surgery alone showed a radiation-dose dependent reduction of local failure in the combined modality arm, with a halving of the local recurrence rate at biologically effective doses of $\geq$ 30 Gy [2]. Pre-operative radiation therapy to a dose of 40-45 Gy in 1.8-2 Gy per fraction, usually combined with 5-fluoro-uracil-based chemotherapy is the standard schedule in many European centers.

Although some reports suggest further improvement in local control for higher doses, especially in high-stage rectal cancer [3, 4], acute and chronic small bowel (SB) and rectal toxicity [5] seem to limit further dose escalation. For small bowel, reported incidences of acute grade III-IV diarrhea vary between 15% and 40%, depending on grading systems, type of surgery, administration of adjuvant chemotherapy and other variables like co-morbidity [6, 7]. Chronic SB radiation toxicity is irreversible and can be life-threatening. Actuarial 5-year estimates of severe chronic SB toxicity vary between 7 and 42% [8, 9] at doses of 45-50 Gy. The incidence of both acute and late SB toxicity is related to the volume of SB in the treatment fields [6, 7, 9]. Several possible methods have been examined for minimizing the portion of SB in the treatment field. For a review of these different techniques, the reader is referred to Letschert [10]. A new possibility to reduce the volume of SB irradiated to high doses consists of Intensity Modulation (IM). IM offers the possibility to spare an Organ At Risk (OAR) lying in the concavity of a Planning Target Volume (PTV). This anatomical relationship occurs in rectal cancer, where SB is partially surrounded by the CTV, consisting of the rectum and its draining lymph node regions. Because of the large internal radius of the concave PTV in rectal cancer, a large number of beam directions may be favorable [11]. With arc therapy, the number of beam directions is infinite, and thus Intensity Modulated Arc Therapy (IMAT) [11, 12] might be a logical approach to this clinical problem. The goals of this manuscript are:

- to present our planning strategy and first experience of IMAT for rectal cancer;
- to report the results of a planning comparison between conventional radiotherapy (3D) and IMAT;
- to validate the IMAT delivery method using polymer gel dosimetry.

Methods and Materials

Delineation

Between February 2003 and November 2003, 7 patients with a histologically proven adenocarcinoma of the rectum were treated with IMAT. All patients signed an informed consent for inclusion in this feasibility study, approved by the local ethics committee. Some clinical data of these patients are shown in Table 1. A planning computed tomography (CT) was performed with the patient in prone position. For patient 5, 6 and 7, a bellyboard was used (Sinmed, Reeuwijk, The Netherlands). CT slice thickness was 0.3 cm, and the scanned volume extended from the third lumbar vertebra down to 10 cm caudal to the obturator foramina. No contrast enhancement was used. No attempts were made to reduce variation of bladder filling. All patients underwent diagnostic magnetic resonance imaging (MRI), which was electronically fused with the planning CT. This was done using the landmark method of the Oncentra Treatment Planning System (Nucletron B.V., Veenendaal, The Netherlands). In those patients who were sent for pre-operative radiotherapy, the gross tumor volume (GTV) was delineated using the fused CT-MRI. The fused CT-MRI was also used for the delineation of all other target subvolumes. These included the following structures: rectum , mesorectal space, presacral space and the lymph node regions along the common iliac (up to and including the level of the first sacral vertebra), the internal iliac, the superior rectal and the internal obturator vessels. In patients with a tumor lying 6 cm or less from the anal verge, the perineal area was also included. The contouring of these

Table 1: Patient and planning description.

	timing	$Vol_{sb_{3D}}$ (cc)	IMAT				3D	
			# arcs	# MUs	CDT (mean±SD)	DRDT	# MUs (W/UW)	DRDT
Pt 1	pre	234.4	5	526	5.8 ± 0.4	5.4	389/109	2.8
Pt 2	pre	29.7	6	508	9.4 ± 0.3	7.6	350/87	2.4
Pt 3	post	22.6	6	421	7.5 ± 0.3	6.3	302/92	2.3
Pt 4	post	8.9	4	476	5.5 ± 0.3	5.5	187/153	2.6
Pt 5	pre	145.8	3	529	3.4 ± 0.0	3.5	304/100	2.5
Pt 6	pre	0.8	5	392	5.8 ± 0.1	5.5	363/92	2.4
Pt 7	post	146.3	4	337	5.6 ± 0.7	4.8	211/144	2.6

The seven patients (Pt) are ordered chronologically. Timing is the order of radiotherapy in relation to the surgery, in which "pre" stands for pre-operative radiotherapy, and "post" for post-operative radiotherapy. $Vol_{sb_{3D}}$ = the volume of small bowel receiving more than 90% of the target prescription dose in the 3D plan. IMAT= Intensity Modulated Arc Therapy. For IMAT the number of arcs is given, as is the total number of monitor units (MUs) for a fraction of 180 cGy. Both clinical delivery time (CDT) as dummy run delivery time (DRDT) is given. All time measurements are given in minutes. For the 3D plans, MUs are split up in the wedged (W) and unwedged (UW) part.

target subvolumes was done together with a radiologist (PS). Due to the fact that the internal motion of the different target subvolumes is different [13], the rectum was expanded anisotropically with 1.5 cm in the antero-posterior direction, and with 0.5 cm in the cranio-caudal and lateral directions. All other subvolumes were expanded isotropically with 0.5 cm. All unexpanded subvolumes were summed to form the CTV, while all expanded subvolumes were summed to the PTV.

The OARs that were contoured were bladder and SB. All SB loops were delineated individually up to the CT slice through the middle of the fourth lumbar vertebra. Structures provided to the optimization algorithm included the PTV, bladder, SB, and three structures generated to aid the optimization towards a desirable solution. A first optimization aid structure was made by subtracting the PTV and an additional margin of 0.6 cm from a 1 cm expansion of the SB, resulting in the structure "small_bowel_exp_optim". Other optimization aid structures were rim_2_cm (= all tissue between 0 and 2 cm around the PTV) and surr (= all tissue more than 2 cm from the PTV). For a discussion about the use of these optimization aid volumes, the reader is referred to De Neve *et al.* [14]. The anatomy-based segmentation tool (ABST) [15] needs an OAR of which the projection on the isocentric plane is larger than the PTV projection in the direction perpendicular to the direction of the leaf motion. For this reason, a segmentation structure (segm_str) was made, consisting of SB and bladder, elongated in the cranio-caudal direction when necessary. Per patient, the same target structures and OARs were used for both plans.

IMAT planning procedure

The IMAT planning procedure has been described in more detail previously [11] and is summarized in Figure 1. Machine states (MSs) are generated using ABST every 8° within the deliverable range. This deliverable range consists of beam directions in which the radiation beam does not traverse metal components of the couch before entering the patient. In the case of the Elekta SL*i*Plus couch, the largest deliverable range is obtained by positioning the metal C-arms of the couch on 120° or 150°, as measured from their lateral position. Considering the relative position of the isocenter to the table and the PTV geometry, possible gantry angels ranged from -136° to 136°. Thus, no arcs were irradiating the patient from below the couch (anterior to the patient). The ABST

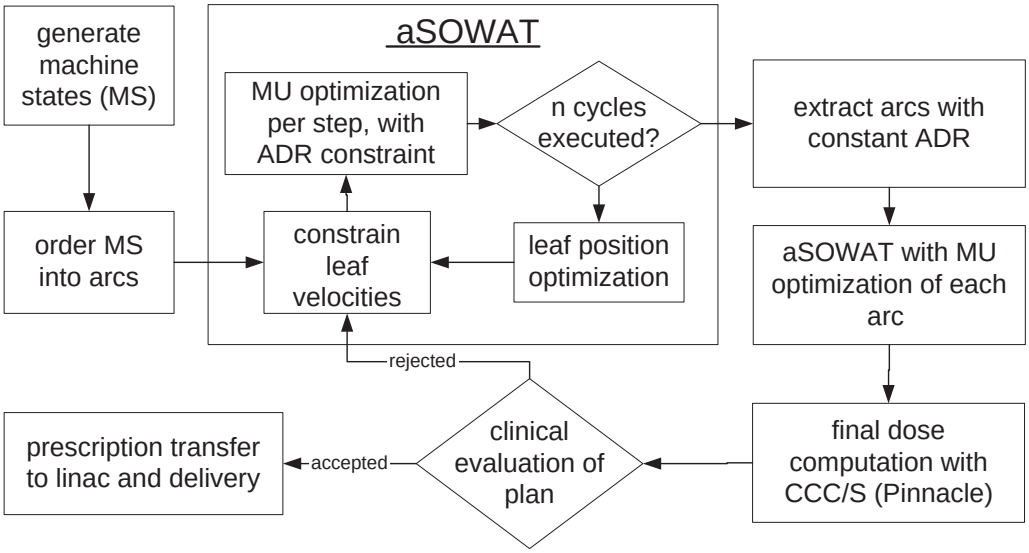

Figure 1: IMAT planning flowchart. *Abbreviations:* ADR: angular delivery rate. aSOWAT: arc-therapy modification of segment outline and weight adaptation tool. CCC/S: collapsed cone convolution/superposition calculation algorithm. MS: machine state. A MS is described by a set of machine parameters that uniquely define beam direction, aperture, photon beam quality. After MS generation, MSs of the same class are then ordered into arcs. These arcs are given as input to aSOWAT. This is our optimization tool, which was adapted for IMAT purposes. aSOWAT starts with a check of the leaf velocities in the transition from one MS to the next. If necessary, leaf positions are adapted in order to meet this constraint. Then, the actual optimization starts with the optimization of the monitor units (MU) per step, in which a step is defined as the transition from one MS to the next. A factor is included in the bio-physical cost function to restrict the MU per degree variation (ADR constraint). When a user-defined number of cycles have been executed, aSOWAT is terminated, and the new MS outlines are saved. This is followed by the interactive extraction of deliverable arcs with constant ADR. After all deliverable arcs have been extracted, these are given as input to aSOWAT, but with optimization of the total number of MUs per arc instead of per step. Finally, a dose calculation with the CCC/S algorithm is done, and the plan is evaluated by the clinical staff.

resulted in (maximally) 4 classes of MSs per beam direction, differing from each other only in the coverage of the PTV (Figure 2). All adjacent MSs of the same class were sorted based on the gantry angle to form an arc (Figure 2), thus resulting in four arcs. These initial arcs were the input of the optimization, which is done by our in-house developed segment outline and weight adaptation tool (SOWAT), modified for IMAT purposes (aSOWAT) (Figure 1) . aSOWAT optimizes the leaf positions of each MS and the monitor unit (MU) values of each step, in which a step is defined as the transition from one MS to the next MS. Additional to the previously described IMAT planning strategy, a factor has been added to the objective function to obtain a fluent angular delivery rate (ADR). This factor takes into account the first and second derivative of the ADR, approximated using the first and second finite differences of the MU values of each step. This first aSOWAT optimization results in arcs with a non-constant ADR, further called virtual arcs, which are presently undeliverable on the Elekta SL*i*Plus linac. These virtual arcs however help to select the start and stop gantry angles of the final, deliverable arcs, for which the ADR has to be constant. The fluently modulating ADR facilitates this extraction of deliverable arcs. To obtain a time-efficient treatment, the number of arcs has to be kept low. Consequently, a one step extraction of deliverable arcs would impose a very rough discretization of the optimized ADR. A more efficient procedure was

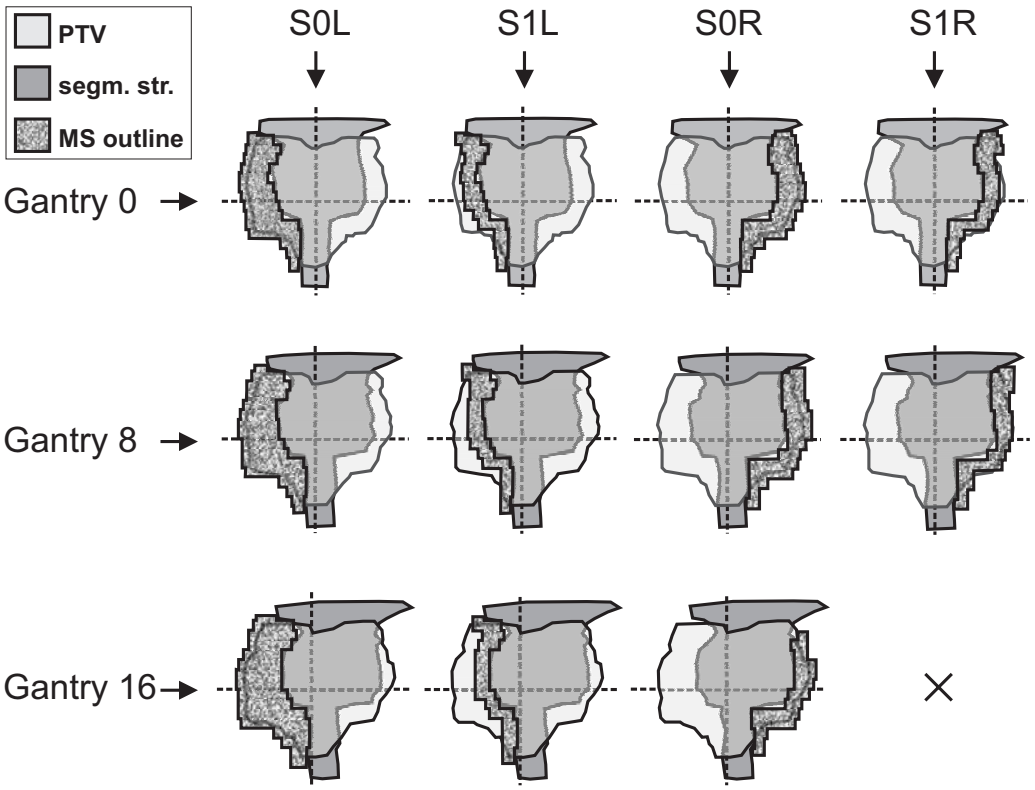

Figure 2: Anatomy-based arc generation shown in beam's eye view (BEV). *Abbreviations:* PTV: planning target volume. Segm. str.: segmentation structure. MS: machine state. S0L: MS covering the total BEV projection of the PTV passing at the left side of the segmentation structure. S1L: MS covering a 2 cm wide area of the PTV at the left side of the segmentation structure. S0R: MS covering the total BEV projection of the PTV passing at the right side of the segmentation structure. S1R: MS covering a 2 cm wide area of the PTV at the right side of the segmentation structure. The ABST-generated machine states are shown for three adjacent beam directions (gantry angles 0°, 8° and 16°). The horizontal position shows how the different classes (S0L, S1L, S0R and S1R) were generated per gantry angle. In the vertical direction, the ordering per arc can be appreciated. As can be seen, the BEV projection of the PTV and the segmentation structure does not differ much when the gantry is rotated over 8°. The S1R MS for the gantry on 16° was not generated, because the width of the S0R MS was less than the user-defined 2 cm for the S1R MS. This means that the S1R arc will end at a gantry angle of 8°.

implemented as follows: each arc is separately (and manually) extracted from the ADR graphs displayed on the planning computer. After each extraction of a deliverable arc, the MUs of all deliverable arcs are re-optimized, together with the remnant ADR of the virtual arcs. During this short optimization, a factor included in the objective function favors the MUs of the deliverable arcs with respect to the ADR of the virtual arcs. Each extraction transfers MUs from the virtual to the deliverable arcs. By downforcing the remnant ADR, only the important parts of the virtual arcs remain to be extracted in the next deliverable arcs. When the remnant ADR falls to zero by optimization, the extraction procedure is finished. The plan is finalized by an aSOWAT optimization cycle, consisting of optimization of the leaf positions of the final arcs, and optimization of the ADR per (extracted) arc instead of per step, which is equivalent to optimization of the total MU-count of an arc (to be delivered at a constant ADR). A final dose computation

was done for 18MV using the collapsed cone convolution/superposition algorithm from Pinnacle (Philips Medical Systems, Best, The Netherlands), which was used for all (IMAT and 3D) plans. Dose distributions of arcs were approximated by computing dose at the 8° interspaced MSs. For this, the MUs of each step were equally split and attributed to the two defining MSs. Thereby, the number of MUs assigned to the first and last MS is the number of MUs of the arc divided by twice the number of steps. The MUs assigned to the other MSs is the number of MUs of the arc divided by the number of steps. Except where explicitly mentioned, all presented results on IMAT calculated dose distributions are based on this 8° discretization.

A last MU optimization per arc was done using the results of the final dose computation. Finally, a prescription file was generated for each arc, and networked to a an Elekta SL*i*Plus 18 MV linear accelerator. The IMAT treatment was delivered in local service mode using prototype dynamic software (Javelin, Elekta), with the same interlock class as used in clinical mode.

Conventional planning

The conventional plan consisted of two lateral beams and one posterior beam, as described earlier. The outlines of the beams were shaped conformally around the PTV with a margin of 0.8 cm, using multileaf collimation. All beams consisted of a wedged and an unwedged part. The weight optimization was done using constrained matrix inversion (CMI) [16]. It was proven previously that CMI resulted in a better plan than achieved by human planners, given that all relevant structures are included in the objective function. The following structures were used in the optimization algorithm: PTV, SB and surr. The last structure was added to avoid unacceptable overdosage outside the PTV.

Treatment evaluation

Treatment delivery time, defined as the time between the start of the first arc and the end of the last arc, was measured for all patients for nearly all fractions. Apart from these clinical time measurements, dummy run delivery time measurements were done for all plans. For the IMAT plans, this was done on Javelin, while for the 3D plans, this was done on the RT Desktop (RTD) linac control software from Elekta. Total time was measured, as well as beam-on time, time for automatic setup and time for system checks. For the different planning techniques, the total number of MUs needed to deliver a 180 cGy fraction, were also compared.

For dose volume histogram (DVH) analysis, all plans were normalized to a median dose of 45 Gy in the PTV. Target dose homogeneity was evaluated using an inhomogeneity factor U (= $\frac{D_{99}-D_1}{D_{med}}$ with D_{99} the dose below which 99% of the PTV volume was treated , D_1 the dose below which 1% of the PTV volume was treated, and D_{med} the median PTV dose). Furthermore, the D_{99} and D_1 (used as a surrogate for maximum and minimum dose, respectively), and the % volume of the target structure receiving more than 95% of the prescribed dose over the total volume ($V_{95\%}$) were compared. For SB, the mean dose (D_{mean}), the % volume receiving more than 90% of the target prescription dose ($V_{90\%}$), and the % volume receiving more than 15 Gy ($V_{>15Gy}$) were evaluated. Finally, the integral dose ($D_{I_{total}}$) given to the patient was approximated as $D_{mean} \times V_{tot}$ with V_{tot} the total scanned volume. The dose deposition efficiency factor (DDEF) was calculated by dividing the integral dose to the PTV ($D_{I_{PTV}}$) by $D_{I_{total}}$. DVHs were recalculated for the group of 7 patients. For all relevant structures of all patients, the volume percentiles at every 0.25 Gy dose level from 0 to 50 Gy were computed from the calculated dose distribution. For every dose level, the mean and standard error of the mean (SEM) was calculated. In order to characterize the different plans in their ability to spare SB, dose "volume difference" histograms (DVDH) were made. A DVDH represents the difference (between two plans) of the % volume receiving specified doses. DVDHs were constructed by calculating the mean (over the seven patients) of difference in % volume receiving a specified dose. These points were calculated every 0.25 Gy between 0 and 50 Gy. For all statistical comparisons, a paired Student t test was used. All tests were two-tailed and $p < 0.05$ was considered statistically significant.

Dosimetric verification

Polymer gel dosimetry (PGD) was used for dose verification. The basis of this dosimetric technique resides in a polymerization reaction of acrylic monomers within a hydrogel. The reaction is initiated by highly reactive radicals, that are formed by radiolysis during irradiation. The amount of polymer formed is related to the absorbed dose, and can be quantified by MRI. Detailed information on PGD can be found elsewhere [17, 18, 19]. A homogeneity study was done to validate PGD for the use of large volumes, and is described elsewhere [20]. A Barex (Cifra, Chateau Thierry, France) cast was vacuum molded on the pelvic region of the RANDO phantom (Alderson Research Laboratories, Stamford, USA). Three supplemental RANDO slices were placed cranially and caudally to the Barex phantom to have full scatter conditions in the gel during irradiation. CT scans (Siemens Somatom Plus 4, Erlangen, Germany) of the gel-filled Barex phantom were transferred to the planning system, and the volumes of interest of a patient case were transferred to the CT set. For this setup, a 3D and an IMAT plan were made as described earlier, and a prescription was made giving a median dose of 7.5 Gy to the PTV. This ensured the maximal response range of the gel, while avoiding saturation effects in the gel. Both techniques were dosimetrically verified using PGD. For the IMAT plan, two measurements were done. First, the plan was delivered in arc therapy mode, thus with dynamic gantry ($IMAT_d$). In a second experiment, the prescription was delivered in a discrete way, i.e. as a static gantry IMRT with gantry positions every 8° ($IMAT_S$). The latter delivery reflects how the plan is calculated. By comparing both results, the effects of the interpolation from discrete, 8°-interspaced, gantry positions to arcs can be seen. For each experiment, gel-filled test tubes were irradiated to doses between 0 and 10 Gy (every 1 Gy) for calibration purposes. The dose distributions, as measured in the gel, were transferred to the planning system. For the transfer of the gel-measured dose distributions, the following positioning procedure was followed: on both the planning CT and the MRI (used for PGD), the content of the Barex cast (=the gel) was automatically contoured. The center of volume (COV) of both structures was positioned onto each other. Rotations were avoided by using laser line positioning on the CT scanner and positioning lines on the MRI scanner. The measured dose distribution was converted to the prescription dose based on the planned versus delivered monitor units. As a consequence, the comparison of converted dose distributions is an absolute dosimetry comparison. The DVHs of all relevant structures, which were clipped to the volume of the gel phantom [11], were computed both for the calculated and the measured dose, and compared. Low's γ-index [21] was calculated in 3D (dose difference criterion = 5%, distance to agreement = 5 mm) and γ-volume histograms (γ-VH) were reconstructed.

Results

Treatment plan and delivery

Details on the delivered IMAT plans are summarized in Table 1. Three to six arcs were used in the IMAT plans. Mean clinical delivery time was 6.3 minutes (range 3.2-12.8 minutes) over all fractions and all patients. For the dummy run delivery, the mean total delivery time was 5.5 minutes (range 3.5-7.6) for the IMAT plans, and 2.5 minutes (range 2.3-2.8) for the 3D plans ($p<0.01$). When considering beam-on time only, this was 3.8 ± 1.0 minutes for IMAT and 1.4 ± 0.2 minutes for the 3D delivery ($p<0.01$). Time for system checks was 1.3 min for the IMAT delivery on the Javelin, and 0.4 min for the 3D plans on the RTD. For the IMAT plans, the number of MUs needed for a fraction of 180 cGy varied between 337 and 529 MUs (mean 456 $\pm$74 MUs) . For the 3D plans, this varied between 340 and 498 MUs (mean 412 ± 56). This difference was not significant ($p=0.16$).

DVH analysis and dose distributions

The compiled DVH data for the 7 patients are summarized in Table 2, and graphically displayed in Figure 3. The minimal dose in the PTV was not significantly different. Inhomogeneity, however, was lower for the 3D plans (9.9% $\pm$ 1.5) than for the IMAT plans (14.4% $\pm$ 3.1). This difference was significant

Table 2: Summary of the DVH data, showing the mean ± the standard deviation.

	3D	IMAT	p
PTV			
V_{95} (%)	97.5 ± 1.4	95.7 ± 2.0	0.16
V_{107} (%)	0.0 ± 0.0	0.2 ± 0.3	0.13
D_{99} (Gy)	46.6 ± 0.1	47.3 ± 0.5	**<0.01**
D_1 (Gy)	42.1 ± 0.6	40.9 ± 1.3	0.12
U (%)	9.9 ±1.5	14.1 ± 3.1	**0.03**
Small bowel			
D_{mean} (Gy)	17.0 ± 7.7	12.4 ± 4.6	**0.02**
V_{90} (%)	19.1 ± 6.5	6.6 ± 2.3	**0.04**
$V_{>15Gy}$ (%)	45.6 ± 8.2	33.0 ± 5.6	**0.04**
Bladder			
D_{mean} (Gy)	34.6 ± 6.8	18.2 ± 2.7	**<0.01**
$D_{I_{total}}$ (J)	262.1 ± 64.5	244.0 ± 47.6	0.24
DDEF (%)	20.7 ± 0.1	22.2 ± 0.1	0.21

Abbreviations: 3D = conventional plan (three beam directions), with conformal portals; IMAT = Intensity Modulated Arc Therapy plan; PTV = Planning target volume; V_{90}, V_{95} and V_{107} = partial volume (%) receiving more than 90%, 95% and 107% of the prescribed dose, respectively; D_1 and D_{99} = the first and the 99^{th} percentile dose; U = inhomogeneity factor, defined as $\frac{(D_{99}-D_1)}{D_{med}}$, with D_{med} the median dose; D_{mean} = mean dose. $D_{I_{total}}$ = the integral dose defined as the mean dose in the total volume multiplied by its volume. $D_{I_{total}}$ was calculated for the total treatment dose (=45 Gy). DDEF = Dose deposition efficiency factor, defined as $\frac{D_{I_{PTV}}}{D_{I_{total}}}$.
p-values represent the result of a two-tailed paired t test.

(p=0.03). Maximal dose in the PTV was 46.6 Gy for the 3D plans, and 47.3 Gy for the IMAT plans (p<0.01). For the CTV, the inhomogeneity for the 3D and IMAT plans was 6.3% and 8.1% (p=0.06). The mesorectal space, surrounding the rectum, received a slightly higher dose in the IMAT plans than in the 3D plans, with a maximal dose of 47.0 Gy vs 46.3 Gy (p=0.01). In the 3D plans, no part of the mesorectal space received a dose higher than 107% of the prescribed dose, while the V_{107} was 0.1% for the IMAT plans. This difference was not significant (p=0.1). For SB, the D_{99} was 45.5 Gy for the 3D plans and 41.5 Gy for the IMAT plans. Mean dose to the SB was significantly lower for the IMAT plans, as was the $V_{>15Gy}$ and the V_{90}. The absolute volume of SB receiving more than 15 Gy was 158 cc (range 21-327 cc) in the 3D plans, and 128 cc (range 13-305 cc) in the IMAT plans. The absolute V_{90} was 84 cc (range 1-234 cc) and 27 cc (range 0-58 cc) for the 3D and IMAT plans, respectively. Figure 4 shows the DVDH for SB, PTV and surr for 3D plans compared to the IMAT plans. This illustrates that the volume of SB receiving any dose is lower for the IMAT plans. The differences in relative volume between 3D and IMAT plans for SB were significant between 13.5 and 42.5 Gy. For the PTV, the DVDH shows the underdosage and overdosage caused by IMAT when compared to 3D. Between 42.25 and 45 Gy, 1-5% of the volume of the PTV receives less by IMAT than by 3D. The bladder received a significantly lower dose in the IMAT plans, with a relative reduction of nearly 50% in D_{mean}. The dose to the surr was lowest for the IMAT plans, with a mean $V_{>30Gy}$ of 9.0% and 4.4% for the 3D and IMAT plan, respectively . This is also reflected in the average DDEF, which was 20.7% for the 3D plans and 22.2% for the IMAT plans. This difference was not significant, but shows that IMAT is at least as efficient as the 3D technique in dose de-

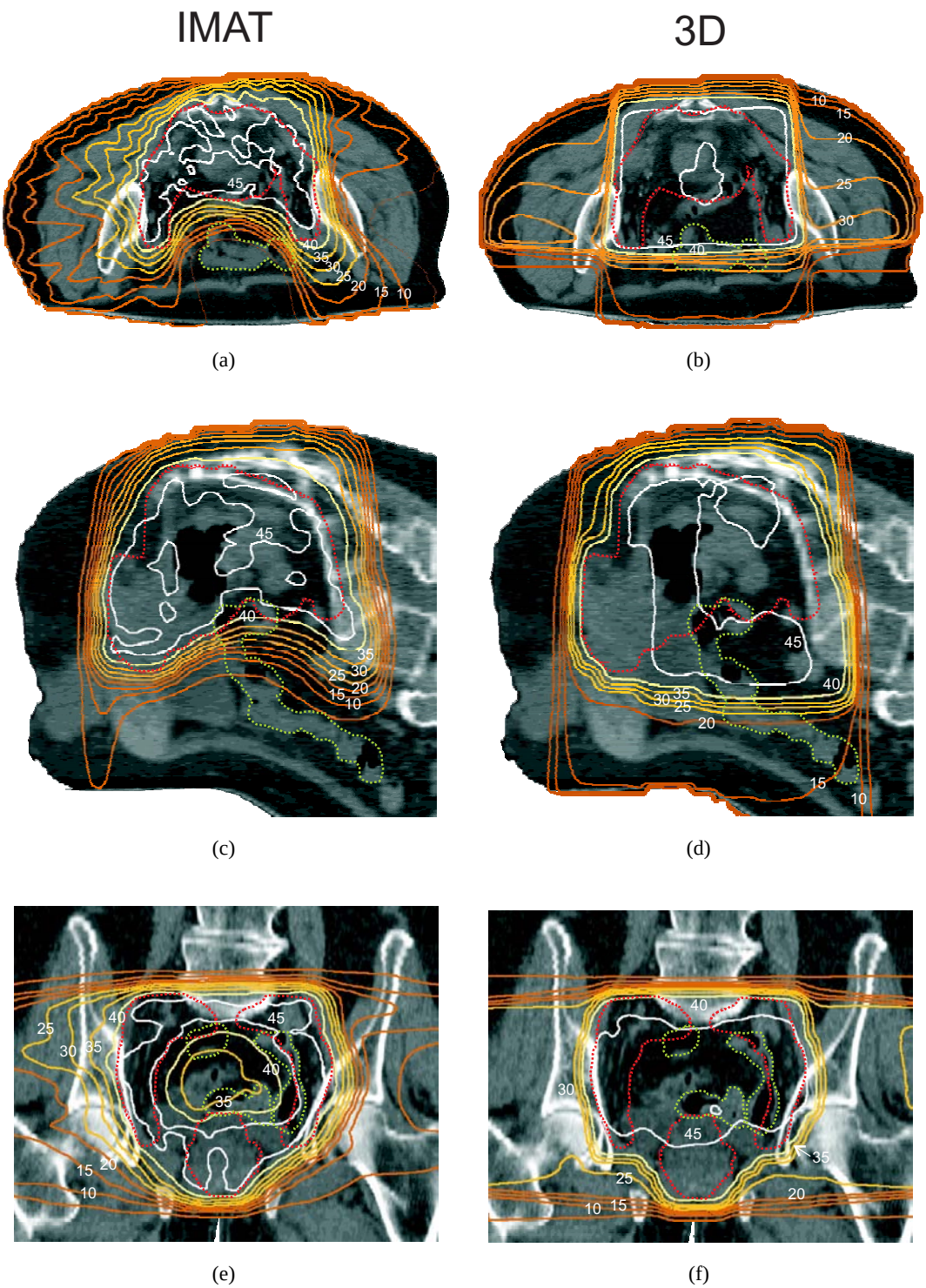

Figure 5: Dose distributions for Patient 5, showing the delivered IMAT plan in a transverse (a), sagittal (c) and coronal (e) plane. The 3D plans (b,d,f) are shown in the same three planes. Isodose values are in Gy. PTV is delineated by a red dotted line, while small bowel is shown by a green dotted line.

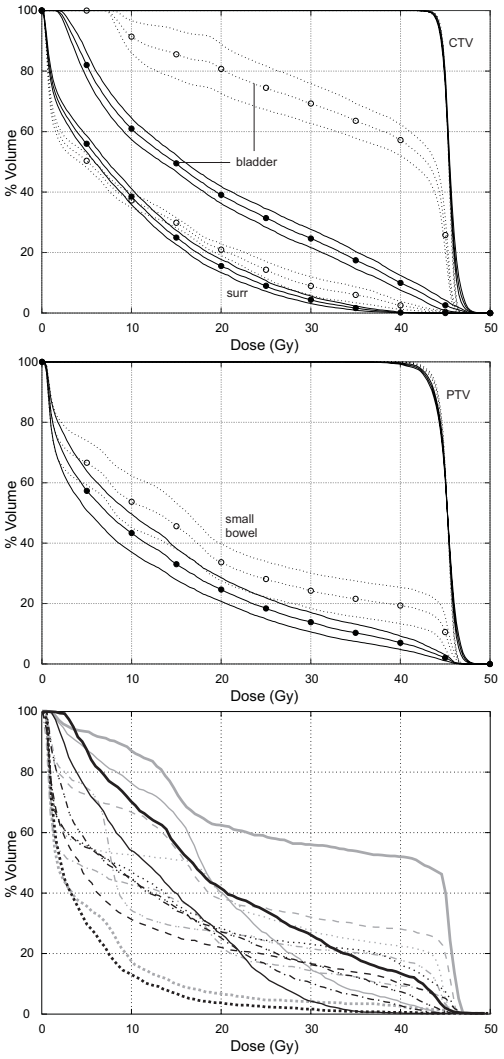

Figure 3: DVHs compiled from the data of the whole group. Solid lines and black-filled circles represent the IMAT plans while the 3D plans are shown by the dotted lines and open circles. For reasons of clarity, all circles were omitted for CTV and PTV. For each plan and each structure, the mean +/- the standard error of the mean is represented. Data are shown for CTV, bladder and surr (*a*), and PTV and small bowel (*b*). In (*c*), the individual DVHs for the seven patients are shown, both for the 3D plans (grey lines) and for the IMAT plans (black lines). The DVHs for patient 1 (solid lines) and for patient 4 (dotted lines) are displayed in bold.

position in the PTV.

Dose distributions for both an IMAT and a 3D

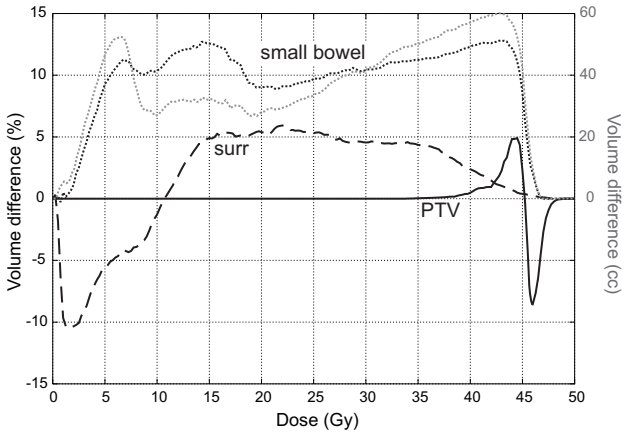

Figure 4: Dose Volume Difference Histograms (DVDH) for PTV (solid line), small bowel (dotted line) and surr (dashed line). The grey dotted line represents the dose absolute volume difference histogram (DAVDH) for the small bowel (in cc). The D(A)VDH is constructed by plotting the mean (over the 7 patients) of $(V_{X_{3D}} - V_{X_{IMAT}})$, in which V_X is the % volume (or the absolute volume for DAVDH) receiving dose x. Points were calculated for 0 Gy < x < 50 Gy with an 0.25 Gy increment of x. Positive values indicate that the volume irradiated to dose x was larger in the 3D plans than in the IMAT plans.

plan are shown in Figure 5. The concave sparing of the SB by the IMAT plan is clearly visible in the three planes. The isodose lines are highly conformal to the PTV form for the IMAT plan. The dose outside the PTV is distributed over a large volume in the IMAT plan, which can also be derived from the DVDH (Figure 4), which shows that IMAT results in deposition of low dose (between 0 and 11 Gy) in a larger volume of the surr. The IMAT plan shows serrated isodose lines (Figure 5a), especially in the low dose region, caused by the discrete gantry angle calculations.

Dosimetric verification

The results of the PGD are summarized in Table 3 and in Figures 6 and 7. Table 3 shows the volumes of the clipped structures, and the relative differences between the measured and the calculated values for some clinically important parameters. The relative differences in D_{med} were insignificant, and varied

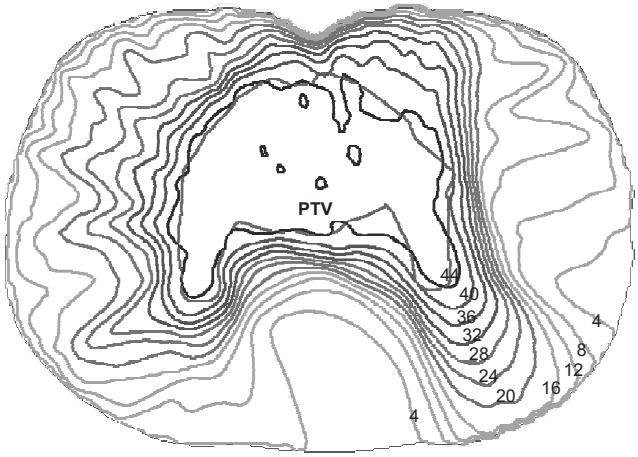

(a) calculated dose: 8 degrees interspacing

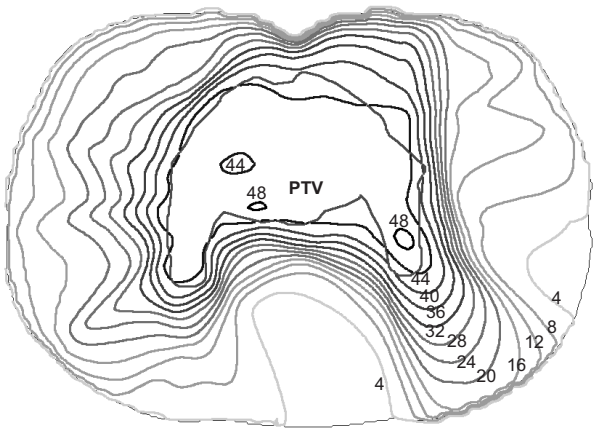

(b) calculated dose: 2 degrees interspacing

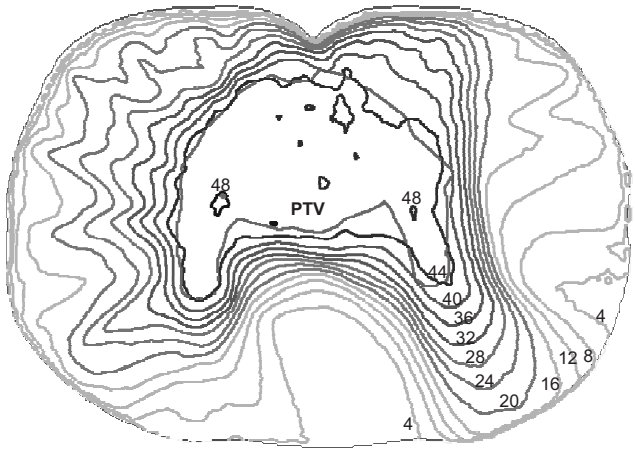

(c) measured dose: static gantry delivery

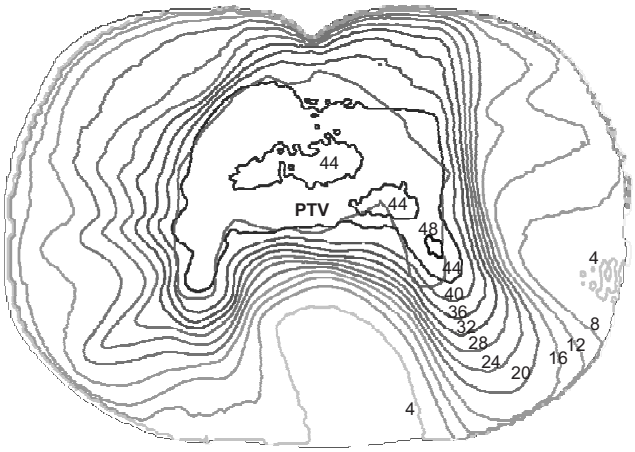

(d) measured dose: dynamic gantry delivery

Figure 6: Dose distributions of the IMAT plan in a transverse plane through the isocenter as it was calculated (a,b) and measured by polymer gel dosimetry (c,d). Isodose values are in Gy. In (a), the calculations are shown for the IMAT plan, with calculated control points every 8° . In (b), the same plan is shown, but additional control points were generated and calculated every 2° by interpolation of the pre-existing control points. (c) The measured IMAT plan, delivered to the phantom in a discrete way, i.e. as a static gantry IMRT with 8° interspaced beams. (d) The measured IMAT plan, delivered in dynamic gantry mode.

between -1.1% for the 3D plan and 0.3 % for the IMAT_d experiment. The relative difference in maximal PTV dose (D_{99}) was nowhere larger than 4%, with the largest difference found for IMAT_S (+4.0%). For all techniques, the D_{99} was underestimated by the dose calculation algorithm, while the minimal dose (D_1) was overestimated by $\pm$2.5% in IMAT, irrespective of the delivery (static vs dynamic gantry). The partial volume of the PTV, in which the γ-index was higher than 1 ($V_{\gamma>1}$), was nowhere higher than 2%. No clear difference was found between the IMAT_S and IMAT_d results. For SB, the relative difference in D_{mean} was largest for the 3D experiment (+5.6%), and smallest for both IMAT experiments

Table 3: Summary of the results of the polymer gel dosimetry.

	Vol_{trunc} (cc)	3D	$IMAT_s$	$IMAT_d$
PTV	952 (97%)			
ΔD_{med} (%)		-1.1	-0.3	+0.3
ΔD_{99} (%)		+2.1	+4.0	+3.2
ΔD_1 (%)		+0.3	-2.8	-2.4
$Vol_{\gamma>1}$ (%)		0.0	1.6	1.1
small bowel	427 (82%)			
ΔD_{mean} (%)		+5.6	-0.5	-0.5
$\Delta V_{90\%}$ (%)		+1.3	-1.8	-2.1
$\Delta V_{>15Gy}$ (%)		+8.4	+3.9	+0.1
$Vol_{\gamma>1}$ (%)		1.6	6.1	9.7
bladder	124 (100%)			
ΔD_{mean} (%)		+3.1	+12.0	+9.9
$Vol_{\gamma>1}$ (%)		0.0	6.0	11.8
surr	6298 (36%)			
$Vol_{\gamma>1}$ (%)		11.7	9.4	5.3
scanned volume				
$Vol_{\gamma>1}$ (%)		9.0	10.2	6.4

Vol_{trunc}: the volume of the structure, clipped to the volume of the MRI-measured gel phantom. The percentage between brackets is the partial volume of the structure in the gel phantom. $IMAT_s$: the IMAT treatment, delivered to the gel phantom in a static gantry mode. $IMAT_d$: the IMAT treatment, delivered to the gel phantom in dynamic gantry mode. ΔD_{med}: relative difference between measured and calculated mean dose, calculated as $\frac{D_{med_{gel}} - D_{med_{calc}}}{D_{med_{calc}}}$, with $D_{med_{gel}}$ the median dose in the specified organ, as measured by gel dosimetry, and $D_{med_{calc}}$ the median dose as calculated. The same reasoning was followed for ΔD_{99}, ΔD_1, ΔD_{mean}, $\Delta V_{90\%}$, and $\Delta V_{>15Gy}$. $Vol_{\gamma>1}$: the partial volume of the clipped structure in which the γ-index was higher than unity.

(<1%). The $V_{\gamma>1}$ for SB was 9.7% for $IMAT_d$, although there is nearly no difference between calculated and measured dose when looking at the DVHs (Figure 7a). The largest differences between measured and calculated dose was seen for bladder, for which the mean measured dose was up to 12% higher than the calculated dose (this was for $IMAT_s$). This is reflected in the high $V_{\gamma>1}$ for $IMAT_s$ (6%) and $IMAT_d$ (11.8%). The $V_{\gamma>1}$ for the total scanned volume was lowest for the $IMAT_d$ (6.4%) and highest for the $IMAT_s$ (10.2%) delivery. On Figure 7, the same data can be found . It shows the good correlation between the measured and calculated dose for PTV. It is also clear that there is no substantial difference between the $IMAT_s$ and the $IMAT_d$ delivery. The DVHs for bladder show a higher measured than calculated dose in all cases, and this is most pronounced in the IMAT deliveries. For SB and surr, DVH comparison shows no clinically relevant differences. Calculated and gel-measured dose distributions are shown in Figure 6. The ripples in the low dose region, which are a consequence of the gantry angle discretization that is done for planning and calculations, are also obvious in the $IMAT_s$ measured dose distributions (Fig 6c). They disappear when the dose computation is done for MSs, interspaced by 2° instead of 8° (Figure 6b), which more closely resembles the results of the $IMAT_d$ delivery (Figure 6d). This $IMAT_d$ is the delivery mode used in the clinical IMAT execution.

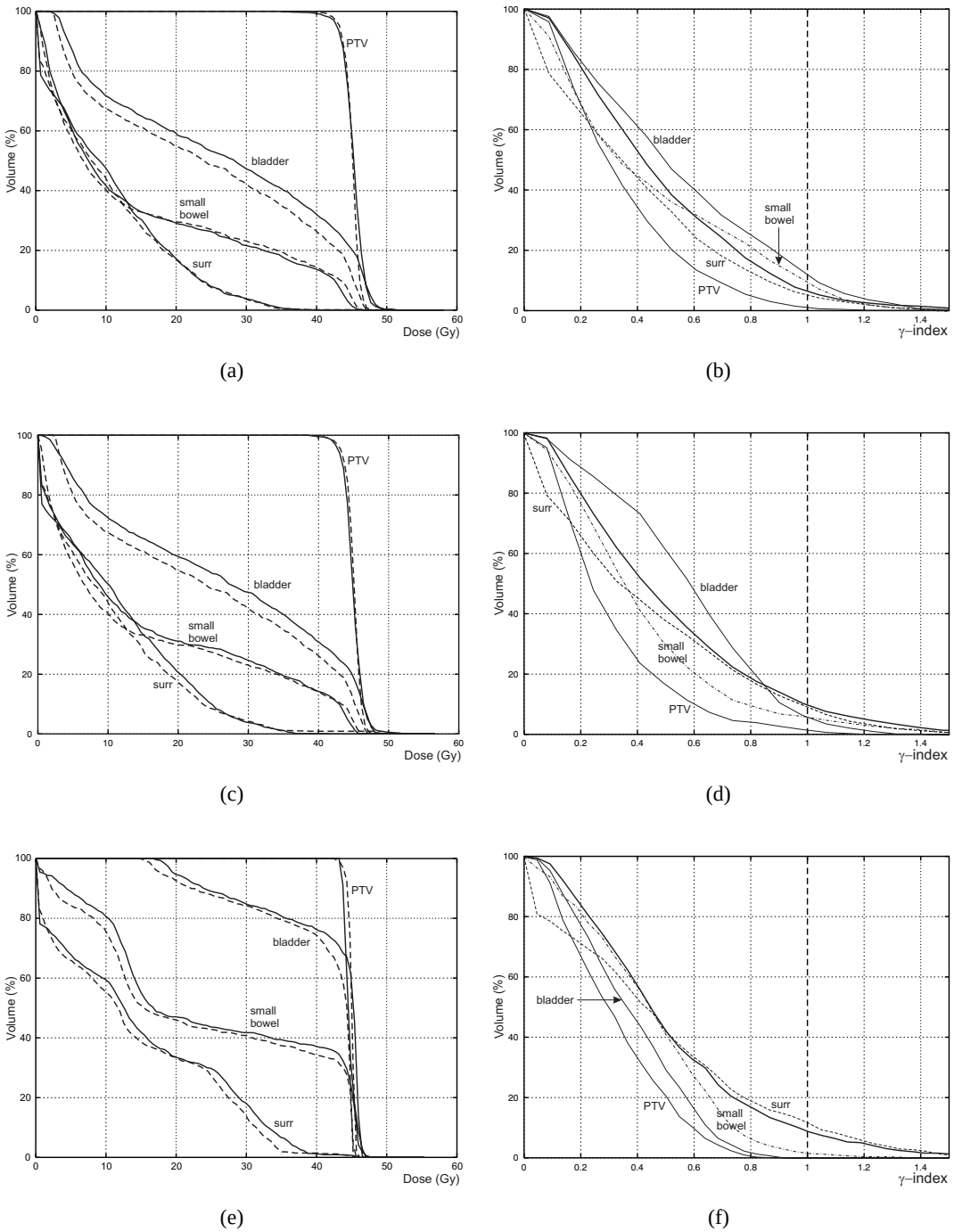

Figure 7: Dose Volume Histograms (*a*,*c*,*e*) and γ-Volume Histograms (*b*,*d*,*f*) for the three polymer gel experiments. In (*a*,*c*,*e*), the dashed lines represent the calculated DVHs, while the solid lines represent the gel-measured DVHs. The DVHs and γ-VHs are shown for PTV, small bowel, bladder and surr. The γ-VHs for the total measured volume are also shown (bold curve). Results are shown for the dynamically delivered IMAT treatment (*a*,*b*), the statically delivered IMAT plan (*c*,*d*) and for the 3D plan (*e*,*f*).

Discussion

Although not significant, the minimal dose was lower for the IMAT plans. The same can be seen for the V_{95} of the PTV, which was lower for the IMAT plans. Still, on the DVH (Figure 3b), it is clear that this underdosage is rather small. The PTV underdosage is partially caused by the SB sparing. The possibility to create concave dose distributions with IMAT leads to a larger PTV surface adjacent to the dose gradient. This, in combination with the leaf position optimization, can result in the observed underdosage, located at the borders of the PTV. Although the PTV underdosage in this group was deemed not to be clinically relevant, assigning a too high importance for SB in the optimization could result in relatively large dose "erosion" at the margins of the PTV. For this reason, we defined the following PTV acceptance criteria for future use in IMAT planning for rectal cancer, based on the results of the present analysis. For the following criteria, we took the observed mean $\pm$ 1 SD, thus resulting in (1) a $V_{95} \geq$ 93.7%, (2) a $D_1 \geq$ 88% of the target prescription dose (for a prescription to 45 Gy, this is 39.6 Gy), and (3) a $V_{107} \leq$ 0.5%. In case of a violation of one of the first two criteria, the IMAT plan should be re-optimized with lower SB importance. The third criterium should not be an absolute one, as the higher maximal dose (and more generally the higher inhomogeneity), is presumably caused by the discretization to deliverable arcs: ADR cannot be modulated in a fine sense due to the required constant ADR. Peeks visible in the ADR graphs cannot be expressed in the final arcs as the Elekta linac is not able to fluently deliver short arcs. Balancing the linac using counterweights and optimization of the settings of the gantry servo-system reduced the problems, but arcs smaller than 56° still cause too many interrupts to be practical. The addition of a few static gantry intensity modulated beams (replacing the practically undeliverable short arcs) to the IMAT arcs may reduce inhomogeneity in the PTV. This possibility has not yet been explored. During planning, it is clear that the arc extraction procedure significantly reduces the quality of the plan (PTV inhomogeneity and dose to the OARs increase, data not shown). This is (partly) solved by leaf position optimization. Earl *et al* [22] also discuss the limitations imposed by the constant ADR, and showed that adding an additional arc could reduce this plan deterioration, but that a variable dose rate or gantry speed would solve this problem. We prefer the implementation of a variable gantry speed over the variable dose rate. In this way, the optimization even has the possibility to insert a static gantry IM beam as a part of an arc by lowering the gantry speed to 0°/min. This solution, which delivers the optimized non-constant ADR, also reduces the number of arcs, the total gantry rotation and most probably also the planning and treatment time. It also removes the complex planning step of arc extraction. We plan to investigate the full impact of variable ADR on planning quality and delivery time.

IMAT offers the possibility to spare SB and bladder in comparison with a 3D technique. A relative reduction of 28% in D_{mean} can be seen for SB. For the V_{90}, a relative reduction of 65% was reached by applying IMAT. The $V_{>15Gy}$, which was found to be strongly associated with acute SB toxicity by Baglan *et al* [6], was reduced with 28%. Whether this sparing of the SB on the planning level will translate into a clinically diminished SB toxicity is beyond the scope of this study, which was focused on clinical implementation of IMAT and its planning comparison with a 3D technique. In the present series, the volume of SB receiving 90% of the target dose in the 3D plans ($\text{Vol}_{\text{sb}_{3D}}$) rather small (mean 84 cc, range 1 - 234 cc) compared to previous reports [6, 9]. This might underestimate the full potential of IMAT, as we could expect a correlation between the $\text{Vol}_{\text{sb}_{3D}}$, and the relative reduction in V_{90}, obtained by IMAT over 3D. A DVH analysis for the subgroup of patients with a $\text{Vol}_{\text{sb}_{3D}}$ greater than 84 cc shows a V_{90} of 32.3% and 9.6% for 3D and IMAT, respectively. For the other four patients, the V_{90} was 9.2% and 4.4%. Of course, the number of patients is too small to draw strong conclusions, but we hypothesize that the IMAT technique gets more efficient as the anatomical situation is more complex. Some subgroups of patients might have a large improvement of their treatment plan quality by IMAT, while the effect might be negligible or clinically irrelevant in others. It was shown that patients who receive post-operative radiotherapy have a larger portion of (fixed) SB in the pelvis [23]. These patients are also at higher risk for SB toxic-

ity than patients who received their radiotherapy in a pre-operative setting [24]. Besides this group of post-operatively treated patients, other patients that might benefit from IMAT could be selected by means of investigations like volumetry of the contrast-filled SB during simulation.

The delivery time of the 3D treatments was significantly shorter than for the IMAT treatments. As mentioned, the 3D treatments were delivered using the RTD. The RTD system operates with a dose rate of $\pm$550 MUs/min (compared to 130 or 260 MUs/min for most of the arcs), and has a faster checking system than the prototype dynamic software used for IMAT. Thus, although clinical IMAT delivery time is within a standard time slot at the moment, it could be reduced even further by adaptations to the linac control software.

Quality assurance of a complex technique like IMAT remains a challenge. As both the gantry and the leaves are constantly moving, tracking their position is not easy. Ramsey *et al* [25] developed an elegant method to evaluate the leaf position errors during arc delivery, based on the logs of a Varian Clinac MLC, and derived a formula to estimate the consequent dosimetrical error. Our strategy was to check the end-of-chain result. Different methods, like ion chamber point dosimetry and 2D film dosimetry have been used by others [22, 26]. Although valuable, these techniques do not offer the possibility to evaluate the IMAT treatment in three dimensions, while dose distributions of IMAT treatment plans typically vary in three dimensions. PGD offers absolute dosimetry in three dimensions with a high resolution. Vergote *et al* [20] optimized PGD for its use in large phantoms. This resulted in a structural root-mean-square deviation between gel-measured and Helax-TMS computed dose distributions of 2% (except in high dose gradient regions, where it was 5%) and a stochastic deviation of 2%, resulting in an accuracy of 2.8% (and 5.4% in high dose gradient regions). We found a good correlation between gel-measured and calculated dose distributions for the PTV ($V_{\gamma>1}$ = 1.1%). The SB sparing, obtained by the IMAT technique, was confirmed by the PGD measurements. These results ensured us that IMAT planning, calculation and delivery were accurate and could be implemented in a clinical setting. The largest deviations were seen for bladder, with a calculated vs measured D_{mean} of 23.7 Gy and 26.0 Gy in the $IMAT_d$ experiment (+9.9%). Nearly the full dose contribution to the bladder is due to scatter and transmission, as the bladder is shielded in all arc apertures. Calculation errors in the computation of both scatter dose and transmission can thus have a high impact on the calculated dose of the bladder. PGD also showed that the interpolation of the 8° angularly interspaced control points to an arc does not produce different dosimetrical results than if it were given as static gantry IM beams. As previously demonstrated [20, 26], decreasing the interspacing distance from 8° to 2° affects the dose distribution for the low dose regions (the ripples disappear), while for high dose regions, there is little or no difference.

To our knowledge, there has been no report on clinically executed IMAT or even IMRT treatment for rectal cancer until now, despite the fact that IMRT has been used in a clinical setting for nearly a decade now. There is one report of a planning comparison between IMRT and 3D [27]. The authors found a relative reduction of 55% to 72% in V_{95} for SB, depending on the PTV inhomogeneity that was tolerated. This is in the same range as our findings, with a V_{95} for SB 72% for IMAT. In pelvic radiotherapy, the first clinical results about the implementation of IMRT for gynecological malignancies have been published. Mundt *et al* have shown that IMRT reduces both acute [28] and chronic [29] SB toxicity in comparison to conventional treatment. In cervical cancer, as in rectal cancer, the internal iliac and obturator nodes are important routes of nodal spread, leading to a concave shaped PTV partially encompassing bladder and SB. Therefore, we hypothesize that a similar toxicity reduction can be achieved in rectal cancer patients as in patients with cervical cancer.

Whether IMAT will prove to be the best option for rectal cancer irradiation (and for other sites) in the future, will largely depend on the improvement of IMAT. A large window for improvement exists for IMAT, including plan optimization and automation of the planning process, and improvements of the linac control software, of which variable gantry speed is

the single most important.

Conclusion

Seven patients with rectal cancer were irradiated with IMAT. On planning, IMAT allowed to spare SB as compared to a conventional 3D technique, without compromising the dose in the PTV. Although treatment time for IMAT was longer in comparison with a 3D technique, it was deliverable within a time slot of 5-10 minutes. Three dimensional PGD showed that IMAT delivery is as accurate as 3D delivery. We identified significant potential for improvements both at the levels of planning and delivery. The single most important technical improvement for IMAT is the implementation of a variable gantry speed.

References

[1] Glimelius B. The role of radiotherapy in rectal cancer. *Eur J Cancer* 2001;37 (Suppl. 7):S203-212

[2] Colorectal Cancer Collaborative Group. Adjuvant radiotherapy for rectal cancer: a systematic overview of 8507 patients from 22 randomised trials. *Lancet* 2001;358:1291-1304

[3] Ahmad NR, Marks G, Mohiuddin M. High-dose preoperative radiation for cancer of the rectum: impact of radiation dose on patterns of failure and survival. *Int J Radiat Oncol Biol Phys* 1993;27:773-778

[4] Chan AK, Wong AO, Langevin J, *et al*. Preoperative chemotherapy and pelvic radiation for tethered or fixed rectal cancer: a phase II dose escalation study. *Int J Radiat Oncol Biol Phys* 2000;48(3):843-856

[5] Kollmorgen CF, Meagher AP, Wolff BG, *et al*. The long-term effect of adjuvant postoperative chemoradiotherapy for rectal carcinoma on bowel function. Ann Surg 1994;220(5):676-682

[6] Baglan KL, Frazier RC, Yan D, *et al*. The dose-volume relationship of acute small bowel toxicity from concurrent 5-FU-based chemotherapy and radiation therapy for rectal cancer. *Int J Radiat Oncol Biol Phys* 2002;52:176-183

[7] Minsky B, Conti JA, Huang Y, *et al*. Relationship of acute gastrointestinal toxicity and the volume of irradiated small bowel in patients receiving combined modality therapy for rectal cancer. *J Clin Oncol* 1995;13:1409-1416

[8] Miller AR, Martenson JA, Nelson H, *et al*. The incidence and clinical consequences of treatment-related bowel injury. *Int J Radiat Oncol Biol Phys* 1999;43:817-825

[9] Letschert JG, Lebesque JV, Aleman BM, *et al*. The volume effect in radiation-related late small bowel complications: results of a clinical study of the EORTC Radiotherapy Cooperative Group in patients treated for rectal carcinoma. *Radiother Oncol* 1994;32:116-123

[10] Letschert JGJ. The prevention of radiation-induced small bowel complications. *Eur J Cancer* 1995;31:1361-1365

[11] Duthoy W, De Gersem W, Vergote K, *et al*. Whole abdominopelvic radiotherapy (WAPRT) using Intensity Modulated Arc Therapy (IMAT): first clinical experience. *Int J Radiat Oncol Biol Phys* 2003; 58:1019-1032

[12] Yu C. Intensity-modulated arc therapy with dynamic multileaf collimation: an alternative to tomotherapy. *Phys Med Biol* 1995;40:1435-1449

[13] Nuyttens JJ, Robertson JM, Yan D, *et al*. The variability of the clinical target volume for rectal cancer due to internal organ motion during adjuvant treatment. *Int J Radiat Oncol Biol Phys* 2002;53:497-503

[14] De Neve W, Duthoy W, Claus F, *et al*. Dose conformation in IMRT for head and neck tumors: which solution to apply? Cancer/Radiotherapie 2002;6 (Suppl. 1):32-36

[15] De Gersem W, Claus F, De Wagter C, *et al*. An anatomy-based beam segmentation tool for intensity-modulated radiation therapy and its

application to head-and-neck cancer. *Int J Radiat Oncol Biol Phys* 2001;51:849-859

[16] De Wagter C, Colle CO, Fortan LG, *et al*. 3D conformal intensity-modulated radiotherapy planning: interactive optimization by constrained matrix inversion. *Radiother Oncol* 1998;47(1):69-76

[17] Maryanski MJ, Gore JC, Kennan RP, *et al*. NMR relaxation enhancement in gels polymerized and cross-linked by ionizing radiation: a new approach to 3D dosimetry by MRI. *MRI* 1993;11:253-258.

[18] De Deene Y, De Wagter C, Van Duyse B, *et al*. Validation of MR-based polymer gel dosimetry as a preclinical three-dimensional verification tool in conformal radiotherapy. *Magnet Reson Med* 2000;43:116-125.

[19] De Deene Y. Gel dosimetry for the dose verification of intensity-modulated radiotherapy treatments. *Z Med Phys* 2002;12:77-88.

[20] Vergote K, De Deene Y, Duthoy W, *et al.* Validation and application of polymer gel dosimetry for the dose verification of an intensity-modulated arc therapy (IMAT) treatment. *Phys Med Biol* 2004;49:287-305

[21] Low DA, Harms WB, Mutic S, *et al*. A technique for the quantitative evaluation of dose distributions. *Med Phys* 1998;25(5):656-661

[22] Earl MA, Shepard DM, Naqvi S, *et al*. Inverse planning for intensity-modulated arc therapy using direct aperture optimization. *Phys Med Biol* 2003;48(8):1075-89

[23] Nuyttens JJ, Robertson J, Yan D, *et al*. The position and volume of the small bowel during adjuvant radiation therapy for rectal cancer. *Int J Radiat Oncol Biol Phys* 2001;51:1271-1280

[24] Minsky BD, Cohen AM, Kemeny N, et al. Combined modality therapy of rectal cancer: decreased acute toxicity with the preoperative approach. J Clin Oncol 1992;10(8):1218-1224

[25] Ramsey CR, Spencer KM, Alhakeem R, *et al*. Leaf position error during conformal dynamic arc and intensity modulated arc treatments. *Med Phys* 2001;28:67-72

[26] Yu C, Li XA, Ma L, *et al*. Clinical implementation of intensity-modulated arc therapy. *Int J Radiat Oncol Biol Phys* 2002;53:453-463

[27] Robertson J, Yan D, Girimonte P, *et al*. The potential benefit of intensity modulated radiation therapy (IMRT) for rectal cancer (Abstr.) *Int J Radiat Oncol Biol Phys* 1999;45(Suppl. 3):248-249

[28] Mundt AJ, Lujan AE, Rotmensch J, *et al*. Intensity-modulated whole pelvic radiotherapy in women with gynecologic malignancies. *Int J Radiat Oncol Biol Phys* 2003;52(5):1330-1337

[29] Mundt AJ, Mell LK, Roeske JC. Preliminary analysis of chronic gastrointestinal toxicity in gynecology patients treated with intensity-modulated whole pelvic radiation therapy. *Int J Radiat Oncol Biol Phys* 2003;56(5):1354-1360

VI Discussion.

VI. 1. IMRT: is it worth all the trouble?

IMRT has been increasingly used in the USA, and somewhat later also in Europe. Whereas IMRT was developed and initially implemented in academic hospitals, it has left its cradle, and is now also implemented in an increasing number of private hospitals. In a recent US survey, about one third of responding radiation oncologists were using IMRT, and more than 90% of the non-users planned to do so in the near future [113]. Although IMRT has been used clinically for more than 10 years, not one randomised trial has been conducted comparing IMRT with less advanced radiation techniques, like 3D-CRT. The evidence of the superiority of IMRT is at best level 3ii (uncontrolled consecutive case series [114]). In this view, it is interesting to note that the NCI (National Cancer Institute) convened a group of experts to address the issue of using IMRT in trial protocols (in which IMRT is not the subject of the trial question!). They allowed the use of IMRT in trials, specifying the requirements to do so [115]. A 2005 update of these NCI IMRT guidelines was recently posted [116]. This permission might reduce the need (and thus the chance) for a prospective randomised trial addressing the benefits of IMRT. However, some specific national reimbursement systems, like in Britain, have encouraged some investigators to start up such a trial [117], but accrual remains a problem for different reasons. The longer IMRT will be used, the fewer physicians will be inclined to enter patients into a randomised trial in which patients might be allotted to an (outmoded) conventional technique.

Nevertheless, it is not obvious that IMRT would result in better clinical results than conventional techniques, and some sound criticism is in its place [118;119]. IMRT planning results might look very attractive when compared to those of 3D-CRT or conventional radiotherapy, they are but an approximate representation of one part of the total treatment chain. Some of the major concerns about IMRT will be discussed here, and IMRT users should be aware of the possible problems associated with IMRT and how to avoid or minimize them:

(1) **Importance of delineation:** As the IMRT planning is entirely based on the delineated structures, the importance of the delineation skills of the planner is evident. This is not a problem that is specific to IMRT, but in fact to all radiation techniques in which the beam outlines are based on the delineated structures, like in 3D-CRT. However, as the dose distribution is more conformal, IMRT will be less forgiving for erroneously delineated structures. Parts of the tumour not defined as such will be underdosed, and parts of the imaged volume that are not defined, will be abused by the optimization algorithm to deposit dose!

(2) **Patient immobilization, changing anatomy and intra-fraction motion:** IMRT is less robust to inter-fraction set-up variability, changing anatomy during treatment and intra-fraction motion. For inter-fraction set-up variability and changing anatomy, this is a direct consequence of the more conformal dose distribution that can be reached. The intra-fraction motion, however, could lead to unwanted underdosage of the target volume, which is directly related to the delivery method of IMRT itself. In all but one IMRT delivery method (the use of compensators), only parts of the target volume will be irradiated at any given time. Therefore, a moving target volume could move in and out these subfields, resulting in a different delivered dose than planned. Although this is found to be true for the dose delivered in one fraction, this effect is diluted over the whole treatment course, typically consisting of 20-35 fractions [120-122].

(3) **Fraction time and biological efficiency:** The delivery time of IMRT treatments is not only of practical and economical importance, but biological effects are to be considered as well [123]. Supposing that the delivery of an IMRT fraction takes 15 minutes, parts of the tumour could be in the first and the last segment only, thus leaving 15 minutes for DNA repair. This possibility has been tested experimentally, and it was found that prolonging the delivery of a 2 Gy fraction resulted in a relatively small but significant decrease of biological effect [124]. This underlines the importance of trying to shorten the delivery time as much as possible. At GUH, the goal is to keep the treatment time (= beam-on time) under 15 minutes. For HNC, the 6-beam coplanar set-up results in treatment times of < 10 minutes, while for the non-coplanar 7-beam set-up used for paranasal sinus cancer, this will rather extend to around 10 to 15 minutes.

(4) **Low-dose hypersensitivity:** this phenomenon denotes the observation that cells are excessively sensitive to low-dose (0.1-0.5 Gy, but observed up to 1 Gy) irradiation, an effect that is not predicted by back-extrapolating the cell survival response from higher doses [125]. The precise molecular basis for this is not yet known. In IMRT treatments, the “unwanted”

dose is spread out over a large volume of normal tissue. This causes large volumes to be irradiated to very low doses per fraction. Although possibly important in IMRT, there has been no report of clinically observed low-dose hypersensitivity so far.

(5) **Secondary radiation-induced tumours:** Radiation is a known carcinogen, and secondary induced cancers represent a serious side effect of a radiation treatment. In the high-dose regions, secondary sarcomas are observed, while radiation-induced carcinomas are seen in the low-dose regions. As previously mentioned, IMRT results in a large volume receiving low doses. Also, the number of MUs needed in IMRT is typically higher than in conventional radiotherapy (and heavily depending on the planning and delivery method). This increase in MUs can result in an increased dose outside the boundaries of the collimated fields/segments, due to leakage and scattered photons. Epidemiologically, it is difficult to assess these radiation-induced secondary cancers, as a multitude of other factors play an important role in the development of secondary induced cancers, like genetic susceptibility and presence of other risk factors like tobacco smoking and other environmental influences. Moreover, the delay between irradiation and the clinical presentation of the secondary tumour can be up to tens of years. Hall *et al* [126] made a theoretical estimate of the risk of secondary induced cancers due to IMRT over conventional radiotherapy, and calculated that an additional 0.75% of surviving patients would develop a radiation-induced secondary malignancy due to the use of IMRT. This figure represents a doubling of the absolute risk of radiation-induced cancers. It is, however, important to mention that the assumptions that are made on IMRT are not always fulfilled for all delivery methods of IMRT or for all sites. Two thirds of the additional cases of radiation-induced cancers were attributed to the larger volume receiving radiation dose. In IMAT for rectal cancer, however, it has been shown that the integral dose was lower in IMAT treatments than in the conventional treatment design [98]. Although the volume of surrounding tissue receiving very low doses (< 40 cGy/fraction) is slightly larger for IMAT than for conventional radiotherapy, the volume of surrounding tissue receiving intermediate doses was higher for the three-field technique. These intermediate dose level could be the most carcinogenic one [119] The other third of the excess of induced cancer cases was ascribed to the increase in MUs. However, this condition is not always present in intensity-modulated techniques [98]. Other investigators estimated an 8-fold increase of secondary cancers due to IMRT [127]. However, this figure was found with the MIMiC-based sliced tomotherapy, typically resulting in treatment plans with a very high number of MUs per

fraction. We can conclude that IMRT can, on theoretical grounds, result in an increase in radiation-induced cancers, but this increase depends on the specific type of IMRT delivery.

Until now, the clinical benefits of IMRT are only suggested in case series, sometimes compared with historical results from the same institution or from literature. This level 3ii evidence suggests that IMRT enables the sparing of OARs. The most studied OAR in HNC is the parotid gland. Numerous groups have shown the possibility of dosimetrical sparing of the parotid gland without compromising local control [53;84], and the resulting preservation of the salivary outflow [52;128]. Our group found a reduction of both the short-term complication of dry eye syndrome [129] as well as a reduction in long-term complications [45]. Altogether, there is increasing evidence in favour of IMRT for OAR sparing without compromising local control. However, so far, no improvement in local recurrence rates has been observed by using IMRT, despite the better target coverage obtained by IMRT.

VI. 2. Comparison between IMAT and Tomotherapy

IMAT was first proposed by Yu as an alternative to tomotherapy [95]. Although IMAT has since then been used clinically, no direct comparison has been made between both delivery techniques. In the comparison that we will give hereunder, IMAT will be compared to the "ring gantry"-based helical tomotherapy, as developed at the University of Wisconsin by Mackie *et al* [94], rather than to the serial tomotherapy, as described earlier (p. 44). It is believed that this helical approach represents the future direction of tomotherapy, rather than the serial tomotherapy with the plug-on MIMiC fan beam MLC [130] (although one could argue that the latter offers the "cheapest" solution for tomotherapy and does not hamper non-coplanar treatments).

The helical tomotherapy treatment unit can be looked at as the fusion between a CT scanner and a linac [130;131]. A 6 megavolt (MV) linear accelerator waveguide and a MV CT detector are installed on a rotating gantry assembly. Power supply and data transmission is achieved by slip-ring technology, allowing continuous rotation. A binary MLC, resembling the MIMiC MLC, is incorporated in the linac head. The treatment couch can be longitudinally moved into the gantry ring. This translation can be quantified by the "pitch", which is defined as the ratio of the longitudinal couch translation per gantry rotation to the slice width. In

tomotherapy, typical values for the pitch are 0.35-0.5, such that each point in the target volume is irradiated during more than one rotation of the gantry. This TomoTherapy Hi-Art System® (further referred to as TomoTherapy) is now commercially available and clinically used in the USA and Europe (http://www.tomotherapy.com). It is sold as a completely integrated treatment package, and includes a dedicated TPS.

A comparison between IMAT and TomoTherpy is summarized in Table 4.

TomoTherapy requires the acquisition of a dedicated treatment unit, while IMAT can be implemented on an MLC-equipped linac, as most of the radiotherapy centres in the Western world have one. Arc therapy is possible on both Elekta [95;96] and Varian linacs [102]. For the Elekta linac, dynamic prescriptions, like for IMAT, are not yet possible in clinical mode. Therefore, IMAT delivery is still done in local service mode, but with the same tolerances as in clinical mode. Varian linacs are capable of IMAT delivery in clinical mode **(**Eugene Wong, personal communication**)**.

	Favourable characteristics	**Unfavourable characteristics**
TomoTherapy	• Fully integrated megavoltage CT for image-guided radiotherapy. • Dedicated TPS, integrated in the treatment unit. • Possibility of transit dosimetry and reconstruction of the delivered dose	• Planning software is a black box. What happens inside? • Treatment times in the range of 20-30 minutes, and dependent on longitudinal PTV length. • Intra-fraction motion might have an impact on tumour control. • Low MU efficiency
IMAT	• Can be executed on widely installed MLC-equipped linacs • Possibility of isocentric table top rotation and sagittal arc set-up • Treatment time +/- independent of longitudinal length of the PTV • More robust against intra-fraction movement than tomotherapy • The outlines of the arcs are intuitive and reflect anatomy.	• No commercially available planning software. • Long planning time needed (interactive and computational). • Sub-optimal gantry acceleration control (on Elekta). • Dynamic delivery still in local service mode (on Elekta)

Table 5: Summary of favourable and unfavourable characteristics of IMAT and tomotherapy. Details about each point are given in the text.

From its architecture, it is clear that there is no possibility of isocentric table top rotation in TomoTherapy. In IMAT, it is possible to use non-coplanar arcs [97], which might be of interest in the treatment of sino-nasal cancer and lung cancer. Although the influence of this possibility to the target dose will be rather small, the use of non-coplanar arcs enables to avoid primary radiation to surrounding structures and OARs.

The fact that the TomoTherapy TPS is a black box might be regarded as a drawback of TomoTherapy. Due to the fact that the IMAT TPS was developed at GUH, precise information on the applied methodology (e.g. on optimization algorithms) is available, and possible improvements can be easily implemented. On the opposite side, information on the details of the TomoTherapy TPS or any possible improvements, have to pass via the company. This is – of course – not a major concern for centers focusing on clinical applications, but might be one if the emphasis is on the development of delivery techniques, like at our institution. The fact that the IMAT TPS is home-made has, besides its mentioned benefits, also the disadvantage of being difficult to export to other centers.

Treatment time (and inversely patient throughput) is an important biological, practical and economical criterion in the choice of radiation techniques. Data on time measurements on a TomoTherapy unit (kindly provided by Paul Bijdekerke, AZ-VUB), shows that the total treatment time (positioning time + radiation time) for head an neck tumours (averaged over 10 patients) is 25 ± 3 minutes (range 21-30 minutes). The radiation time (up to the exit of the patient) was 11 ± 3 minutes. The positioning time (including patient positioning, acquisition of the MV CT, registration of MV CT and planning CT and subsequent analysis and repositioning) is estimated to be 14 minutes. No direct comparison can be made with IMAT (not implemented for HNC).

Intra-fraction motion is an important issue that has to be considered in all delivery techniques in which (a part of) the “beams” cover only a part of the PTV [132]. Unlike conformal field treatments, where intra-fraction organ motion only affects the boundaries creating broad dose penumbra, the interplay of the movement of the beam aperture and the movement of the patient anatomy can create regions of over- and underdosage throughout the field. Clearly, the latter situation is encountered in all IMRT techniques. Due to the fact that TomoTherapy delivery implies a continuous translation in cranio-caudal direction of the PTV through the slit-beam, over- and underdosage in the PTV can be expected for moving targets with a relatively large amplitude in cranio-caudal direction (e.g. lung tumours) [133]. These hot and cold spots are minimized by using a large jaw width, and when the couch translation velocity

is small relative to the motion amplitude and frequency. On the other hand, conformal arc therapy is relatively insensitive to intra-fraction motion (only the borders can be affected). In IMAT, the whole extent of the PTV (in cranio-caudal direction) is within the beam aperture at any moment. Therefore, intra-fraction target motion in cranio-caudal direction will have less influence on the dose distribution. It has to be mentioned that the problem of hot and cold spots in TomoTherapy will be blurred after multiple fractions, but the effect might be important for treatments with a low number of fractions.

TomoTherapy integrates image-guided radiation therapy (IGRT) in its design [134]. The aim of IGRT is to reduce uncertainties of the relevant anatomical structures at the time of radiation. By the MV CT detectors that are built on the rotating ring, MV tomograms can be made with TomoTherapy. Fusion software then performs the registration of the planning CT and the MV-CT. Corrections can be made by translations of the table couch. Rotational positioning errors around the longitudinal axis can be corrected by modifying the gantry start angle. Although this CT-based position verification is ingrained in TomoTherapy, it is not an exclusive feature. Other linac companies are developing tomographic position verification systems as well, with cone-beam kilo-voltage CT (Elekta, Varian), or a separate CT, lined up with the linac (Siemens). These cone-beam CT scanners, which are mounted orthogonally to the linac gantry, offer the same possibilities as the MV-CT of TomoTherapy, with even higher quality CT (better soft tissue contrast due to the kilo-voltage) [135]. Another feature of TomoTherapy is the possibility for transit dosimetry and – given a MV CT is provided - reconstruction of the delivered dose [136]. Indeed, the measured photon intensities can be back-projected through the MV CT (or another relevant data set), and a 3D dose distribution can be computed. Again, transit dosimetry is not an exclusive characteristic of TomoTherapy, and is also possible using electronic portal imaging devices on linacs [137]. Nevertheless, TomoTherapy is – at the moment – the commercially available system that offers the most integrated form of ready-to-use solutions for IGRT, and offers the most advanced opportunities to apply adaptive radiotherapy.

The need for adaptive radiotherapy becomes clear from the clinical example in Figure 19 and is also shown in publication V. 1, Figure 5. In most treatment protocols, one snapshot (i.e. the planning CT) is taken as the basis for the delineation and planning for the whole treatment course. Safety margins for microscopic extension and set up errors are applied, but in most cases, no attention is given to the changing anatomy, which can be a result of the treatment

itself, as shown in the presented case. Other investigators have observed the same finding in lung cancer [138]. Tumour shrinkage could lead to unwanted high-dose irradiation of OARs,

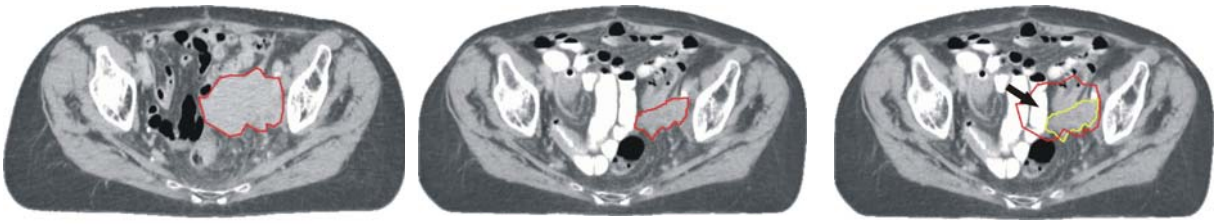

(a) (b) (c)

Figure 19: Illustration of changing anatomy during treatment. A patient with a recurrent squamous cell carcinoma of the cervix was treated with concomitant radiotherapy and chemotherapy. Radiotherapy was prescribed as 25 fractions of 1.8 Gy to a PTV around the GTV and the elective pelvic lymph nodes, followed by a boost of 5 fractions of 1.8 Gy to a PTV around the GTV. (a) Planning CT scan before the start of the concomitant treatment (CT_{0Gy}). The GTV is indicated in red. (b) Planning CT of the same patient at 45 Gy (CT_{45Gy}). Again, the (shrunken) GTV is indicated in red. (c) Back-projection of the original GTV (in red) on the CT_{45Gy} after registration of both CT scans. The space occupied by the original GTV on the GTV_{0Gy} is now taken by a (contrast-filled) small bowel loop (black arrow). This clearly illustrates that, if no re-imaging had been done, the high-dose region would have encompassed small bowel.

which move into the high-dose region, as the tumour disappears (see presented case). Therefore, an adaptive therapy process, in which the planning is adapted to the new anatomical situation (or to the previously reconstructed dose distributions) will lead to a higher uncomplicated cure rate, as both OARs will receive less dose, and the smaller target volumes will allow higher doses to be delivered. Adaptive radiotherapy will also allow to incorporate patient-specific motion and set-up errors into the re-planning, possibly allowing for smaller margins to be used. A review of adaptive radiotherapy is given elsewhere [139].

A subject that is closely related to adaptive radiotherapy is the ease and speed of the planning process. Adaptive radiotherapy will need a fast (and ultimately “online”) planning procedure. Planning time can be divided in computational time and interactive time. In the total planning time, computational time is less important than the interactive time, as these processes can be done over-night, while the interactive time necessitates human input (and time). The IMAT planning process in the GUH approach is, in its present state, cumbersome and requires long computational and interactive time. This is a major drawback for IMAT in comparison with TomoTherapy. When placed in a historical perspective, however, the same situation was seen in the early days of the static-gantry IMRT at GUH. The first IMRT plans at GUH started

with the manual creation of leaf settings per segment, and even with manual weight optimization through trial and error [1]. It was only after a while that planning tools were developed for the automation of both the creation of segments [21], as for the optimization of weights [13;14] and segment outlines [27]. These additional tools, in association with the development of class solutions and scripts, have led to the present situation, in which the largest part of the static-gantry IMRT planning process is executed by trained radiation technologists and assisted and supervised by radiation oncologists. The lack of effective planning tools for IMAT is probably the major reason why IMAT has not been implemented on a larger scale [17].

We can state that IMAT is not only an alternative to tomotherapy, but rather a delivery technique that allows creating dose distributions of the same quality, and with some distinct advantages over tomotherapy. In that view, it is hard to understand the lack of interest from the commercial linac vendors for IMAT. At least two linac companies (Elekta and Varian) produce linacs that are mechanically capable of delivering IMAT treatments. Still, nearly no development in hardware or planning software is done in that area, despite of feeling TomoTherapy breathing down their neck (as of June 2005, 35 treatment centers installed TomoTherapy, most of them in the USA). The most likely reason for this is, again, the difficulty of the IMAT planning process, to which the linac and TPS vendors do not have a solution. Resuming the chronology of IMAT planning, the first approach was the inverse planning strategy of Yu [95]. However, in the reports on the clinical implementation of the same research group, an anatomy-based approach was used [97;140], indicating the difficulties they had to implement the inverse planning strategy first proposed. The group states, however, that the full potential of IMAT will only be reached using inverse planning [97], whereas we believe that the anatomy-based approach is the most logical way to follow, as there is a firm physical background to do so [1;9] and it elegantly minimizes the constraint of MLS [96]. It is interesting to note that both approaches are converging [104].

In the IMAT planning and delivery process, as applied at GUH, there is still a large window for improvement. In our view, the most important improvement would be the possibility of delivering arcs with a variable gantry speed, thus allowing arcs with an non-constant ADR [96;98;104]. A variable gantry speed would obviate the need for the extraction of arcs with a constant ADR, as explained on p. 56 and shown in Figure 18a. This step of arc extraction is the most complex and time-consuming one, and leads to a deterioration of the planning quality, and to a higher number of arcs (and a longer treatment time). We prefer a variable

gantry speed above a variable dose rate because with the former option, static beams are possible within an arc, when the gantry speed is brought to zero. The possibility of a variable gantry speed would of course bring along the need to explore the possible gantry acceleration, and to incorporate this constraint in the TPS. Another possible improvement in the IMAT planning would be the optimization of the start and stop angles of the arcs. At this moment, the start and stop angles are determined manually during the arc extraction step. The optimization of the start and stop angle could be done in a parallel way as is done for the LPO: calculating the dose contribution for a small arc, computing the influence of the addition/omission of the small arc to/from the already existing arc on the objective function, and accepting or rejecting the new situation. This method, however, has not yet been implemented at GUH.

VI. 3. Future perspectives

Although much research is still ongoing and needed, it is fair to state that IMRT has now become a clinically implemented and widely accepted radiation technique. As shown in the current thesis (publications V. 2 and V. 3, reviewed in publication V. 1), and by others [141], IMRT in HNC results in lower chronic toxicity. Unfortunately, there are no data (that is: not from controlled trials!) suggesting a better local control by the use of IMRT over conventional RT techniques. Still, IMRT creates the possibility to escalate the dose to small volumes [85]. In publication V. 4, this possibility was explored, together with the use of FDG-PET as a guide for delineation and dose escalation. This was done within the frame of a clinical Phase I trial, in which the dose is escalated stepwise. Lauve *et al* [142] have used a similar approach, and found a maximal tolerable dose 70.8 Gy (in 30 fractions, and as the sole treatment modality). The analysis of clinical results from these trials will help us to select the maximal tolerable dose. This dose level could then be used in a controlled trial, to investigate whether this would result in a better local control.

As shown in Figure 1, a growing body of literature on IMRT becomes available, both on IMRT physics and on clinical (toxicity) outcome. Thus, knowledge on dose-volume effects on toxicity is increasing, but fragmented. The actual NTCP models are still largely based on clinical data from the pre-3D-CRT era [24]. Although useful, these data are only rough estimates and cannot fully reflect the biological effects of inhomogeneous irradiation [143].

There is an obvious need for new models, and efforts should be made to pool all clinically available data, in order to construct NTCP models adapted to IMRT [144].

IMAT planning and delivery will need to be further developed and automated. This process will require mutual input from researchers and linac/TPS vendors. Ultimately, this should result in a TPS and delivery technique that are not only available at specialized university hospitals, but can be dispersed on a larger scale. As shown in Table 4, a quite large number of radiation techniques are at the disposal of the radiation oncologist. Choosing the best available radiation technique for a given clinical case is not always trivial, and should be examined for each group of clinical problems. However, the diversity of delivery techniques should no longer impede multicenter trials on IMRT/IMAT. Solutions to overcome this heterogeneity consist of meticulously formulated planning goals and constraints (section III. 4.2.3) that have to be met by all participating centers, and an end-of-chain dosimetrical control [145], for which PGD is a promising candidate.

VII Bibliography

[1] De Neve W, De Wagter C, De Jaeger K, Thienpont M, Colle C, Derycke S et al. Planning and delivering high doses to targets surrounding the spinal cord at the lower neck and upper mediastinal levels: Static beam-segmentation technique executed with a multileaf collimator. Radiother Oncol 1996; 40(3):271-279.

[2] Wu Q, Mohan R, Morris M, Lauve A, Schmidt-Ullrich R. Simultaneous integrated boost intensity-modulated radiotherapy for locally advanced head-and-neck squamous cell carcinomas. I: dosimetric results. Int J Radiat Oncol Biol Phys 2003; 56(2):573-585.

[3] Claus F, Duthoy W, Boterberg T, De Gersem W, Huys J, Vermeersch H et al. Intensity modulated radiation therapy for oropharyngeal and oral cavity tumors: clinical use and experience. Oral Oncol 2002; 38(6):597-604.

[4] Claus F, Boterberg T, Ost P, De Neve W. Short term toxicity profile for 32 sinonasal cancer patients treated with IMRT. Can we avoid dry eye syndrome? Radiother Oncol 2002; 64(2):205-208.

[5] Intensity Modulated Radiation Therapy Collaborative Working Group. Intensity-modulated radiotherapy: Current status and issues of interest. Int J Radiat Oncol Biol Phys 2001; 51(4):880-914.

[6] Webb S, Lomax T. There is no IMRT? Phys Med Biol 2001; 46(12):L7-L8.

[7] Webb S. Intensity-modulated radiation therapy. Bristol: Institute of Physics Publishing, 2001.

[8] Mundt AJ, Roeske JC. Intensity modulated radiation therapy: A clinical perspective. First ed. Hamilton: BC Decker Inc, 2005.

[9] Brahme A, Roos JE, Lax I. Solution of an integral equation encountered in rotation therapy. Phys Med Biol 1982; 27(10):1221-1229.

[10] Webb S. The physical basis of IMRT and inverse planning. Br J Radiol 2003; 76(910):678-689.

[11] De Neve W. Rationale of intensity modulated radiation therapy: A clinician's point if view. In: Bortfeld T, Schmidt-Ullrich R, De Neve W, Wazer DE, editors. Image-Guided IMRT.1st ed. Berlin: Springer, 2005: 3-9.

[12] Mohan R, Bortfeld T. The potential and limitations of IMRT: a physicist's point of view. In: Bortfeld T, Schmidt-Ullrich R, De Neve W, Wazer DE, editors. Image-Guided IMRT.1st ed. Berlin: Springer, 2005.

[13] De Wagter C, Colle CO, Fortan LG, Van Duyse BB, Van den Berge DL, De Neve WJ. 3D conformal intensity-modulated radiotherapy planning: interactive optimization by constrained matrix inversion. Radiother Oncol 1998; 47(1):69-76.

[14] De Gersem WRT, Derycke S, De Wagter C, De Neve WCJ. Optimization of beam weights in conformal radiotherapy planning of stage III non-small cell lung cancer: Effects on therapeutic ratio. Int J Radiat Oncol Biol Phys 2000; 47(1):255-260.

[15] Xing L, Chen GT. Iterative methods for inverse treatment planning. Phys Med Biol 1996; 41(10):2107-2123.

[16] Webb S. Optimization by simulated annealing of three-dimensional conformal treatment planning for radiation fields defined by a multileaf collimator. Phys Med Biol 1991; 36(9):1201-1226.

[17] Xing L, Wu Q, Yang Y, Boyer A. Physics of IMRT. In: Mundt AJ, Roeske JC, editors. Intensity modulated radiation therapy: A clinical perspective.1st ed. Hamilton: BC Deckers Inc, 2005: 20-52.

[18] Schlegel W, Bortfeld T, editors. A comparison of IMRT planning systems in the treatment of colon-rectal cancer. 00 May 22; Heidelberg: Springer, 2000.

[19] De Neve W, De Gersem W, Derycke S, De Meerleer G, Moerman M, Bate MT et al. Clinical delivery of intensity modulated conformal radiotherapy for relapsed or second-primary head and neck cancer using a multileaf collimator with dynamic control. Radiother Oncol 1999; 50(3):301-314.

[20] Sherouse GW, Chaney EL. The Portable Virtual Simulator. Int J Radiat Oncol Biol Phys 1991; 21(2):475-482.

[21] De Gersem W, Claus F, De Wagter C, De Neve W. An anatomy-based beam segmentation tool for intensity-modulated radiation therapy and its application to head-and-neck cancer. Int J Radiat Oncol Biol Phys 2001; 51(3):849-859.

[22] Burman C, Kutcher GJ, Emami B, Goitein M. Fitting of Normal Tissue Tolerance Data to An Analytic-Function. Int J Radiat Oncol Biol Phys 1991; 21(1):123-135.

[23] Kutcher GJ, Burman C, Brewster L, Goitein M, Mohan R. Histogram Reduction Method for Calculating Complication Probabilities for 3-Dimensional Treatment Planning Evaluations. Int J Radiat Oncol Biol Phys 1991; 21(1):137-146.

[24] Emami B, Lyman J, Brown A, Coia L, Goitein M, Munzenrider JE et al. Tolerance of Normal Tissue to Therapeutic Irradiation. Int J Radiat Oncol Biol Phys 1991; 21(1):109-122.

[25] Vaarkamp J, Krasin M. Reduction of target dose inhomogeneity in IMRT treatment planning using biologic objective functions. Int J Radiat Oncol Biol Phys 2001; 49(5):1518-1519.

[26] De Neve W, De Gersem W, De Meerleer G, Claus F, De Wagter C. Reduction of target dose inhomogeneity in IMRT treatment planning using biologic objective functions - In response. Int J Radiat Oncol Biol Phys 2001; 49(5):1519-1520.

[27] De Gersem W, Claus F, De Wagter C, Van Duyse B, De Neve W. Leaf position optimization for step-and-shoot IMRT. Int J Radiat Oncol Biol Phys 2001; 51(5):1371-1388.

[28] Galvin JM, Smith AR, Lally B. Characterization of A Multileaf Collimator System. Int J Radiat Oncol Biol Phys 1993; 25(2):181-192.

[29] Claus F, De Gersem W, Vanhoutte I, Duthoy W, Remouchamps V, De Wagter C et al. Evaluation of a leaf position optimization tool for intensity modulated radiation therapy of head and neck cancer. Radiother Oncol 2001; 61(3):281-286.

[30] Shepard DM, Earl MA, Li XA, Naqvi S, Yu C. Direct aperture optimization: a turnkey solution for step-and-shoot IMRT. Med Phys 2002; 29(6):1007-1018.

[31] Alber M, Nusslin F. Optimization of intensity modulated radiotherapy under constraints for static and dynamic MLC delivery. Phys Med Biol 2001; 46(12):3229-3239.

[32] Siebers JV, Lauterbach M, Keall PJ, Mohan R. Incorporating multi-leaf collimator leaf sequencing into iterative IMRT optimization. Med Phys 2002; 29(6):952-959.

[33] Hamilton RJ, Lachaine ME, Armbruster B. Treatment planning. In: Mundt AJ, Roeske JC, editors. Intensity modulated radiation therapy: A clinical perspective.1st ed. Hamilton: BC Deckers Inc, 2005: 149-165.

[34] UICC TNM classification of malignant tumours. 6th ed. New York: John Wiley & Sons, 2002.

[35] McBride WH, Withers HR. Radiobiology of subclinical disease. Front Radiat Ther Oncol 1994; 28:46-50.

[36] Fogliata A, Cozzi L, Bieri S, Bernier J. Critical appraisal of a conformal head and neck cancer irradiation avoiding electron beams and field matching. Int J Radiat Oncol Biol Phys 1999; 45(5):1331-1338.

[37] Dorr W. Acute radiation effects in normal tissues--translational aspects of biological research. Front Radiat Ther Oncol 2002; 37:1-8.

[38] Williams J, Chen YC, Rubin P, Finkelstein J, Okunieff P. The biological basis of a comprehensive grading system for the adverse effects of cancer treatment. Semin Radiat Oncol 2003; 13(3):182-188.

[39] Lee SP, Leu MY, Smathers JB, McBride WH, Parker RG, Withers HR. Biologically effective dose distribution based on the linear quadratic model and its clinical relevance. Int J Radiat Oncol Biol Phys 1995; 33(2):375-389.

[40] Trott KR. Experimental radiotherapy of late-responding tissues--recent advances and future development. Front Radiat Ther Oncol 2002; 37:9-16.

[41] De Neve W, Claus F, Duthoy W, De Meerleer G, De Wagter C. Intensity modulation techniques for improvement of normal tissue tolerance. Front Radiat Ther Oncol 2002; 37:163-173.

[42] Bijl HP. "Dose-volume effects in rat spinal cord irradiated with protons: Radiobiological studies of inhomogeneous dose distributions," Ph.D. dissertation, Rijksuniversiteit Groningen, 2005.

[43] Parsons JT, Bova FJ, Fitzgerald CR, Mendenhall WM, Million RR. Radiation Optic Neuropathy After Megavoltage External-Beam Irradiation - Analysis of Time-Dose Factors. Int J Radiat Oncol Biol Phys 1994; 30(4):755-763.

[44] Claus F. "Intensity modulated radiation therapy for ethmoid sinus cancer," Ph.D. dissertation, Ghent University Hospital, 2002.

[45] Duthoy W, Boterberg T, Claus F, Ost P, Vakaet L, Bral S et al. Postoperative intensity-modulated radiotherapy in sinonasal carcinoma. Cancer 2005; 104(1):71-82.

[46] Parsons JT, Bova FJ, Fitzgerald CR, Mendenhall WM, Million RR. Radiation Retinopathy After External-Beam Irradiation - Analysis of Time-Dose Factors. Int J Radiat Oncol Biol Phys 1994; 30(4):765-773.

[47] Takeda A, Shigematsu N, Suzuki S, Fujii M, Kawata T, Kawaguchi O et al. Late retinal complications of radiation therapy for nasal and paranasal malignancies: Relationship between irradiated-dose area and severity. Int J Radiat Oncol Biol Phys 1999; 44(3):599-605.

[48] Eisbruch A, Ten Haken RK, Kim HM, Marsh LH, Ship JA. Dose, volume, and function relationships in parotid salivary glands following conformal and intensity-modulated irradiation of head and neck cancer. Int J Radiat Oncol Biol Phys 1999; 45(3):577-587.

[49] Nagler RM. The enigmatic mechanism of irradiation-induced damage to the major salivary glands. Oral Dis 2002; 8(3):141-146.

[50] Maes A, Weltens C, Flamen P, Lambin P, Bogaerts R, Liu X et al. Preservation of parotid function with uncomplicated conformal radiotherapy. Radiother Oncol 2002; 63(2):203-211.

[51] Eisbruch A, Ship JA, Dawson LA, Kim HM, Bradford CR, Terrell JE et al. Salivary gland sparing and improved target irradiation by conformal and intensity modulated irradiation of head and neck cancer. World J Surg 2003; 27(7):832-837.

[52] Munter MW, Karger CP, Hoffner SG, Hof H, Thilmann C, Rudat V et al. Evaluation of salivary gland function after treatment of head-and-neck tumors with intensity-modulated radiotherapy by quantitative pertechnetate scintigraphy. Int J Radiat Oncol Biol Phys 2004; 58(1):175-184.

[53] Dawson LA, Anzai Y, Marsh L, Martel MK, Paulino A, Ship JA et al. Patterns of local-regional recurrence following parotid-sparing conformal and segmental intensity-modulated radiotherapy for head and neck cancer. Int J Radiat Oncol Biol Phys 2000; 46(5):1117-1126.

[54] Morrish RB, Jr., Chan E, Silverman S Jr, Meyer J, Fu KK, Greenspan D. Osteonecrosis in patients irradiated for head and neck carcinoma. Cancer 1981; 47(8):1980-1983.

[55] Glanzmann C, Gratz KW. Radionecrosis of the mandibula: a retrospective analysis of the incidence and risk factors. Radiother Oncol 1995; 36(2):94-100.

[56] Reuther T, Schuster T, Mende U, Kubler A. Osteoradionecrosis of the jaws as a side effect of radiotherapy of head and neck tumour patients--a report of a thirty year retrospective review. Int J Oral Maxillofac Surg 2003; 32(3):289-295.

[57] Regulation of gastrointestinal function. In: Ganong W.F., editor. Review of medical physiology.16th ed. East Norwalk: Appleton & Lange, 1993: 438-467.

[58] Eisbruch A, Lyden T, Bradford CR, Dawson LA, Haxer MJ, Miller AE et al. Objective assessment of swallowing dysfunction and aspiration after radiation concurrent with chemotherapy for head-and-neck cancer. Int J Radiat Oncol Biol Phys 2002; 53(1):23-28.

[59] Duthoy, W. IMRT protocol for Head and Neck Tumours. http://krtkg1.rug.ac.be/personnel/download/IMRT_HN_Protocol.pdf - accessed 7-8-2005

[60] Mohan R, Wu Q, Manning M, Schmidt-Ullrich R. Radiobiological considerations in the design of fractionation strategies for intensity-modulated radiation therapy of head and neck cancers. Int J Radiat Oncol Biol Phys 2000; 46(3):619-630.

[61] Fowler JF, Harari PM, Leborgne F, Leborgne JH. Acute radiation reactions in oral and pharyngeal mucosa: tolerable levels in altered fractionation schedules. Radiother Oncol 2003; 69(2):161-168.

[62] Eisbruch A. Head and Neck cancer: overview. In: Mundt AJ, Roeske JC, editors. Intensity modulated radiation therapy: A clinical perspective.1st ed. Hamilton: BC Deckers Inc, 2005: 264-275.

[63] Wu Q, Manning M, Schmidt-Ullrich R, Mohan R. The potential for sparing of parotids and escalation of biologically effective dose with intensity-modulated radiation treatments of head and neck cancers: a treatment design study. Int J Radiat Oncol Biol Phys 2000; 46(1):195-205.

[64] Kankerincidentie in Vlaanderen, 1997-1999. Van Eyken E, editor. 2002. Brussels, Vlaams Kankerregistratienetwerk. (Report)

[65] Dulguerov P, Jacobsen MS, Allal AS, Lehmann W, Calcaterra T. Nasal and paranasal sinus carcinoma: Are we making progress? A series of 220 patients and a systematic review. Cancer 2001; 92(12):3012-3029.

[66] Jansen EPM, Keus RB, Hilgers FJM, Haas RLM, Tan IB, Bartelink H. Does the combination of radiotherapy and debulking surgery favor survival in paranasal sinus carcinoma? Int J Radiat Oncol Biol Phys 2000; 48(1):27-35.

[67] Shukovsky LJ, Fletcher GH. Retinal and optic nerve complications in a high dose irradiation technique of ethmoid sinus and nasal cavity. Radiology 1972; 104(3):629-634.

[68] Ellingwood KE, Million RR. Cancer of the Nasal Cavity and Ethmoid-Sphenoid Sinuses. Cancer 1979; 43(4):1517-1526.

[69] Claus F, De Gersem W, De Wagter C, Van Severen R, Vanhoutte I, Duthoy W et al. An implementation strategy for IMRT of ethmoid sinus cancer with bilateral sparing of the optic pathways. Int J Radiat Oncol Biol Phys 2001; 51(2):318-331.

[70] Friedman M, Roberts N, Kirshenbaum GL, Colombo J. Nodal size of metastatic squamous cell carcinoma of the neck. Laryngoscope 1993; 103(8):854-856.

[71] Adams S, Baum RP, Stuckensen T, Bitter K, Hor G. Prospective comparison of 18F-FDG PET with conventional imaging modalities (CT, MRI, US) in lymph node staging of head and neck cancer. Eur J Nucl Med 1998; 25(9):1255-1260.

[72] Apisarnthanarax S, Chao KS. Current imaging paradigms in radiation oncology. Radiation Research 2005; 163:1-25.

[73] Daisne JF, Duprez T, Weynand B, Lonneux M, Hamoir M, Reychler H et al. Tumor volume in pharyngolaryngeal squamous cell carcinoma: Comparison at CT, MR imaging, and FDG PET and validation with surgical specimen. Radiology 2004; 233(1):93-100.

[74] Ling CC, Humm J, Larson S, Amols H, Fuks Z, Leibel S et al. Towards multidimensional radiotherapy (MD-CRT): biological imaging and biological conformality. Int J Radiat Oncol Biol Phys 2000; 47(3):551-560.

[75] Brun E, Kjellen E, Tennvall J, Ohlsson T, Sandell A, Perfekt R et al. FDG PET studies during treatment: prediction of therapy outcome in head and neck squamous cell carcinoma. Head Neck 2002; 24(2):127-135.

[76] Van de Wiele C. PET and SPECT in IMRT: Future Prospects. In: Bortfeld T, Schmidt-Ullrich R, De Neve W, Wazer DE, editors. Image-Guided IMRT.1st ed. Berlin: Springer, 2005: 171-176.

[77] Verhey L, Chuang C, Pirzkall A. Magnetic resonance imaging for IMRT. In: Bortfeld T, Schmidt-Ullrich R, De Neve W, Wazer DE, editors. Image-Guided IMRT.1st ed. Berlin: Springer, 2005: 177-186.

[78] Yang T, Chao KSC. Functional imaging in head and neck cancer. In: Mundt AJ, Roeske JC, editors. Intensity modulated radiation therapy: A clinical perspective.1st ed. Hamilton: BC Deckers Inc, 2005: 307-318.

[79] Ceelen W, Smeets P, Backes W, Van Damme N, Boterberg T, Demetter P et al. Noninvasive monitoring of radiotherapy induced microvascular changes using dynamic contrast enhanced magnetic resonance imaging (DCE-MRI) in a colorectal tumour model. Int J Radiat Oncol Biol Phys 2006; (in press).

[80] Minn H, Joensuu H, Ahonen A, Klemi P. Fluorodeoxyglucose imaging: a method to assess the proliferative activity of human cancer in vivo. Comparison with DNA flow cytometry in head and neck tumors. Cancer 1988; 61(9):1776-1781.

[81] Pugachev A, Ruan S, Carlin S, Larson SM, Campa J, Ling CC et al. Dependence of FDG uptake on tumor microenvironment. Int J Radiat Oncol Biol Phys 2005; 62(2):545-553.

[82] Chao KS, Ozyigit G, Tran BN, Cengiz M, Dempsey JF, Low DA. Patterns of failure in patients receiving definitive and postoperative IMRT for head-and-neck cancer. Int J Radiat Oncol Biol Phys 2003; 55(2):312-321.

[83] Feng M, Jabbari S, Lin A, Bradford CR, Chepeha DB, Teknos TN et al. Predictive factors of local-regional recurrences following parotid sparing intensity modulated or 3D conformal radiotherapy for head and neck cancer. Radiother Oncol 2005; 77(1):32-38.

[84] Bussels B, Maes A, Hermans R, Nuyts S, Weltens C, Van den BW. Recurrences after conformal parotid-sparing radiotherapy for head and neck cancer. Radiother Oncol 2004; 72(2):119-127.

[85] Zhou J, Fei D, Wu Q. Potential of intensity-modulated radiotherapy to escalate doses to head-and-neck cancers: what is the maximal dose? Int J Radiat Oncol Biol Phys 2003; 57(3):673-682.

[86] Allal AS, Dulguerov P, Allaoua M, Haenggeli CA, El Ghazi EA, Lehmann W et al. Standardized uptake value of 2-[F-18] fluoro-2-deoxy-D-glucose in predicting outcome in head and neck carcinomas treated by radiotherapy with or without chemotherapy. J Clin Oncol 2002; 20(5):1398-1404.

[87] Geets X, Daisne JF, Gregoire V, Hamoir M, Lonneux M. Role of 11-C-methionine positron emission tomography for the delineation of the tumor volume in pharyngo-laryngeal squamous cell carcinoma: comparison with FDG-PET and CT. Radiother Oncol 2004; 71(3):267-273.

[88] Daisne JF, Sibomana M, Bol A, Doumont T, Lonneux M, Gregoire V. Tri-dimensional automatic segmentation of PET volumes based on measured source-to-background ratios: influence of reconstruction algorithms. Radiother Oncol 2003; 69(3):247-250.

[89] Vanderstraeten B, Duthoy W, De Gersem W, De Neve W, Thierens H. [18F]fluoro-deoxy-glucose positron emission tomography ([18F]FDG-PET) voxel intensity-based intensity-modulated radiation therapy (IMRT) for head and neck cancer. Radiother Oncol 2006; (submitted).

[90] Proimos BS, Tsialas SP, Coutroubas SC. Gravity-oriented filters in arc cobalt therapy. Radiology 1966; 87(5):933-937.

[91] Webb S. A gravity-oriented-device for IMRT can never rival other IMRT delivery methods. Phys Med Biol 2004; 49(5):L5-L9.

[92] Carol M, Targovnik H, Smith D, Cahill D. 3-D planning and delivery system for optimized conformal therapy. Int J Radiat Oncol Biol Phys 1992; 24(Suppl 1):158.

[93] Low DA, Mutic S, Dempsey JF, Markman J, Goddu SM, Purdy JA. Abutment region dosimetry for serial tomotherapy. Int J Radiat Oncol Biol Phys 1999; 45(1):193-203.

[94] Mackie TR, Holmes T, Swerdloff S, Reckwerdt P, Deasy JO, Yang J et al. Tomotherapy - A New Concept for the Delivery of Dynamic Conformal Radiotherapy. Med Phys 1993; 20(6):1709-1719.

[95] Yu CX. Intensity-Modulated Arc Therapy with Dynamic Multileaf Collimation - An Alternative to Tomotherapy. Phys Med Biol 1995; 40(9):1435-1449.

[96] Duthoy W, De Gersem W, Vergote K, Coghe M, Boterberg T, De Deene Y et al. Whole abdominopelvic radiotherapy (WAPRT) using intensity-modulated arc therapy (IMAT): First clinical experience. Int J Radiat Oncol Biol Phys 2003; 57(4):1019-1032.

[97] Yu CX, Li XA, Ma LJ, Chen DJ, Naqvi S, Shepard D et al. Clinical implementation of intensity-modulated arc therapy. Int J Radiat Oncol Biol Phys 2002; 53(2):453-463.

[98] Duthoy W, De Gersem W, Vergote K, Boterberg T, Derie C, Smeets P et al. Clinical implementation of intensity-modulated arc therapy (IMAT) for rectal cancer. Int J Radiat Oncol Biol Phys 2004; 60(3):794-806.

[99] De Neve W, Duthoy W, Claus F, De Gersem W, Coghe M, De Meerleer G et al. Dose conformation in IMRT for head and neck tumors: which solution to apply? Cancer Radiother 2002; 6 Suppl 1:32s-36s.

[100] Gillis S, Bral S, De Wagter C, Derie C, Paelinck L, Van Vaerenbergh K et al. Evaluation of the Sinmed Mastercouch((R)) as replacement for a standard couch. Radiother Oncol 2005.

[101] Bratengeier K. Applications of two-step intensity modulated arc therapy. Strahlenther Onkol 2001; 177(8):394-403.

[102] Wong E, Chen JZ, Greenland J. Intensity-modulated arc therapy simplified. Int J Radiat Oncol Biol Phys 2002; 53(1):222-235.

[103] Wong E, D'Souza DP, Chen JZ, Lock M, Rodrigues G, Coad T et al. Intensity-modulated arc therapy for treatment of high-risk endometrial malignancies. Int J Radiat Oncol Biol Phys 2005; 61(3):830-841.

[104] Earl MA, Shepard DM, Naqvi S, Li XA, Yu CX. Inverse planning for intensity-modulated arc therapy using direct aperture optimization. Phys Med Biol 2003; 48(8):1075-1089.

[105] De Deene Y, De Wagter C, Van Duyse B, Derycke S, Mersseman B, De Gersem W et al. Validation of MR-based polymer gel dosimetry as a preclinical three-dimensional verification tool in conformal radiotherapy. Magn Reson Med 2000; 43(1):116-125.

[106] De Deene Y, De Wagter C, Van Duyse B, Derycke S, De Neve W, Achten E. Three-dimensional dosimetry using polymer gel and magnetic resonance imaging applied to the verification of conformal radiation therapy in head-and-neck cancer. Radiother Oncol 1998; 48(3):283-291.

[107] De Deene Y. "Verificatie van de dosisverdeling bij hoge-precisie radiotherapie met behulp van NMR gel-dosimetrie," Ph.D. dissertation, University of Ghent, 2000.

[108] Vergote K. "Development of polymer gel dosimetry for applications in intensity-modulated radiotherapy," Ph.D. dissertation, University of Ghent, 2005.

[109] Maryanski MJ, Gore JC, Kennan RP, Schulz RJ. Nmr Relaxation Enhancement in Gels Polymerized and Cross-Linked by Ionizing-Radiation - A New Approach to 3D Dosimetry by Mri. Magn Reson Imaging 1993; 11(2):253-258.

[110] Vergote K, De Deene Y, Duthoy W, De Gersem W, De Neve W, Achten E et al. Validation and application of polymer gel dosimetry for the dose verification of an intensity-modulated arc therapy (IMAT) treatment. Phys Med Biol 2004; 49(2):287-305.

[111] Low DA, Harms WB, Mutic S, Purdy JA. A technique for the quantitative evaluation of dose distributions. Med Phys 1998; 25(5):656-661.

[112] Duthoy W, Vergote K, De Gersem W, De Deene Y, De Wagter C, De Neve W. Clinical validation of intensity modulated arc therapy (IMAT) by means of polymer gel dosimetry. Journal of Physics: Conference Series 2004;276-279.

[113] Mell LK, Roeske JC, Mundt AJ. A survey of intensity-modulated radiation therapy use in the United States. Cancer 2003; 98(1):204-211.

[114] National Cancer Institute. Levels of Evidence for Adult Cancer Treatment Studies (PDQ®). http://www.cancer.gov/cancertopics/pdq/levels-evidence-adult-treatment/healthprofessional/allpages - accessed 20-9-2005

[115] Cumberlin, R. L. and Kaplan, R. NCI IMRT Guidelines Letter - 2002. http://www.rtog.org/pdf_document/IMRT-RTOG.pdf - accessed 6-8-2005

[116] Abrams, J. and Coleman, N. The National Cancer Institute Guidelines for the Use of Intensity-Modulated Radiation Therapy in Clinical Trials. http://www.rtog.org/pdf_document/IMRT_NCI_Guidelines_v4.0.doc - accessed 6-8-2005

[117] Nutting C. A multicentre randomised study of parotid sparing intensity modulated radiotherapy versus conventional radiotherapy in patients with head and neck cancer. 2003. (Personal Communication)

[118] Glatstein E. Intensity-modulated radiation therapy: the inverse, the converse, and the perverse. Semin Radiat Oncol 2002; 12(3):272-281.

[119] Santiago RJ, Glatstein E. Pros and cons of IMRT: what's been swept under the rug? In: Mundt AJ, Roeske JC, editors. Intensity modulated radiation therapy: A clinical perspective.1st ed. Hamilton: BC Deckers Inc, 2005: 628-637.

[120] Chui CS, Yorke E, Hong L. The effects of intra-fraction organ motion on the delivery of intensity-modulated field with a multileaf collimator. Med Phys 2003; 30(7):1736-1746.

[121] Jiang SB, Pope C, Al Jarrah KM, Kung JH, Bortfeld T, Chen GT. An experimental investigation on intra-fractional organ motion effects in lung IMRT treatments. Phys Med Biol 2003; 48(12):1773-1784.

[122] Naqvi SA, D'Souza WD. A stochastic convolution/superposition method with isocenter sampling to evaluate intrafraction motion effects in IMRT. Med Phys 2005; 32(4):1156-1163.

[123] Chmura SJ, Farrey K, Wang S, Garofalo MC, Roeske JC. Impact of prolonged treatment times. In: Mundt AJ, Roeske JC, editors. Intensity modulated radiation therapy: A clinical perspective.1st ed. Hamilton: BC Deckers Inc, 2005: 337-343.

[124] Mu X, Lofroth PO, Karlsson M, Zackrisson B. The effect of fraction time in intensity modulated radiotherapy: theoretical and experimental evaluation of an optimisation problem. Radiother Oncol 2003; 68(2):181-187.

[125] Joiner MC, Marples B, Lambin P, Short SC, Turesson I. Low-dose hypersensitivity: current status and possible mechanisms. Int J Radiat Oncol Biol Phys 2001; 49(2):379-389.

[126] Hall EJ, Wuu CS. Radiation-induced second cancers: the impact of 3D-CRT and IMRT. Int J Radiat Oncol Biol Phys 2003; 56(1):83-88.

[127] Verellen D, Vanhavere F. Risk assessment of radiation-induced malignancies based on whole-body equivalent dose estimates for IMRT treatment in the head and neck region. Radiother Oncol 1999; 53(3):199-203.

[128] Eisbruch A, Kim HM, Terrell JE, Marsh LH, Dawson LA, Ship JA. Xerostomia and its predictors following parotid-sparing irradiation of head-and-neck cancer. Int J Radiat Oncol Biol Phys 2001; 50(3):695-704.

[129] Claus F, Boterberg T, Ost P, De Neve W. Short term toxicity profile for 32 sinonasal cancer patients treated with IMRT. Can we avoid dry eye syndrome? Radiother Oncol 2002; 64(2):205-208.

[130] Beavis AW. Is tomotherapy the future of IMRT? Br J Radiol 2004; 77(916):285-295.

[131] Mackie TR, Balog J, Ruchala K, Shepard D, Aldridge S, Fitchard E et al. Tomotherapy. Semin Radiat Oncol 1999; 9(1):108-117.

[132] Yu CX, Jaffray DA, Wong JW. The effects of intra-fraction organ motion on the delivery of dynamic intensity modulation. Phys Med Biol 1998; 43(1):91-104.

[133] Kissick MW, Boswell SA, Jeraj R, Mackie TR. Confirmation, refinement, and extension of a study in intrafraction motion interplay with sliding jaw motion. Med Phys 2005; 32(7):2346-2350.

[134] Mackie TR, Kapatoes J, Ruchala K, Lu WG, Wu C, Olivera G et al. Image guidance for precise conformal radiotherapy. Int J Radiat Oncol Biol Phys 2003; 56(1):89-105.

[135] Jaffray DA, Siewerdsen JH, Wong JW, Martinez AA. Flat-panel cone-beam computed tomography for image-guided radiation therapy. Int J Radiat Oncol Biol Phys 2002; 53(5):1337-1349.

[136] Kapatoes JM, Olivera GH, Balog JP, Keller H, Reckwerdt PJ, Mackie TR. On the accuracy and effectiveness of dose reconstruction for tomotherapy. Phys Med Biol 2001; 46(4):943-966.

[137] Vieira SC, Dirkx ML, Heijmen BJ, de Boer HC. SIFT: a method to verify the IMRT fluence delivered during patient treatment using an electronic portal imaging device. Int J Radiat Oncol Biol Phys 2004; 60(3):981-993.

[138] Kupelian PA, Ramsey C, Meeks SL, Willoughby TR, Forbes A, Wagner TH et al. Serial megavoltage CT imaging during external beam radiotherapy for non-small-cell lung cancer: Observations on tumor regression during treatment. Int J Radiat Oncol Biol Phys 2005.

[139] Yan D, Lockman D, Martinez AA, Wong J, Brabbins D, Vicini F et al. Computed tomography guided management of interfractional patient variation. Semin Radiat Oncol 2005; 15(3):168-179.

[140] Ma LJ, Yu CX, Earl M, Holmes T, Sarfaraz M, Li XA et al. Optimized intensity-modulated arc therapy for prostate cancer treatment. Int J Cancer 2001; 96(6):379-384.

[141] Lin A, Kim HM, Terrell JE, Dawson LA, Ship JA, Eisbruch A. Quality of life after parotid-sparing IMRT for head-and-neck cancer: a prospective longitudinal study. Int J Radiat Oncol Biol Phys 2003; 57(1):61-70.

[142] Lauve A, Morris M, Schmidt-Ullrich R, Wu Q, Mohan R, Abayomi O et al. Simultaneous integrated boost intensity-modulated radiotherapy for locally advanced head-and-neck squamous cell carcinomas: II--clinical results. Int J Radiat Oncol Biol Phys 2004; 60(2):374-387.

[143] Bijl HP, van Luijk P, Coppes RP, Schippers JM, Konings AW, Der Kogel AJ. Regional differences in radiosensitivity across the rat cervical spinal cord. Int J Radiat Oncol Biol Phys 2005; 61(2):543-551.

[144] Deasy JO, Niemierko A, Herbert D, Yan D, Jackson A, Ten Haken RK et al. Methodological issues in radiation dose-volume outcome analyses: summary of a joint AAPM/NIH workshop. Med Phys 2002; 29(9):2109-2127.

[145] Gillis S, De Wagter C, Bohsung J, Perrin B, Williams P, Mijnheer BJ. An inter-centre quality assurance network for IMRT verification: results of the ESTRO QUASIMODO project. Radiother Oncol 2005; 76(3):340-353.

Kruisdankwoordraadsel

Een promovendus moet aanvaarden dat het dankwoord het meest gelezen deel zal zijn van de thesis. Van U, beste lezer, weet ik dat U eerst de thesis las, en dit stukje voor het laatst hebt gehouden, maar geloof me, er zijn er anderen….

Een thesis maak je niet alleen, dat is algemeen geweten. Een netwerk van mensen staat naast en achter je, gedurende al die tijd. Ieder van hen draagt op zijn manier bij aan het geheel, soms heel direct, soms meer achter de schermen. De onderstaande mensen wil ik in het bijzonder bedanken:

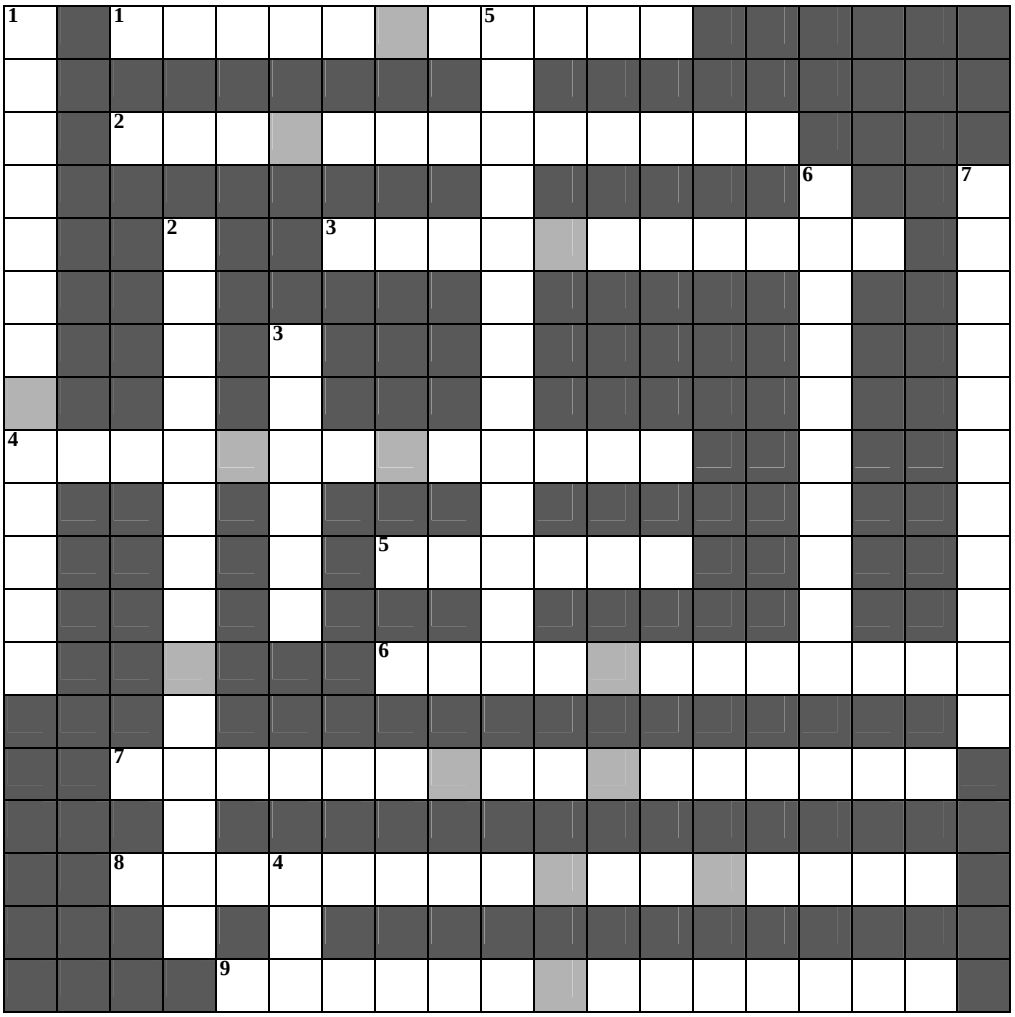

Blanco

Spatie

Horizontaal

(1) Bedankt om voor mij het pad te effenen, en mij die eerste jaren geduldig te leren wat er te leren viel. Je manier van werken, je zelfkritiek,… het was allemaal inspirerend voor mij. Hoe je met die "broken pipe" omging, getuigde van diep inzicht (U asked 4 it).

(2) Officieus lid van de leescommissie, maar bovenal begeleider in bange uren en laatste loodjes. Als U een Engelse tekst wil laten nalezen, bent U beter af bij hem dan bij een "native speaker" (trouwens; je aanvraag voor de 170-uren werkweek is afgewezen).

(3) "Eminence grise" van de dienst. Zijn a-dogmatische vragen mogen dan al eens verward worden met naïviteit, voor mij waren ze een belangrijke reden om voor radiotherapie te kiezen.

(4) The Irish soul backing. Ta gra agam ort.

(5) Vereenzelvigd worden met een tak van de wetenschap: het is niet iedereen gegund. Interface tussen mens en machine, menigmaal hebben Bart en Marc me uit de nood geholpen (ik had dat commando zelf óók al geprobeerd, echt waar…)

(6) De samenwerking met jou was één van de leukste momenten tijdens mijn doctoraat. Je introduceerde me in de wondere wereld van de geldosimetrie (werkt dat nu eigenlijk?), en bracht een stukje Jamaïca op P7, op zich een kunst.

(7) Schippert tussen Poperinge en de krtkg6. De inzet waarmee hij keer op keer streeft naar het onbereikbare, optimale plan is indrukwekkend. Bedankt voor het samen werken: je gunde me een blik achter het (mist)gordijn van algoritmes en C++ (soms begreep ik het).

(8) Bedankt om mij en dit werk te "promoten". Zonder Uw nooit aflatende ideeënstroom (die mij soms tsunami-gewijs overspoelde), zou dit werk niet mogelijk geweest zijn.

(9) Heerlijk boontje (nee, niet mijn vrouwtje) met onvolprezen kwaliteiten. Presteert het best onder hoge druk.

Verticaal

(1) Mijn lieverd, mijn boontje: bedankt voor al je liefde, het opgebrachte geduld (telkens weer) en het gezonde tegengewicht dat je bood (there is life out there!). Wat we samen schreven is (eindelijk) aanvaard door "Nature". Ik verlang naar het ogenblik dat het ter perse gaat!

(2) Bedankt voor al het stille werk dat je verricht hebt. Dossiers opvragen, databases aanvullen, ik kon het met een gerust hart aan jou overlaten.

(3) Mama en papa, zonder jullie zou ik hier niet staan: waarschijnlijk helemaal niet, en dan toch alleszins niet als de persoon die ik nu ben. Bedankt!

(4) Instelling met mooi briefpapier. Stelde mij in staat om dit werk uit te voeren en tóch betaald te worden.

(5) Net voor de eindmeet durft het schrijven van een thesis nogal eens "tegensteken", en wordt het allemaal "fuzzy". De kandidaat durft dan al eens dingen op papier te zetten die hij uiteráárd niet zo bedoeld had. Ik dank dan ook de professoren Yves De Deene, Marc Peeters, Guy Storme en Eugene Wong voor hun kritische nalezing en waardevolle suggesties. Zij hebben dit werk verbeterd.

(6) Zelf het beste plan is niet veel waard zonder mensen die het – elke dag weer - met toewijding en zorg ten uitvoer brengen. Gelukkig hebben wij zulke mensen op de dienst radiotherapie.

(7) Mijn rechtstreekse collega's over de loop der jaren: Ilse Vanhoutte, Joost Nuyttens, Samuel Bral, Frederic Duprez, Valerie Fonteyne, Sabine Meersschout, Nathalie Meireson, Katrien Vandecasteele en Benedict Engels (de lengte van de lijst begint me zorgen te baren). Bedankt voor de samenwerking, de babbels en de vervangingen alom.

B	■	F	I	L	I	P	■	C	L	A	U	S	■	■	■	■	■	■
A	■	■	■	■	■	■	■	■	E	■	■	■	■	■	■	■	■	■
R	■	T	O	M	■	B	O	T	E	R	B	E	R	G	■	■	■	■
B	■	■	■	■	■	■	■	■	S	■	■	■	■	■	V	■	■	A
A	■	C	■	■	M	A	R	C	■	M	A	R	E	E	L	■	■	S
R	■	R	■	■	■	■	■	O	■	■	■	■	■	R	■	■	■	S
A	■	I	■	■	O	■	■	M	■	■	■	■	■	P	■	■	■	I
■	■	S	■	■	U	■	■	M	■	■	■	■	■	L	■	■	■	S
B	A	R	T	■	D	E	■	W	I	L	D	E	■	E	■	■	■	T
O	■	I	■	■	E	■	■	S	■	■	■	■	■	G	■	■	■	E
O	■	N	■	■	R	■	F	Y	S	I	C	A	■	I	■	■	■	N
N	■	A	■	■	S	■	■	I	■	■	■	■	■	N	■	■	■	T
E	■	■	■	■	■	■	K	O	E	N	■	V	E	R	G	O	T	E
■	■	D	■	■	■	■	■	■	■	■	■	■	■	■	■	■	■	N
■	■	W	E	R	N	E	R	■	D	E	■	G	E	R	S	E	M	■
_	_	■	R	■	■	■	■	■	■	■	■	■	■	■	■	■	■	_
_	_	W	I	L	F	R	I	E	D	■	D	E	■	N	E	V	E	_
■	■	■	E	■	W	■	■	■	■	■	■	■	■	■	■	■	■	■
■	■	■	■	C	O	F	F	E	A	■	A	R	A	B	I	C	A	■